Stony Brook University

Submarine groundwater discharge as an integral environmental "currency" limiting population and development within the ecosphere of small islands.

A Dissertation Presented

by

Ruth Coffey

to

The Graduate School

in Partial Fulfillment of the

Requirements

for the Degree of

Doctor of Philosophy

in

Marine and Atmospheric Science

Stony Brook University

December 2014

Stony Brook University

The Graduate School

Ruth Coffey

We, the dissertation committee for the above candidate for the

Doctor of Philosophy degree, hereby recommend

acceptance of this dissertation.

Henry Bokuniewicz – Dissertation Advisor
Professor, School of Marine and Atmospheric Sciences (SoMAS)

Robert Swanson - Chairperson of Defense
Professor, School of Marine and Atmospheric Sciences (SoMAS)

Warren Sanderson
Professor, Department of Economics

John Rapaglia
Assistant Professor, Department of Biology, Sacred Heart University

Leonard Nurse
Senior Lecturer, Centre for Resource Management and Environmental Studies, University of the West Indies

This dissertation is accepted by the Graduate School

Charles Taber
Dean of the Graduate School

Abstract of the Dissertation

Submarine groundwater discharge as an integral environmental "currency" limiting population and development within the ecosphere of small islands.

by

Ruth Coffey

Doctor of Philosophy

in

Marine and Atmospheric Science

Stony Brook University

2014

Submarine groundwater discharge (SGD) from oceanic islands has been estimated to contribute over a third of the global SGD due to orographic precipitation, short aquifer pathways and poorly developed surface drainage. This seepage of groundwater across the sea floor connects land and coastal ocean resources, and is hereby proposed as a parameter to evaluate the interconnections between coastal environmental quality and coastal populations and development. Relatively few islands have been studied, but SGD is typically found to be an important, and often the only, source of nutrients to coastal waters. Freshwater and its pollutant load are delivered to the coastal zone *via* SGD with consequent impacts on tourism and fisheries thus linking the land-based and marine economic sectors. The characteristics of SGD were investigated on Barbados, Guam and Bimini, islands all of, at least partly, carbonate origin, This study evaluates the similarities and differences between these islands and assesses the applicability of using SGD as a parameter within a population-development-environment model. Model scenarios can be used to explore the integrated coastal impacts of wastewater treatment practices and changes in seasonal rainfall due to climate change. This study also presents novel analytical methods for SGD field data.

Dedication Page

For my family.

Your love, support and encouragement keep me moving forward.

Table of Contents

List of Figures

Chapter 3

Chapter 4

Chapter 5

Chapter 6

List of Tables

Acknowledgments

I am eternally grateful to my advisor, Henry Bokuniewicz, and the other members of my dissertation committee, Larry Swanson, Leonard Nurse, John Rapaglia and Warren Sanderson, for their support and patience. Their guidance has helped me mold this dissertation into the best possible product.

This work would not have been possible without field support in each of my field sites:

From Barbados, I would like to thank the Cave Hill Campus of the University of the West Indies and the Barbados Water Authority for providing housing and logistical support. I am particularly grateful for the help of Barry Mayers from the University of the West Indies, and Gregory Thompson of the Barbados Water Authority for their help both in field sampling and in securing the needed resources and data to complete this project.

Supporting my study of Guam, was Matthew Charette of the Woods Hole Oceanographic Institution. I am also thankful for Michael Slattery from Stony Brook University for his invaluable help in the field on Guam.

The Bimini study was conducted with Michael White, Aaron Macy and Cody Roldan, who assisted with field and laboratory work. I am also grateful for the transportation assistance from the members of the Bimini Biological Field Station. This study was a part of the School of Marine and Atmospheric Sciences Research Experience for Undergraduates 2010 summer program.

I am also incredibly grateful for the immense help of Eileen Doyle, Carol Dove, Kim Knoll and all of the support staff at the School of Marine and Atmospheric Sciences, without whom, equipment would never have been paid for, forms would not have been submitted on time, and my sanity would be in even worse shape.

Last, and certainly not least, I extend thanks to my family and friends, who have been sounding boards and supportive pillars throughout my career. This dissertation would not exist without their love, support and encouragement, and there will never be enough ways to express my infinite gratitude for each and every one of them.

Chapter 1 Introduction

There are fifty-one small island nations in the world's oceans (United Nations Department of Economic and Social Affairs, 2014) and many thousands of oceanic islands. Although globally they span the full geological and climatic range, island populations face the common problem of having limited resources. Potable water is particularly critical as sustainable island economies often depend on agriculture and, increasingly, on tourism, both of which place heavy demands on freshwater resources which are solely dependent on the island's precipitation or on its resources to artificially augment the water supply. Thorough characterization of the local water cycle, including the hydrogeological resources, is important in assessing the vulnerability of potable water resources. This includes the phenomenon known as submarine groundwater discharge, which can play an important role, linking terrestrial freshwater management to ocean water quality.

Submarine groundwater discharge (SGD) is any flow of groundwater up across the sea floor (Burnett *et al.*, 2006). This includes both freshwater from the land that seeps under the shoreline, known as the underflow, as well as seawater circulated through the coastal aquifer. The underflow, that is the flow of freshwater out under the shoreline, may be seen as a loss of potable water, and in fact, several water-stressed coasts have tried to recover freshwater from submarine springs (Nymphea, 2013). This "loss", however, serves a critical purpose in curtailing saltwater intrusion into the freshwater aquifer. It is also one of the principle drivers of SGD.

SGD is largely, though not exclusively, a diffuse (non-point) loss of freshwater and is a function of the hydraulic gradient between the surface of the freshwater aquifer and sea level. The terrestrial hydraulic gradient combined with the density difference between freshwater and seawater maintains the location of the freshwater interface. In coastal aquifers, the zone between fresh, meteoric groundwater and groundwater of oceanic salinity is referred to as a 'subterranean estuary' (Moore, 1999). The diversity of subterranean estuaries worldwide are similar to that of open-water, surface estuaries due to changes in the amount of flow laterally across the boundary, changes in permeability, and strong variations in salinity, temperature, dissolved oxygen, nutrient concentrations and other properties. As a mechanism for transport of terrestrially derived dissolved constituents, SGD has been found to be an important, and occasionally the only, source of nutrients to coastal waters (*e.g.* Bokuniewicz, 1980; Capone and Bautista, 1985). On isolated islands, the importance of SGD is enhanced by the short distances between the areas of recharge inland and discharge at the shoreline.

Pollutants from agriculture, sewage and other wastewater can enter the coastal ocean *via* SGD (*e.g.* Taniguchi *et al.*, 2008; Burnett *et al.*, 2006; Rodellas *et al.*, 2014). Where SGD is the primary source of nutrients to the coastal waters, the productivity and sustainability of coastal fisheries may depend upon it. However, excess nutrients and contaminant input *via* SGD can also degrade water quality, having negative impacts on living marine resources as well as tourism.

In addition to the local importance of SGD at oceanic islands, island SGD may have disproportionately large global implications, not just on water budgets but also on geochemical budgets as well. More than a third of global SGD has been estimated to originate at oceanic islands (Zektser, 2000). Because of the high relief found on some of these islands orographic lift enhances total precipitation that ultimately supplies SGD. For example, the island of Mauritius with its elevation in excess of 800 m receives peak rainfall amounting to 4000 mm per year (Povinec *et al*., 2012). In addition, small islands typically lack well-formed river drainage systems (point source discharges); during rainstorm events, transport of water is primarily in the form of ephemeral surface runoff. In the long term, however, the more diffuse, non-point source, and more persistent SGD fuels the underflow. Nutrient transport by SGD is important on small islands for several reasons, geographical and economical. Flow paths from the land into the ocean also are short, so time for attenuation, adsorption and alteration of nutrients (*e.g.* denitrification) within the aquifer is limited. Small islands are often restricted in natural resources for export, tourism may then play a larger role in supporting the residents, and the production of fisheries is important not only for subsistence but also for export. Poor soil quality may not only add to the stress on water quality from excess fertilizer nitrogen but also may limit the viability of agriculture itself, which places a larger burden on other sectors to support the economy.

Given the potential importance of island SGD, what is needed, then, is an efficient strategy to assess island-specific SGD because the economies of many small islands cannot afford the benefit of extensive (and expensive) research, measurements must then be coupled with a method to translate field SGD studies with management policy. Population-development-environment (PDE) models have been used to describe the interactions among population demography, societal and economic development and environmental conditions in Mauritius and on the Yucatan Peninsula (Lutz, 1994; Lutz *et al*., 2000). The environmental parameters in these models, however, have neglected SGD and its tie to the coastal water quality. The goal, therefore, of this study is primarily to develop strategies to characterize the primary baseline trends in groundwater discharge but also to suggest an approach to anticipate the role of SGD ultimately with economic parameters.

A critical constraint to consider is that small island nations, like Barbados, may not be willing and able to fund a full range of developed SGD sampling regimes with long study periods, dedicated staff, well-stocked equipment. To overcome some of these hurdles, I have developed an expedient sampling scheme to determine basic characteristics of SGD patterns by using vented benthic chambers (a.k.a. manual seepage meters) to measure SGD. With adequate

manpower and relatively few measurements, SGD patterns can be used to determine basic spatial and temporal variations in the system, and the implications for nutrient input. Using a few measurements to extrapolate to a larger shoreline can give a first order approximation of overall potential impact of SGD for application in PDE models.

Approaching a PDE model, six categories of parameters need to be considered. These are: geography/geology, climate, population, nutrient, economic and, in the context of this thesis, SGD (Table 1-1). Geographic and geologic parameters include shoreline length, land area, aquifer depth and hydrologic characteristics, and percent cultivated land. These parameters define the reservoir for the water and nutrient model. Climatic parameters include seasonal rainfall, the duration of the seasons and the percentage of rainfall that recharges the aquifer. These define the input of freshwater. Population characteristics include the projected changes in the resident population, tourism visitation numbers and residence time and population water use, all of which define both the demand and the input of wastewater and associated nutrients. Economic parameters include the contribution of tourism to the GDP as well as any costs associated with the mitigation of water quality degradation, such as the implementation and maintenance of sewage treatment strategies. Finally, as I will discuss, SGD will need to be characterized by the integrated flow per meter of shoreline, the extent of measurable flow and the fraction of freshwater being discharged at the shoreline. These determine the concentration of nutrients and freshwater being supplied to the coastal ocean.

The goal of my research has been to explore strategies for characterizing SGD on oceanic islands in the context of sustainable management of water resources.

Previous Work

Despite the importance of SGD on small oceanic islands, relatively few studies have been done and SGD has not been integrated into issues of water management. Notably, studies of SGD have been done on Hawaii (Knee *et al*., 2008) and Jeju, Korea (Lee and Kim, 2007; Kim *et al*., 2003). Other research has been done on small islands, including Mauritius (Burnett *et al*., 2006; Povinec *et al*., 2012), the Philippines (Senal *et al*., 2011), Mallorca (Basterretxea, 2010; Rodellas *et al*., 2014), and Barbados (Lewis, 1987).

It can be difficult, however, to compare SGD studies done for different objectives, in part because the operable parameters are evaluated in different units. Total SGD is sometimes reported as a total volume per unit time, like m^3/y, although this presupposed a well-delimited body of receiving water, like a bay. Other techniques report total SGD per meter of shoreline while still others report specific SGD as volume per area per time. The units of cm/d are actually cubic centimeters of groundwater per square centimeter per day. Specific SGD can be converted to SGD per meter of shoreline by multiplying by the extent of the seepage face from shore. This

can be converted to total SGD by multiplying by the shoreline length. Translating the results of one particular study into comparable terms as reported in another study often requires certain assumptions, such as the width of the offshore zone of discharge or the relevant shoreline length. I will do my best to make these conversions, but they will ultimately add uncertainty.

Mauritius

Mauritius is a tropical volcanic island covering 1865 km^2 in the Indian Ocean (20° 18' S; 57° 35' E). Mauritius has a million residents in urban and rural settings, so degradation of the quality of both potable groundwater and coastal water is of large concern. Nitrate transported into coastal lagoons *via* SGD has been implicated as a cause of algal blooms and eutrophication events (Bokuniewicz et al., 2007). Annual precipitation can be up to 4000 mm/y (Povinec *et al*., 2012), nearly half of which occurs at the end of the summer, that is January through March (Falkland, 1991). The coastal zone is made predominantly of lagoons shaped by barrier or fringing reefs (Bokuniewicz *et al*., 2007). The primary aquifer is the Curipipe Aquifer, which covers approximately 95 km^2 and is comprised of highly permeable lava flows (Povinec *et al*., 2012). More than fifty percent of the potable water demands in Mauritius are met by withdrawal from its aquifers (Burnett *et al*., 2006). Sugarcane and other agricultural industries also depend on groundwater supplies (Povinec *et al*., 2012).

A 2005 field excursion to Mauritius was part of an intercomparison project to evaluate different methods for measuring SGD, including manual seepage meters, automated seepage meters, piezometers, electrical conductivity and isotopic tracers. Water balance estimates predicted an average rate of discharge of 64 cm/d (Burnett *et al*., 2006). (N.B. SGD units are reported as cm/d, which is shorthand notation for the volume flux discharge across an area of seafloor, $cm^3/cm^2/day$). Seepage meters recorded average flow of 54.5 cm/d, however samples in the vicinity of a submerged spring had flow rates as high as 490 cm/d. At the highest rates o f discharge, SGD showed evidence of freshwater dilution. The use of geochemical tracers and other methods showed similar rates of both SGD and freshwater dilution. The variability of the results is likely due to preferential flow through the coralline shore and lava tubes (Burnett *et al*., 2006).

Hawaii

The volcanic Hawaiian island chain stretches across 2450 km of the tropical Pacific Ocean (Falkland, 1991). The six major islands (Kauai, Oahu, Molokai, Lanai, Maui and Hawaii) combined have a 16,390 km^2 land area (Falkland, 1991). Mean annual rainfall is 1850 mm (Falkland, 1991). The high values are a result of the orographic effect from the relief of each

individual island. A number of studies have looked at SGD on the Big Island (Hawaii), and the islands of Kauai and Oahu.

On the western coast of the Big Island, Peterson *et al*. (2009) used aerial thermal infrared imaging to detect SGD and suggest that point-source groundwater discharges dominate over diffuse seepage along the coastline. These point-source discharges are likely a result of the high permeability of the fractured basalt bedrock and the presence of lava tubes (Peterson *et al*., 2009). In addition to the thermal imaging, they also determined SGD fluxes using radium and radon isotopes. These naturally occurring radionuclides are elevated in groundwater and are routinely used as indicators of SGD. Models used to convert isotope activity into fluxes give values in terms of total volumetric discharge rather than the vertical advection flux normally reported for manual seepage meters (Peterson *et al*., 2009). They found average SGD fluxes from 1,100 m^3/d to 12,000 m^3/d and freshwater fluxes from 630 m^3/d to 8,600 m^3/d. To convert these values to SGD values that can be compared with manual seepage meter results, I divided the total discharge values by the area of the freshwater plume. Total SGD flows ranged between 62 cm/d and 320 cm/d with an average of 130 cm/d. The freshwater component ranged from 22% to 89%, averaging 63%. In this study, Peterson *et al*. (2009) saw inverse correlation with the tide, with the highest flow occurring during low water and negative flow during high water (influx of seawater into the sediment).

On the north shore of Kauai, Knee *et al*. (2008) studied SGD as a source of nutrients and a possible source of fecal-indicator bacteria. Volumetric discharges determined from concentrations of radium isotopes ranged from 408 m^3/d to 35,352 m^3/d (Knee *et al*., 2008), which is comparable to those found by Peterson *et al*. (2009), however, when converted, this corresponded to SGD rates ranging from 1.8 cm/d to 11.8 cm/d, averaging 5.8 cm/d, much lower than those found on the Big Island.

On the island of Oahu, Garrison *et al*. (2003) found SGD to be a substantial source of dissolved nutrients to Kahana Bay. Nutrient concentrations were elevated due to sediment diagenesis in the submarine aquifer. In total, nutrient input into the bay by SGD was equal to or greater than surface runoff. Averaged SGD rates were 42 cm/d with a 20% freshwater component (Garrison *et al*., 2003).

Jeju, Korea

Jeju Island is a 1,828 km^2 volcanic island in the South Sea of Korea. It receives substantial precipitation, especially during the summer months when it receives up to 1,900 mm/y (Kim *et al*., 2003). The vast majority of this precipitation infiltrates the highly permeable volcanic rocks with little sustained stream flow (Hwang *et al*., 2005). Several studies of SGD have been conducted on Jeju using a variety of methods; including manual seepage meters,

geochemical tracers and water budget analysis (*e.g.* Kim *et al*., 2003; Hwang *et al*., 2005; Lee and Kim, 2007 respectively). High rainfall, high permeability and limited over-land flow contribute to fluxes of SGD between 14 and 82 cm/d (Kim *et al*., 2003). There are two different hydrologic regimes on Jeju; in the western portion of the island the highly permeable volcanic units are underlain by a low-permeability sedimentary unit causing artesian flow along the coast (Hahn *et al*., 1997) and the eastern side of the island is composed of a permeable volcanic unit overlain by an unconsolidated sand unit (Kim *et al.*, 2011). This sets up a dichotomy of groundwater discharging into the coastal waters (I will discuss similar dichotomies in Barbados and Guam). Western Jeju SGD is comprised of 18% freshwater while eastern Jeju SGD is dominated by recirculated seawater, comprised of only 2% freshwater (Kim *et al*., 2003). Despite the low freshwater component, Hwang *et al*. (2005) found SGD to be an important source of nutrients to Bangdu Bay on the eastern side of Jeju, which they suggest is responsible for benthic eutrophication as well as influencing phytoplankton community structure within the bay. Kim *et al.* (2011) found that SGD contributed over 90% of dissolved organic nitrogen in two bays, one in each of two hydrologic regimes.

Philippines

SGD studies in the Philippines underscore the importance of SGD in accounting for nutrient inputs to the coastal ocean and embayments. Taniguchi *et al.* (2008) looked at groundwater discharge into Manila Bay, a semi-enclosed embayment on the Philippine island of Luzon. Manual seepage meters, automatic seepage meters and geochemical tracers were used to evaluate SGD input, freshwater contribution, nutrient loading and then compare these values to previously documented contributions by stream flow and surface runoff. The Botan Peninsula, the location for the study, is a 11.2 km^2 peninsula on the western edge of Manila Bay. There are two pronounced seasons – wet (November-April) and dry (May-October) – and an average annual rainfall is 3,000 mm/y (Taniguchi *et al.*, 2008). The aquifers are primarily volcaniclastic sediments with a few confining clay layers of fine ash; the partially confined layers have low hydraulic conductivities; 2.2-5.1 m/d (Taniguchi *et al*., 2008). SGD flow rates during the dry season vary between 0 and 26 cm/d with an inverse correlation to the tidal elevation (Taniguchi *et al.*, 2008). Fluxes of SGD-contributed inorganic nitrogen are of the same magnitude as those discharged by the rivers draining into Manila Bay (Taniguchi *et al.*, 2008).

Senal *et al.* (2011) studied nutrient input *via* SGD on Santiago Island in the Philippines. Santiago Island is surrounded by a 32-km^2 limestone and carbonate sediment reef flat (Senal *et al.*, 2011). They found higher average SGD in the dry season (16 cm/d) than in the wet season (7 cm/d) with higher inorganic nitrogen flux in the wet season; 4.4 mmol $N/m^2/d$ during the wet season, 0.9 mmol $N/m^2/d$ during the dry season (Senal *et al.*, 2011). Despite lower average SGD flux in the wet season there is a higher freshwater component in discharged water.

Methods

I will report on SGD measurements on Barbados, Guam and Bimini islands. Common methods were used at all of these locations and will be described here.

Direct Measurement of SGD

Although various methods have been developed to measure SGD, the use of a vented benthic chamber, a.k.a. "seepage meter", has been widely employed and has the advantage of being inexpensive and requiring little technical training, although being labor intensive. As a result, it may be well suited to use in areas where financial resources are limited but workers are available. I will rely on this relatively simple but effective technique for characterizing SGD on oceanic islands.

This technique was originally designed to measure fluid flow through canal sediments in the 1940s, and was modified by Lee (1977) to be used for measuring SGD seepage in lake and coastal systems. The manual seepage meter is constructed using the top or bottom ~10-30 cm of a 55-gallon drum with a nozzle inserted in the end of the drum (Figure 1.1). The meter is installed open end down into the sediment so that only a few centimeters of the top of the meter is above the sediment surface (Figure 1.2). A bag is attached to the nozzle so that water vented through the nozzle can be collected and measured. The seepage rate can be calculated from the volume collected as:

$$v = \frac{V}{tA} \qquad [1.1]$$

where v is the volume flux, V is volume of water collected, t is the elapsed time, and A is the area of the seepage meter. The units of volume flux, $cm^3/cm^2/d$, reduce to that of SGD velocity, commonly cm/d.

Ideally, the SGD measured by the seepage meter would be a function of the hydraulic gradient and hydraulic conductivity in the sediment. However, there has been some discussion regarding other factors that may affect seepage meter measurements. There are two main categories for potential artifacts caused by the seepage meter itself, that is, anomalies induced by flow over the meter and those induced by characteristics of the collection bag.

The device itself creates topography over the sediment surface; it can perturb the ambient stream flow. Shinn *et al.* (2002) devised an experiment to quantify the artifacts due to the topography the meter creates within the flow. They installed meters into sand-filled child's play pools that were submerged into water, both in a controlled laboratory experiment with no ambient flow and in the environment (Florida Keys and Tampa Bay) where the meters were

subjected to flow conditions from tides and waves. Since the bottoms of the meters were effectively sealed off from any natural submarine groundwater discharge, the seepage that the meters would record would be solely due to an artifact of the meter. In the laboratory experiment with no ambient flow, the classic Lee-type seepage meter recorded 0.2 cm/d, and 1-3 cm/d in the environmental sites where there was ambient flow (Shinn *et al.*, 2002). These values are at or below the generally accepted lower limit of seepage meters to reliably measure flow in the field (Bokuniewicz, 2004, personal communication). Shinn *et al.* (2002) suggest that the flow they measured in the environment is due primarily to the Bernoulli Effect.

Bernoulli's principle is:

$$E = P + \frac{1}{2}\rho v + \rho g h \qquad [1.2]$$

where E is energy, P is pressure, ρ is the density of the fluid, v is the velocity, g is the acceleration due to gravity and h is the water depth. For energy to remain conservative, if the velocity is increased, there must be a resultant decrease in pressure. (Of course, this is the principle that governs the flight of airplanes and the motion of sailboats. The airfoil shape makes the air or fluid speed up over one side and the resulting decrease in pressure creates a lift force.) A seepage meter or any other surface topography, like ripples, will act like an airfoil in the presence of horizontal bottom flow. Huettel *et al.* (1996, 1998) demonstrated that small topographic features do create zones of upward flow in the sediments. Flume experiments show that there can be a seven-fold increase in fluid exchange in sandy sediments with small-scale surface topography (Huettel and Gust, 1992). While Shinn *et al.* (2002) documented flow artifacts from meters in areas with moderate tidal and wave affects, they did not quantify any of the ambient flow velocities. A study by Garrison *et al*. (2003) in Hawaii used a seepage meter isolated from groundwater discharge by a kiddie pool as a control during their field experiment and found no significant artificial flux as a result of wave action.

Recently the seepage meter has been redesigned and tested in Australia (Brodie *et al*., 2009) with the conclusion that, due to the Bernoulli Effect, seepage meters should not be used to quantify seepage flux in absolute terms, but can be useful in determining relative changes in flux and should be accompanied by other indirect means of measuring groundwater flux. It should be noted, however, that Brodie *et al*. (2009) constructed their seepage meters out of galvanized steel sheeting with a diameter comparable with 55-gallon drums, but with a height of roughly 75 cm (Brodie *et al*., 2009). One could reasonably expect that a seepage meter more than twice the height of the seepage meters constructed for this thesis would have a greater contribution *via* the Bernoulli Effect due to the greater relief off of the seafloor, though Brodie *et al.* (2009) do not provide data to evaluate an error. The Brodie *et al*. (2009) design also included a chamber to house the collection bag as well as a tube kept above the water level to allow for gas venting.

The gas-vent tube is susceptible to flooding and kinking (Brodie *et al*., 2009), which would introduce further artifacts in the measurement.

Another source of flow artifacts can be the hydraulic gradient within an empty bag. Corbett and Cable (2003), in response to the Shinn *et al.* (2002) article, suggest this as an additional factor in the observed flow that was unaccounted for. They cited an experiment done by Shaw and Prepas (1989) that demonstrated in laboratory and field tests an anomalous short-term flux attributed to a pressure differential between the collection bag and the surrounding water. In a tank filled with stagnant water, they measured a lower hydraulic potential in an empty collection bag than that of the water level in the tank. Water would flow into the bag until the pressure gradient was eliminated. Once the gradient was eliminated, flow into the bag would be proportional to the seepage rate, until the bag began to reach its capacity, at which time the flow would slow and eventually cease. Pre-filling the collection bag with 1000 mL was found to effectively eliminate the short-term influx of water. There will likely still be some short-term influx of water despite the initial volume of water within the bag as it will still need to equilibrate with the surrounding water, but pre-filling will reduce the impact on seepage measurements.

A study by Murdoch and Kelly (2003) combined a field and laboratory study with a theoretical analysis to study the effects of bag characteristics and ambient flow on the seepage meter performance. In order to evaluate these factors, they had to define relationships between all of the variables that contribute to the volume flux measured by seepage meters. Effective resistance (E_R) is a function of the hydraulic conductivity of the sediment (K), the radius of the device (R), and bag conductance (C) (Equation 1.3). Bag conductance is the ratio between volume flux and hydraulic head required to cause flow.

$$E_R = \frac{KR}{C} \qquad [1.3]$$

Murdoch and Kelly (2003) also defined two flux ratios one that combined both the velocity head[1] of the ambient water and the effective resistance of the bag (Q_R), and one that accounts for the effects of bag resistance alone (Q_{R1}):

$$Q_R = \frac{Q_s}{Q_o} = \frac{b + m - mh^*_{vel}}{(b+m)(1 - E_R m)} \qquad [1.4]$$

[1] Velocity head is due to the motion of the fluid (kinetic energy). Murdoch and Kelly (2003) used the equation $v^2/2g$ to determine the velocity head, where v is the velocity and g is the acceleration due to gravity.

$$Q_{R1} = \frac{1}{1 - E_R m} \qquad [1.5]$$

where b and m are empirical constants, h^*_{vel} is the velocity head of the water, Q_s is the flux from the sediment to the collection bag, and Q_o is the ambient flow rate where effective resistance is zero and the velocity head is zero. These theoretical relationships, when expressed graphically, show that a decrease in effective resistance leads to an increase in a higher flow ratio. In a situation where there is no ambient flow, the velocity head is zero and the velocity ratio for a particular effective resistance can be increased by increasing the meter dimensions (d* = d/R). For effective resistance less than 0.2, an increase in the meter dimensions can optimize the performance of the meters. At low effective resistance, the flow ratio approaches one, which indicates that the flux into the bag corresponds with the flux out of the sediments. For a fixed meter size where d* = 1, an increase in the velocity head also results in higher flow ratios; at velocity heads greater than zero, the theoretical analysis shows a "suction" artifact ($Q_R > 1$), which is likely due to the Bernoulli effect as described earlier.

Bag conductance, an important factor in the theoretical analysis by Murdoch and Kelly (2003), is affected by size, shape and the thickness of the collection bag. A thin membrane bag is expected to have a high conductance and thus a low effective resistance optimal for fieldwork (Murdoch and Kelly, 2003). However, thin membrane bags can be fragile and easy to puncture. Murdoch and Kelly (2003) investigated two different bag types in the field and in the laboratory; a thin membrane bag and a thicker more durable bag. The thin bag had a 25 µm thick membrane and a 3500 mL capacity, and in field and laboratory testing it showed a lower effective resistance. The more durable bag had a 150 µm thick membrane, a 3000 mL capacity and was prone to kinks and creases that increased the effective resistance of the bag. In field tests, Murdoch and Kelly (2003) report that thin bags were unable to resolve consistent patterns of groundwater flux where thicker, more durable bags were able to resolve consistent patterns. They recommend a rigid container to isolate the collection bag to reduce velocity-induced artifacts (Murdoch and Kelly, 2003). Such a chamber (an inverted bucket with small holes in it) had been used earlier to serve as a "stilling well" around the collection bag to isolate it from high-frequency fluctuations caused by waves (Bokuniewicz and Zeitlin, 1980).

To summarize, both seepage meter and bag characteristics may create flow artifacts in areas where there is substantial ambient stream flow. It is also possible to minimize error by minimizing the seepage meter relief off of the seafloor, pre-filling collection bags, and choosing a collection bag with low effective resistance. Fieldwork done with discretion, accounting for all sources of error in the methodology have demonstrated it is possible to produce reliable and consistent results. Seepage meters have been shown to resolve spatial patterns such as a decrease in flow with distance from shore (*e.g.* Bokuniewicz, 1980), as well as temporal patterns like those showing tidal influences (*e.g.* Paulsen *et al*., 2004; Taniguchi, 2002).

For this thesis, seepage meters were constructed from 55-gallon drums; the top and bottoms of the drum were cut down to have 20-35 cm sides. The tops of the 55-gallon drums include two threaded holes; the smaller of which was fitted with a nozzle, the larger was used as an air-escape during installation and was fitted with a stopper prior to SGD collection. Bottoms required drilling of one hole to attach a nozzle and another hole to allow air and water to escape quickly during placement. In the field, the meters were installed in sand as deeply as possible, typically with 5-10 cm of the side of the meter in the sand, leaving 10-15 cm of headspace within the drum (Figure 1.2). The meters were installed in each location for between five and eight hours. The devices were sampled hourly with more frequent samples taken for high flow areas where the flow in an hour exceeded the volume of the sample bags.

The SGD was vented from the meters and collected in 4L plastic bags (typically small kitchen garbage bags). The bags were not prefilled so that discharged water would not be diluted, allowing nutrient samples to be taken. For the interpretation of water quality of the samples, the residence time could be calculated using the height of the headspace and the SGD rate. With a headspace, h, that is the height of the top of the device above the seabed, and the SGD flow rate, the flushing time without mixing would be at least h/SGD.

I have found that expelling as much air from the collection bags as possible prior to attachment to the seepage meter vent minimizes anomalous flow due to the hydraulic gradient as does reusing bags, which retain trace amounts of water from the previous sample. A rigid container, as suggested by Murdoch and Kelly (2003), was tried but not used, as buckets proved difficult to attach securely enough so as not to introduce a pumping effect as the bucket rocked in the wave action while both keeping construction simple and retaining the integrity of the seepage meter.

Seepage meters were placed in one of three possible configurations: (a) randomly, (b) in shore perpendicular transects, or (c) in shore-parallel lines. In some places, placement was constrained to patches large enough with a thick enough sand layer to allow for installation and partly because each seepage meter was intended to be a random sample of flow. SGD has been shown to be variable due to the heterogeneity of porosity and permeability (Brock *et al*., 1982), particularly in karstic aquifers. Because of this, adjacent seepage meters may record substantially different rates of discharge. However, the average flow rate can be calculated arrays of randomly placed seepage meters, which can also give the frequency distribution of occurrences of seepage rates in the area. Three or four seepage meters were deployed on each sampling date in shore-parallel or shore-perpendicular transects to sample an array of flow patterns.

Freshwater Component

SGD includes not only freshwater seeping under the shoreline from the land, but also seawater circulated in the coastal aquifer (Burnett *et al*., 2006). While both components are important, the freshwater component is that which carries terrestrial pollutants to the sea and also is directly related to the potable water supply. If the salinity of the water collected is measured, the freshwater component of SGD can be calculated as:

$$f_{FW} = 100 * \left(1 - \frac{S_{SGD}}{S_{amb}}\right) \quad [1.6]$$

where f_{FW} is the fraction of fresh water expressed as a percentage, S_{SGD} is the salinity of the discharged water and S_{amb} is the salinity of the ambient surface water. For a reliable measurement, the seepage meter should be in place long enough for complete flushing.

Offshore Decrease of Discharge

Seepage meters are point measurements. In order to extrapolate available measurements over extended areas, it is necessary to characterize a distribution of SGD along the coast. SGD can occur either as a diffuse seepage, fairly uniform over large areas, or as small areas of concentrated flow, perhaps as submerged springs. Early modeling of groundwater discharge into a freshwater lake in an isotropic and homogeneous aquifer found that diffuse discharge decreased approximately exponentially offshore (McBride and Pfannkuch, 1975). Analytical calculations for the same situation subsequently showed that the decrease was not strictly exponential (Bokuniewicz, 1992), but given the inherent variability of natural systems, the exponential decrease has proven useful. An (approximately) exponential decrease is not always expected or detected, but when it is evident, the decrease can be described as:

$$y = Ae^{-Cx} \quad [1.7]$$

Integrating the area under this curve provides a total value of SGD flow per meter of shoreline. The integral for this type of equation provides an integrated SGD value of:

$$\int_0^\infty y\,dx = {}^{A}/_{C} \quad [1.8]$$

which has units of cubic meters per day per meter of shoreline.

To the extent that measured SGD decreases regularly offshore, fitting an exponential decrease provides an expedient for calculating the total discharge per meter of shoreline without having to assume a limited extent of the seepage face, although 100 m is usually assumed (Burnett *et al*., 2006). Departure (outliers) around this exponential decrease might be considered as an isolated area of enhanced seepage or as a submerged spring.

Conclusion

In the chapters to follow, I will use results of manual seepage meters, salinity measurements to calculate freshwater components and the exponential decrease to calculate total SGD per meter of shoreline. I will provide a strategy that managers might use to determine relevant characteristics of SGD at the shore of an oceanic island. This strategy will include some new and innovative procedures for treating temporal, tidal variations of SGD and the influence of seiching on measurement of SGD. I will present three applications of this strategy to characterize SGD on Barbados, Guam and Bimini. I will then proffer a suggestion about how SGD might be integrated into some broader considerations of water management.

References

Basterretxea, G., A. Tovar-Sanchez, A.J. Beck, P. Masqué, H.J. Bokuniewicz, R. Coffey, C.M. Duarte, J. Garcia-Orellana, E. Garcia-Solsona, L. Martinez-Ribes, R. Vaquer-Sunyer. 2010. Submarine Groundwater Discharge to the Coastal Environment of a Mediterranean Island (Majorca, Spain): Ecosystem and Biogeochemical Significance. Ecosystems. 13(5) pp. 629-643.

Bokuniewicz, H.J. 1980. Groundwater Seepage into Great South Bay, New York. Estuarine and Coastal Marine Science 10 pp. 437-444.

Bokuniewicz, H.J. 1992. Analytical Descriptions of Subaqueous Groundwater Seepage. Estuaries15:458-462

Bokuniewicz, H.J. 2004. Personal Communication. Stony Brook University.

Bokuniewicz, H., J. Rapaglia and A. Beck. 2007. Submarine groundwater discharge (SGD) from a volcanic island: A case study in Mauritius Island. International Journal of Oceans and Oceanography, submitted.

Bokuniewicz, H.J. and M.J. Zeitlin. 1980. Characteristics of Ground-Water Seepage into Great South Bay. Marine Sciences Research Center. Special Report 35. pg. 30.

Brock, T.D., D.R. Lee, D. Janes and D. Winek. 1982. Groundwater seepage as a nutrient source to a drainage lake; Lake Mendota, Wisconsin. Water Research. 16: 1255-1263.

Brodie, R.S., S. Baskaran, T. Ransley and J. Spring. 2009. Seepage meter: progressing a simple method of directly measuring water flow between surface water and groundwater systems. Australian Journal of Earth Sciences. 56(1): 3-11.

Burnett, W.C., P.K. Aggarwal, A. Aureli, H. Bokuniewicz, J.E. Cable, M.A. Charette, E. Kontar, S. Krupa, K.M. Kulkarni, A. Loveless, W.S. Moore, J.A. Oberdorfer, J. Oliveira, N. Ozyurt, P. Povinec, A.M.G. Privitera, R. Rajar, R.T. Ramessur, J. Scholten, T. Stieglitz, M. Taniguchi, J.V. Turner. 2006. Quantifying submarine groundwater discharge in the coastal zone *via* multiple methods. Science of the Total Environment. 367(2-3): 498-543.

Capone, D.G. and M.F. Bautista. 1985. A groundwater source of nitrate in nearshore marine sediments. Nature. 313: 214-216.

Corbett, D.R. and J.E. Cable. 2003. Seepage Meters and Advective Transport in Coastal Environments: Comments on "Seepage Meters and Bernoulli's Revenge" by EA Shinn, CD Reich and TD Hickey. 2002. Estuaries. 25: 126-132.

Falkland, A. 1991. Hydrology and water resources of small islands: a practical guide. United Nations Educational, Scientific and Cultural Organization, Paris. 435 pp.

Garrison, G.H., C.R. Glenn and G.M. McMurtry. 2003. Measurement of Submarine Groundwater Discharge in Kahana Bay, O'ahu, Hawai'i. Limnology and Oceanography. 48(2): 920-928.

Hahn, J., Y. Lee, N. Kim, C. Hahn and S. Lee. 1997. The groundwater resources and sustainable yield of Cheju volcanic island, Korea. Environmental Geology. 33(1): 43-53.

Huettel, M., G. Gust. 1992. Impact of bioroughness on interfacial solute exchange in permeable sediments. Mar. Ecol. Prog. Series. 89: 253-267.

Huettel, M., W. Ziebis and S. Forster. 1996. Flow-induced uptake of particulate matter in permeable sediments. Limnology and Oceanography. 41(2): 309-322.

Huettel, M., W. Ziebis, S. Forster and G.W. Luther III. 1998. Advective transport affecting metal and nutrient distributions and interfacial fluxes in permeable sediments. Geochim.

Cosmochim. Acta. 62(4): 613-631.
Hwang, D.-W., Y.-W. Lee and G. Kim. 2005. Large submarine groundwater discharge and benthic eutrophication in Bangdu Bay on volcanic Jeju Island, Korea. Limnology and Oceanography. 50(5): 1393-1403.
Kim, G., K.-K. Lee, K.S. Park, D.-W. Hwang and H.-S. Yang. 2003. Large submarine groundwater discharge (SGD) from a volcanic island. Geophysical Research Letters. 30(21): 2098.
Kim, G., J.-S. Kim and D.-W. Hwang. 2011. Submarine groundwater discharge from oceanic islands standing in oligotrophic oceans: implications for global biological production and organic carbon fluxes. Limnology and Oceanography. 56(2): 673-682.
Knee, K.L., B.A. Layton, J.H. Street, A.B. Boehm, A. Paytan. 2008. Sources of Nutrients and Fecal Indicator Bacteria to Nearshore Waters on the North Shore of Kaua'i (Hawai'i, USA). Estuaries and Coasts 31: 607-622.
Lee, D.R. 1977. A device for measuring seepage flux in lakes and estuaries. Limnology and Oceanography. 22(1): 140-147.
Lee, J.-M. and G. Kim. 2007. Estimating submarine discharge of fresh groundwater from a volcanic island using a freshwater budget of the coastal water column. Geophysical Research Letters. 34: L11611.
Lewis, J.B. 1987. Measurements of groundwater seepage flux onto a coral-reef – spatial and temporal variations. Limnology and Oceanography. 32(5): 1165-1169.
Lutz, W. (Ed.) 1994. Population-Development-Environment: Understanding their Interactions in Mauritius. Springer-Verlag, Berlin, Germany. 400 pp.
Lutz, W., L. Prieto and W. Sanderson. 2000. Population, Development and Environment on the Yucatan Peninsula: from Ancient Maya to 2030. International Institute for Applied Systems Analysis, Laxenburg, Austria. 257 pp.
McBride, M.S., and H.O. Pfannkuch. 1975. The distribution of seepage within lake beds. Journal of Research of the United States Geological Survey. 3: 505-512.
Moore, W.S. 1999. The subterranean estuary: a reaction zone of ground water and sea water. Marine Chemistry 65(1-2): 111-125.
Murdoch, L.C. and S.E. Kelly. 2003. Factors affecting the performance of conventional seepage meters. Water Resour. R. 39(6): 1163, doi:10.1029/2002WR001347.
Nymphea Middle East. 2013. Company Profile. http://www.oceanologyinternational.com/__novadocuments/43497?v=635242597726870000 Last accessed: 28 January 2014.
Paulsen, R.J., D. O'Rourke, C.F. Smith and T.F. Wong. 2004. Tidal load and salt water influences on submarine groundwater discharge. Ground Water. 42(7): 990-999.
Peterson, R.N., W.C. Burnett, C.R. Glenn and A.G. Johnson. 2009. Quantification of point-source groundwater discharges to the ocean from the shoreline of the Big Island, Hawaii. Limnology and Oceanography 54(3) p 890-904.
Povinec P.P, W.C. Burnett, A. Beck, H. Bokuniewicz, M. Charette, M.E. Gonneea, M. Groening, T. Ishitobi, E. Kontar, L. Lion Wee Kwong, D.E.P. Marie, W.S. Moore, J.A. Oberdorfer, R. Peterson, R. Ramessur, J. Rapaglia, T. Stieglitz, Z. Top. 2012. Isotopic, geophysical and biogeochemical investigation of submarine groundwater discharge: IAEA-UNESCO intercomparison exercise at Mauritius Island. Journal of Environmental Radioactivity. 104(2012): 24-45.
Rodellas, V., J. Garcia-Orellana, A. Tovar-Sánchez, G. Basterretxea, J. M. López-Garcia, D.

Sánchez-Quiles, E. Garcia-Solsona, P. Masqué. 2014. Submarine groundwater discharge as a source of nutrients and trace metals in a Mediterranean bay (Palma Beach, Balaeric Islands). Marine Chemistry. 160(2014): 56-66.

Senal, M.I.S., G.S. Jacinto, M.L. SanDiego-McGlone, F. Siringan, P. Zamora, L. Soria, M. B. Cardenas, C. Villanoy and O. Cabrera. 2011. Nutrient inputs from submarine groundwater discharge on the Santiago reef flat, Bolinao, Northwestern Philippines. Marine Pollution Bulletin. 63(2011):195-200.

Shaw, R.D. and E.E. Prepas. 1989. Anomalous, short-term influx of water into seepage meters. Limnology and Oceanography. 34(7): 1343-1351.

Shinn, E.A., C.D. Reich and T.D. Hickey. 2002. Seepage Meters and Bernoulli's Revenge. Estuaries. 25: 126-132.

Taniguchi, M., W.C. Burnett, J.E. Cable and J.V. Turner. 2002. Investigation of submarine groundwater discharge. Hydrolical Processes. 16: 2115-2129.

Taniguchi, M., W.C. Burnett, H. Hulaiova, F. Siringan, J. Foronda, G. Wattayakorn, S. Rungsupa, E.A. Kontar and T. Ishitobi. 2008. Groundwater Discharge as an Important Land-Sea Pathway into Manila Bay, Philippines. Journal of Coastal Research. 24(sp1):15-24.

United Nations Department of Economic and Social Affairs, Division for Sustainable Development. 2014. SIDS Members. URL: http://sustainabledevelopment.un.org/index.php?menu=1520 Last accessed: 10 September 2014.

Zektser, I.S. 2000. Groundwater and the Environment: Applications for the Global Community. Lewis Publishers, Boca Raton: 175 pp.

Figures

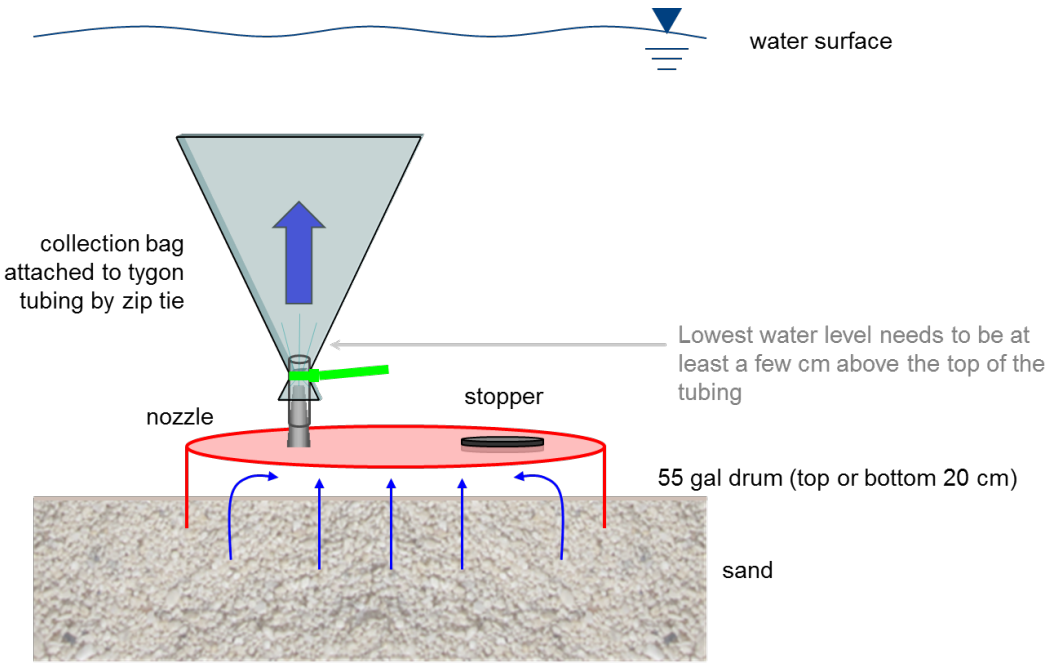

Figure 1.1. Schematic of Lee-type seepage meter (after Lee, 1977)

Figure 1.2. Photograph of seepage meter in-situ. Credit Ruth Coffey.

Tables

Table 1-1. Classifications of model parameters.

Geographic Parameters	Land Area
	Shoreline Length
	Volume of Aquifer
	Estimated Aquifer Thickness
	Porosity
	Specific Yield
	Volume of Water in Aquifer
	Cultivated land
Field Parameters	Dry Season SGD_m
	Wet Season SGD_m
	Dry Season Shoreline Flux
	Wet Season Shoreline Flux
Climate Parameters	Dry Season Precipitation
	Wet Season Precipitation
	Duration of Dry Season
	Recharge to Aquifer
Population Parameters	Tourists for Dry Season (initial)
	Tourists for Wet Season (initial)
	Available Beds (initial)
	Available Beds (limit)
	Tourists Supported by Dry Season Water (limit)
	Tourists Supported by Wet Season Water (limit)
	Tourist arrivals (minimum)
Nutrient Parameters	Nitrogen Contributed *per Capita*
	Fertilizer application
	Fertilizer Leaching to Groundwater
	Aquifer "Cleaning" Capacity
Economic Parameters	Tourist Expenditure
	Contribution to GDP
	Sewage Treatment Plant Construction Cost
	Sewage Treatment Plant Maintenance Cost
	Sewage Nitrogen Removal
	Sewage Treatment Plant Capacity

Chapter 2 Tidal Modulation

Introduction

Submarine groundwater discharge (SGD) rates are determined by the inland hydraulic gradient between the sea surface and the water table or confining unit hydraulic head. This gradient can vary on a wide spectrum of time scales. Seasonal influences (months) have been documented by many researchers (*e.g.* Michael *et al*., 2005) and tidal influences (diurnal, semi-diurnal) are common (*e.g.* Taniguchi, 2002). Shorter-term (<30 min) seiche effects have been observed (Basterretxea *et al*., 2011) and are explored further in Chapter 3 of this thesis.

The tide is a major modulating force of groundwater discharge, but there is, inherent in the system, a lag between the two signals. This time lag has been well documented, for example, on Shelter Island, New York (Paulsen *et al*., 2004), on Oahu, Hawaii (Garrison *et al*., 2003) and can also be seen in data from Osaka Bay, Japan (Taniguchi, 2002). As a result of this lag, a plot of groundwater discharge against water levels will often yield a hysteresis loop rather than a simple linear relationship. The ellipse that describes this loop has some useful properties that can be used to describe groundwater discharge, which I will explore here for the sake of finding the most efficient use of resources to determine the average SGD in light of tidal variations.

The intersection of two sinusoidal curves, like the tide and a tidally modulated SGD, the axes of which are at right angles to each other, generates an ellipse known as a Lissajous Curve or a Bowditch Curve (Figure 2.1). The eccentricity of an ellipse is the degree to which the ellipse is elongated. Ellipses have two axes – the semimajor and semiminor axes – which are perpendicular to each other and which are, respectively, the longest and shortest distances that can be drawn from two symmetric points around the ellipse. Eccentricity is related to the lengths of the semiaxes by the equation:

$$e = \sqrt{1 - \frac{b^2}{a^2}} \qquad [2.1]$$

where *a* is the semimajor axis and *b* is the semiminor axis (Weisstein, 2014a). Eccentricity can range from 0 to (but not equal to) 1; a circle has an eccentricity of 0 (Weisstein, 2014a; Weisstein 2014b).

The important properties of an ellipse for this study are the Cartesian coordinates for the intersection between the semiaxes and the range along the y-axis. In the case of SGD modulated by the tide, the ellipse is generated from the time-series of each as a Lissajous/Bowditch Curve with the additional properties of the direction of progression (clockwise/counterclockwise) of data points along the ellipse. The Cartesian location of the center of the ellipse (i.e. the intersection of the major and minor axes) is expected to provide the average groundwater discharge and average tidal height, or mean sea level. This should be true as long as (a) SGD is directly proportional to the hydraulic gradient, as it should be with hydraulic conductivity as the constant of proportionality, and (b) the hydraulic gradient is inversely proportional to the tidal elevation.

Calculating the average SGD in this manner is a more robust method than a strict average of collected data points, as it will give a more accurate value when the data covers only a portion of the tidal cycle. In principle, only five points would be needed to determine the ellipse; *e.g.* two coordinates to specify the center, one each to specify the lengths of the semi-major and semi-minor axes and one to specify the angle of rotation. Only four points are necessary if the mean water level is known, that is, if the x_0 coordinate of the center is known. As described above, the expectation is that the ellipse will expand or contract depending on the tidal modulation but remain centered on the average conditions, that is, determining the average SGD in light of all tidal variation. Manual seepage meters are labor-intensive. Where applicable, this method may be used to determine average flow conditions with minimal effort.

Methods

Sinusoids were first used to set standards for the interpretation of the appropriate ellipse-fit method. Two sine curves were plotted against each other. Tests varied the offset between them (lag/lead) and the amplitude difference to determine their relationship to ellipse parameters. Field data from Guam and Bimini (presented in Chapters 4 and 5 of this thesis) as well as from Shelter Island, New York (Paulsen *et al.*, 2004) were then analyzed with the method for a proof of concept. All data were analyzed using Matlab (ver. R2012a).

A search of the Matlab community resources will result in many m-scripts that purport to describe an ellipse given a set of points. However, tests with sine curves where I knew what answers to expect showed many of these to be inconsistent in their results. The best of these m-scripts was written by Fitzgibbon *et al.* (1999), and when this script was used with field data, all but a few sites produced results that appeared to fit the data well, so it was chosen as the m-script

for the SGD ellipse fit method. Fitzgibbon *et al.* (1999) designed a least-squares fitting method that fit an ellipse to data and dealt reasonably with noise within the data. Other m-scripts tried did not always yield ellipse parameters with short datasets that appeared parabolic, and with the test sine curves, other m-scripts could not resolve consistent ellipse orientations for the test scenarios.

Results

Sinusoid Tests

Sinusoid tests plotted the time series of water level on the x-axis and SGD on the y-axis and tested the effects of changing the phase shift or amplitude (Figure 2.2 and Figure 2.3, respectively). In the sinusoid tests, evaluations varying the phase shift of the SGD signal showed that data points progressed in a clockwise pattern when SGD lagged behind the tide. When the data points plotted in a counterclockwise pattern, SGD lead the tide. Phase shift is also linked to the eccentricity of the ellipse. Increasing phase shift (up to a phase shift of three hours) leads to decreasing eccentricity (Figure 2.2 and Figure 2.4). The axial tilt is due to amplitude differences between SGD and tide signals (Figure 2.3 and Figure 2.5). Because this is dependent on the ratio of the magnitudes along the two axes, that is as the SGD range over the range in water level, the angle of tilt must be calibrated to each situation in order to interpret its significance.

Field Data Reanalysis

The field data from Shelter Island, NY (Paulsen *et al.*, 2004) consisted of a time series of SGD and tide measurements taken approximately every half hour for eight consecutive full tidal cycles (Figure 2.6). With this data set, I can demonstrate the utility of the ellipse fit method as well as estimate the resolution limits of the data collected over a portion of the tidal cycle.

A visual inspection shows that the ellipses fit well with the data points (Figure 2.7). Ellipses for each individual tidal cycle are similar to the ellipse for the full dataset, and while they do not precisely overlap (Figure 2.8), SGD averages for individual ellipses are within 16% of the SGD average for the full dataset (Table 2-1). In this test case, the average SGD, that is the vertical coordinate of the center of the ellipse, varies by 16% from tidal cycle to tidal cycle; thus it only approximates the long-term average to ±8%. It is unlikely that the hydraulic conductivity is changing, so the variation would mean that the effective hydraulic gradient is not solely linearly dependent on the tidal elevation. As I will discuss below, given the non-linearity of the coastal hydraulic water table elevation and the tidally driven changes in the water table near shore, this is perhaps not surprising. An average of each of the individual cycle average SGD values provides a closer value to the average SGD for the full dataset. With this technique, the

eccentricity of the full data set was 0.97, which corresponds to a time lag of 1 hour. The eccentricity of the individual tidal cycle ellipses ranged from 0.94 to 0.99 corresponding to a time lags ranging between 0.4 and 1.3 hours.

One of the primary difficulties with using manual seepage meters to evaluate SGD is the time-intensive nature of the sampling. To that end, I have evaluated the accuracy of the ellipse fit for different subsampling regimes. Five points selected at 1-hour intervals around either low or high tide show poor ellipse accuracy, while 2-hour interval sampling as well as 0.5-hour sampling for only half a tidal cycle fit the full cycle ellipse fairly well (Figure 2.9; Table 2-2).

Discussion

I would expect that the characteristics of the ellipse would depend on the following characteristics of the coastal aquifer. The range of SGD should be determined by the magnitude of the terrestrial hydraulic gradient. The water-table gradient at the shoreline is the primary driver for the underflow (Q_N), although leakage from deep, confined aquifers may also contribute to the underflow (Burnett *et al*., 2006). Modeling exercises have shown that non-tidal SGD seemed to be linearly related to groundwater underflow, SGD is related to the underflow modified by the tidal range (Figure 2.10; Destouni and Prieto, 2003; Prieto and Destouni, 2005). Notably, non-tidal SGD exists even if Q_N is zero, presumably due to the circulation of seawater, probably driven by density gradients in the pore water, probably driven by density gradients in the pore water.

Total SGD is elevated further in the presence of the tides (Prieto and Destouni, 2005). In tidal environments, coastal hydraulic gradients, driving SGD, are elevated by tidal pumping (Nielsen, 1990) and SGD is often modulated by changes in the water level over the tidal cycle (Smith *et al.*, 2009; Taniguchi, 2002; Michael *et al.*, 2003). The basic hydraulic gradient at a shoreline as elevated by tidal pumping (Nielsen, 1990) depends upon the beach slope, the tidal range and the hydraulic conductivity among other parameters. Because the effective distance over which the gradient drives SGD cannot be determined a priori, the absolute values for SGD cannot be known, but the vertical extent of the ellipse should be expected to increase with increases with increases in the hydraulic conductivity, beach slope and tidal range. Both the beach slope (Sunamura, 1984) and the hydraulic conductivity (Salarashayeri and Siosemarde, 2012) have been correlated to the grain size (D) of the sediment. Taking such empirical relationships into account, we might expect SGD to be directly dependent on the square of the tidal range, and approximately inversely proportional to the grain size, or $D^{0.75}$.

Modeling of tidally-induced circulation of seawater showed an elevated circulation during intertidal flow, increasing the exchange between groundwater underflow, SGD, by three orders of magnitude (Xin *et al.*, 2010; Rocha, 2000). When the underflow is low, SGD is most sensitive to the tidal range (Rocha *et al.*, 2000).

This time lag is expected to depend on the propagation of tidal changes in the hydraulic gradient of the coastal water-table. Emery and Foster (1948) monitored water-table changes in response to the tide along the California coast. The water-table position lagged one to three hours behind the tide with an increasing lag time farther inshore. The lag time of the water-table response to the tides depended on the hydraulic conductivity of the coastal aquifer. Changes in the elevation of the water-table in a highly permeable beach were similar to the tide; amplitude gradually decreases landward. Small time lags between the tide and SGD would be expected. Conversely, the water-table elevation changes in a low-permeability beach decrease sharply landward and would be anticipated to cause large time lags. The time-varying elevation of the water table at any point will not be symmetric but rather will change more rapidly near the maximum elevations and more slowing during minimum elevations. The degree of asymmetry will decrease with the decreasing amplitude so that it will be greatest near the shore and least farther inland. The maximum water-table elevation will propagate landward in the beach at a rate dependent on the square root of the hydraulic conductivity and the tidal frequency (Metcalf *et al*., 1995). I might expect the time lag indicated by the ellipse to show the same dependence.

Conclusion

Presumably, as the tide changes, say through a spring-neap cycle, the ellipse would expand and contract, but one may assume that the center, that is the average SGD, would remain the same. The eccentricity of the ellipse can indicate the degree of lag between the initial tidal signal and the response of the groundwater. I have shown that the labor intensive nature of SGD field work can be minimized by either sampling frequently for half a tidal cycle, making sure to capture either low or high tide, or sampling infrequently (2-hour intervals) over a full tidal cycle.

While this method of reanalysis of field data shows promise, there is still work that needs to be done to address accuracy issues. Another avenue of expansion of this method is to standardize the tide by the rate of change in water level rather than the water level itself. This way both axes would be in the same units, which would provide a more direct way to compare ellipses from different field locations and tease out the differences in SGD regimes. The coarse time resolution of the manual seepage meters precluded this refinement in my study.

Example m-script

```
%% Shelter Island Hour Sample 1HT Even Distribution

  clear all
  close all
  clc

  %Read in field data
    %Tide in cm (u)
    %SGD in cm/d (v)
    u = xlsread('Shelter_Island_data.xlsx','1hoursamples','C5:C9');
    v = xlsread('Shelter_Island_data.xlsx','1hoursamples','D5:D9');
    %Title for sample
    L = {'SI Tide Hour Sample 1HT Even'};

  %Ellipse fit m-script from Fitzgibbon et al. 1999
    fitellipse(u,v);

  %Write results to Excel Worksheet
    xlswrite('Shelter_Island_data.xlsx',L,'1HourEllipse','A3')
    xlswrite('Shelter_Island_data.xlsx',ans,'1HourEllipse','B3:F3')
    xlswrite('Shelter_ISland_data.xlsx',tf,'1HourEllipse','G3')

  %Plot the ellipse on the same figure as the data
    %Center of Ellipse
    x0 = xlsread('Shelter_Island_data.xlsx','1HourEllipse','B3');
    y0 = xlsread('Shelter_Island_data.xlsx','1HourEllipse','C3');

    %Major and Minor radius
    a = xlsread('Shelter_Island_data.xlsx','1HourEllipse','D3');
    b = xlsread('Shelter_Island_data.xlsx','1HourEllipse','E3');

    %Orientation (radians)
    phi = xlsread('Shelter_Island_data.xlsx','1HourEllipse','F3');

    %Smoothness (# of points)
    num = 100;

    theta = linspace(0,2*pi,num);
    p(1,:) = a*cos(theta);
    p(2,:) = b*sin(theta);

    Q = [cos(phi) -sin(phi)
       sin(phi) cos(phi)];
    p = Q*p;

    p(1,:) = p(1,:) + x0;
    p(2,:) = p(2,:) + y0;

    figure(1), hold on
    filename = 'SI Tide Hour Sample 1HT Even';
    plot(p(1,:),p(2,:),'LineWidth',0.5)
    plot(x0, y0, 'r+')
```

```
plot(u,v,'b.')
axis equal;
axis([0 200 0 200]);
title(filename);
xlabel('Water Level (cm)');
ylabel('SGD (cm/d)');
print(figure(1),'-dpng',filename);
```

References

Basterretxea, G., A. Jordi, E. Garces, S. Angles, A. Rene. 2011. Seiches stimulate transient biogeochemical changes in a microtidal coastal ecosystem. Marine Ecology Progress Series: V423: 15-28.

Burnett, W.C., P.K. Aggarwal, A. Aureli, H. Bokuniewicz, J.E. Cable, M.A. Charette, E. Kontar, S. Krupa, K.M. Kulkarni, A. Loveless, W.S. Moore, J.A. Oberdorfer, J. Oliveira, N. Ozyurt, P. Povinec, A.M.G. Privitera, R. Rajar, R.T. Ramessur, J. Scholten, T. Stieglitz, M. Taniguchi, J.V. Turner. 2006. Quantifying submarine groundwater discharge in the coastal zone *via* multiple methods. Science of the Total Environment. 367(2-3): 498-543.

Destouni, G. and C. Prieto. 2003. On the possibility for generic modelling of submarine groundwater discharge. Biogeochemistry. 66: 171-186.

Emery, K.O. and J.P. Foster. 1948. Water Tables in Marine Beaches: Journal of Marine Research. 7(3): 644-654.

Fitzgibbon, A.W., M. Pilu and R.B. Fisher. 1999. Direct Least Squares Fitting of Ellipses. IEEE Transactions on Pattern Analysis and Machine Intelligence. 21(5): 476-480.

Garrison, G.H., C.R. Glenn and G.M. McMurtry. 2003. Measurement of Submarine Groundwater Discharge in Kahana Bay, O'ahu, Hawai'i. Limnology and Oceanography. 48(2): 920-928.

Metcalf, W., H. Bokuniewicz and A. Terchunain. 1995. Water-table variations on a reflective ocean beach: Quoque Beach, New York. Northeastern Geology. 17(1): 61-67.

Michael, H.A., J.S. Lubetsky and C.F. Harvey. 2003. Characterizing submarine groundwater discharge: A seepage meter study in Waquoit Bay, Massachusetts. Geophysical Research Letters. 30: 1297.

Michael, H.A., A.E. Mulligan and C.F. Harvey. 2005. Seasonal oscillations in water exchange between aquifers and the coastal ocean. Nature. 436(25): 1145-1148.

Nielsen, P. 1990. Tidal Dynamics of the Water Table in Beaches. Water Resources Research. 26: 2127-2134.

Paulsen, R.J., D. O'Rourke, C.F. Smith and T.F. Wong. 2004. Tidal load and salt water influences on submarine groundwater discharge. Ground Water. 42(7): 990-999.

Prieto, C. and G. Destouni. 2005. Quantifying hydrological and tidal influences on groundwater discharges into coastal waters. Water Resources Research. 41: W12427.

Rocha, C. 2000. Density-driven convection during flooding of warm, permeable intertidal sediments: the ecological importance of the convective turnover pump. Journal of Sea Research. 43: 1-14.

Salarashayeri A.F. and M. Siosemarde 2012. Prediction of Soil Hydraulic Conductivity from Particle-Size Distribution. World Academy of Science, Engineering and Technology 6: 395-399.

Smith, A.J., D.E. Herne and J.V. Turner. 2009. Wave effects on submarine groundwater seepage measurement. Advances in Water Resources. 32: 820-833.

Sunamura, T. 1984. Quantitative predictions of beach-face slope. Geological Society of America Bulletin 95: 242-245.

Taniguchi, M. 2002. Tidal effects on submarine groundwater discharge into the ocean. Geophysical Research Letters. 29(12): 1561.

Weisstein, Eric W. 2014a "Eccentricity." From MathWorld--A Wolfram Web Resource. http://mathworld.wolfram.com/Eccentricity.html Last accessed: 3 February 2014.

Weisstein, Eric W. 2014b "Conic Section." From MathWorld--A Wolfram Web Resource. http://mathworld.wolfram.com/ConicSection.html Last accessed: 3 February 2014.
Xin, P., C. Robinson, L. Li, D.A. Barry and R. Bakhtyar. 2010. Effects of wave forcing on a subterranean estuary. Water Resources Research. 46.

Figures

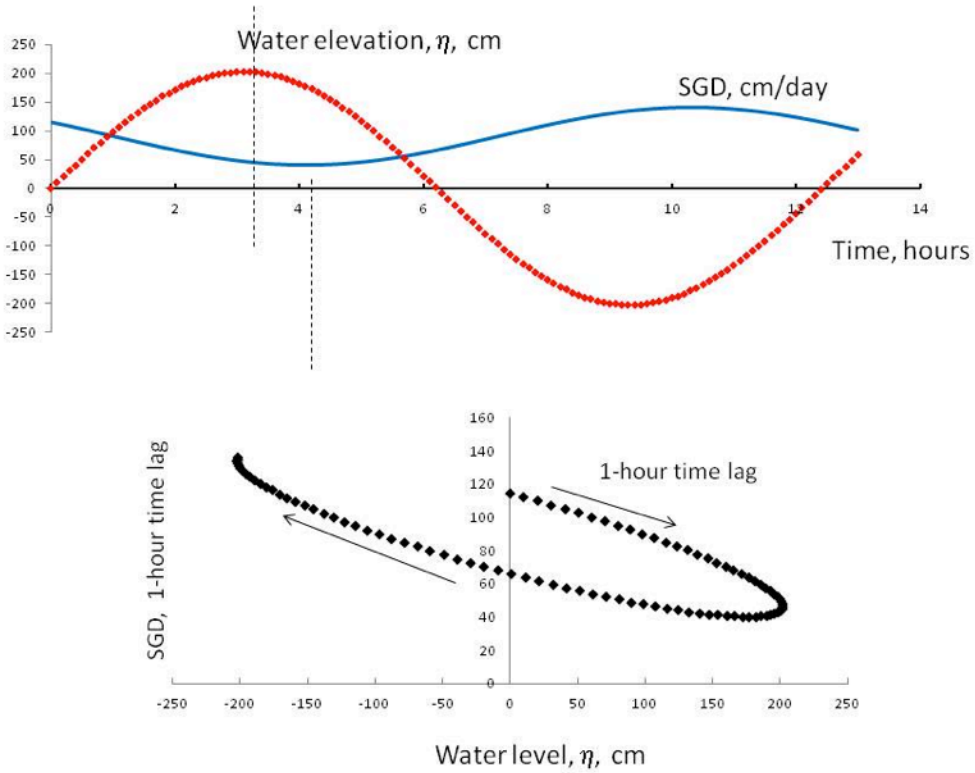

Figure 2.1. Lissajous or Bowditch Curve. Top graph shows a time series with plots of water elevation (red dashed line) and SGD (blue solid line). The bottom graph shows the same data plotted with water level on the x-axis and SGD plotted on the y-axis. The resulting curve is a Lissajous or Bowditch Curve.

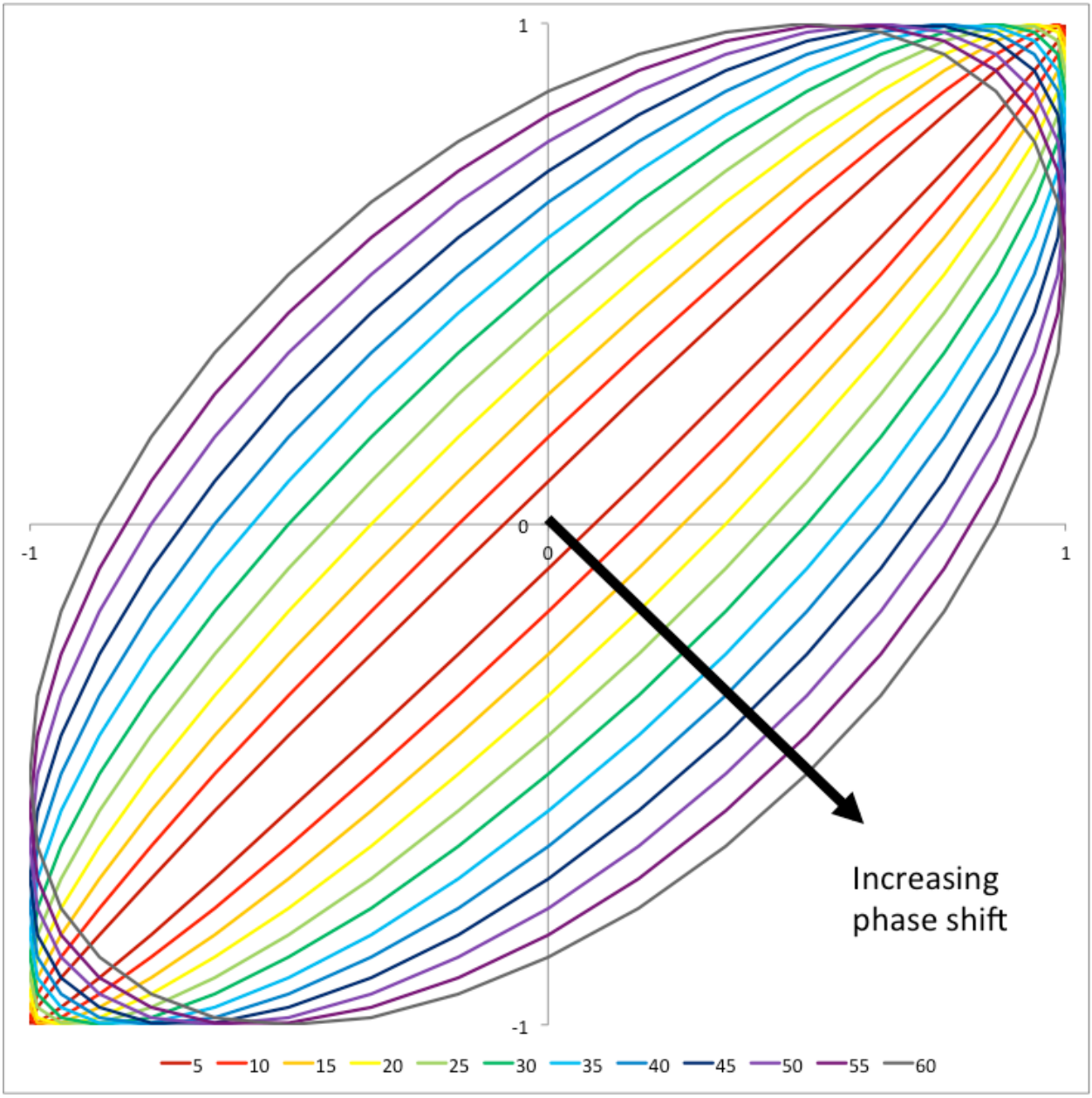

Figure 2.2. Phase Shift. Ellipses of increasing lagging phase shift (water level in m on the x-axis; SGD in m/d on the y-axis). Looking at the width of the ellipse at the semiminor axis, the smallest phase shift gives the narrowest ellipse and the largest phase shift gives the widest ellipse. Phase shift is in degrees offset. For a semidiurnal (tidal) period, one degree equals (12.42/360) hours.

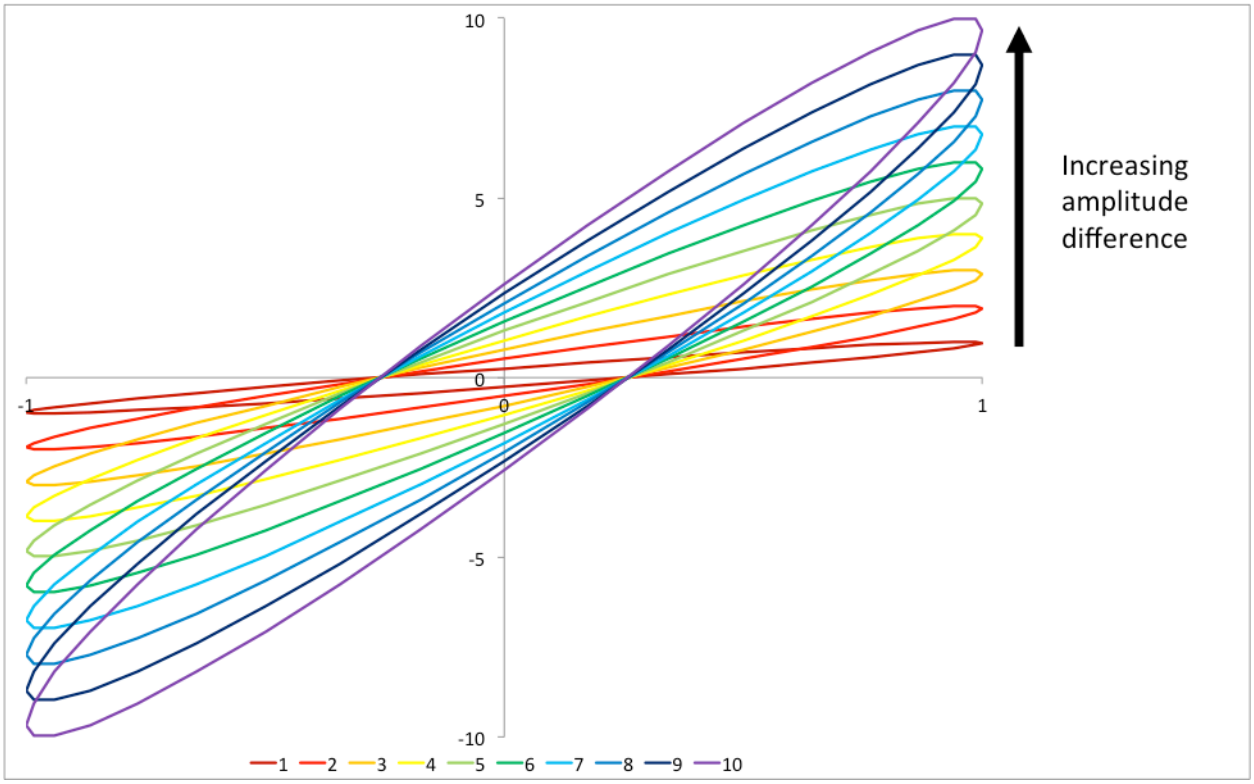

Figure 2.3. Amplitude. Ellipses of increasing amplitude difference (water level in cm on the x-axis; SGD in cm/d on the y-axis.

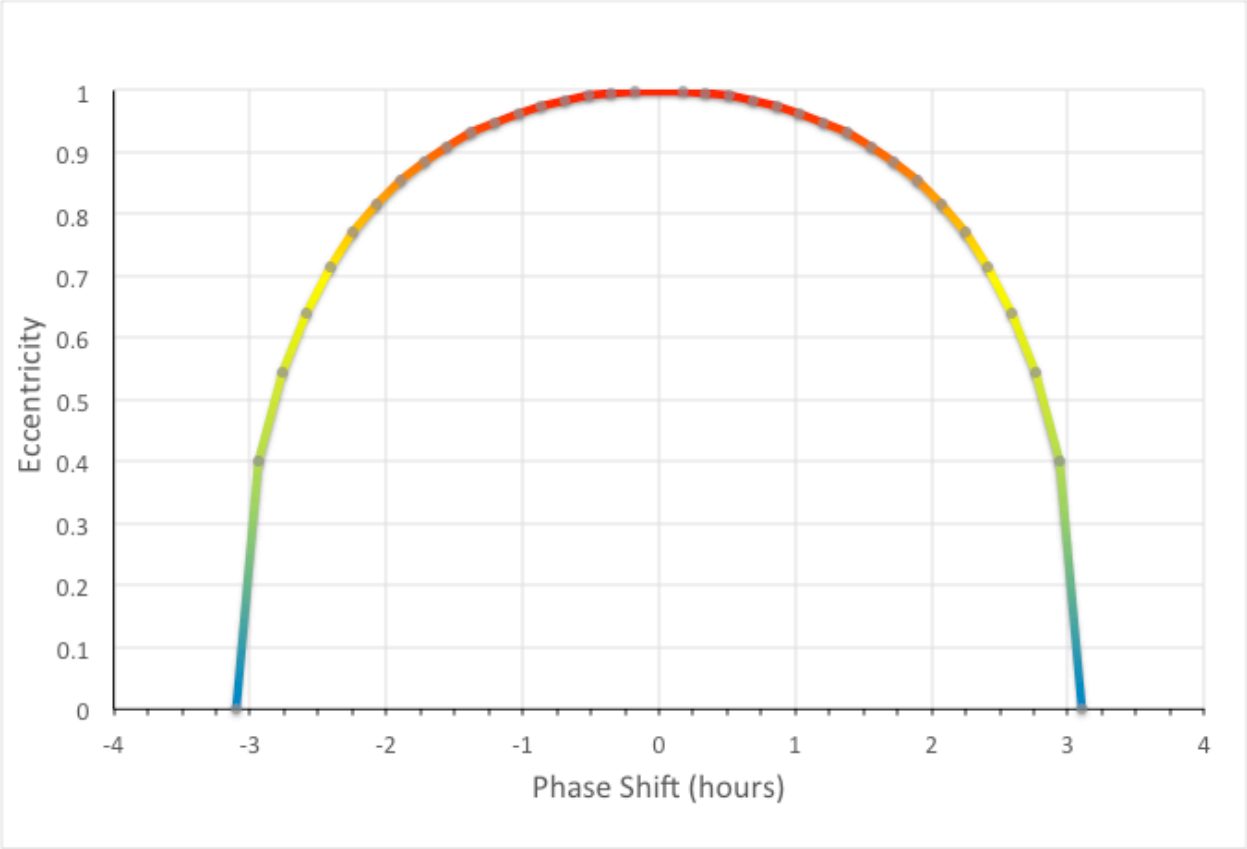

Figure 2.4. Phase shift and eccentricity. Phase shift (hours) on the x-axis, eccentricity on the y-axis.

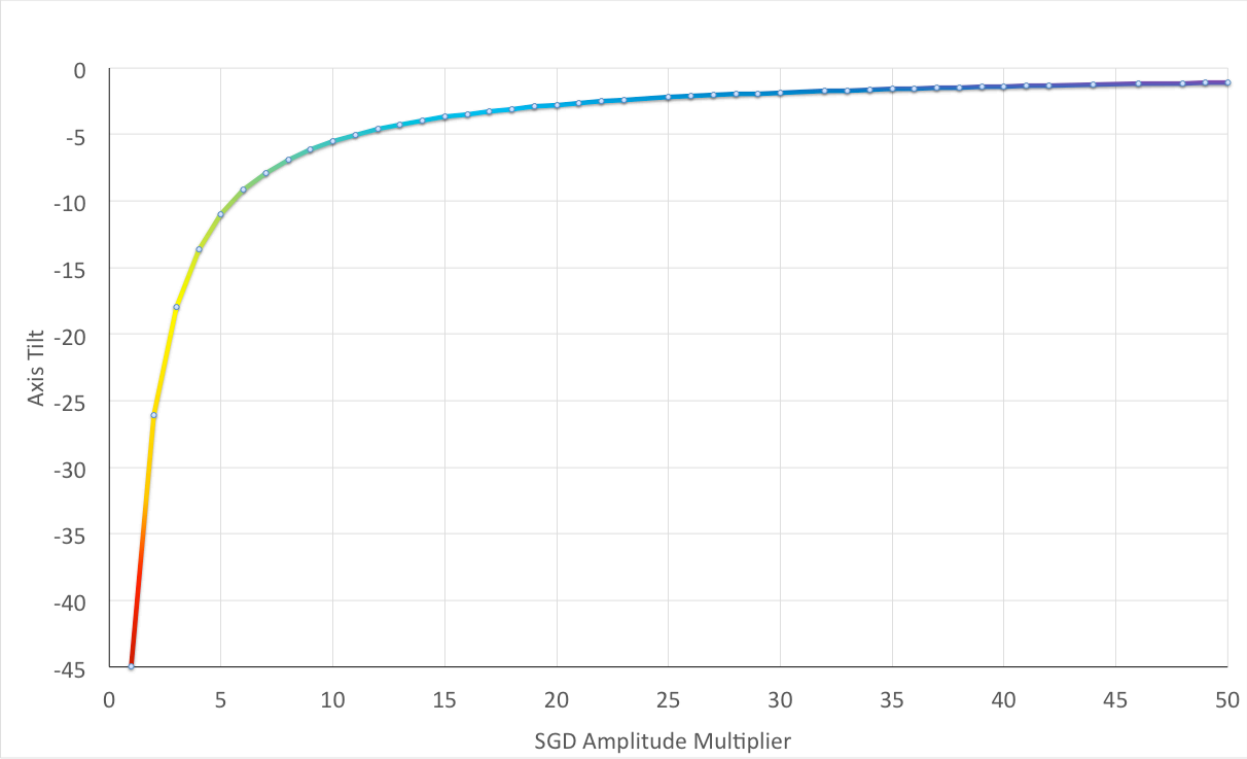

Figure 2.5. Amplitude and axis tilt. SGD amplitude multiplier on the x-axis, axial tilt on the y-axis.

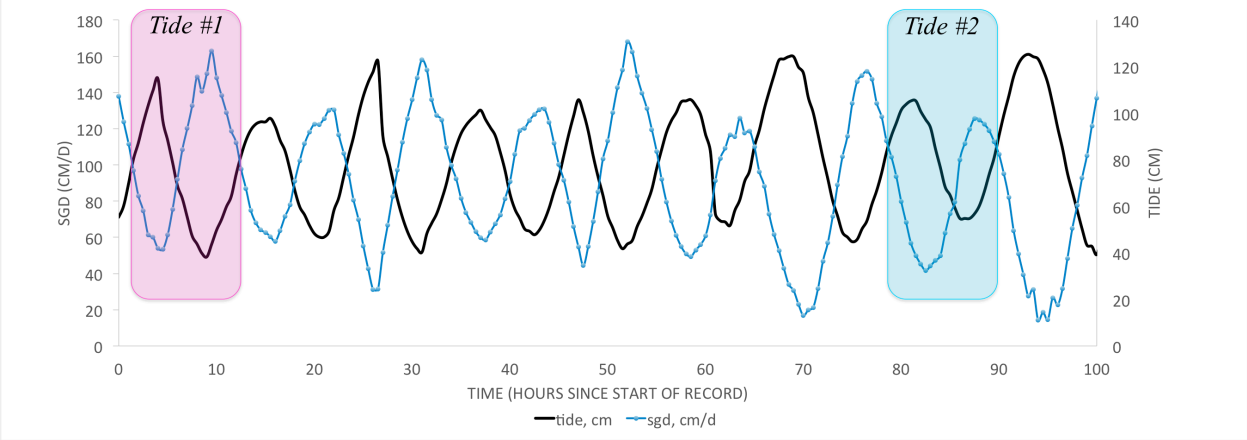

Figure 2.6. Shelter Island time series. Eight full tidal cycles showing tide (black line) and SGD (blue line) data from Shelter Island, NY (Paulsen et al., 2004). Bars indicate individual tides #1 and #2.

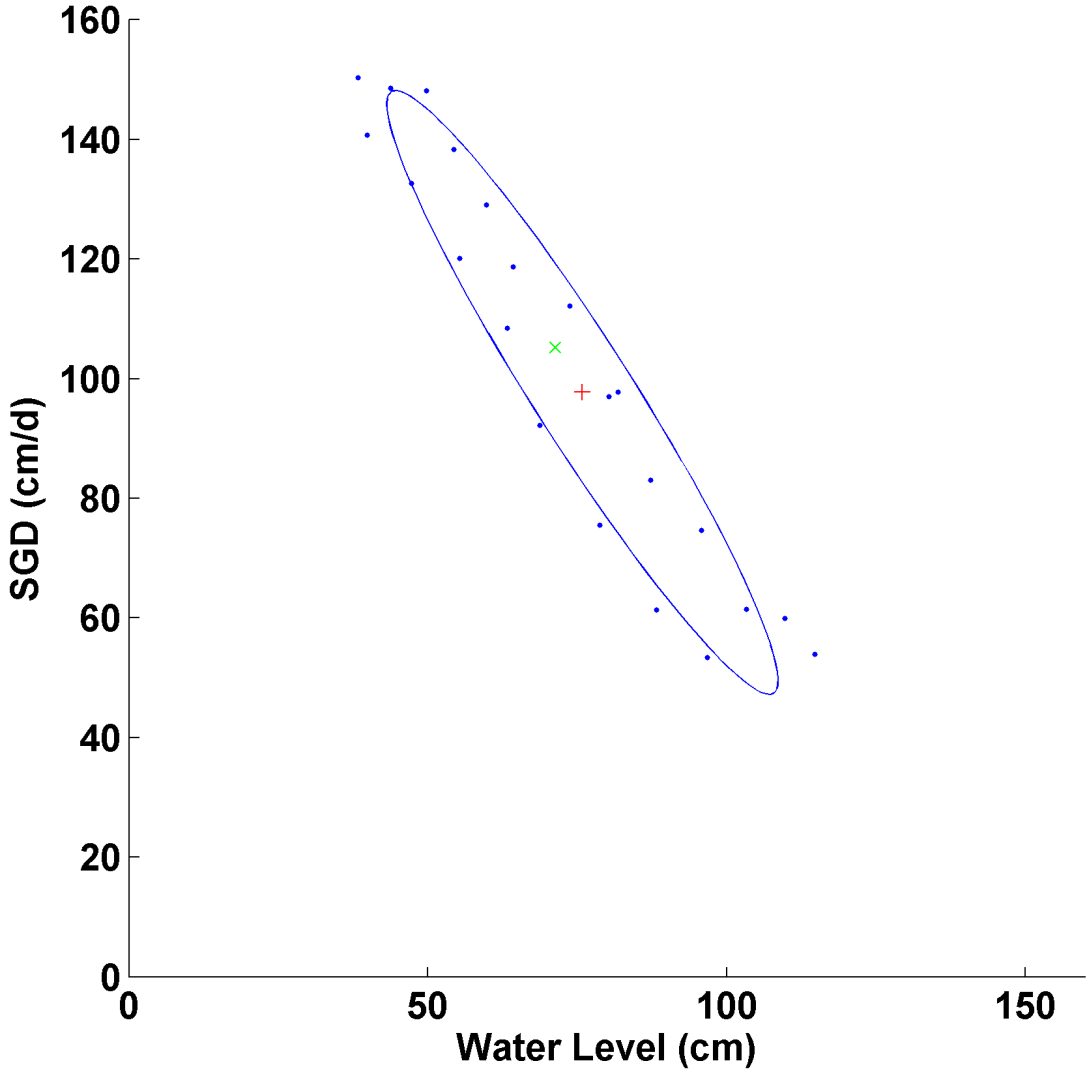

Figure 2.7. Ellipse fit. Tide #1 ellipse fit (blue line) with data points (blue circles), ellipse average SGD (red +), and arithmetic average(green x).

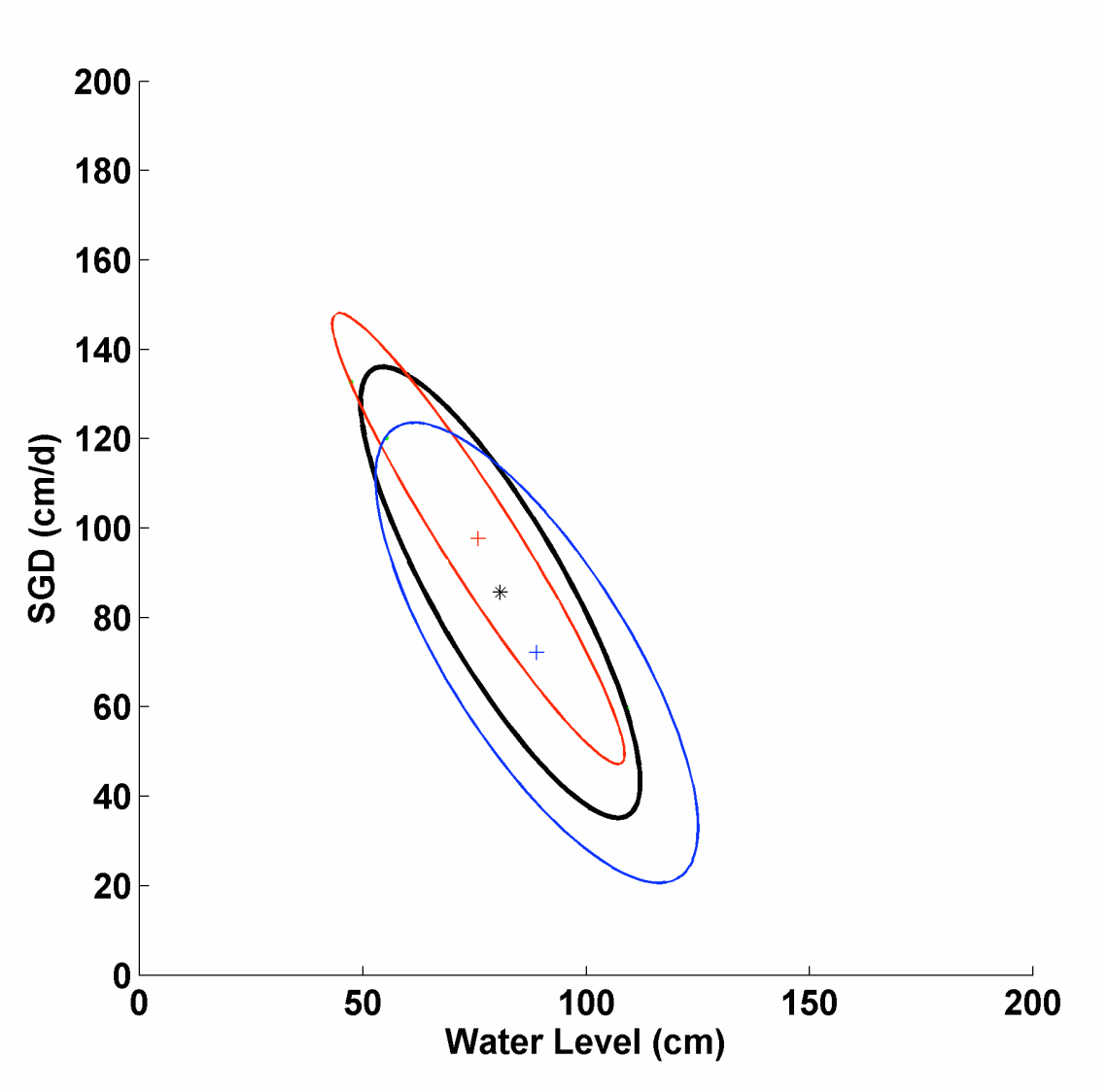

*Figure 2.8. Ellipse fit comparisons. Comparison of ellipses and ellipse averages from full dataset (black line and *), tide #1 (red line and +) and tide #8 (blue line and +).*

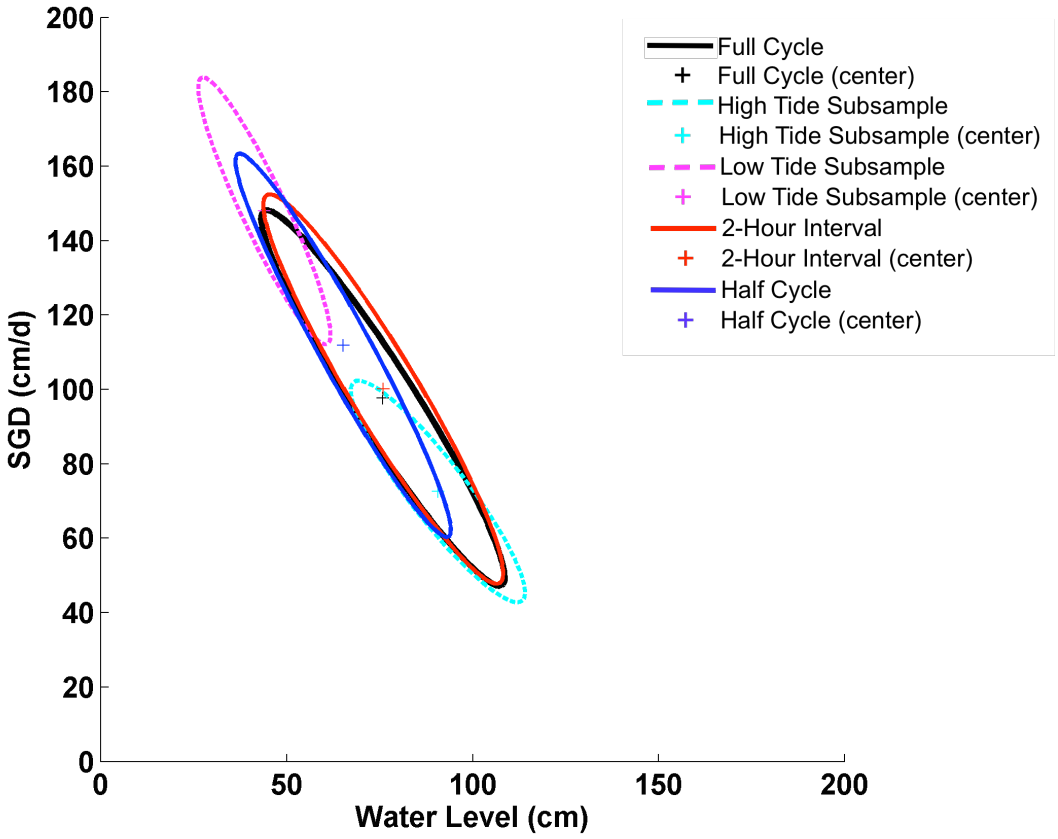

Figure 2.9. Sub-sampling results. Tide #1 ellipse fit for full cycle (black line), high and low tide subsamples (cyan and pink dashed lines respectively), 2-hour interval sampling (red solid line) and sampling over half a cycle (blue solid line)

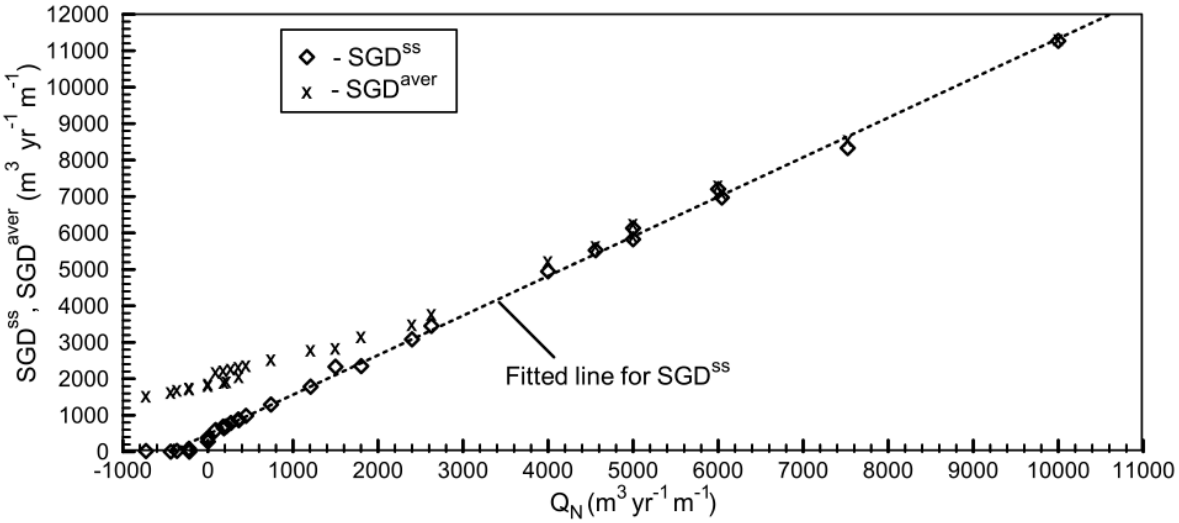

Figure 2.10. SGD and tidal effects. "Resulting temporal average SGD (SGD^{aver}, crosses) for the diurnal sea boundary oscillation with amplitude 0.65 m is compared with corresponding previous [Destouni and Prieto, 2003] nontidal simulation results, SGD^{ss} (diamonds with dashed best fitted line), with both shown as functions of the net land determined groundwater drainage, Q_N. Q_N is defined as the total large-scale fresh groundwater recharge (natural groundwater recharge from precipitation, possible artificial recharge, and groundwater inflow into the coastal aquifer zone from upstream areas) minus the large-scale groundwater extraction (pumping) in the coastal aquifer system." (From Prieto and Destouni, 2005)

Tables

Table 2-1. SGD averages based on the center coordinate for ellipse fit method comparing tidal cycles. Averages for individual tidal cycles and percent difference from the average for all cycles.

	SGD Average (cm/d)	*% Difference*
Full data set (8 Tidal Cycles)	*85.65*	
Tide 1	*97.73*	*14%*
Tide 2	*97.32*	*14%*
Tide 3	*78.72*	*-8%*
Tide 4	*94.61*	*10%*
Tide 5	*99.35*	*16%*
Tide 6	*74.31*	*-13%*
Tide 7	*89.09*	*4%*
Tide 8	*72.14*	*-16%*
Arithmetic Average of Tides 1-8	*87.91*	*3%*

Table 2-2: SGD averages for ellipse fit method comparing subsamples. For the same tide (Tide #1) a comparison between a full cycle, subsamples taken at either high or low tide in 1-hour intervals, subsamples taken at a 2-hour interval, and a half cycle.

Ellipse Fit Trial	**SGD Average (cm/d)**	**% Difference**
Full Cycle	97.73	
High Tide Subsample	57.33	-47%
Low Tide Subsample	152.00	63%
2-Hour Interval	100.11	3%
Half Cycle	111.88	17%

Chapter 3 Barbados

Introduction

With a population density of over 635 people/km^2, Barbados is an island nation with one of the highest population densities in the world. Submarine groundwater discharge (SGD) is the critical parameter linking land-use to coastal environments that should be integrated into the coastal zone management of Barbados. SGD is the flux of groundwater, terrestrially derived fresh water and circulated seawater, into the coastal ocean. Previous studies have shown SGD to be an important phenomenon on small oceanic islands (Burnett *et al*., 2006), coral reef systems (Paytan *et al*., 2006), and on Barbados in particular (Lewis, 1987). The flow of groundwater retards saltwater intrusion, but fresh SGD also serves as a vector to transport fertilizers, wastewater, pesticides and other dissolved constituents into coastal water bodies. It is a substantial source of nutrients to the coastal ocean (*e.g.* Crotwell and Moore, 2003; Moore, 2006). Elevated nutrient concentrations in SGD can lead to eutrophication (Burnett *et al*., 2001) and may have repercussions through the food web and into society. Societal concerns include losses in tourism as a result of unsightly algae washed up on the beaches as well as changes in economically important fisheries. For many small islands, like Barbados, Mauritius and the Hawaiian islands, the linkage between nutrients introduced *via* SGD and the tourism and fishery economies is an important parameter that needs to be better investigated. Such an investigation is the intent of the present study. Especially for an island nation like Barbados, where 15% of the economy is based on tourism (Wellington and Moore, 2004), coastal water quality is an economic concern as well as an aesthetic one.

In this chapter, I will describe a field campaign intended to characterize SGD around Barbados with relatively inexpensive seepage meters and minimal expenditure of time to gather basic information that will be incorporated into model that could be incorporated into resource management. I will explore how this might be done in Chapter 6 of this thesis.

Previous Work

Barbados is a karstic island (13.0667 N; 59.61667 W) in the Caribbean Sea characterized by a series of carbonate ridges (Figure 3.1; Jones, 2002). It covers an area of 431 km^2 and is

fringed with coral reefs. The average coastal salinity is 34.5, and the mean tidal range is 1.7 m (NOAA, 2007). Two hundred and seventy thousand inhabitants rely on its unconfined, limestone aquifer for more than 80% of their freshwater requirements. The other 20% of freshwater demand is provided by desalinization. The average rainfall is 1450 mm/y corresponding to 640 million m^3/y. It exceeds 140 mm/month during the wet season (June through November). Annual recharge has been estimated to be 149 million m^3 (Jones, 2002). Water withdrawals amount to 19 million m^3/y (AQUASTAT, 2000) and are used primarily in agriculture, dominated by the sugar cane crop. The Barbados Water Authority distributes 26 million m^3/y of potable water to its customers, including a transient tourist population estimated to reach 500,000 additional persons (AQUASTAT, 2000). Sewage is treated in Bridgetown and discharged into the sea. Over the rest of the island sewage is introduced to the aquifer through a variety of septic systems. The coastal economy is based to a large extent on tourism but there are substantial subsistence fisheries and recreational fisheries that also rely on the maintenance of an appropriate coastal water quality.

SGD has been measured along the west coast of Barbados to occur at rates over a meter per day (Lewis, 1987). Direct measurements using vented benthic chambers (Lee, 1977) had been made at eight sites (Figure 3.1). SGD was found to decrease with increasing tidal elevation from about 20 cm/d at low tide to 2 cm/d at high tide (Lewis, 1987). Maximum rates of SGD average about 94 cm/d in the dry season (May) and about 140 cm/d in the wet season (November; Lewis, 1987). Nitrate concentrations in the SGD reached values of 1.05 mg/L and decreased with increasing salinity (Lewis, 1987) as expected with an in-mixing of sea water in the subterranean estuary. From these measurements a total nitrate discharge of 1.08×10^8 m^3/y was estimated in the wet season (November) and 4.67×10^7 m^3/y in the dry season (May); compared to estimates between 1.58×10^7 m^3/y and 6.50×10^7 m^3/y provided by a numerical hydrologic model (Harris, 1971 and Proctor and Redfern, 1983 respectively, as cited in Lewis, 1987).

Since this pioneering work by Lewis (1987) in Barbados, SGD has attracted the attention by the global scientific community (Burnett *et al*., 2006). In addition, new modeling studies had been initiated on Barbados (Mayers, 2007, personal communication) and it is my intention to revisit SGD here.

Some additional measurements had been made at Worthing Beach (Cable *et al*., 2010). Worthing Beach is backed by a 0.25 km^2 mangrove swamp forming a ring around a brackish pond which appeared to be groundwater fed. This beach contained a subterranean estuary (STE) of an inverted nature, that is, a layer of saline groundwater overlying a freshwater wedge. The usual salt wedge would be expected at depth, but was not found in the wells. The underflow was calculated to be 0.15 to 0.38 m^3/d per meter of shoreline. Groundwater from the upland behind the swamp drained into the swamp. The low hydraulic gradients in the beach were driven by water levels in the mangrove swamp. A flux of nitrogen was calculated to be 34.2 mmoles/d per meter of shoreline.

Methods

This study was conducted at two sites on the western Barbados shoreline: Alleynes Bay (13.20427 N; 59.64028 W) and Queens Fort Beach (13.19466 N; 59.64128 W; Queens Fort Beach is an informal name given to the site located in Heron Bay) (Figure 3.1). All sites were located on a narrow, Quaternary beach in front of the First High Cliff. The First High Cliff is a 125,000 year old uplifted reef tract, one of two such major geographic features (Mesolella *et al*., 1969). The sites were in areas of high infiltration capacity (50 to 100 mm/hr; Jones, 2002). The beaches studied are composed of carbonate sand overlying a limestone aquifer. Worthing Beach forms a barrier separating a freshwater wetland from the sea. Alleynes Bay and Queens Fort Beach are the margins of a carbonate terrace in front of the First High Cliff. Offshore, the sites were characterized by limestone rocks on the seafloor covered by patches of sand. Alleynes Bay and Queens Fort Beach were sampled twice; August 2006, at the peak of the wet season, and January 2007, during the dry season, in order to capture seasonal changes in SGD.

Sediment samples were taken and analyzed for size distribution by the Barbados National Standards Institution Soils Mechanic Laboratory during the dry season of 2012. Average grain size, sorting and skew are calculated according to Folk (1966). Grain size class is according to the Wentworth Scale (Wentworth, 1922).

Alleynes Bay and Queens Fort beach are both sandy beaches underlain by limestone aquifer material. Sand in the swash zone of Alleynes Bay was very coarse, moderately well sorted and negatively skewed. The back beach at Alleynes Bay also was very coarse sand, moderately sorted and positively skewed. Queens Fort Beach was slightly coarser, though still very coarse sand, moderately well sorted in both the swash zone and the back beach areas. The swash zone at Queens Fort Beach was positively skewed and the back beach was negatively skewed. See Table 3-1 for sand grain values for both sites. Offshore both sites were characterized by limestone rocks on the seafloor covered by patches of sand. Sand remained in place for the duration of a daily sampling, with the exception of twelve instances where the bottom edge of the seepage meter was exposed through wave action. During each hourly sample collection meters were checked for signs of scouring. If a meter's bottom edge was exposed, the meter was either moved to a new location or removed from sampling, depending on the remaining time available for sampling and the availability of suitable sand patches. From day to day or season to season, exact locations could not be re-occupied because the devices had to be placed in sand to provide good contact with the sea floor, and patches of sand were ephemeral.

Measurements were made using Lee-type benthic seepage meters using the method previously described in Chapter 1. Placement of seepage meters at each site was constrained, in

part, to sand patches large and thick enough to allow for installation and, partly, because I was considering each seepage meter to be a random sample of the distribution of SGD. It was noted when meters were deployed in line with visible seeps exposed on the shore face.

Salinity was determined using a YSI 556 MPS, a multi-probe system which can simultaneously measure dissolved oxygen, conductivity, temperature, pH and oxygen reduction potential. Calculations of the freshwater component were calculated using Equation 1.6.

Samples taken August 2006 and January 2007 for nutrient analysis were collected in 25 mL acid-washed plastic bottles and frozen for transport and storage. For inorganic nitrogen, freezing prior to filtration is adequate for preserving field concentrations (Dore *et al*., 1996). To be prepared for nutrient analysis, the samples were thawed, filtered through a 0.4 µm polycarbonate Nuclepore® membrane filter to remove particulates and kept refrigerated until analysis. The nutrient analyte of interest, NO_x (nitrate plus nitrite), was analyzed on a Lachat Instruments FIA-6000 flow injection type automated analyzer.

During the dry season, in addition to the samples from seepage meters and ambient seawater, I also collected samples from public supply wells and monitoring wells within the catchment basin (Figure 3.1). These samples were analyzed for NO_x in order to provide a freshwater end member for nitrogen.

A pressure sensor was not available, so approximate tide measurements were taken hourly, measured against a temporary tide staff. The timing of tidal measurements did not coincide with SGD sample collection, as a result of these limitations, I could not use the ellipse method described in Chapter 2 to determine average discharge; numerical averages are used here instead.

Results

Wet Season 2006

At Alleynes Bay, measurements were made at seven sites during the wet season, although not all simultaneously (Figure 3.2A). The wet season measurements at Alleynes Bay were conducted on August 23 and 27, 2006. Arithmetic average flow for four seepage devices (A, B, C, D; Figure 3.2A) on August 23 was 66 cm/d with a maximum of 152 cm/d and a minimum of 11 cm/d. Two devices (A and D) were removed after 2.5-3.5 hours due to scouring issues. The remaining two (B and C) remained in place for 8-9 hours. There was an inverse relationship with the tide, shown by devices B and C (Figure 3.3). Devices A and D potentially show a similar tidal modulation, but were not sampled long enough for the trend to be clear. Average ambient

salinity was 31.9. Salinity decreased over the sampling period in devices B and C yielding freshwater components of 37% and 39% respectively. Devices A and D had salinities that were within the range of variations in ambient salinity, however the data set for these devices is too short to determine freshening. Additionally, a freshwater seep was exposed at low tide was sampled for salinity measurements (Figure 3.4). It had an average salinity of 8.3, with an average freshwater component of 74%.

Arithmetic average flow for three devices (A', B' and C'; Figure 3.2A) on August 27 was 39 cm/d with a maximum of 91 cm/d and a minimum of 15 cm/d. One device (A'), at a distance of 23 m from shore, was directly offshore from a seep exposed on the beach at low tide; this device recorded an average flow of 62 cm/d and ranged from 23-91 cm/d. All three devices, in place for 7.5 hours, showed an inverse relationship with the tide, though A' also showed a higher frequency variation superimposed upon the tidal frequency (Figure 3.5). Ambient salinity was 32.2. Salinity decreased over the sampling period in all three devices: A' was 49% fresh, B' was 23% and C' was 22%. Additionally, on August 27, the seep exposed at low tide was sampled for salinity and nutrient measurements. The seep had an average salinity of 6.5 with an average freshwater component of 80%.

Overall arithmetic average discharge at Alleynes Bay during the wet season was 55 cm/d with an average freshwater component of 34%. Because SGD showed a tendency to decrease offshore, I used an exponential functional trend, as described in Chapter 1, to calculate a total discharge per meter of shoreline. This mathematical expedient avoided the need to choose an arbitrary width to the seepage zone. In the process, however, it was necessary to discriminate two groups of measurements. An evaluation of the arithmetic averages for each devices by distance from shore, the data fall into two groups, one that approximated the exponential decrease offshore as discussed in Chapter 1, and another group of higher discharge that do not fit this pattern (Figure 3.6) were considered as outliers. The three devices that fit the exponential decrease, D, B' and C', were all in a transect offshore with C closest to shore and C' furthest from shore, with flow rates decreasing from 47 cm/d at 12.9 m from shore to 25 cm/d at 26.8 m from shore. Using Equation 1.8 with $A = 0.79$ m/d and $C = 0.045$ m^{-1} (R-squared = 0.93; Figure 3.6), the total integrated flux is 18 m^3 per meter of shoreline per day. With an average freshwater component of 34%, total integrated flux of freshwater is 6 m^3 per meter of shoreline per day.

Measurements at Queens Fort Beach were made on August 24, 2006. Four devices were deployed at Queens Fort Beach during the wet season (Figure 3.7A). Arithmetic average flow was 15 cm/d with a minimum flow of 6 cm/d and a maximum of 25 cm/d. One device (C) may have been showing a response to the tide but the others did not and any tidal modulation was small (Figure 3.8). Although the flow rate varied over time, it increased or decreased over a range of about ±5 cm/d without consistent pattern at any one device. Average ambient seawater had a salinity of 33.9. There was no observable freshening of the seepage samples. At Queens Fort Beach SGD decreased offshore (Figure 3.9). It could be represented as an exponential decrease as before with A = 0.46 m/d and C = 0.066 m^{-1} (R-squared= 0.82) to give a total

discharge per meter of shoreline of 7 m^3 per meter of shoreline per day. No freshwater seeps or submerged areas with higher discharge were found here.

Dry Season 2007

The dry season measurements at Alleynes Bay were conducted on January 17 and 18, 2007 at seven locations, although not all locations were occupied simultaneously (Figure 3.2B). Arithmetic average flow for four seepage devices on January 17 was 28 cm/d with a maximum of 52 cm/d and a minimum of 9 cm/d. Only one device remained in place for the entire duration of the 8 hour sampling day (C) the others had the sand scoured away from the bottom edge due to wave action; B remained in place for 3 hours, D was replaced after 2 hours yielding two data sets (D1 and D2), D2 remained in place for 5.5 hours. C and D2 showed an inverse relationship with the tide, B and D1 were not in place long enough to determine a trend though they do show a decrease in flow rates with a rising tide indicating that a similar inverse relationship may hold for this location also (Figure 3.10). Ambient salinity was 33.7. Device C showed some freshening with a freshwater component of 30%, B and D1 were not in place long enough to detect freshening, and D2 salinity was within the range of variation of the ambient water and thus had no freshwater.

Arithmetic average flow for three devices on January 18th was 26 cm/d with a maximum of 61 cm/d and a minimum of 10 cm/d. These three devices were all in place for 8 hours and two (B' and D') seemed to show a tidal modulation (Figure 3.11). Ambient salinity was 32.0. Devices B', C' and D' all showed freshening with freshwater components of 32%, 21% and 24% respectively. A systemic decrease away from shore was not clearly resolved for either day nor for a composite of the two days at Alleynes Bay. As a result, I did not attempt to apply an exponential expedient to calculate SGD per meter of shoreline. On January 24, 2007, a freshwater seep exposed at low tide was sampled for salinity and nutrients. It had a salinity of 20.4. Arithmetic average flow for Alleynes Bay in the dry season is 27 cm/d with an average freshwater component of 26%.

Measurements at six locations were made over two days, January 21 and 22, 2007 at Queens Fort Beach (Figure 3.7B). Arithmetic average flow for three devices on January 21 was 16 cm/d with a minimum flow of 5 cm/d and a maximum of 30 cm/d. All three devices were deployed for about six hours. Average ambient salinity was 34.0. As before, there was weak to no tidal modulation and no observable freshening of the SGD samples (Figure 3.12).

Arithmetic average flow for three devices on January 22 was 29 cm/d with a minimum flow of 14 cm/d and a maximum of 49 cm/d. The three devices were deployed for about two hours, which was too short to determine a firm correlation with the tide or observe any freshening. It appeared that one and possibly two of the three devices may have been inversely

correlated with the tide (Figure 3.13). Average ambient salinity was 35.4. All salinity variations of the devices were within the range of ambient variability.

Arithmetic average flow for Queens Fort Beach in the dry season is 22 cm/d with no discernable freshwater influence. All devices were at the same distance from shore; no relationship between SGD and distance from shore could be determined. Because an offshore transect was not measured, it was inappropriate to try to estimate a total flux per meter of shoreline.

Nutrients 2006-2007

In Alleynes Bay during the wet season there was an inverse correlation of NO_x with salinity. At a salinity of 34, concentrations of NO_x were less than 7 µM/L and below detection limits. At a freshwater seep on the beach, water with a salinity of 3.2 had a NO_x value of 179.9 µM/L (Figure 3.14). The only sample taken at Queens Fort Beach during the wet season had a concentration below detection. The inverse linear relationship between salinity and NO_x concentration in µM/L at Alleynes Bay took the form:

$$[NO_x] = -4.8\,S + 166 \qquad [3.1]$$

where *S* is the salinity (R-squared= 0.67).

During the dry season, Alleynes Bay also displayed an inverse correlation between salinity and NO_x; at a salinity of 34 the NO_x concentration below detection and at a salinity of 15.9 the NO_x was 182.0 µM/L (Figure 3.14). NO_x concentrations in fresh well water ranged from below detection to 390.4 µM/L (Figure 3.14). The linear trend between salinity and NO_x concentration yields the relationship (R-squared= 0.42)**:**

$$[NO_x] = -6.8\,S + 250 \qquad [3.2]$$

Queens Fort Beach in the dry season had NO_x concentrations below detection with the exception of meter C from January 21st, which had 8.6 µM/L. This seepage meter had an average SGD of 14 cm/d with a range of 4-20 cm/d.

Discussion

In the wet season, Alleynes Bay had an arithmetic average flow rate of 55 cm/d with a freshwater component of 34%. Queens Fort Beach had an arithmetic average flow rate of 15

cm/d and a freshwater component of 0%. In the dry season, Alleynes Bay (average flow rate of 27 cm/d with a freshwater component of 26%) had higher flow rates and a greater freshwater component than Queens Fort Beach (average flow rate of 22 cm/d with a freshwater component of 0%). At Alleynes Bay where the NO_x concentrations are inversely correlated with salinity, the fresh water component of SGD appears to be a principal vector for nitrogen input into the coastal ocean. The seasonal differences in the slope of the trend between salinity and NO_x at Alleynes Bay can represent dilution from increased precipitation during the wet season. In the wet season, the nitrogen was transported to the coastal ocean at lower concentrations more frequently with the likely consistent daily precipitation, where as in the dry season the higher concentration of nitrogen is likely input into the coastal ocean in pulses of higher concentrations after rain events. The differences in SGD and fresh water component were apparent in the NO_x concentrations at these two sites; Alleynes Bay had much higher concentrations, which varied with salinity, but Queens Fort Beach remained consistently very low and had no relationship with salinity. These indicate different source waters for SGD at the two sites; SGD at Alleynes Bay incorporated terrestrially derived freshwater while SGD at Queens Fort Beach was principally circulated seawater. Circulation of seawater is not an appreciable source of additional nutrients to the coastal waters.

Using the characteristic differences between Alleynes Bay and Queens Fort Beach, I attempted to extrapolate the results along the extent of the shoreline studied by Lewis (1987). The strategy was to apply an SGD typology for the extrapolation (Bokuniewicz, 2001). A typology is not a model, but rater an attempt to classify the shoreline using a relevant and available shoreline characteristic as a surrogate for potential SGD. In this case, differences between the wet and dry seasons were used to discriminate two classes of SGD. In Lewis' study, sites that showed little to no change in SGD between seasons were represented by the situation at Queens Fort Beach. Sites where the SGD was low in the dry season and high in the wet season (Lewis, 1987) are analogous to the situation at Alleynes Bay. Using this comparison, 60% of the western shoreline of Barbados displays characteristics similar to Alleynes Bay. This percentage of shoreline is indicative of a substantial fresh water input into the coastal ocean, supplying 9.6×10^7 m^3 of fresh water during the wet season and 5.7×10^7 m^3 of fresh water during the dry season.

An interesting question is the cause of the high frequency variation superimposed upon the tidal frequency shown in device A' on August 27 at Alleynes Bay. This device showed variations up to 62 cm/d within 41 minutes. One possible explanation could be a hydraulic gradient set up by the presence of a seiche within the embayment. It is interesting to note that the salinity within this device decreased steadily reaching a freshwater component of 49%. The exploration of a seiche signal within SGD measurements can be found in Chapter 4 of this thesis.

All of the above considerations apply only to the west coast of Barbados. The east coast is an upraised platform exposed to considerably higher wave energy. It was beyond the ability and scope of this to document SGD on the east coast. It might be expected that general aquifer

characteristics are similar but hydraulic gradients may be greater, and, while tidally induced circulation of seawater would be comparable, an elevated component of wave-induced circulation (Li *et al*., 1999) would increase total SGD.

Conclusion

The Barbados coast appears to be characterized by two types of coastal groundwater hydrologies. In one type, SGD is primarily recirculated seawater with little tidal or seasonal modulation. Along other stretches of the coast, SGD contains a freshwater component amounting to an annual average of 30% of the total discharge and it is tidally and seasonally modulated. Nitrogen inputs from land-based sources are associated with this latter type of coastline.

Submarine groundwater discharge in Barbados has the potential to substantially impact on the properties and quality of the coastal ocean from the substantial freshwater contribution and also the concentrations of nutrients. While the results from this study should not be extrapolated to characterize the entire shoreline of Barbados, they are likely characteristic of much of the western shoreline, and thus characterize most of the developed area.

Small oceanic islands with high population densities, like Barbados, need to be acutely aware of the impact that development and economy has on the natural environment. An increase in population will likely not change the net flow of SGD unless there is substantial diversion of wastewater to an oceanic outfall offshore. However, there could be a decline in the quality of the freshwater flux. The SGD source-water can be contaminated by different land uses – urban, agriculture, forested – each of which will leave a different signature upon the water being discharged. It is also important to identify where the discharge occurs – both the spatial variability and the use for the coastal water body – as SGD into a lagoon will have different environmental repercussions than SGD into the open ocean, especially SGD on the exposed, high energy eastern coast. In addition, a tourism-dominated area will have different economic repercussions than will a fisheries-dominated area. Such considerations will be considered further in Chapter 6.

References

AQUASTAT. 2000. Food and Agriculture Organization of the United Nations. Information System on Water and Agriculture: Barbados. http://www.fao.org/nr/water/aquastat/countries/barbados/index.stm Last accessed: 12 August 2008.

Bokuniewicz, H.J. 2001. Towards a coastal groundwater typology. Journal of Sea Research: 46: 99-108.

Burnett, W.C., M. Taniguchi, J. Oberdorfer. 2001. Measurement and significance of the direct discharge of groundwater into the coastal zone. Journal of Sea Research 46(2): 109-116.

Burnett, W.C., P.K. Aggarwal, A. Aureli, H. Bokuniewicz, J.E. Cable, M.A. Charette, E. Kontar, S. Krupa, K.M. Kulkarni, A. Loveless, W.S. Moore, J.A. Oberdorfer, J. Oliveira, N. Ozyurt, P. Povinec, A.M.G. Privitera, R. Rajar, R.T. Ramessur, J. Scholten, T. Stieglitz, M. Taniguchi, J.V. Turner. 2006. Quantifying submarine groundwater discharge in the coastal zone *via* multiple methods. Science of the Total Environment. 367(2-3): 498-543.

Cable, J.E., J.B. Martin, C. Pounder, L. Inniss, A. Moseley and E. Smith. 2010. Submarine Groundwater Discharge from a Carbonate Aquifer, Worthing Beach, Barbados. American Society for Limnology and Oceanography Summer Meeting. June 6-11, 2010. Santa Fe, New Mexico, USA.

Crotwell, A.M., and W.S. Moore. 2003. Nutrient and radium fluxes from submarine groundwater discharge to Port Royal Sound, South Carolina. Aquatic Geochemistry 9(3): 191-208.

Dore, J.E., T. Houlihan, D.V. Hevel, G. Tien, L. Tupas and D.M. Karl. 1996. Freezing as a method of sample preservation for the analysis of dissolved inorganic nutrients in seawater. Marine Chemistry 53: 173-185.

Folk, R.L. 1966. A Review of Grain-Size Parameters. Sedimentology 6(1966): 73.93.

Harris, W.H. 1971. Groundwater-carbonate rock chemical interactions, Barbados, West Indies. Ph.D. thesis, Brown Univ. 384 pp.

Jones, I.C. 2002. Geochemical evolution of groundwater in the Pleistocene limestone aquifer of Barbados. Doctoral Thesis. University of Texas, Austin, TX. 273 pp.

Lee, D.R. 1977. Device for measuring seepage flux in lakes and estuaries. Limnology and Oceanography. 22(1): 140-147.

Lewis, J.B. 1987. Measurements of groundwater seepage flux onto a coral-reef – spatial and temporal variations. Limnology and Oceanography. 32(5): 1165-1169.

Li L., D. Barry, F. Stagnitti, J.P. Parlange. 1999. Submarine groundwater discharge and associated chemical input to a coastal sea. Water Resource Research. 35: 3253–3259.

Mayers, B. 2007. Personal Communication. January 2007, University of the West Indies, Cave Hill Campus, Barbados.

Mesolella, K.J., R.K. Matthews, W.S. Broeker and D.L. Thurber. 1969. The astronomical theory of climatic change: Barbados Data. Journal of Geology. 77: 250-274.

Moore, W.S. 2006. The role of submarine groundwater discharge in coastal biogeochemistry. Journal of Geochemical Exploration 88(1-3): 389-393.

NOAA. 2007. Tidal Station Locations and Ranges. http://tidesandcurrents.noaa.gov/tides07/tab2ec4.html#117. Accessed 12 August 2008.

Paytan, A., G.G. Shellenbarger, J.H. Street, M.E. Gonneea, K. Davis, M.B. Young, W.S. Moore. 2006. Submarine groundwater discharge: an important source of new inorganic nitrogen

to coral reef ecosystems. Limnology and Oceanography. 51(1): 343-348.
Proctor and Redfern International Ltd. 1983. Coastal conservation project, V.2; sect. 8: Drainage and groundwater models. 50 p.
Wellington, C. and R. Moore. 2004. Barbados' first national communications to the United Nations Framework Convention on Climate Change. http://unfccc.int/essential_background/library/items/3599.php?rec=j&priref=3229 Last accessed: 12 August 2008.
Wentworth, C.K. 1922. A Scale of Grade and Class Terms for Clastic Sediments. Journal of Geology 30(5): 377-392.

Figures

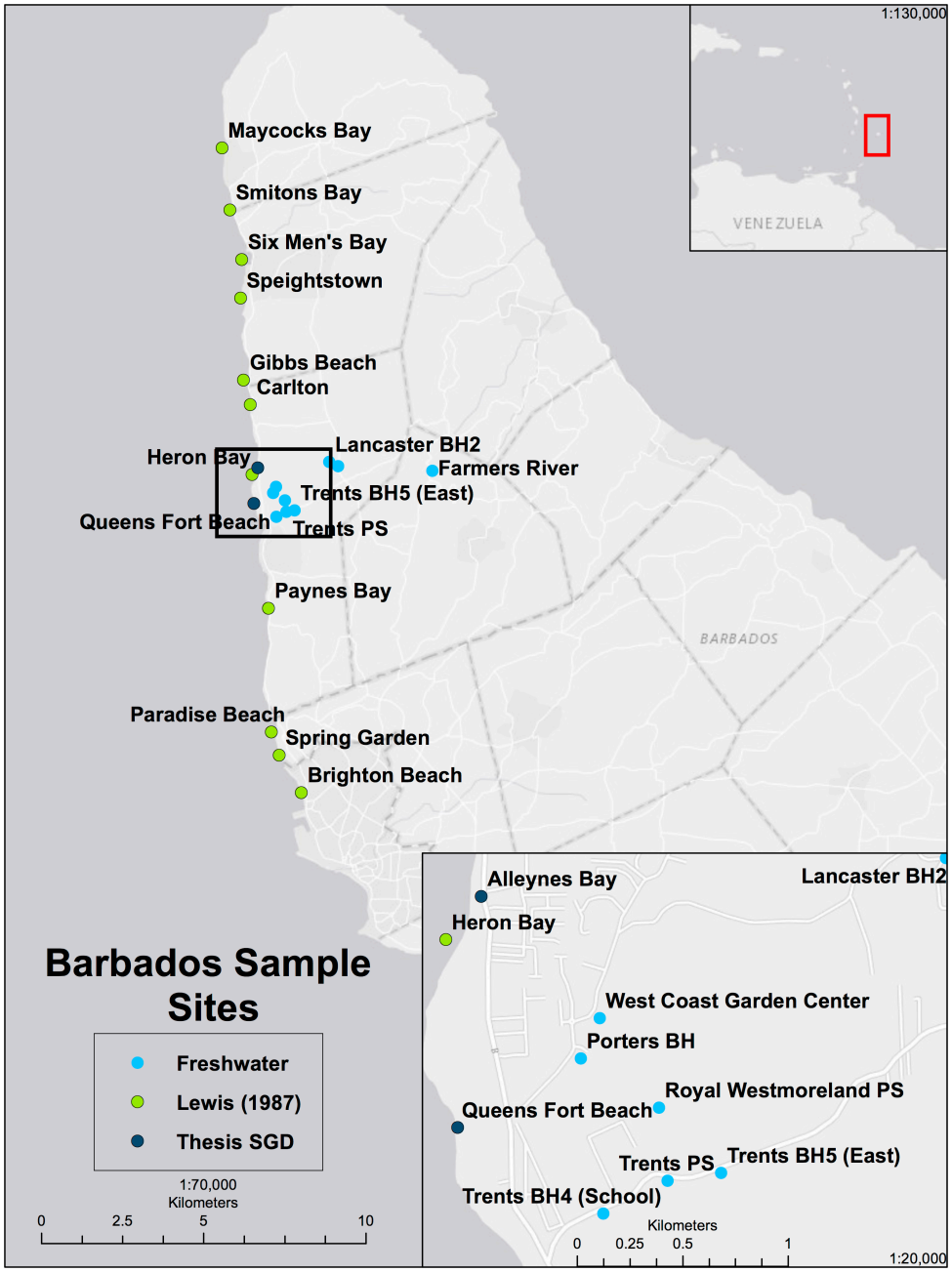

Figure 3.1. Barbados sample sites. Map showing locations of 11 of 15 field sites from Lewis 1987 (green markers); two manual seepage meter field sites for this study (dark blue markers) and catchment basin sites (teal markers). The bottom inset map shows a close up view of the area surrounding the two manual seepage meter field sites. Map produced by Michael White, SoMAS.

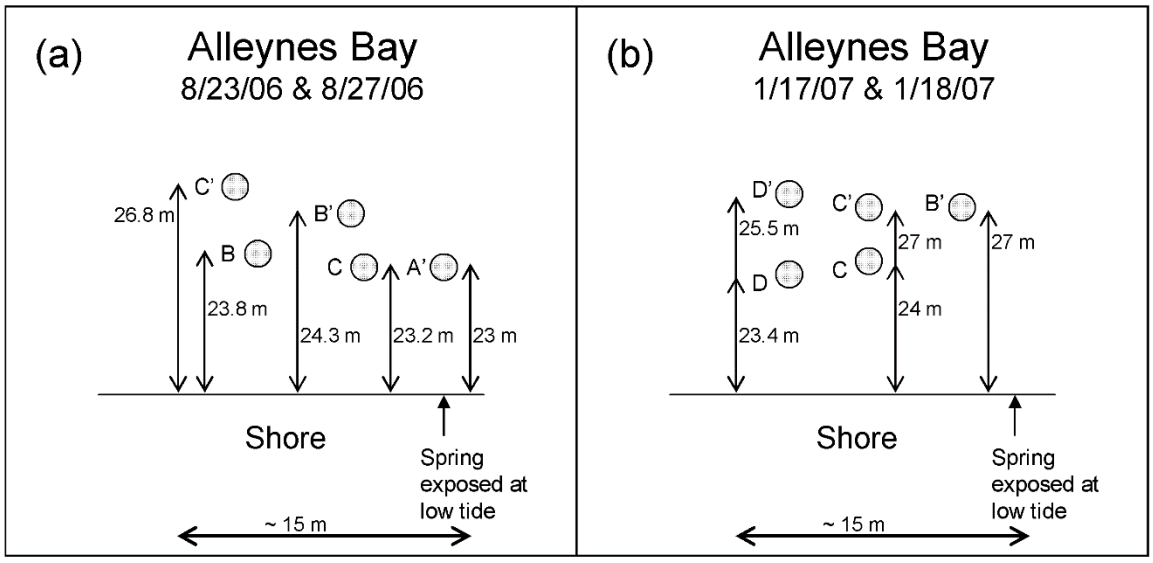

Figure 3.2. Alleynes Bay schematic. Locations of seepage meter sites during the wet season (a) and dry season (b).

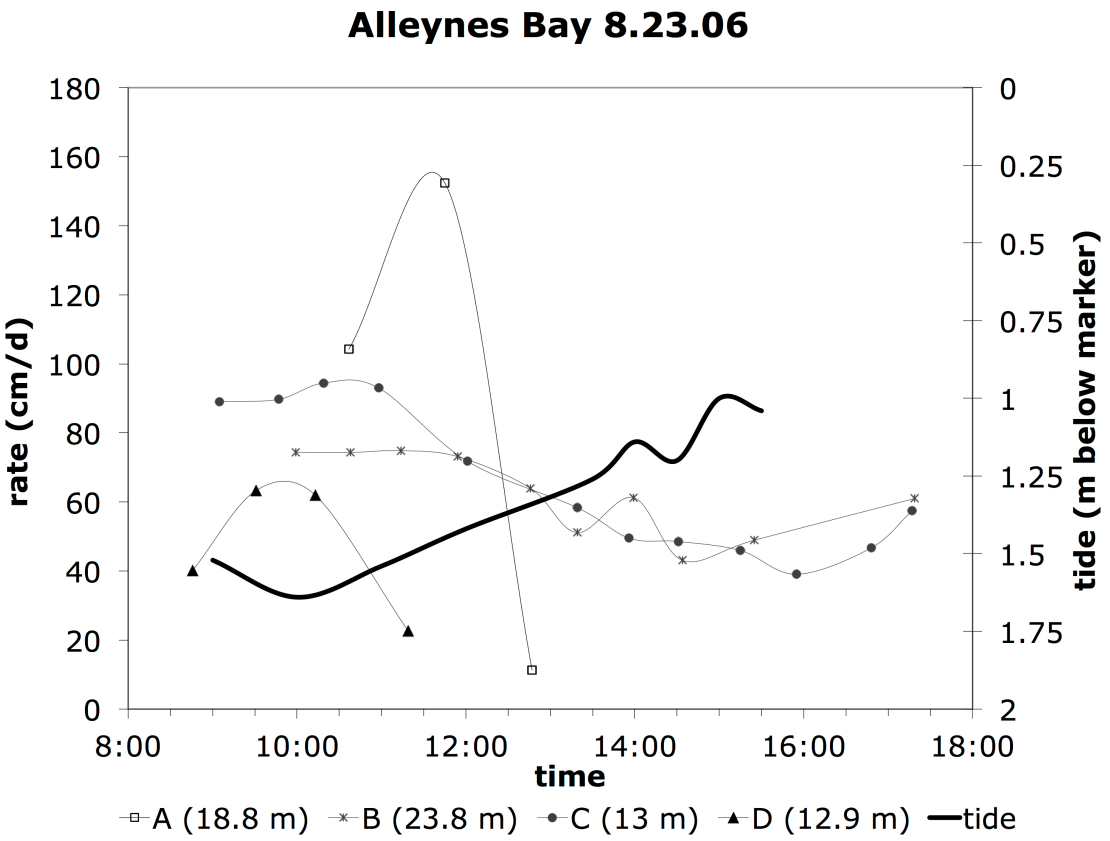

Figure 3.3: Alleynes Bay flow rate and tidal height (8/23/06). Time series of tide (thick black line) and SGD (meters A, B, C and D).

Figure 3.4. A seep – groundwater flowing directly out of the beach face at low tide at Alleynes Bay. Inset photo is close up of the squared off region of the photo of the shoreline. Credit Ruth Coffey.

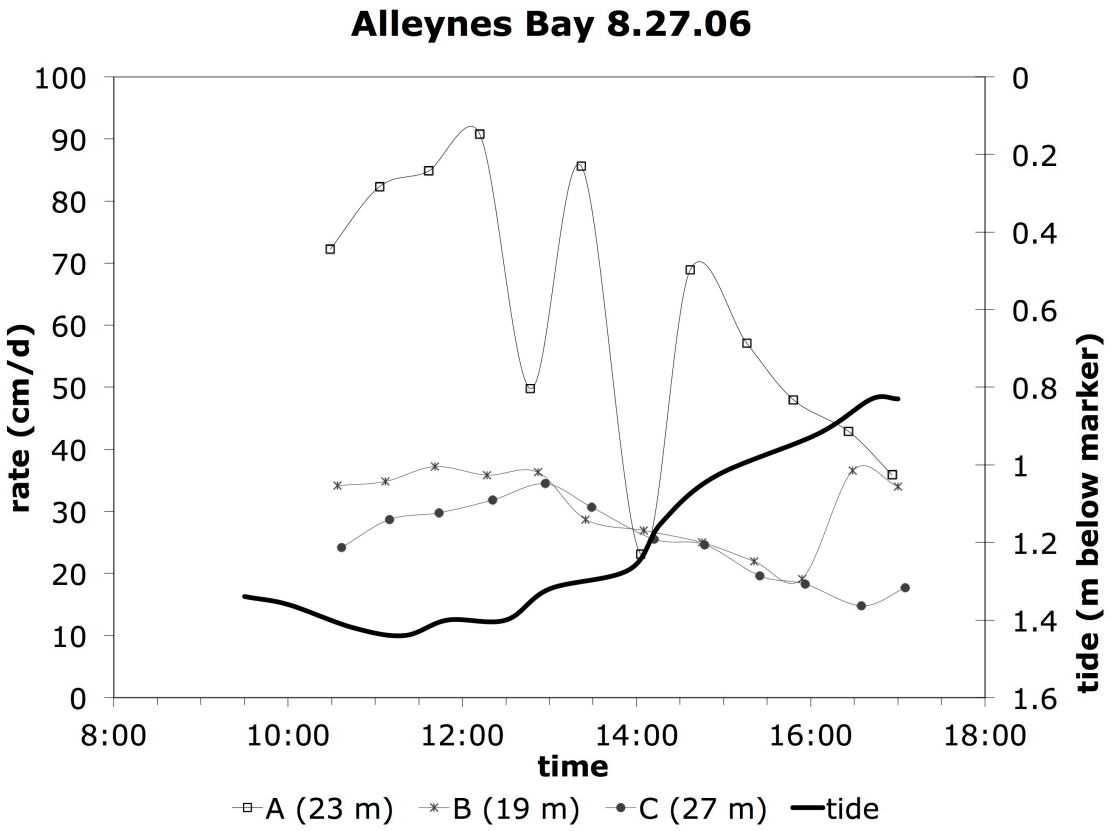

Figure 3.5. Alleynes Bay flow rate and tidal height (8/27/06). Seepage device A' (x) shows high frequency variations superimposed upon tidal frequency. Devices B' (*) and C' (•) show flow rates inverse to the tide (thick black line).

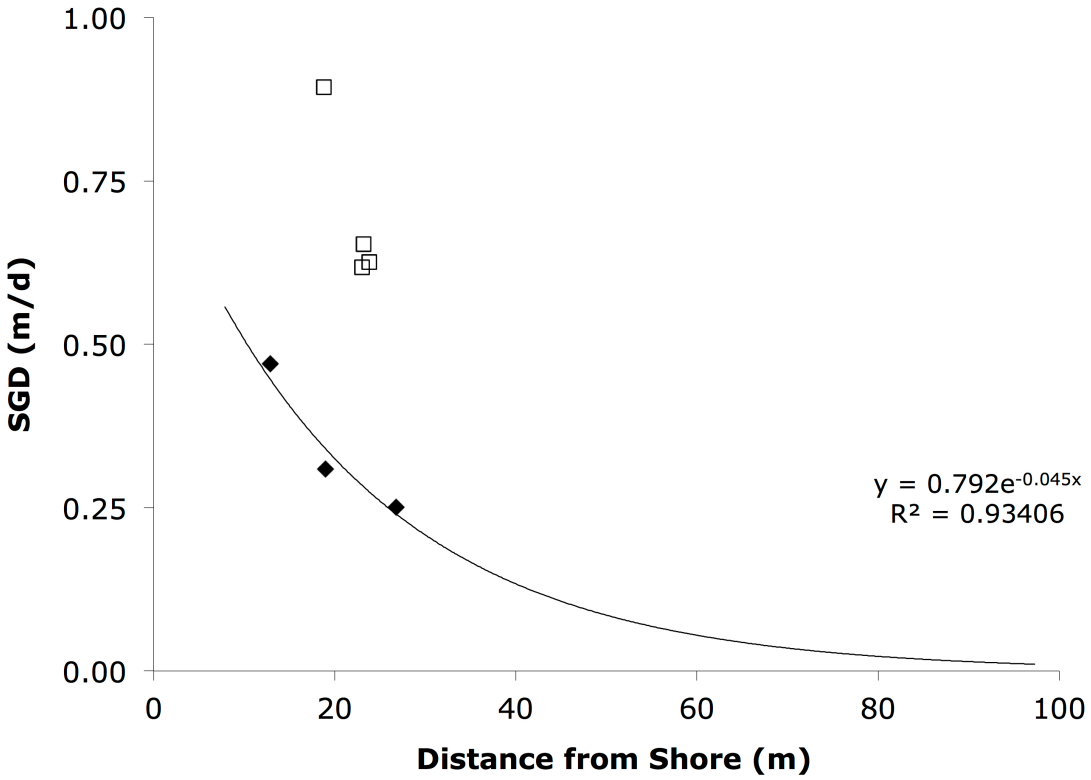

Figure 3.6. Alleynes Bay compiled, distance from shore vs. SGD flux. Devices with exponential decrease from shore are shown in solid diamonds, the anomalously high discharge devices are shown in open squares.

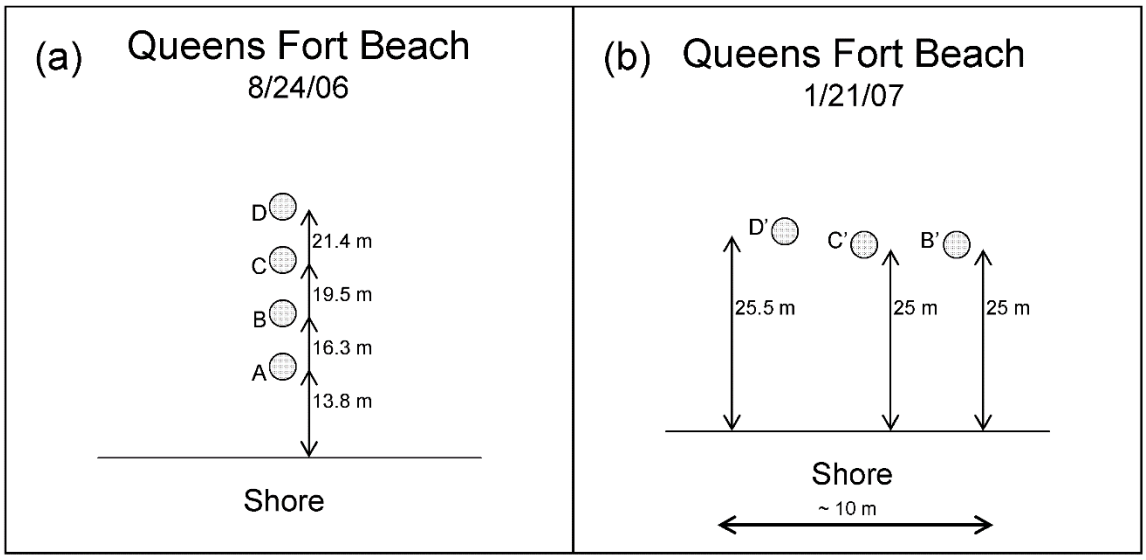

Figure 3.7. Queens Fort Beach sites. Locations of seepage meter sites during the wet season (a) and dry season (b).

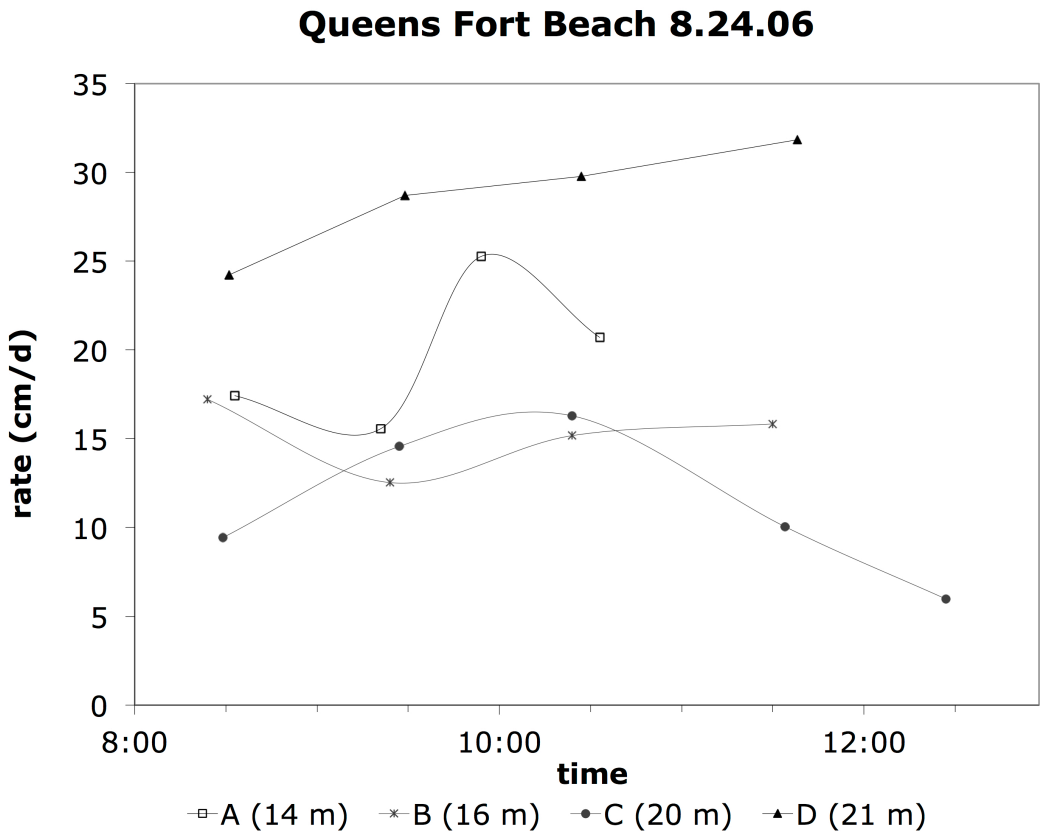

Figure 3.8: Time series at Queens Fort Beach (8/24/06) of SGD at four seepage meters. Low water occured at 10:30 am.

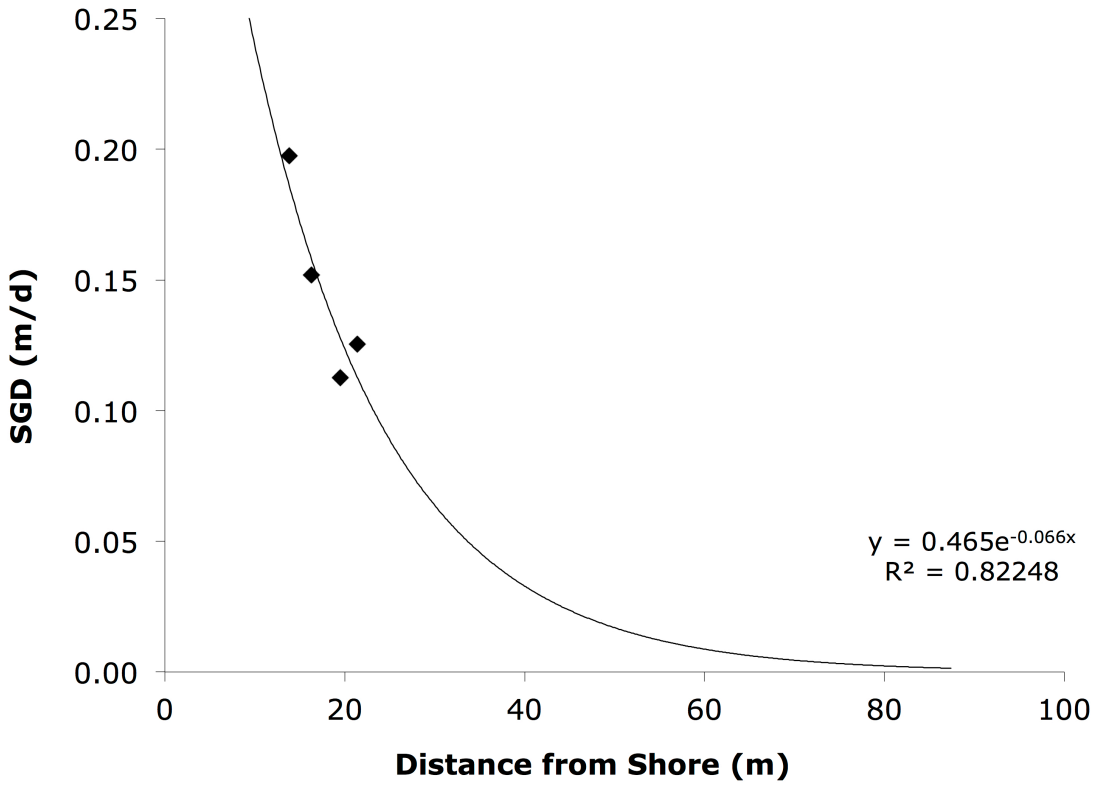

Figure 3.9. Queens Fort Beach distance from shore vs. flow rate. An exponential line (line) is fit to the flow rate data (diamonds) with equation and R-squared value.

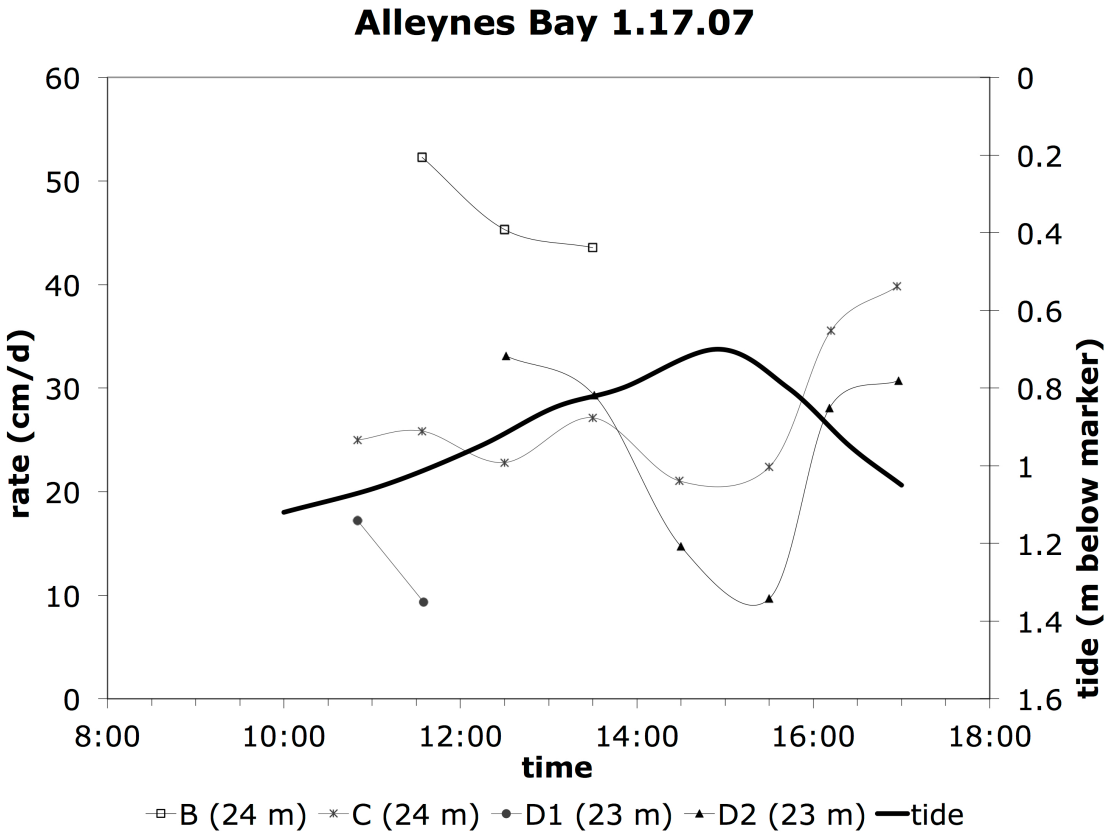

Figure 3.10: Time series at Alleynes Bay (1/17/06). Tide (thick black line) and SGD at four seepage meters.

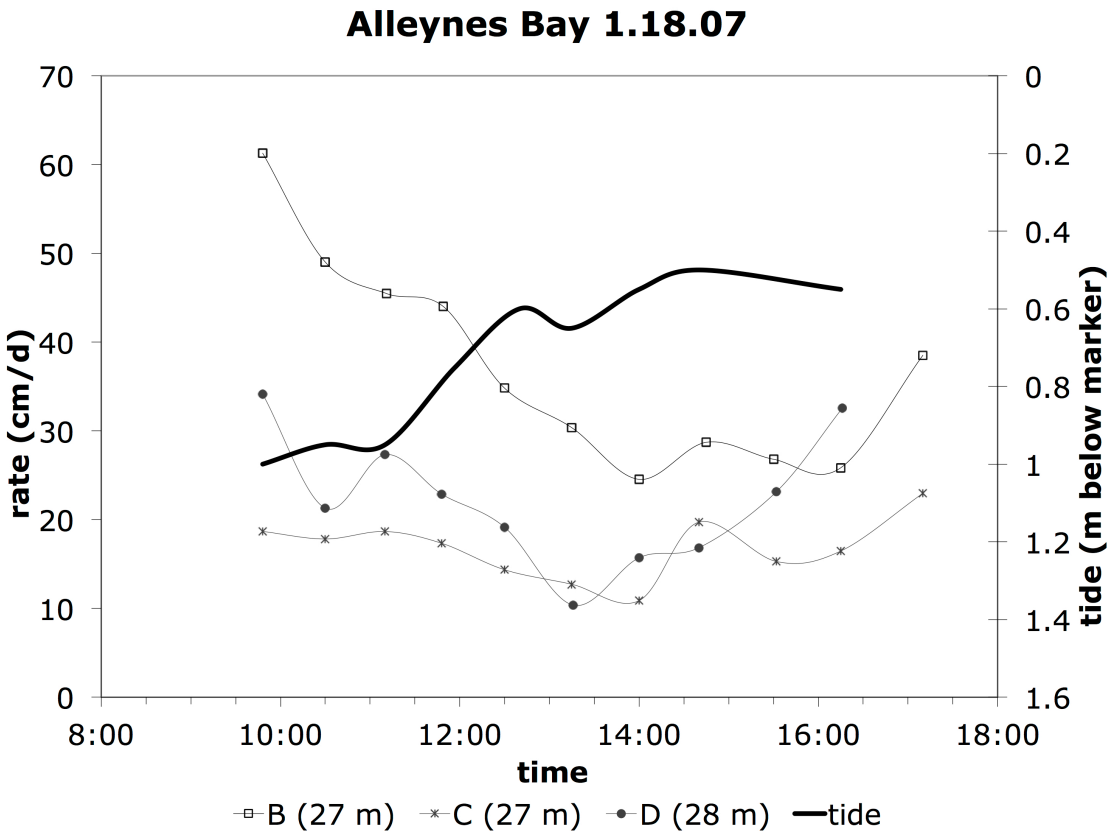

Figure 3.11: Time Series at Alleynes Bay (1/18/07). Tide (thick black line) and SGD at three seepage meters.

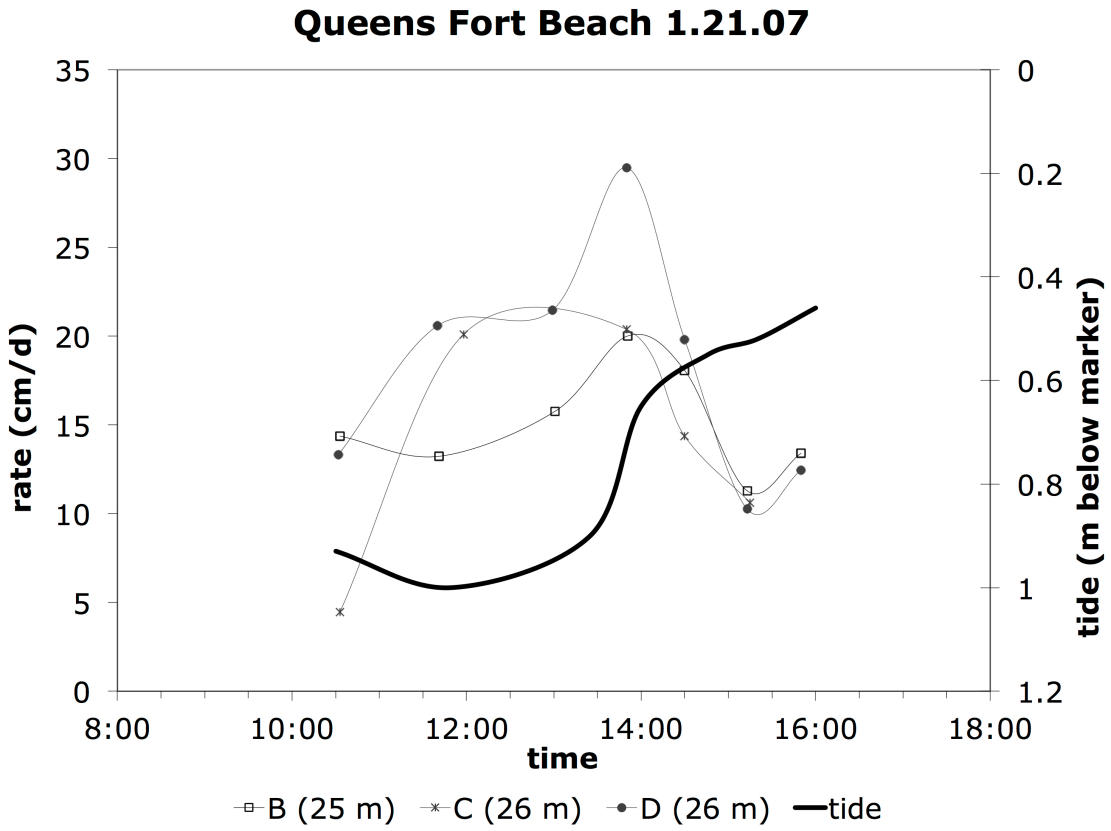

Figure 3.12: Time Series at Queens Fort Beach (1/21/07). Tide (thick black line) and SGD at four seepage meters.

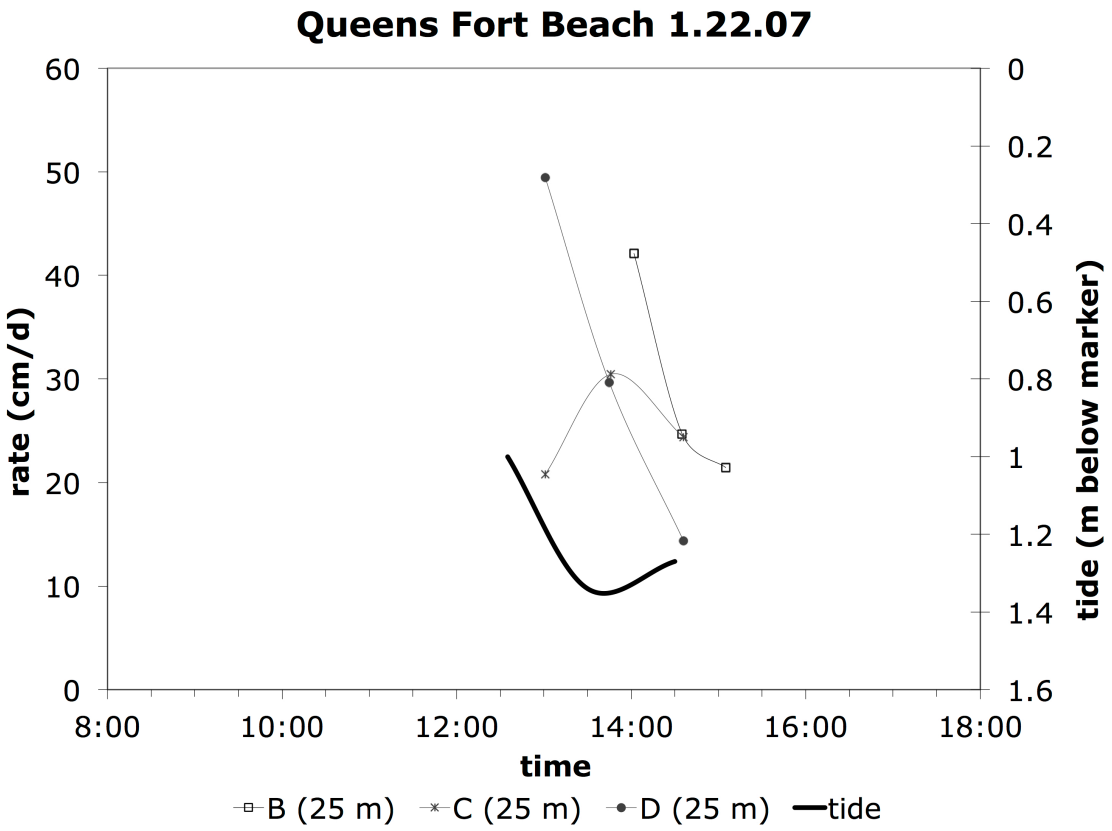

Figure 3.13: Time series at Queens Fort Beach (1/22/07). Tide (thick black line) and SGD at four seepage meters.

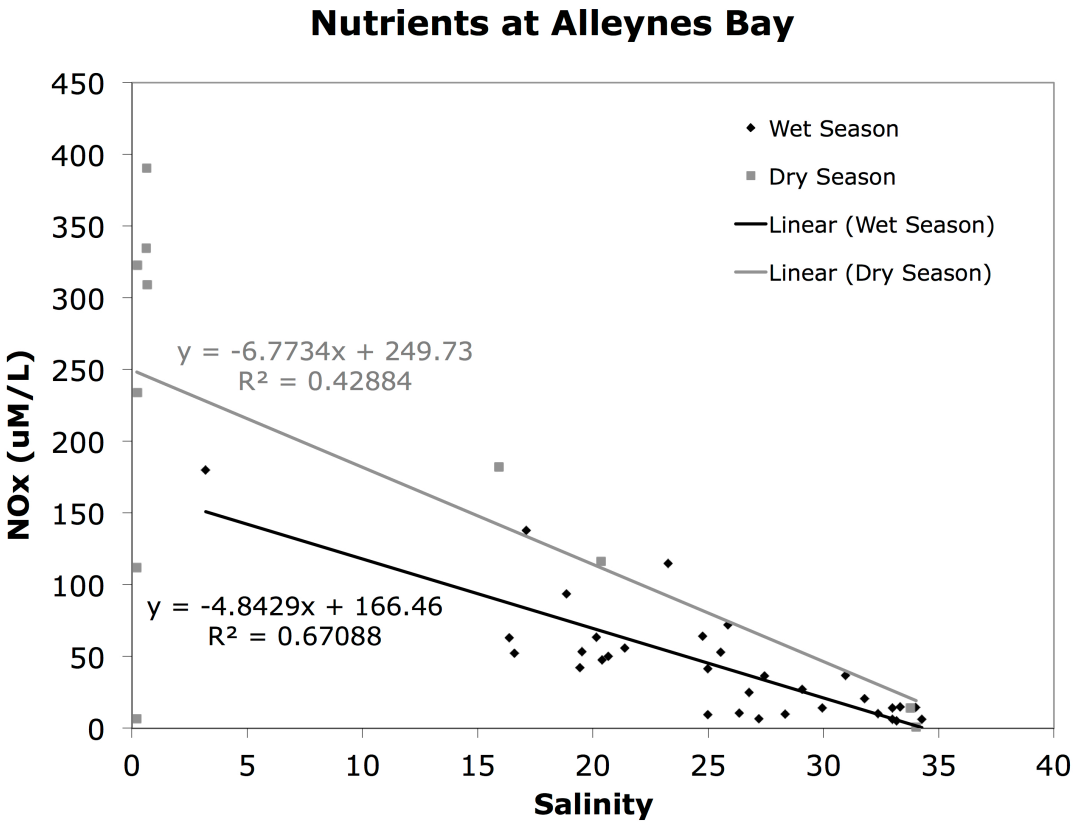

Figure 3.14. Nutrients at Alleynes Bay. Salinity vs. NOx samples for wet season (black diamonds) and dry season (gray squares). Linear trend line equations and R-squared values are included.

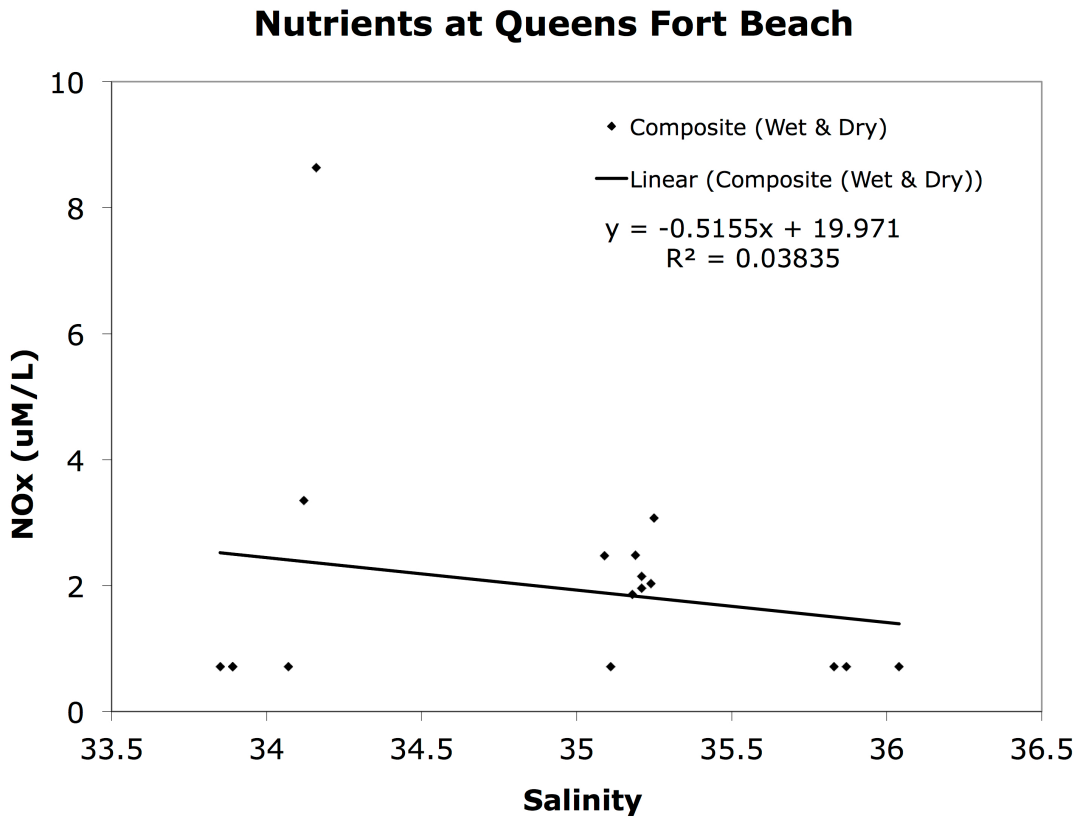

Figure 3.15. Nutrients at Queens Fort Beach. Composite of wet and dry samples, almost entirely below detection (7 µM/L), linear equation and R-squared value.

Tables

Table 3-1. Grain size results for Alleynes Bay and Queens Fort Beach.

Site	**Graphic Mean (φ)**	**Sorting (φ)**	**Skew**
Alleynes Bay Swash Zone	1.37	.62	-0.05
Alleynes Bay Back Beach	1.36	.59	0.08
Queens Fort Beach Swash Zone	1.81	.53	0.14
Queens Fort Beach Back Beach	1.73	.51	-0.57

Chapter 4 Guam

Introduction

Guam is a 544 km^2 island in the western Pacific Ocean and it consists of two geologically disparate terrains: a gently sloping limestone plateau interspersed with three volcanic hills in the north and a predominantly volcanic mountainous region fringed by limestone plains in the south (Ward *et al*., 1965). Rainfall amounts up to 2500 mm/y near the coast and in excess of 2800 mm/y upland (Lander and Guard, 2003). The high permeability of the northern region leads to high rates of recharge 67% (Jocson *et al.* 2002). The southern volcanic region is much less permeable and most rainfall contributes to surface flows (Ward *et al*., 1965). A water budget for the northern part of the island estimated SGD to contribute a flux of groundwater of 6.8 m^3 m^{-1} d^{-1} to the coastal ocean (Matson, 1993). This represents 40% of the river discharge for the whole island, but because the river discharge is primarily located on the southern end of Guam, SGD on the northern part is the predominant terrestrial influence on the coastal water. The sites representative of the northern region were located Tumon Bay, a partially closed embayment in the northern region of the island, exchange with the open ocean is limited by a fringing reef stretching from the western peninsula to the eastern boundary of the bay (Burdick, 2006).

Guam is home to over 170,000 residents, and the island is visited by over one million tourists annually. The economy primarily relies on tourism, U.S. military spending, and exportation of fish and hand-made crafts. Tourism and the military have high demand for fresh water and both the tourism and the fisheries depend upon the quality of the coastal water. Tumon Bay is the center of Guam's tourism industry, providing prime waterfront property for a number of first-class hotels. Tracking the growth and development of Tumon Bay is the increasing presence of a benthic filamentous green alga, *Enteromorpha clathrata* (Denton *et al*., 2005). In order to keep the aesthetic of Tumon Bay, hotels invest in daily removal of the algae from the beaches (FitzGerald, 1978). Groundwater, reaching the bay as SGD, has been implicated among the sources of nutrients fueling the algal growth, and characterization of the patterns of discharge is an important step towards determining the best management practices for Tumon Bay.

Methods

Direct measurements of submarine groundwater discharge were made at three sections of the shoreline around Guam between November 11 and November 18, 2008 (Figure 4.1). During this period, four sites were sampled in Tumon Bay and two sites were sampled in southern Guam.

Measurements were made using Lee-type seepage meters (method previously described in Chapter 1). A Schlumberger CTD-Diver pressure sensor (model DI261: 10m/80 mS/cm) was attached to a seepage meter to record changes in water level. Average SGD reported are those derived by the ellipse fit method described in Chapter 1, except where noted.

Salinity was determined using a YSI 556 MPS, a multi-probe system which can simultaneously measure dissolved oxygen, conductivity, temperature, pH and oxygen reduction potential. Samples for nutrient analysis were collected in 25 mL acid-washed plastic bottles and frozen for transport and storage. For inorganic nitrogen, freezing prior to filtration is adequate for preserving field concentrations (Dore *et al*., 1996). Nutrients were analyzed by the Woods Hole Oceanographic Institution using a Lachat QuickChem 8000 nutrient auto-analyzer. The freshwater component of the SGD was calculated using Equation 1.6.

Data was analyzed using MATLAB (ver. R2012a) for coefficient of correlation determination. Coefficients of correlation (R) and significance (p) were calculated to determine the connections between average high flow rate, peak high flow rate, average flow rate, flow rate range and freshwater component among all samples in Tumon Bay. Average high flow rate was calculated as the average flow for the hour surrounding low tide or, for days when low tide was not captured, the average seepage for the two consecutive measurements nearest low tide. Peak high flow rate is the highest discharge rate measured for each device. Average flow rate is the average determined by fitting an ellipse to simultaneous pairings of tidal elevation and SGD, the SGD-coordinate of the center of the ellipse was taken as the average SGD. BIOMstat Statistical Analysis for Biologists (ver. 3.30o; Applied BioStatistics Inc.) was used for the analysis of covariation with ancova statistics.

Results

Tumon Bay

Tumon Bay was sampled in four different locations over five days: south, central, north-central, and north (Figure 4.1). At each site, four devices were deployed for a total of 20 samples.

South Tumon was sampled November 11, 2008 with four devices installed parallel to shore, 18 m from the shoreline and spaced 35 m apart (Figure 4.2), which were all sampled for

eight hours. SGD ranged between 14 and 119 cm/d. Three of the devices (B, C and D) recorded measurements between 14 and 44 cm/d, and only one device (A) recorded measurements in excess of 100 cm/d (Table 4-1). Average SGD was determined by fitting an ellipse to the hysteresis loops. Although the scatter was fairly large, ellipses showed moderate discharge for devices B, C and D, and high flow for device A (Table 4-1). All four devices showed an inverse relationship with the tide (Figure 4.3 and Figure 4.4A-D). Salinities decreased in all devices, though the effect was most pronounced in the high flow device (A) (Figure 4.5). The devices with moderate flow (B, C and D) also had a moderate freshwater component ranging from 17% to 19% (Table 4-1). A high flow device (A) recorded a much higher freshwater component (66%). The average of all SGD samples had 32 μM nitrogen as nitrate plus nitrite (NO_x) and 8 μM silicate. Also present at this site during low tide were visually discernable seeps above the water line where groundwater was freely flowing (similar in appearance to those found in Barbados at Alleynes Bay; Chapter 3, Figure 3.4). This direct seep had an average salinity of 4.22 and a freshwater component of 87%. The direct seep had 44 μM NO_x and 7 μM silicate. There is an inverse relationship between salinity and NO_x (R-squared 0.61; Figure 4.6) and no significant relationship between salinity and silicate (R-squared 0.02; Figure 4.7).

Central Tumon was sampled on November 13, 2008 and November 18, 2008. On November 13, four devices were installed for six to eight hours perpendicular to shore (Figure 4.8; device C was installed for six hours, the other three for eight) to determine shore normal variability. SGD ranged between 0 and 143 cm/d and average SGD at each device ranged from 16 to 76 cm/d (Table 4-1; Figure 4.9). One device (D) showed SGD in excess of 100 cm/d indicative of a high discharge anomaly. Figure 4.10A-D show ellipse fits for all devices. Average ambient salinity was 33.67 (Figure 4.11) and the freshwater component ranged between 5% and 60% (Table 4-1). The lowest freshwater component was recorded in the device that also recorded the lowest range in SGD (C1; ranging 8 to 26 cm/d). Samples had an average of 26 μM NO_x and 3 μM silicate. There was an inverse linear relationship between salinity and NO_x (R-squared 0.70 Figure 4.12) and an inverse linear relationship between salinity and silicate (R-squared 0.69; Figure 4.13).

On November 18, four devices were installed for seven hours in a tight cluster (Figure 4.8) to determine fine-scale spatial variability. SGD ranged between 19 and 111 cm/d. Average SGD at each device ranged from 35 to 76 cm/d. Two devices (A2, B2) showed SGD in excess of 100 cm/d and could be classified as high discharge anomalies. Two devices showed an inverse relationship with the tide (C2 and D2) and two (A2 and B2) showed a direct relationship with the tide (increasing seepage with increasing water height) (Figure 4.14). Figure 4.15A-D show ellipse fits for all devices. Average ambient salinity was 34.16 for November 18 (Figure 4.16). Freshwater component ranged between 5% and 46% (Table 4-1). The lowest freshwater component was recorded in the device that also recorded the lowest range in SGD (C1; ranging 8 to 26 cm/d). Samples had an average of 13 μM NO_x and 11 μM silicate. There was a weak

inverse linear relationship between salinity and NO_x (R-squared 0.47; Figure 4.17) and an inverse linear relationship between salinity and silicate (R-squared 0.90; Figure 4.18).

North-Central Tumon was sampled for 8 hours on November 12, 2008 with four devices installed parallel to shore 9 m from the shoreline and 48 m apart (Figure 4.19). Device A was installed within the extent of a perceptible submerged spring of cold water that could be felt coming up through the sediment. The sediment within the spring appeared to be finer than the neighboring sediment, and small black snails were seen concentrated within the vicinity of device A. SGD ranged between 8 and 246 cm/d. Three devices (A, B and C) recorded SGD in excess of 100 cm/d (average SGD for these three ranged from 73 to 147 cm/d) (Figure 4.20). Device A recorded a maximum flow of 246 cm/d, the highest flow recorded in this study, this device also had the highest average SGD of 147 cm/d (ranging from 65 to 246 cm/d). Three of the devices (A, B and D) showed an inverse relationship with the tide. Device C showed no trend with the tide despite a range of SGD from 23 to 153 cm/d. Figure 4.21A-D show the ellipse fits for the four devices. Average ambient salinity was 33.90. The freshwater component at this location ranged from 9% to 90%. The highest freshwater component was found in the cold-water spring at device A. The lowest freshwater component was found in device C despite high flow rates; this was also the device unmodulated by the tide (Figure 4.22). Samples had an average of 34 μM NO_x and 6 μM silicate. There was an inverse linear relationship between salinity and NO_x (R-squared 0.77; Figure 4.23) and no significant relationship between salinity and silicate (R-squared 0.15; Figure 4.24).

North Tumon was sampled for 7 hours on November 17, 2008 with four devices parallel to shore 13 m from the shoreline (Figure 4.25). SGD ranged between 6 and 160 cm/d. Three devices (B, C and D) recorded flow in excess of 100 cm/d. Average discharge for these three devices was between 71 and 80 cm/d (Table 4-1). The third device (A) had an average discharge of 35 cm/d ranging between 12 and 63 cm/d. All four devices showed an inverse relationship with the tide (Figure 4.26). Figure 4.27A-D show the ellipse fits for all four devices. Average ambient salinity is 31.85. Freshwater trends are shown in Figure 4.28. The freshwater component ranged from 31% to 74%. The lowest freshwater component was in device A, which had the smallest range of SGD. The highest freshwater component was in device B, which recorded a maximum flow of 160 cm/d and a minimum of 6 cm/d (Table 4-1). Samples had an average of 34 μM NO_x and 11 μM silicate. There was a weak inverse linear relationship between salinity and NO_x (R-squared 0.21; Figure 4.29) and no significant relationship between salinity and silicate (R-squared 0.04; Figure 4.30).

Sites in Tumon Bay showed substantial freshening. Based on the salinity measurements (Table 4-1), the freshwater component ranged from 5% to 90% with an average of 39%. Pooling together all of the Tumon Bay NO_x data, there is an inverse linear relationship between salinity and NO_x (R-squared 0.64), which determines a freshwater end-member with 70 μM nitrogen as nitrate plus nitrite (Figure 4.31).

In an attempt to calculate an integrated discharge per meter of shoreline, the integrated exponential decrease from shore as described in Equation 1.8 was used. As described earlier in Chapter 3, this expedient allowed an integrated SGD per meter of shoreline to be calculated without an arbitrary assumption concerning the width of the seepage face; however, to obtain a reasonable exponential fit, some anomalous outliers of high SGD were removed from the data. These outliers were then added back into the calculated flux as a percentage of the transect data that were judged o show anomalous values multiplied by the average SGD calculated for the anomalous data alone. Three devices in Central Tumon in the shore-normal transect (November 13) can be used to represent a decreasing SGD which gives a total integrated flux of 18.8 m^3 per meter of shoreline per day. This curve fitting seemed to give a reasonable approximation of background seepage decreasing offshore. However, outliers above this curve needed to be incorporated into the total discharge separately. These high SGD "anomalies" were classified separately according to the percentage of devices that fall off the fitted exponential approximation. The background seepage showed an average freshwater component (31%) means that there is a volume of 5.9 m^3 per meter of shoreline per day of freshwater discharged into Tumon Bay.

Of the twenty seepage devices, ten were judged to be outliers in which SGD exceeded 100 cm/d. Because the devices were randomly placed, this would indicate that 50% of the bay floor might contain high flow anomalies. Arithmetic average discharge for the high flow anomalies is 80 cm/d, which yields a total flux of 400 m^3 per meter of shoreline with the equation:

$$Flux = D * L \qquad [4.1]$$

where D is the measured discharge rate and L is the width of Tumon Bay, 500 m. Using the linear relationship between flow rate and freshwater component, discharge at 80 cm/d should have a freshwater component of 55%, which would give a freshwater flux of 222 m^3 per meter of shoreline per day.

An "integrated" flux proportionally combines the average anomaly discharge with the more traditional exponential integrated flux. Using the 50/50 split between anomalous and non-anomalous, the daily flux is 114 m^3 per meter of shoreline.

Coefficients of correlation (R) and significance (p) were calculated to search for correlation among average high flow rate, peak high flow rate, average flow rate, flow rate range and freshwater component among all samples in Tumon Bay. Average and peak high flow rates, average flow rate and flow rate range were all significantly correlated with the freshwater component (Table 4-1). The best predictor of freshwater was found to be the average high flow rates with a correlation coefficient of 0.83 ($p = 7.1 \times 10^{-6}$)

To determine whether there is any variation with North-South location within Tumon Bay, an analysis of covariance was conducted using location, distance from shore and average flow rate (as determined by ellipse fitting, as described in the methods). Location was coded from 1 to 4 by site with 1 being the southernmost site and 4 being the northernmost site. The analysis of covariance did not find any North-South trend (P = 0.76).

Tumon Bay Seiche

The presence of higher frequency fluctuations in discharge present in seventeen of the twenty seepage meters deployed in Tumon Bay is an unexpected phenomenon that cannot be accounted for by tidal variations (e.g. Figure 4.3). These short-term fluctuations were spread about 66 minutes apart, about equal to the sampling interval. The average amplitude of these SGD fluctuations is 26 cm/d and reached a maximum of 87 cm/d. The average amplitude of the discharge fluctuations is 45% of the average discharge, indicating there is an additional non-negligible force acting on the hydrologic system driving SGD. One possible explanation is the influence of a seiche within Tumon Bay.

Submarine groundwater discharge rates are determined by the hydraulic gradient between the sea surface and the water table or confining unit hydraulic head. This gradient can vary on a wide spectrum of time scales, from seasonal influences (months), documented by many researchers (*e.g.* Michael *et al*., 2005), tidal influences (diurnal, semi-diurnal), also documented by many researchers (*e.g.* Taniguchi, 2002), to short-term (<30 min) seiche effects. The short-term variability of groundwater discharge as a result of seiching has been documented within lakes and the marine environment. Taniguchi and Fukuo (1996) used numerical analyses and automated seepage meters to connect groundwater flow and seiche in Lake Biwa, Japan. Rosenberry *et al*. (2013) found seiche-induced fluctuations in groundwater discharge in the Great Salt Lake, Utah, and also suggested that it enhanced selenium and mercury flux from the sediments. Artifacts due to seiching have also been suggested within the marine environment. A study in Brazil showed a seiche period of 10 to 20 minutes corresponded to modulated SGD (Bokuniewicz *et al*., 2004). A study in Mallorca found evidence for nutrient fluxes and changes in plankton community structure as a result of seiche-induced variability in groundwater discharge (Basterretxea *et al.*, 2011). There has been no previous identification of groundwater discharge influences by seiching within Tumon Bay.

Tumon bay is at least partially enclosed by a fringing reef. A seiche in a closed bay has a period *T*:

$$T = \frac{2L}{\sqrt{gD}} \qquad [6.1]$$

where L is the length of the bay, g is the gravitational acceleration and D is the depth of the bay. The depth of the bay was estimated to be 2 m. Across the length of Tumon Bay, 2,650 m (Figure 4.32), the seiche period would be 20 minutes and the width of the bay, 500 m (Figure 4.32), would yield a seiche period of 4 minutes. It is possible that the bay behaves as an open bay, in which case the seiche periods would be

$$T = \frac{4L}{\sqrt{gD}} \qquad [6.2]$$

or 40 minutes longitudinally and 8 minutes across the bay. To examine the theory that a seiche is present within Tumon Bay, I compared the period of the groundwater data, the periods expected from the equation for a closed bay seiche and periods determined from a spectral analysis of the pressure sensor data.

To search for these periods in the actual water level changes in the bay, five days of data from the pressure sensor were aggregated and adjusted for differences in installation depth. Each sequential record was normalized to start at the level the previous record had ended on. The data was then analyzed in Matlab with the spectrum.m function to calculate the spectrum using Fast Fourier Transforms. Spectral analysis revealed two peaks of energy within the range of frequencies corresponding to the calculated seiche periods (Figure 4.33). The period of the first peak is 14 minutes, it ranges between 7 and 23 minutes and it is marginally significant. The second peak has a period of 4 minutes, ranges between 3 and 7 minutes, and is highly significant. Surface wind waves were also detected at periods of 7 seconds and 12 seconds.

The presence of periods in the spectral analysis that match well with calculated seiche periods for a closed embayment but not as well for the open embayment suggest that the force driving the changes in SGD is related to a closed bay seiche effect. The periods from the calculations and spectral analysis were much shorter than the 66-minute periodicity seen within the field measurements, however, the sampling rate for the field measurements were made approximately 30 minutes apart, or with a frequency of 0.5 mHz. The Nyquist rate for the highest frequency seiche is 8 mHz, and the Nyquist rate for the low frequency seiche is 2 mHz, both of which are much larger than the frequency of the SGD sampling, indicating that there is substantial aliasing of the field data. However, in any particular sampling interval the integration of seiche sycles might include more (or fewer) episodes of high (or low) SGD driven by the variations in hydraulic head.

The next question that arises is whether a seiche can drive the scale of changes in seen in SGD fluxes. As mentioned earlier, the average amplitude of the SGD fluctuations is 26 cm/d and reached a maximum of 87 cm/d. Visual inspection of the tidal record suggests that the amplitude of the seiche is approximately 10 cm. Using the ellipse plot, it is possible to evaluate the magnitude to which a change in water level affects a change in SGD. The site in the south of Tumon Bay sampled on November 11th showed one device (A) with the characteristic high frequency variability in SGD (Figure 4.3), of which, the largest variation was 39 cm/d. Using a

seiche amplitude of 10 cm, the ellipse for that SGD series shows a corresponding change of up to 70 cm/d (Figure 4.34). The observed changes in SGD fit reasonably well within the possible range of SGD deviations corresponding to a 10 cm change in water level using the ellipses. It is difficult to more rigorously compare the measured variability with expected variability due to the aliasing of the seepage meter measurements, which may affect the apparent amplitude in the measured record.

Southern Guam

Two sites were visited on the southern area of Guam: South-East Pacific and Nimitz Bay (Figure 4.1). At each site four devices were installed.

The South-East Pacific site was sampled on November 15, 2008 for between 3.5 and 6.5 hours with four devices installed parallel to shore 8 m from the shoreline and with an average spacing of 35 m (B, C and D were sampled 6.5 hours; A was disturbed by a beach-goer and removed after 3.5 hours; Figure 4.35). SGD ranged between 0 and 36 cm/d. Average discharge for the four devices was between 4 and 23 cm/d (Table 4-3). All four devices also showed an inverse relationship with the tide, as well as the shorter-term variability indicative of a seiche (Figure 4.36). Figure 4.37A-C show ellipse fits for three of the four devices (B-D), for device A, the ellipse fit script assigned an ellipse that did not visually fit the data points and provided an average SGD far in excess of any recorded measurements for that device (ellipse average of 58; range of SGD 1-23 cm/d). Ambient salinity was 34.75. There was very little change in salinity in any of the devices (Figure 4.38); the average freshwater component is 1%. Samples had an average of 6μM NO_x and 8 μM silicate.

The Nimitz Bay site was sampled on November 16, 2008 for 6.5 hours with four devices installed parallel to shore 18 m from the shoreline and spaced about 19 m apart (Figure 4.39). SGD ranged from 9 to 22 cm/d with averages from 12 to 18 cm/d (Table 4-3). All four devices showed an inverse relationship with the tide and three of the devices (A, B and C) showed clear short-term seiche variability (Figure 4.40). Figure 4.41A-D show ellipse fits for all four devices. Ambient salinity was 34.08. There was very little change in salinity (Figure 4.42); the average freshwater component is 2%. Samples had an average of 4 μM NO_x and 18 μM silicate.

Samples from stations in Southern Guam had no significant trend between salinity and NO_x (R-squared 0.10; Figure 4.43), however there was a marginally significant inverse relationship between salinity and silicate (R-squared 0.47; Figure 4.44).

Discussion

Outside of the anomalously high discharge areas, the discharge freshwater flux was 5.9 m^3 per meter of shoreline per day while the anomalous discharge flux reached 222 m^3 per meter of shoreline per day. Combined, assuming a 50/50 split between spring and non-spring flux, estimated total fresh groundwater discharge to Tumon Bay was 114 m^3 per meter of shoreline per day. This value, however, is two orders of magnitude higher than the previous shoreline estimate of 6.8 m^3 per meter of shoreline per day, and is the same as the highest observed shoreline seep rate of 110 m^3 per meter of shoreline per day for the same study area (Matson, 1993). Net annual recharge for the northern region of Guam is 14 m^3 per meter of shoreline per day (Matson, 1993), which is also much smaller than our estimated fresh groundwater discharge. This may mean that the use of randomly placed seepage meters as representative of general discharge patterns overestimates discharge into Tumon Bay or that the earlier estimates underestimated the importance and distribution of submerged springs. The non-spring discharge flux calculated here (5.9 m^3 per meter of shoreline per day), while high compared to previous estimates of discharge, is close to the integrated flux found in Barbados (6.0 m^3 per meter of shoreline per day; Chapter 3 of this thesis).

The presence of a seiche in Tumon Bay is likely the source of the small-scale variations in discharge observed in Tumon Bay and in the South Guam sites. A recent study in Mallorca, Spain by Basterretxea *et al*., (2011) has shown seiche-induced variability in groundwater discharge has effects on nutrient fluxes and plankton community structure. Seiches increase porewater exchange, increasing nutrient input into the embayment followed by a rapid response in the plankton community (Basterretxea *et al*., 2011). In Tumon Bay, nutrient input *via* groundwater has already been implicated in the pervasiveness of the nuisance algae, *Enteromorpha clathrata*, and further investigation into the groundwater-seiche link is necessary to fully understand the water quality and ecosystem effects.

The driving force for seiching seemed to have persisted for the five days of the experiment. It could have been persistent, diurnal wind patterns or interaction with the ocean tide. Resolution of the driving force was beyond the scope of available data. From the water-level records, the amplitude of the seiche seems to have been about 0.1 m, which translates to a change in SGD of up to 80 cm/d using the ellipse.

Conclusion

Despite uncertainties involved with extrapolations to the entire bay, distinct differences appear in groundwater discharge patterns between the northern and southern portions of Guam. The geological differences between the northern and southern portions of Guam define distinctly different hydrological regimes. In the northern, karstic, region of Guam Tumon Bay spring flow may dominate up to half of the seafloor and freshwater input has a substantial effect, both in reducing salinity and in transporting nutrients, primarily NO_x, into the bay. Sites on Southern Guam in the volcanic terrain showed much lower SGD and the discharged water consists of recirculated seawater. Nutrient transport *via* SGD is low.

References

Basterretxea, G., A. Jordi, E. Garces, S. Angles, A. Rene. 2011. Seiches stimulate transient biogeochemical changes in a microtidal coastal ecosystem. Marine Ecology Progress Series: V423: 15-28.

Bokuniewicz, H, E Kontar, M Rodrigues, DA Klein. 2004. Submarine Groundwater Discharge (SGD) Patterns through a fractured rock: A case study in the Ubatuba, coastal area, Brazil. Asociacion Argentina de Sedimentologia Revista, 11: 9-16.

Burdick, D. 2006. Guam Coastal Atlas. University of Guam Marine Laboratory. Technical Report 114. http://www.guammarinelab.com/coastal.atlas/ (last accessed 5/24/11)

Denton, G.R.W., L.P. Concepcion, H.R. Wood and C.M. Sian Denton. 2005. Nutrient Status of Tumon Bay in Relation to Intertidal Blooms of the Filamentous Green Alga, *Enteromorpha clathrata*. Water and Environmental Research Institute of the Western Pacific, University of Guam. Technical Report No. 110.

Dore, J.E., T. Houlihan, D.V. Hevel, G. Tien, L. Tupas and D.M. Karl. 1996. Freezing as a method of sample preservation for the analysis of dissolved inorganic nutrients in seawater. Marine Chemistry 53: 173-185.

FitzGerald, W.J. 1978. Environmental Parameters Influencing the Growth of *Enteromorpha clathrata* (Roth) J. Ag. In the Intertidal Zone on Guam. Botanica Marina: V21 pp. 207-220.

Jocson, J.M.U., J.W. Jenson and D.N. Contractor. 2002. Recharge and aquifer response: Northern Guam Lens Aquifer, Guam, Mariana Islands. Journal of Hydrology 260: 231-254.

Lander, M.A. and C.P. Guard 1. 2003 Creation of a 50-Year Rainfall Database, Annual Rainfall Climatology, and Annual Rainfall Distribution Map for Guam. Water & Environmental Research Institute of the Western Pacific, University of Guam. Technical Report No. 102.

Matson, E.A. 1993. Nutrient flux through soils and aquifers to the coastal zone of Guam (Mariana Islands). Limnology and Oceanography 38(2), 361-371.

Michael, H.A., A.E. Mulligan and C.F. Harvey. 2005. Seasonal oscillations in water exchange between aquifers and the coastal ocean. Nature. 436(25): 1145-1148.

Rosenberry, D.O., R.W. Sheibley, S.E. Cox, F.W. Simonds and D.L. Naftz. 2013. Temporal variability of exchange between groundwater and surface water based on high-frequency direct measurements of seepage at the sediment-water interface. Water Resources Research. 49: 2975-2986.

Taniguchi, M. 2002. Tidal effects on submarine groundwater discharge into the ocean. Geophysical Research Letters. 29(12): 1561.

Taniguchi, M. and Y. Fukuo. 1996. An effect of seiche on groundwater seepage rate into Lake Biwa, Japan. Water Resources Research 32(2), 333-338.

Ward, P.E., S.H. Hoffard and D.A. Davis. 1965. Hydrology of Guam. Geological Survey Professional Paper 403-H, Washington, H1-H28.

Figures

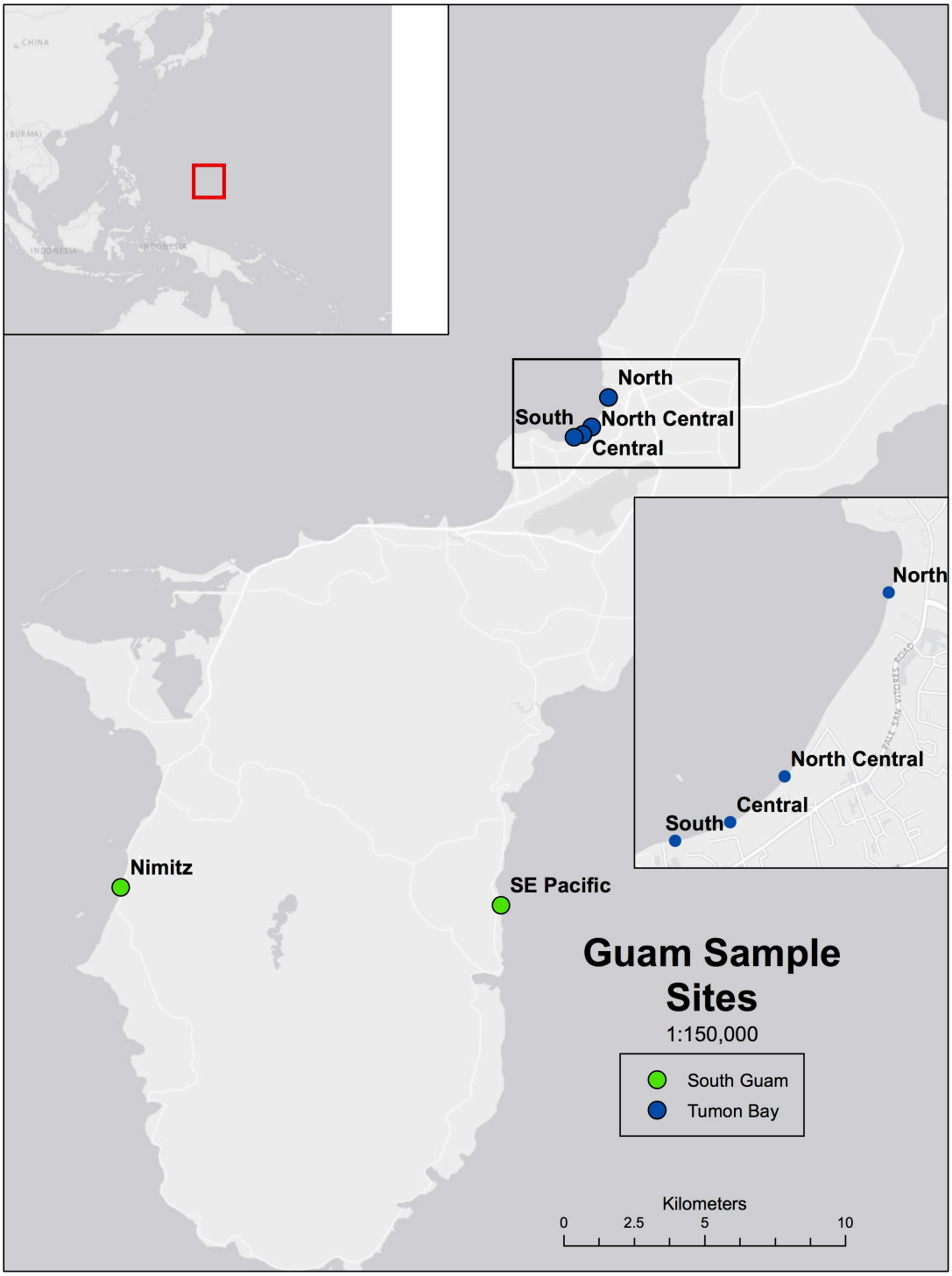

Figure 4.1. Map of field sites. Call out shows four sites (dark blue markers) in Tumon Bay for Northern Guam, Green markers indicate two Southern Guam sites: Nimitz Bay and SE Pacific. Map produced by Michael White SoMAS.

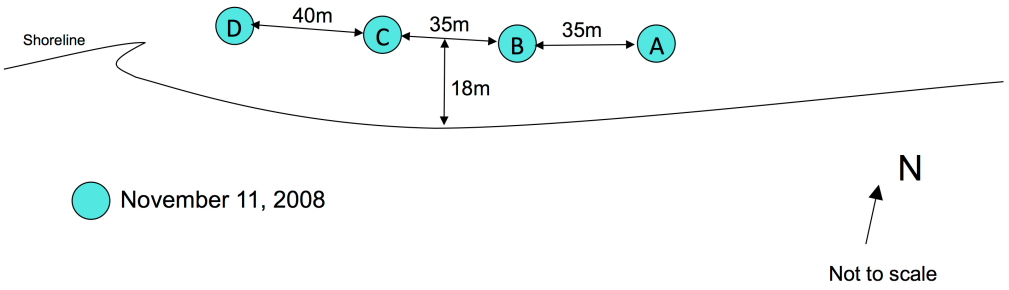

Figure 4.2. Sketch of South Tumon Bay site. Lettered circles represent device locations, solid black line indicates shoreline position and large arrow indicates north. Figure is not to scale.

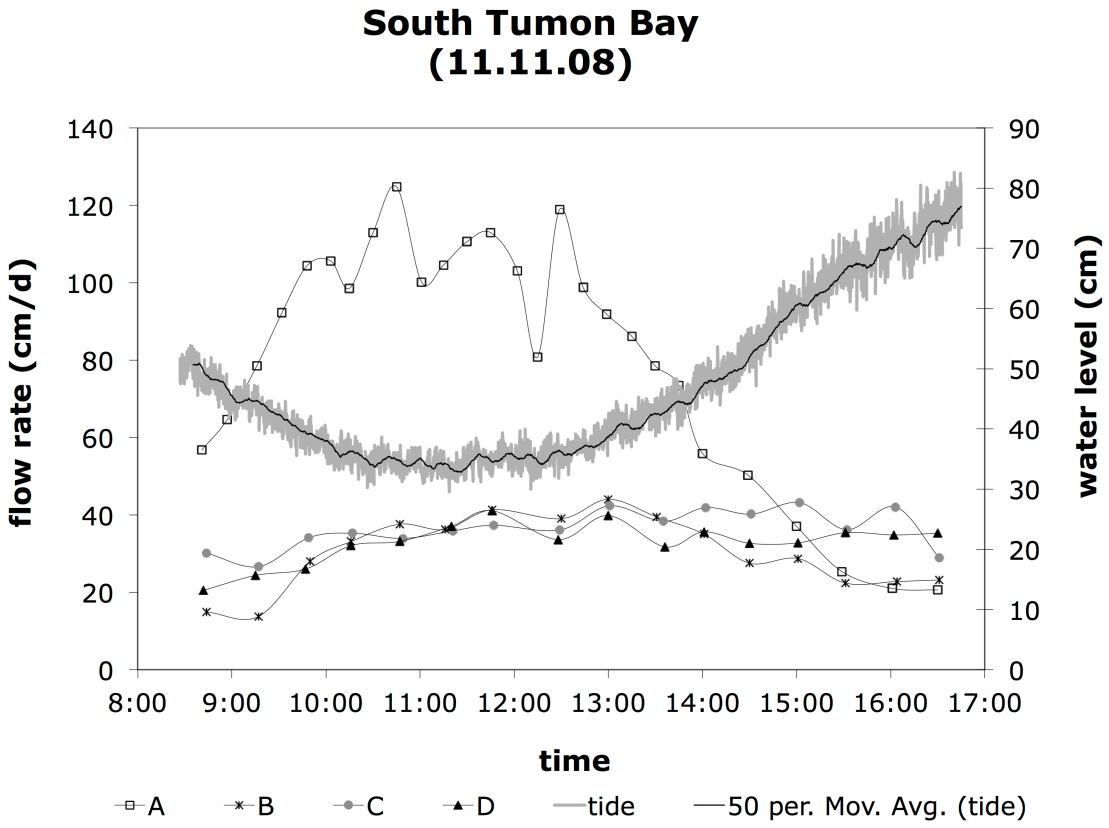

Figure 4.3. SGD results for South Tumon Bay on November 11, 2008: the tide (grey line) is fitted with a 50 point moving average (black line) and four SGD time series, devices A (open squares), B (star), C (gray solid circle), and D (black solid triangle).

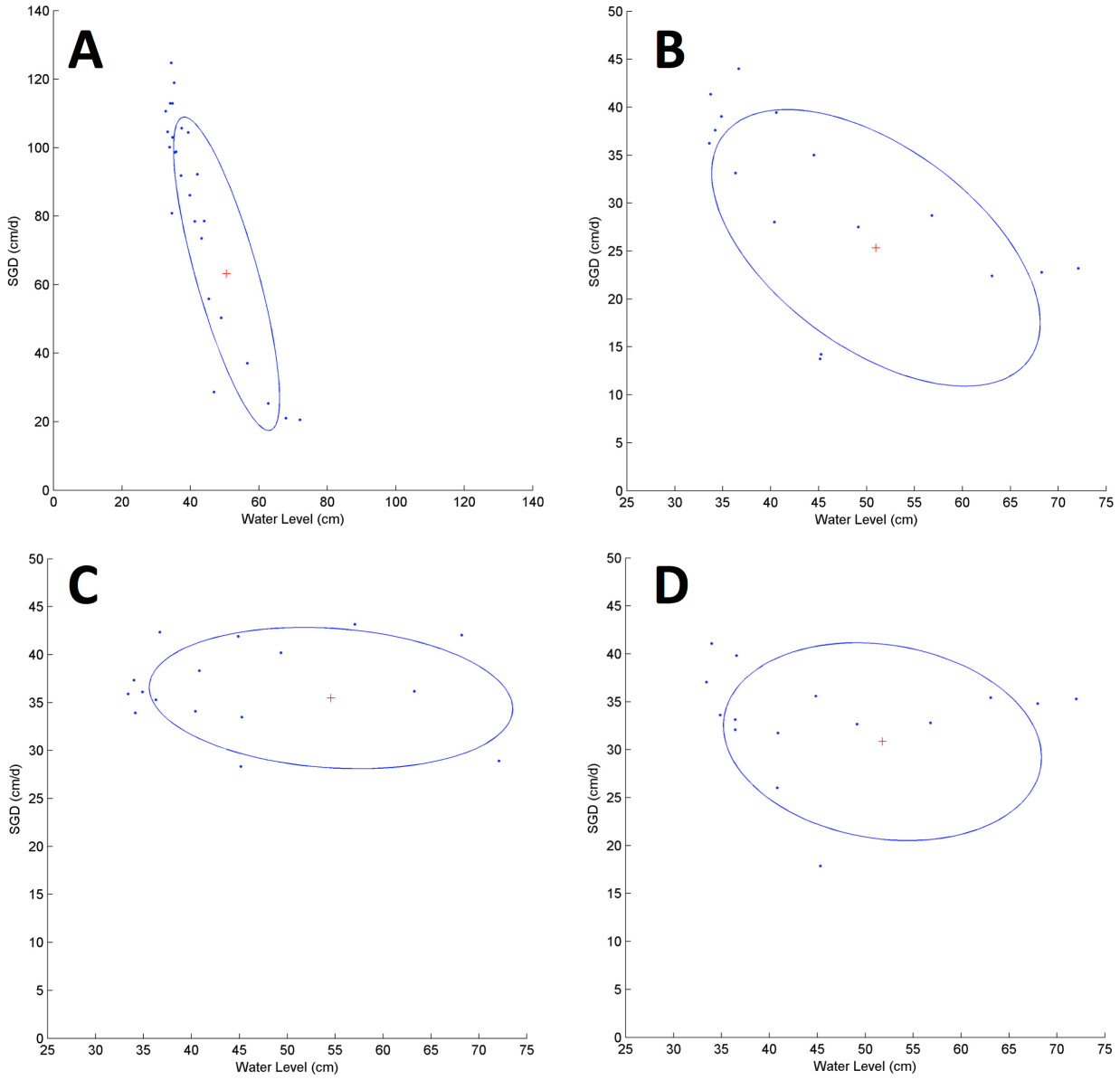

Figure 4.4 A-D. South Tumon ellipse fit for November 11, 2008. Upper left (A) is device A, upper right (B) is device B, lower left (C) is device C and lower right (D) is device D. Blue points are data, blue ellipse is the fit ellipse, and the red cross is the center of the ellipse. Note different axes on subplots.

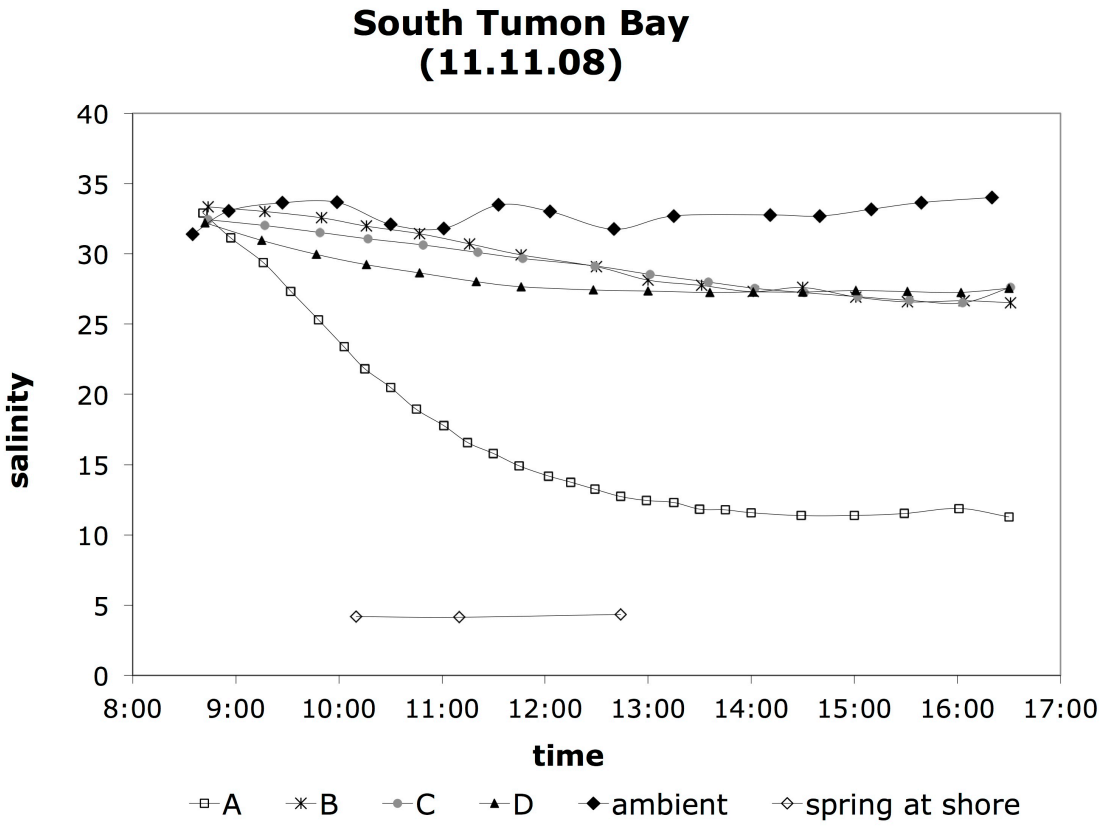

Figure 4.5. Salinity trends at South Tumon Bay for November 11, 2008. Time vs. salinity for devices A (open squares), B (black star), C (solid gray circle), and D (solid black triangle), ambient salinity (solid black diamond) and a spring exposed on the beach face that was directly sampled (open diamond).

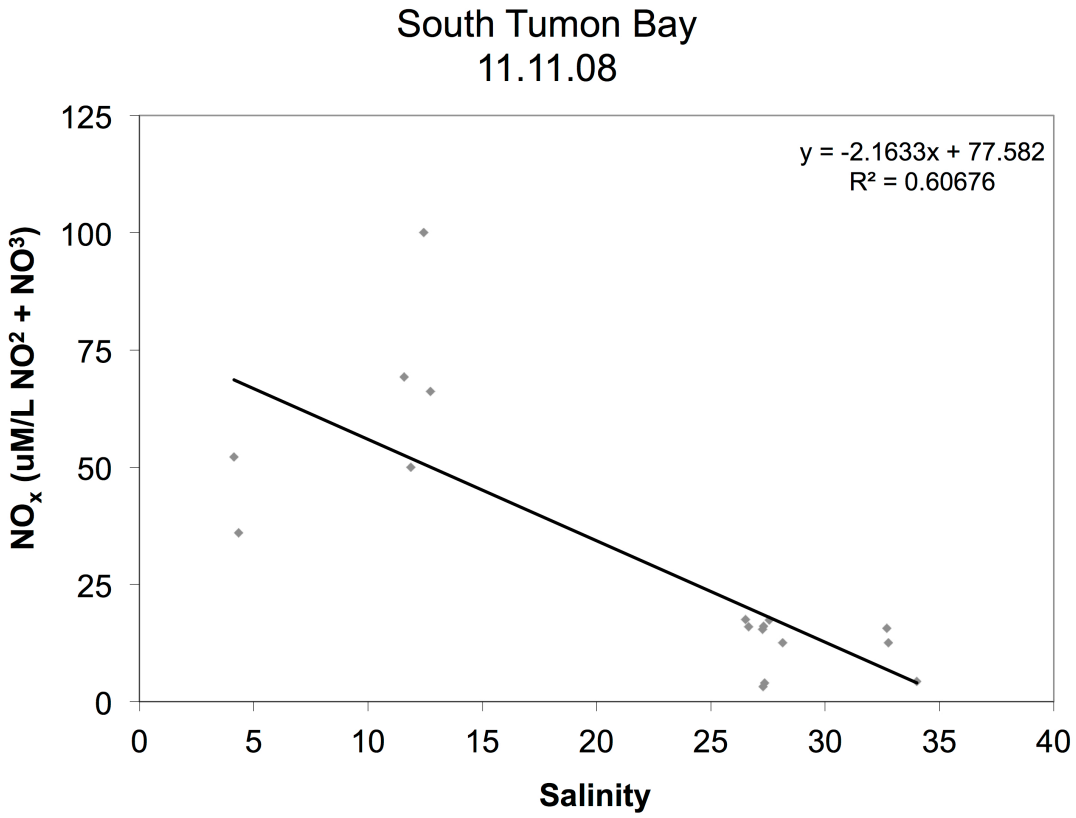

Figure 4.6 Salinity vs. NO_x (solid gray diamonds) at South Tumon Bay on November 11, 2008 fitted with a linear trendline (black line).

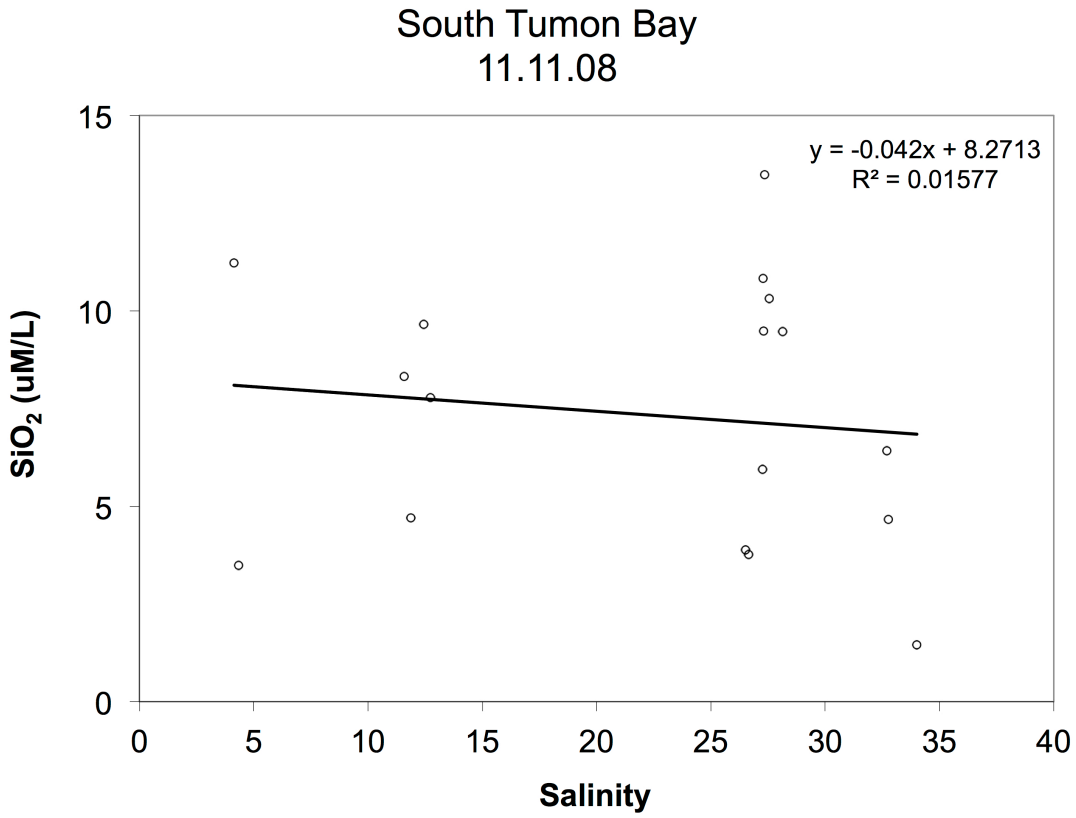

Figure 4.7. Salinity vs. SiO_2 (open circles) at South Tumon Bay on November 11, 2008 fitted with a linear trendline (black line).

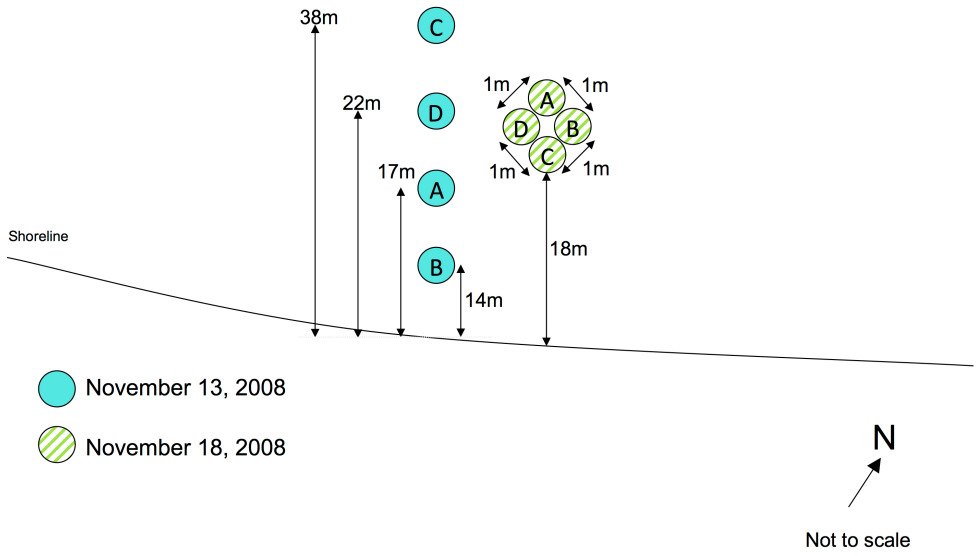

Figure 4.8. Sketch of Central Tumon Bay site. Lettered circles represent device locations (fill patterns indicate different sampling dates), solid black line indicates shoreline position and large arrow indicates north. Figure is not to scale.

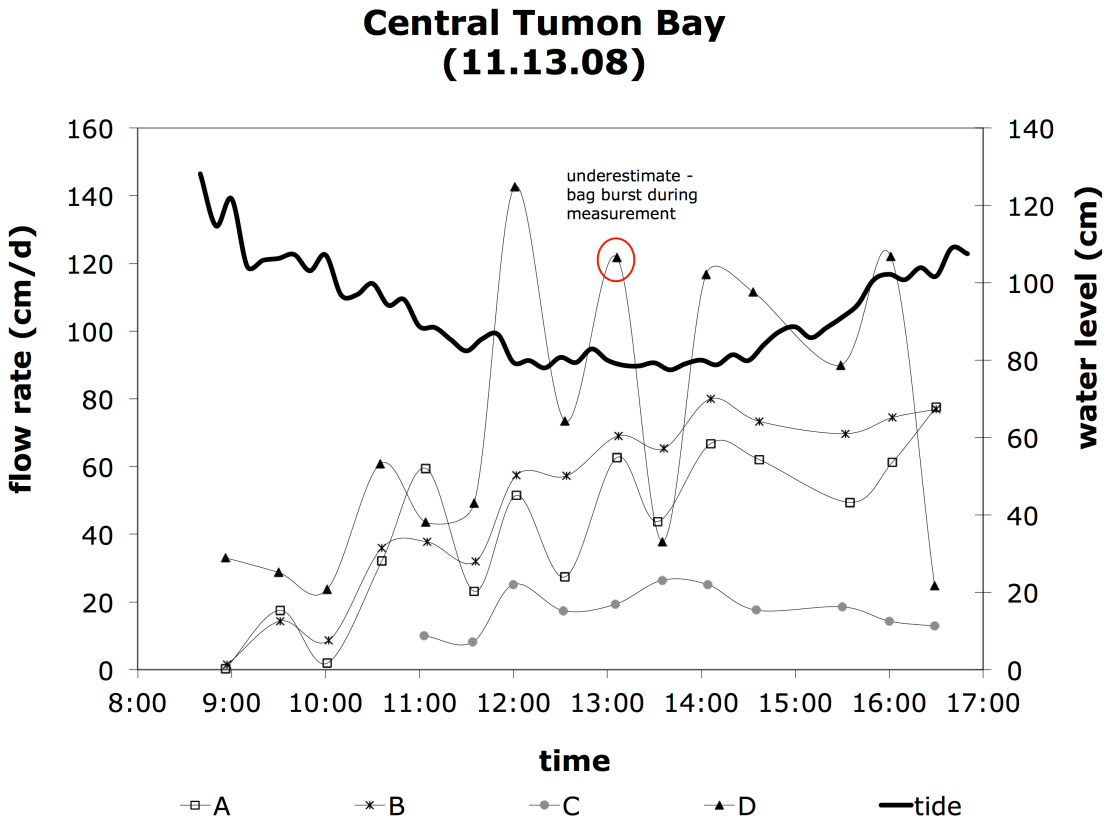

Figure 4.9. SGD results for Central Tumon Bay on November 13, 2008: tide (black line) and four SGD time series, devices A (open squares), B (star), C (gray solid circle), and D (black solid triangle). Note an underestimated measurement on device D as a result of a broken bag during measurement.

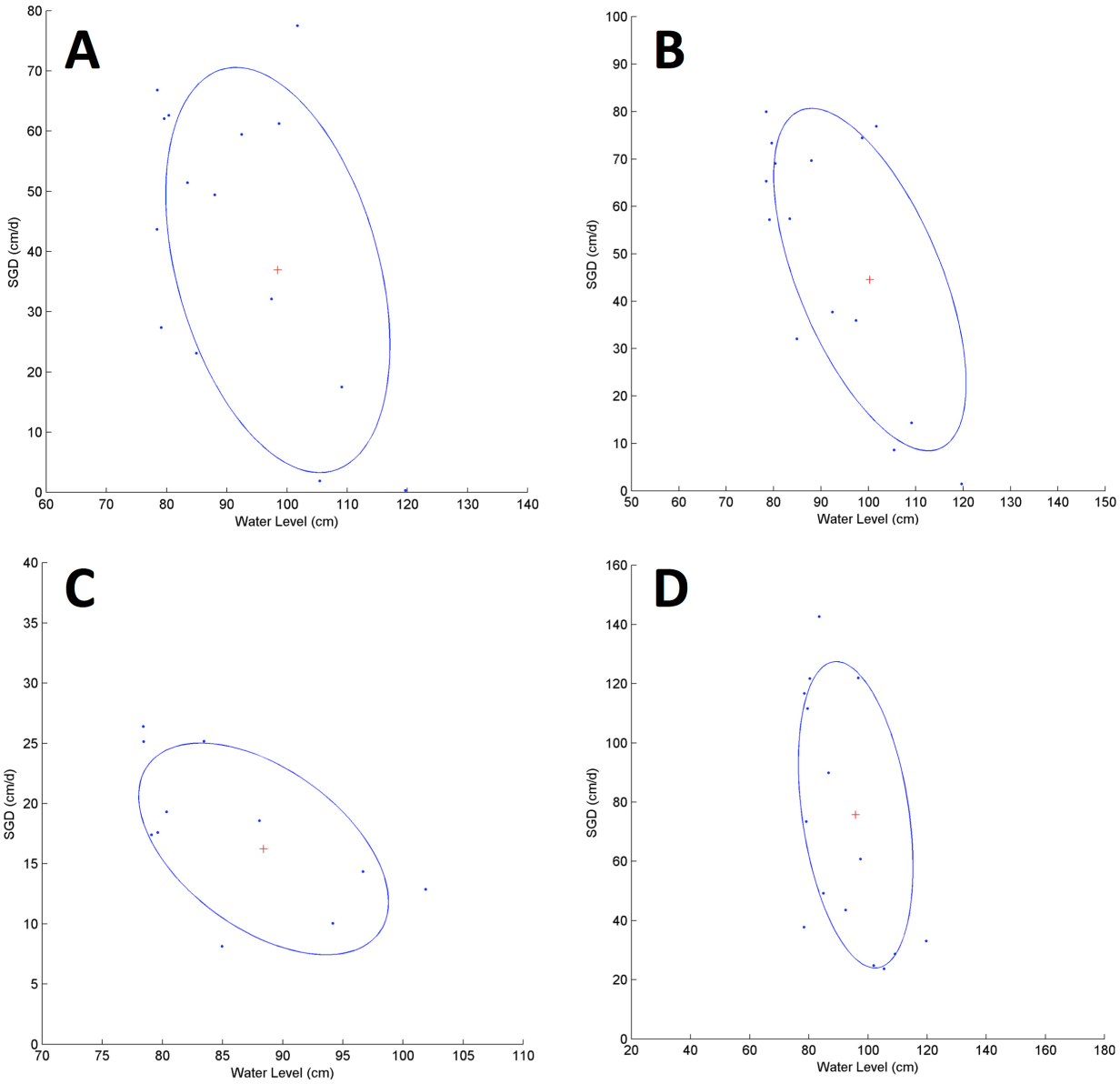

Figure 4.10 A-D. Central Tumon ellipse fit for November 13, 2008. Upper left (A) is device A, upper right (B) is device B, lower left (C) is device C and lower right (D) is device D. Blue points are data, blue ellipse is the fit ellipse, and the red cross is the center of the ellipse. Note different axes on subplots.

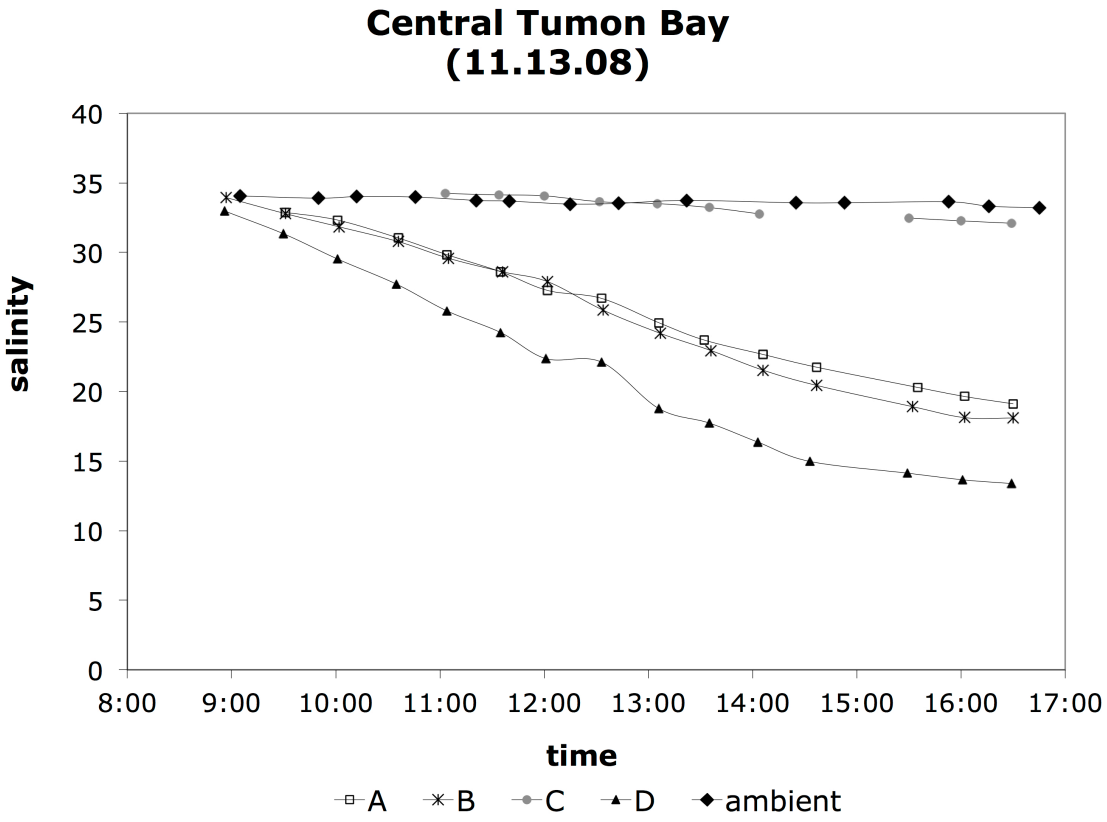

Figure 4.11 Salinity trends at Central Tumon Bay for November 13, 2008. Time vs. salinity for devices A (open squares), B (black star), C (solid gray circle), and D (solid black triangle), ambient salinity (solid black diamond) and a spring exposed on the beach face that was directly sampled (open diamond).

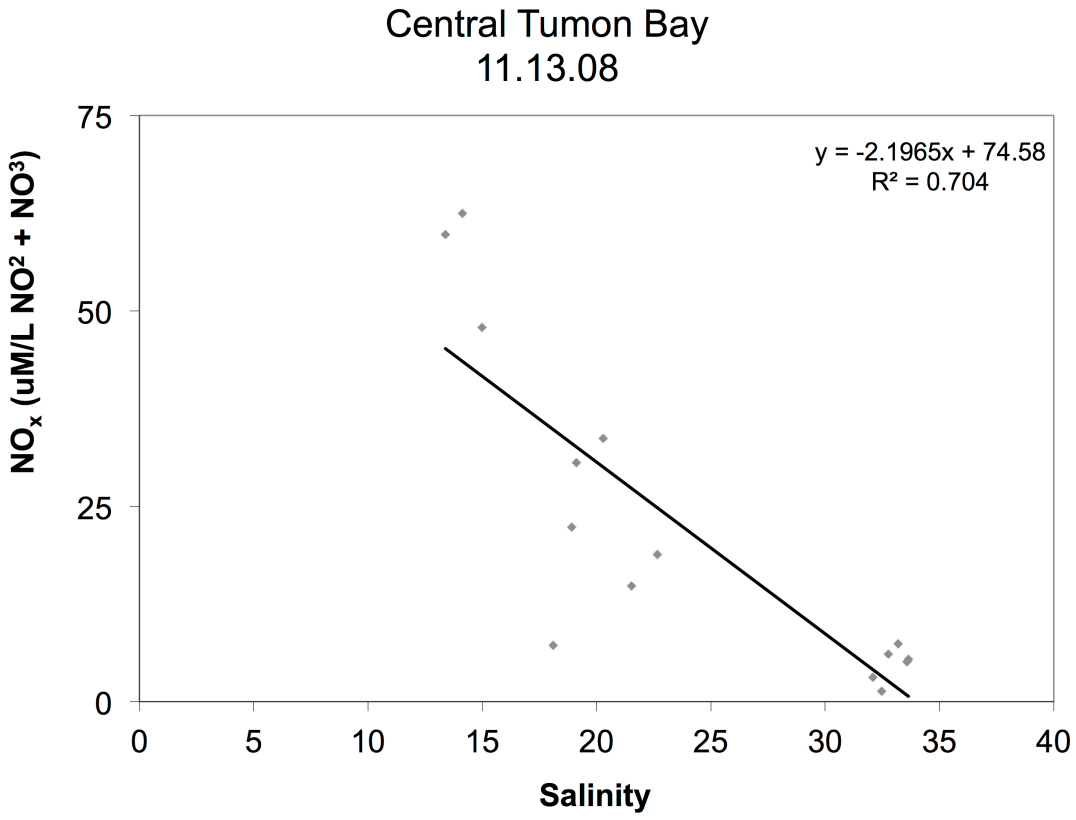

Figure 4.12. Salinity vs. NO_x (solid gray diamonds) at Central Tumon Bay on November 13, 2008 fitted with a linear trendline (black line).

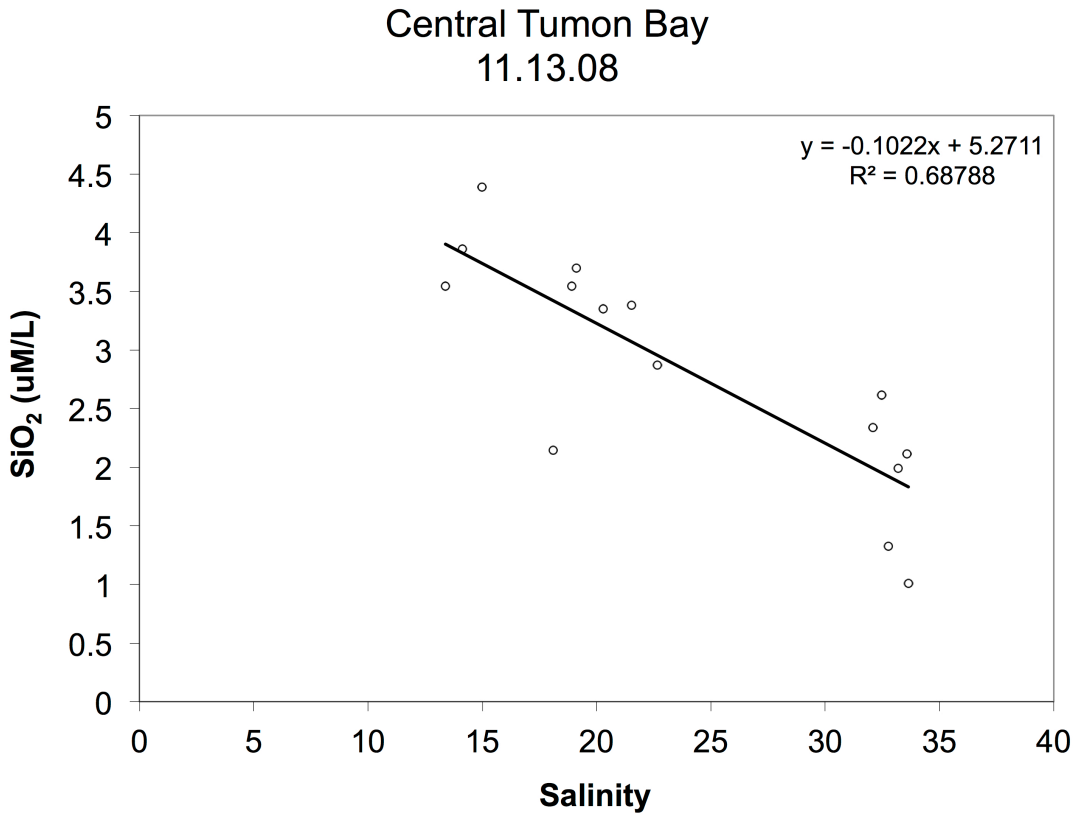

Figure 4.13. Salinity vs. SiO_2 (open circles) at Central Tumon Bay on November 13, 2008 fitted with a linear trendline (black line).

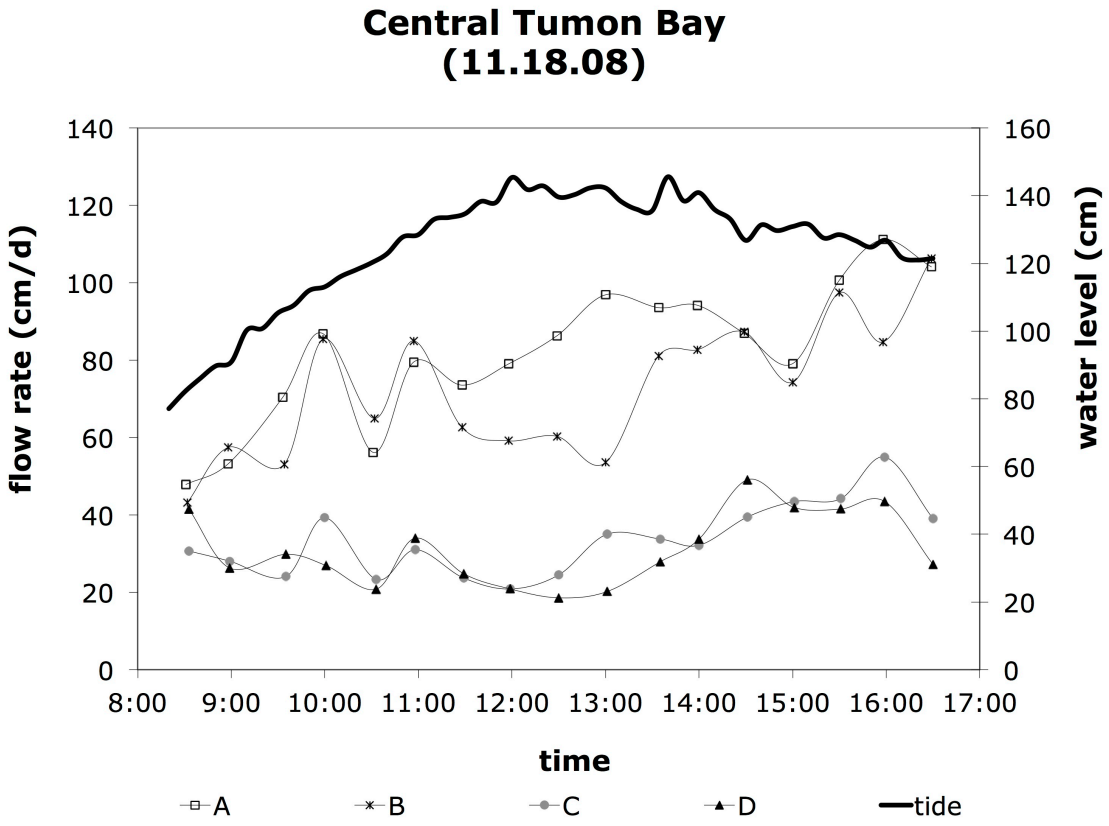

Figure 4.14. SGD results for Central Tumon Bay on November 18th, 2008: tide (black line) and four SGD time series, devices A (open squares), B (star), C (gray solid circle), and D (black solid triangle).

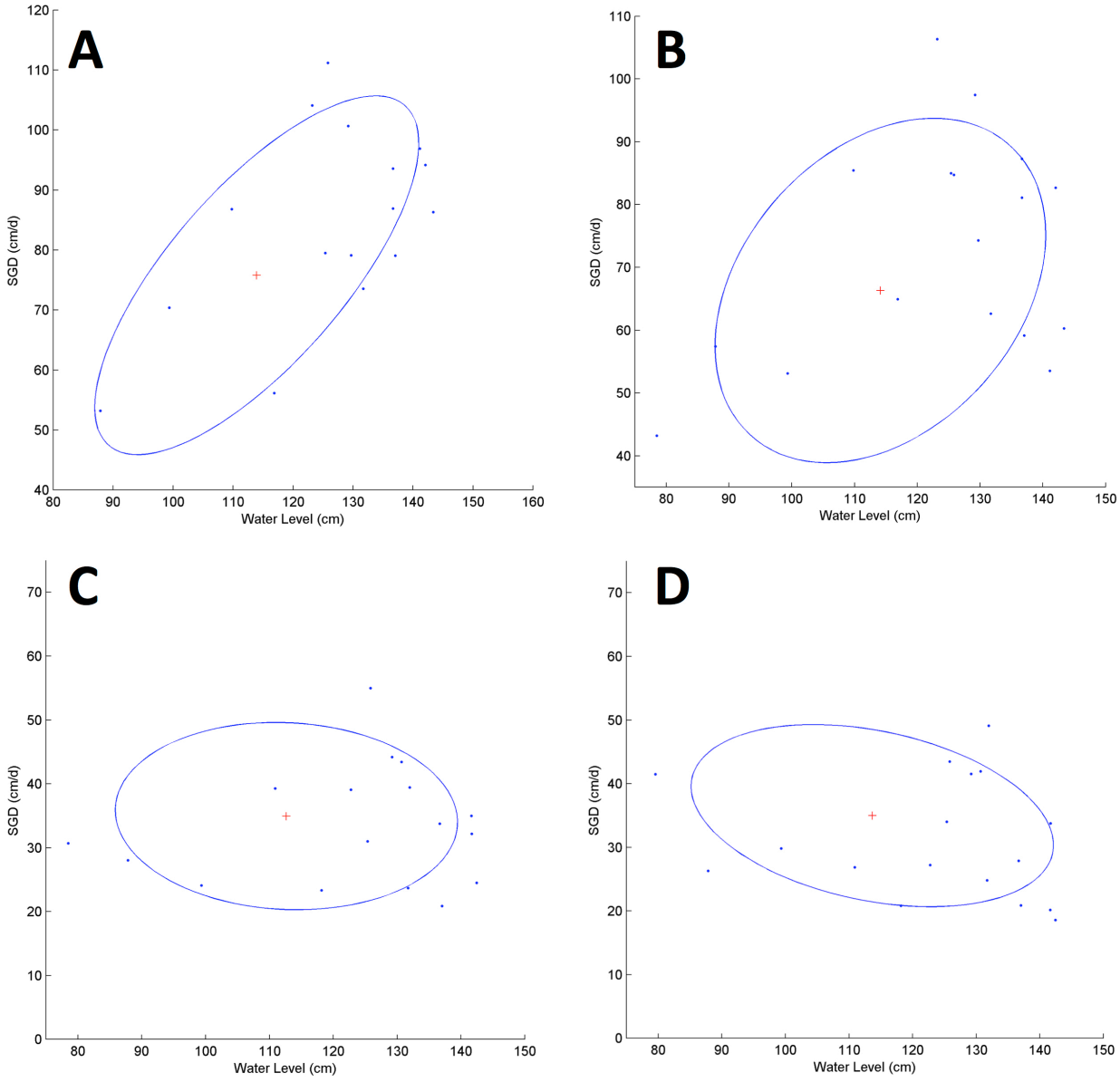

Figure 4.15 A-D. Central Tumon ellipse fit for November 18, 2008. Upper left (A) is device A, upper right (B) is device B, lower left (C) is device C and lower right (D) is device D. Blue points are data, blue ellipse is the fit ellipse, and the red cross is the center of the ellipse. Note different axes on subplots.

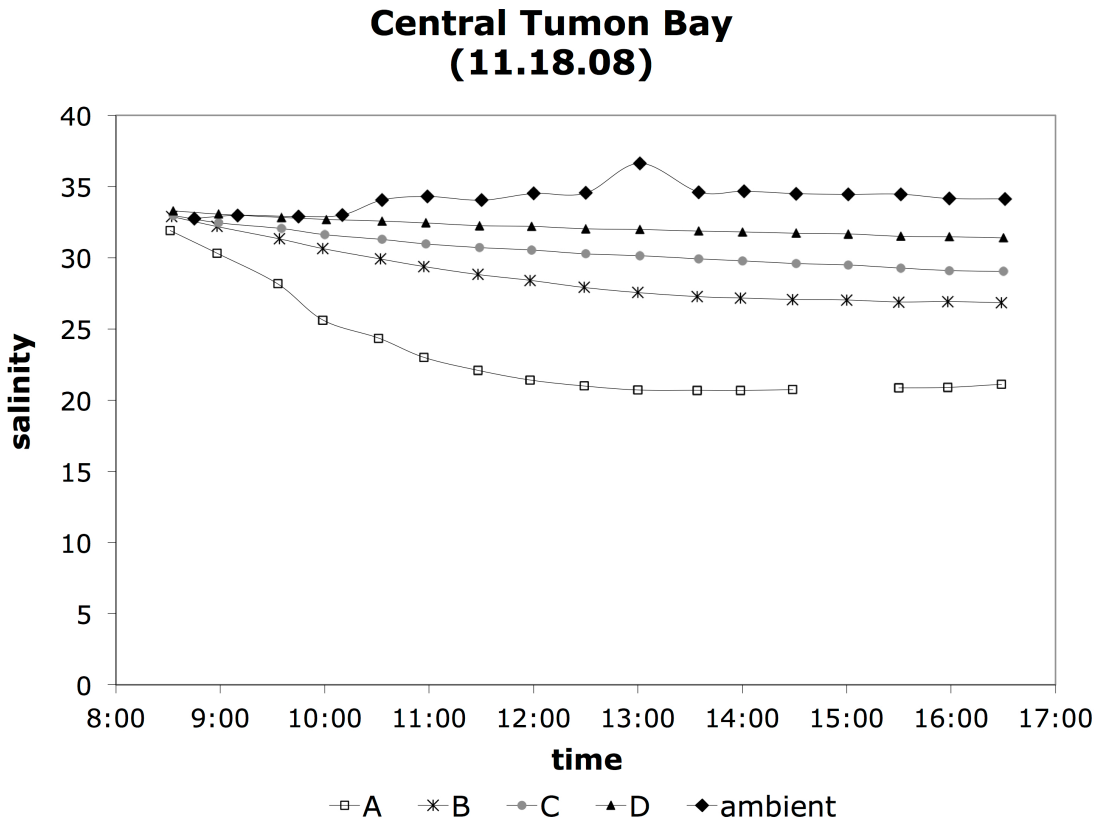

Figure 4.16. Salinity trends at Central Tumon Bay for November 18, 2008. Time vs. salinity for devices A (open squares), B (black star), C (solid gray circle), and D (solid black triangle), ambient salinity (solid black diamond) and a spring exposed on the beach face that was directly sampled (open diamond).

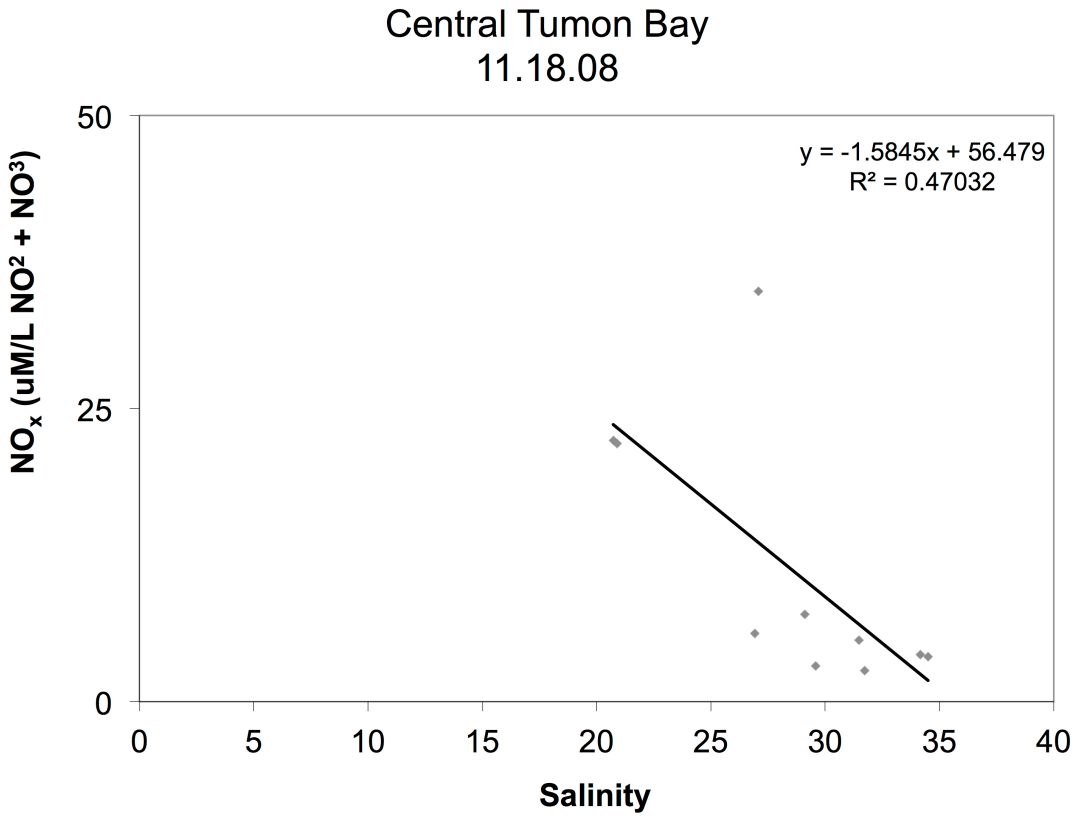

Figure 4.17. Salinity vs. NO_x (solid gray diamonds) at Central Tumon Bay on November 18, 2008 fitted with a linear trendline (black line).

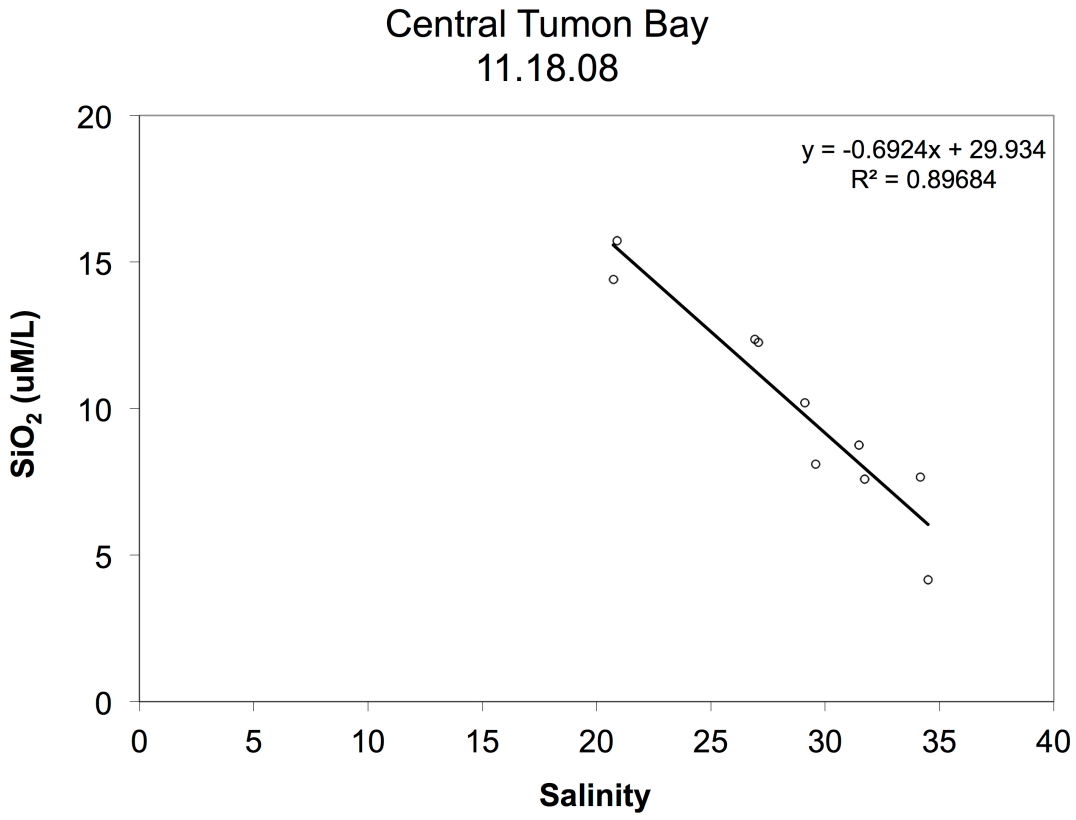

Figure 4.18. Salinity vs. SiO_2 (open circles) at Central Tumon Bay on November 18, 2008 fitted with a linear trendline (black line).

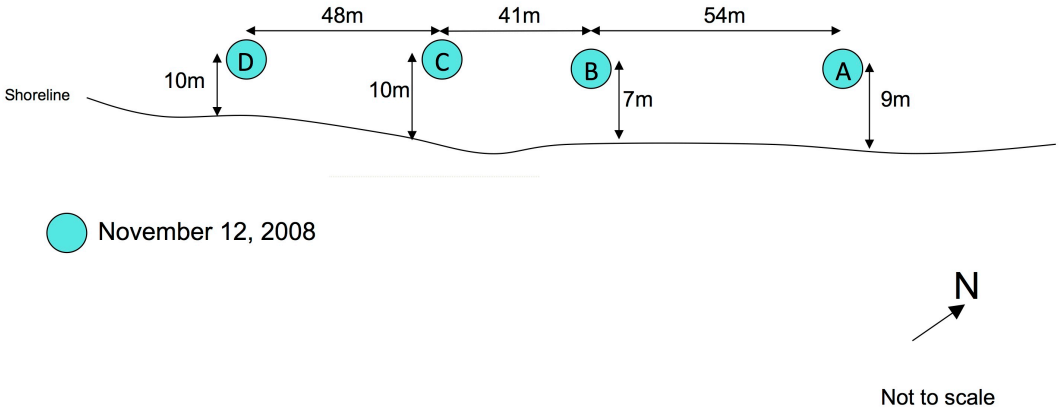

Figure 4.19. Sketch of North-Central Tumon Bay site. Lettered circles represent device locations, solid black line indicates shoreline position and large arrow indicates north. Figure is not to scale.

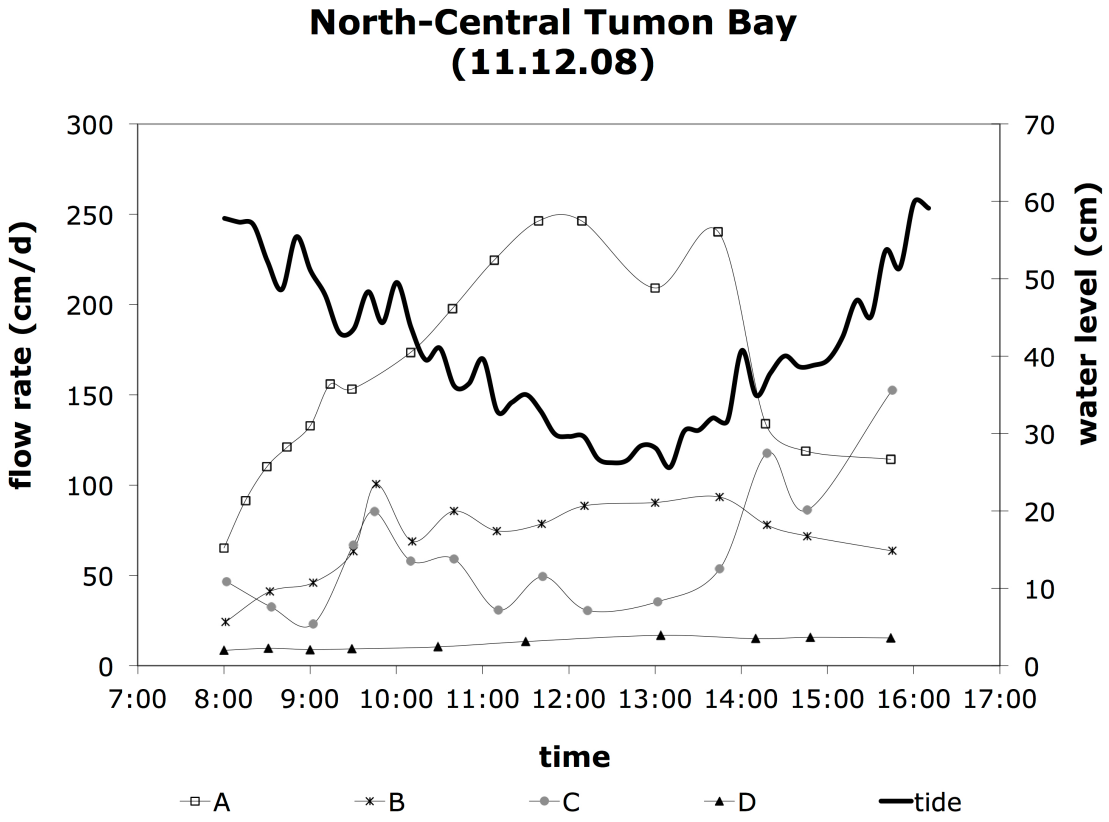

Figure 4.20. SGD results for North-Central Tumon Bay on November 12, 2008: tide (black line) and four SGD time series, devices A (open squares), B (star), C (gray solid circle), and D (black solid triangle).

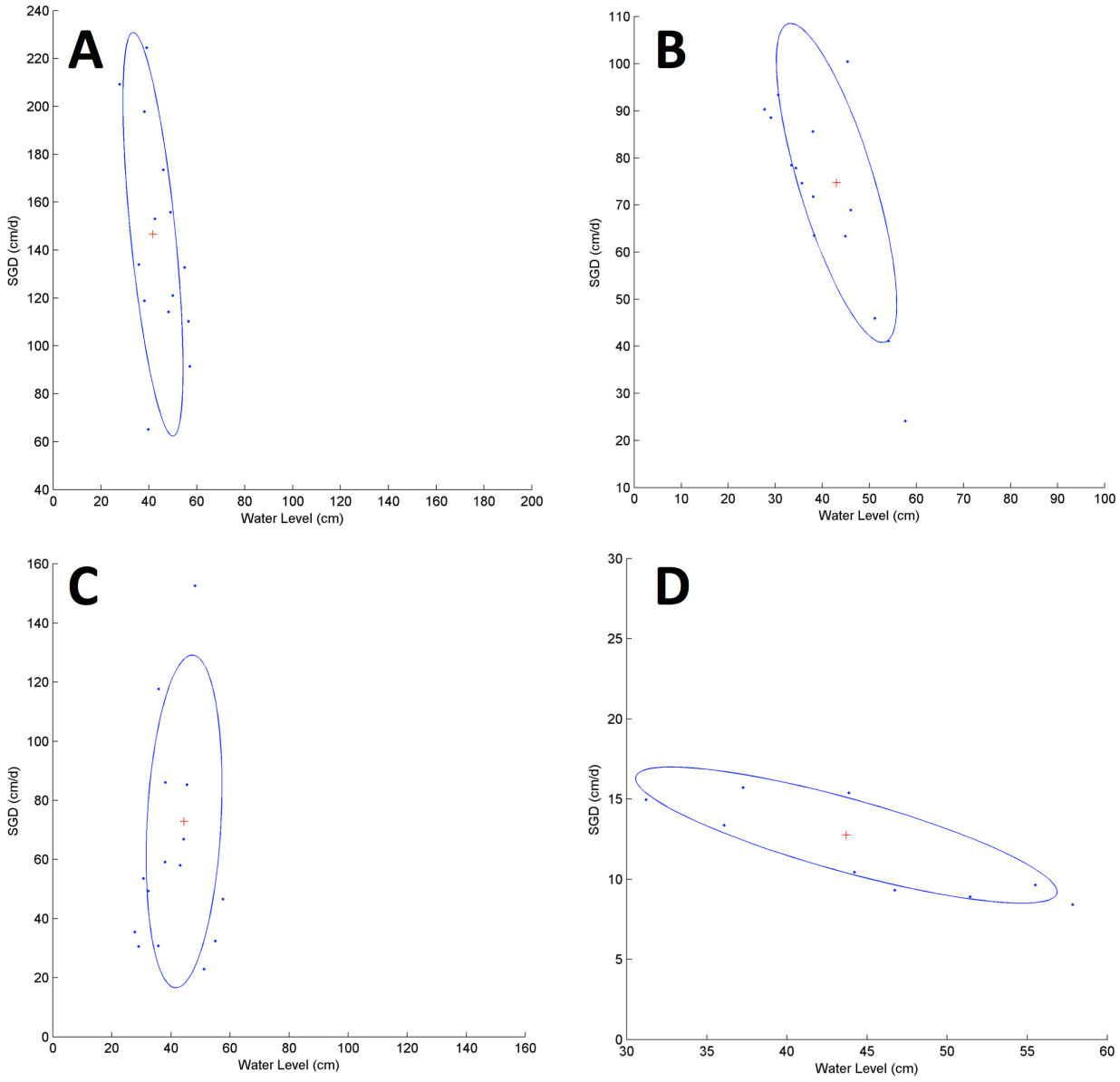

Figure 4.21 A-D. North-Central Tumon ellipse fit for November 12, 2008. Upper left (A) is device A, upper right (B) is device B, lower left (C) is device C and lower right (D) is device D. Blue points are data, blue ellipse is the fit ellipse, and the red cross is the center of the ellipse. Note different axes on subplots.

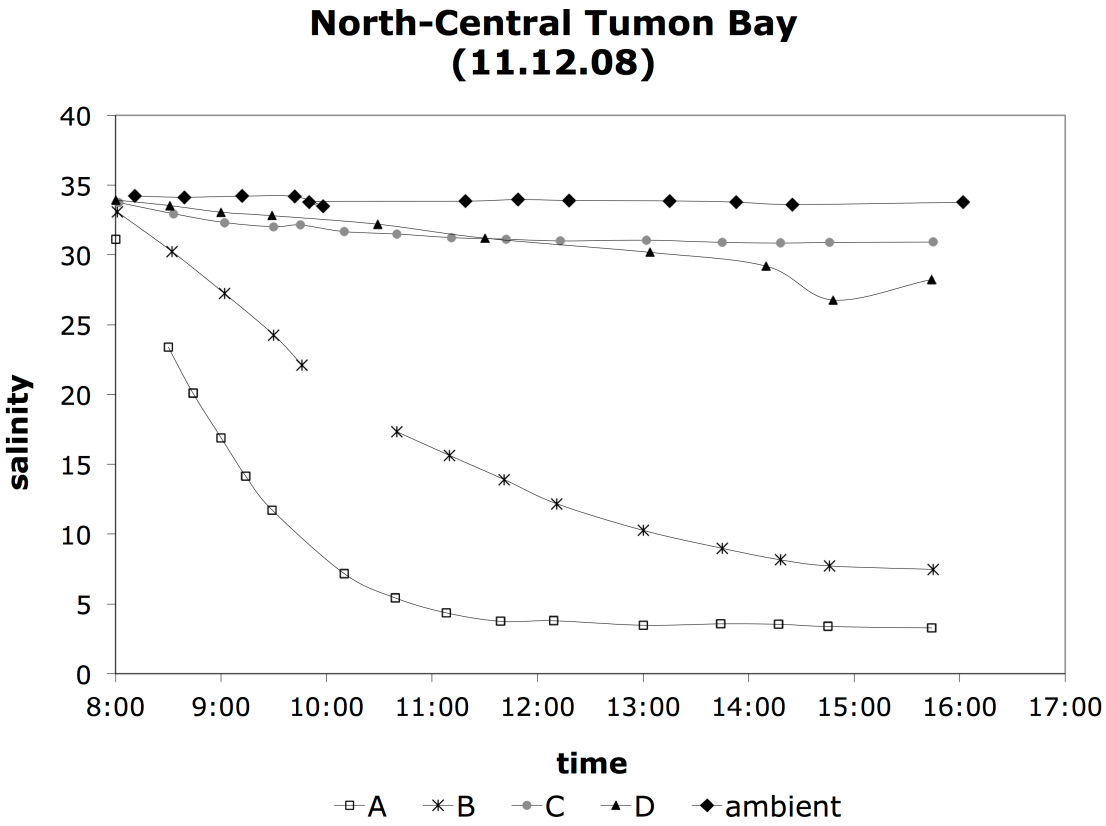

Figure 4.22. Salinity trends at North-Central Tumon Bay for November 12, 2008. Time vs. salinity for devices A (open squares), B (black star), C (solid gray circle), and D (solid black triangle), ambient salinity (solid black diamond) and a spring exposed on the beach face that was directly sampled (open diamond).

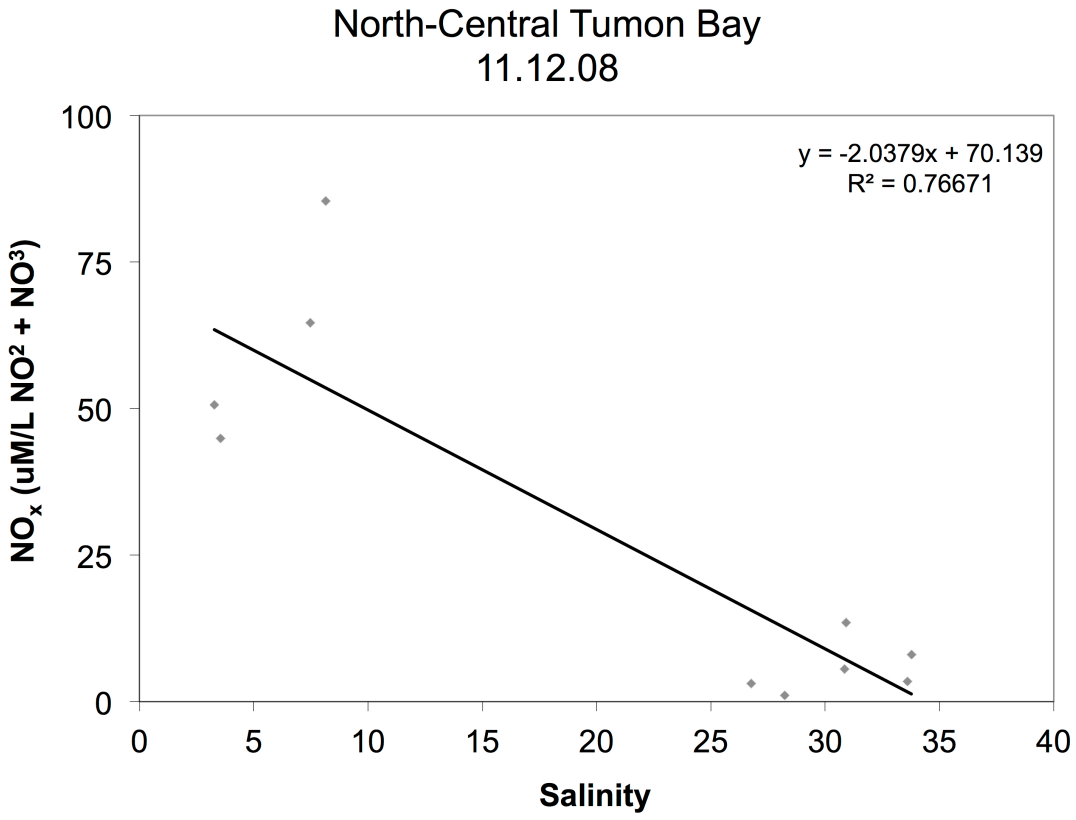

Figure 4.23. Salinity vs. NO_x (solid gray diamonds) at North-Central Tumon Bay on November 12, 2008 fitted with a linear trendline (black line).

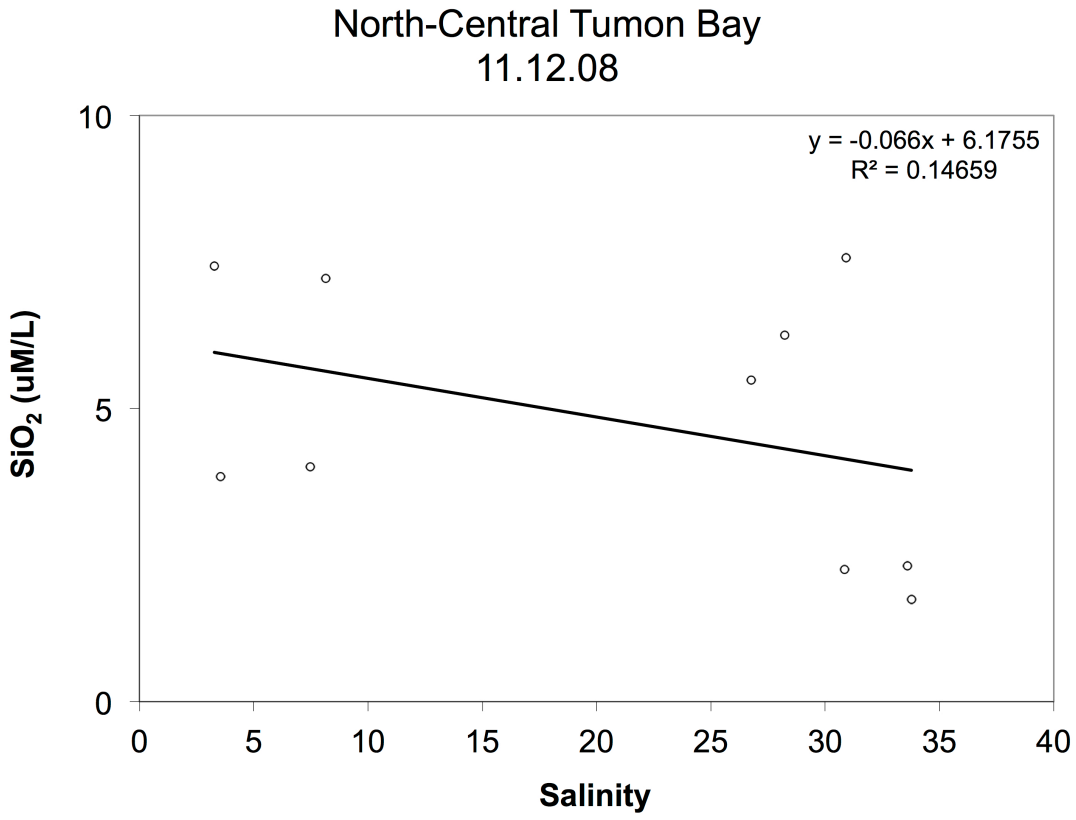

Figure 4.24. Salinity vs. SiO_2 (open circles) at North-Central Tumon Bay on November 12, 2008 fitted with a linear trendline (black line).

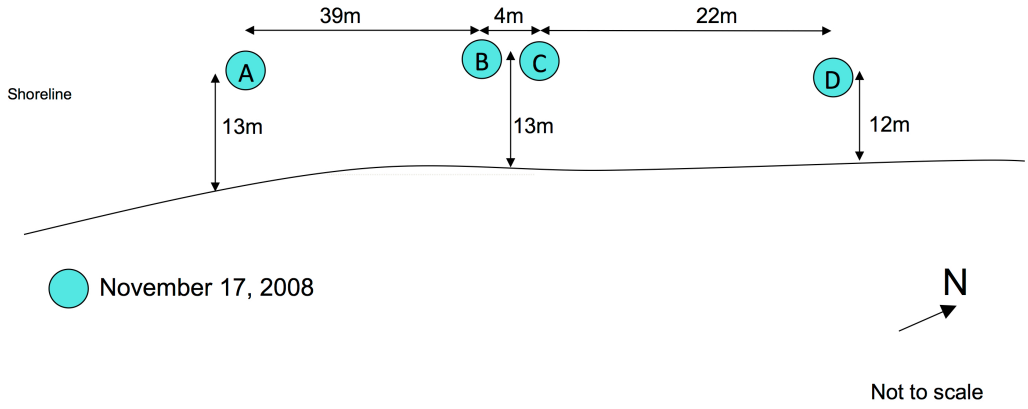

Figure 4.25. Sketch of North Tumon Bay site. Lettered circles represent device locations, solid black line indicates shoreline position and large arrow indicates north. Figure is not to scale.

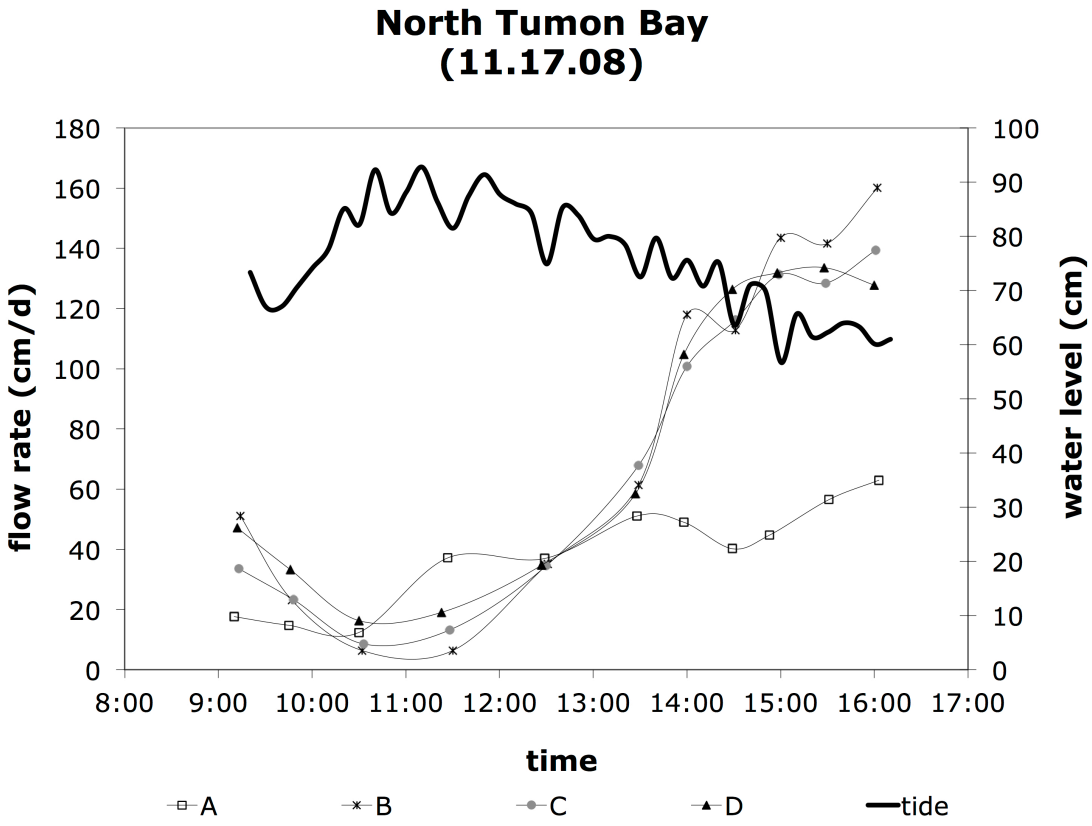

Figure 4.26. SGD results for North Tumon Bay on November 17th, 2008: tide (black line) and four SGD time series, devices A (open squares), B (star), C (gray solid circle), and D (black solid triangle).

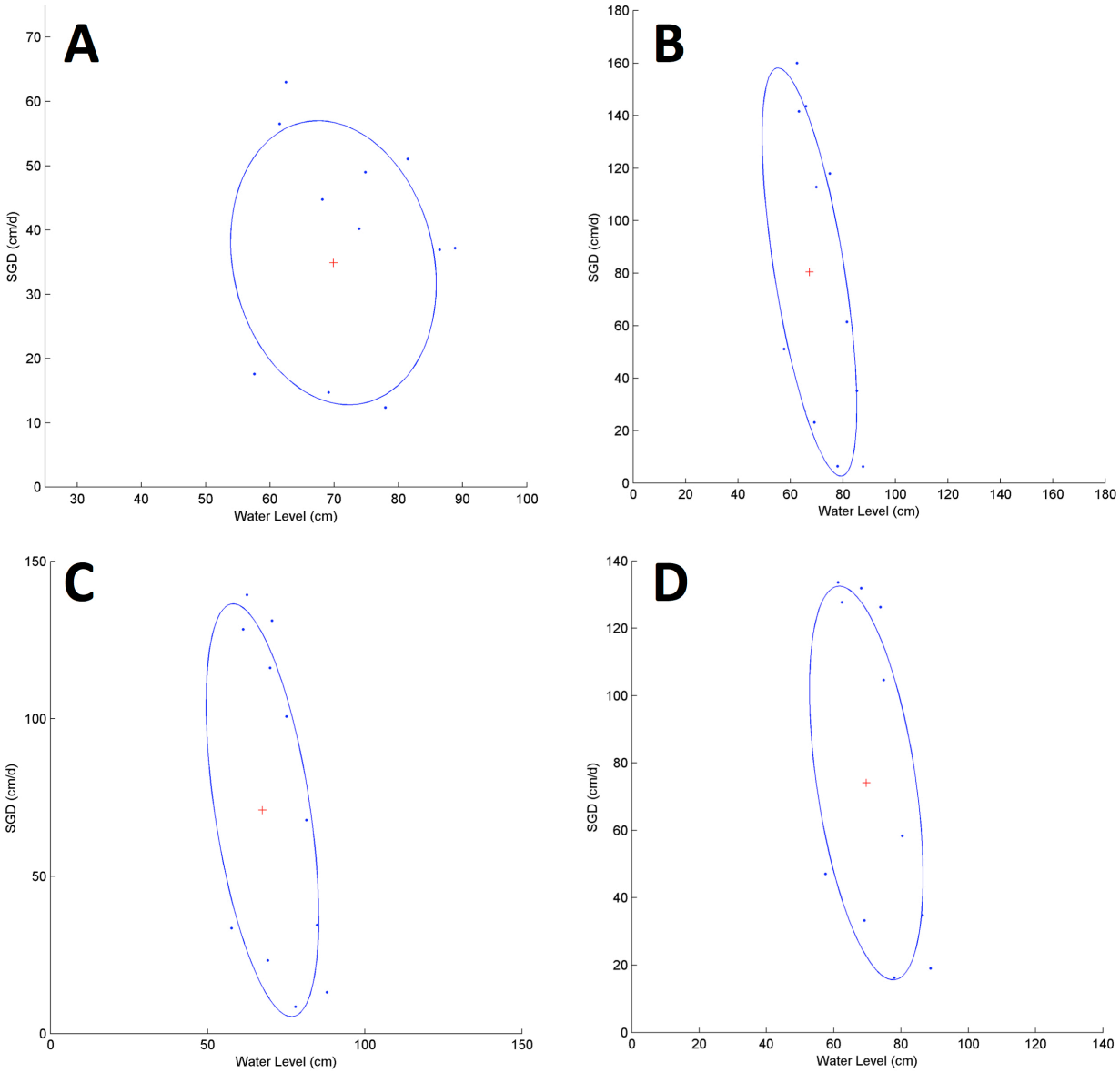

Figure 4.27A-D. North Tumon ellipse fit for November 17, 2008. Upper left (A) is device A, upper right (B) is device B, lower left (C) is device C and lower right (D) is device D. Blue points are data, blue ellipse is the fit ellipse, and the red cross is the center of the ellipse. Note different axes on subplots

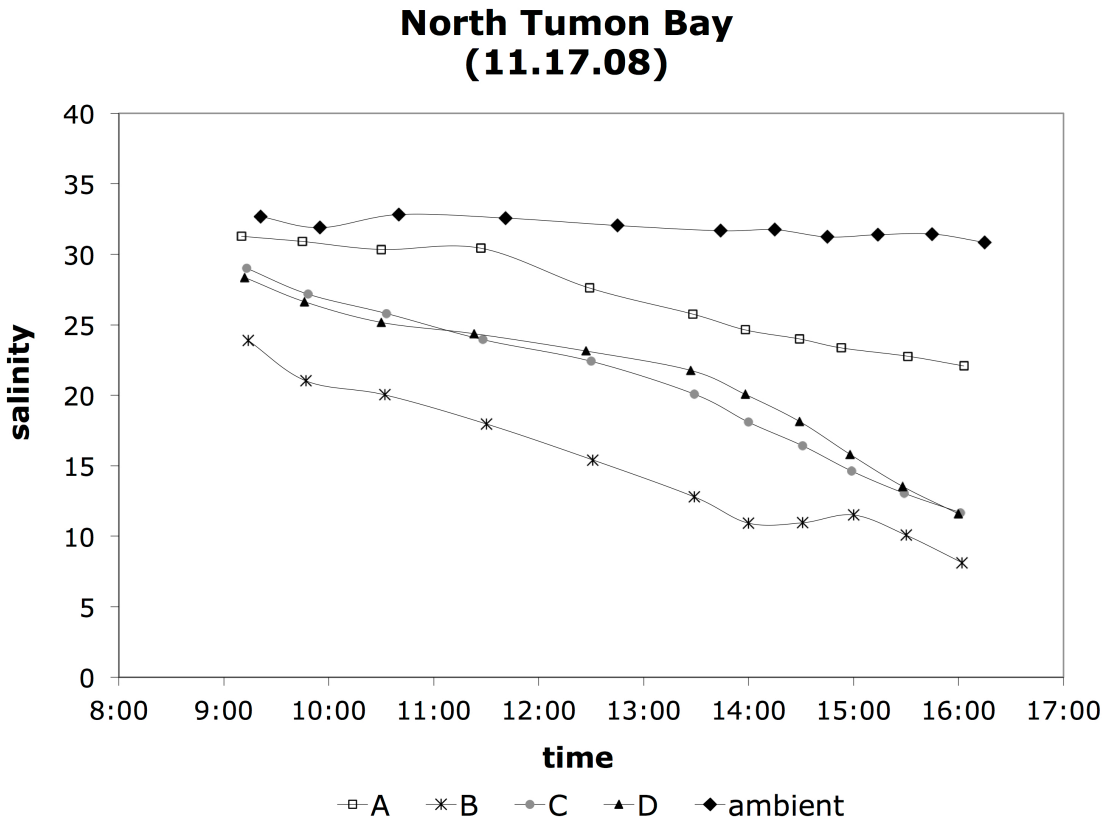

Figure 4.28. Salinity trends at North Tumon Bay for November 17, 2008. Time vs. salinity for devices A (open squares), B (black star), C (solid gray circle), and D (solid black triangle), ambient salinity (solid black diamond) and a spring exposed on the beach face that was directly sampled (open diamond).

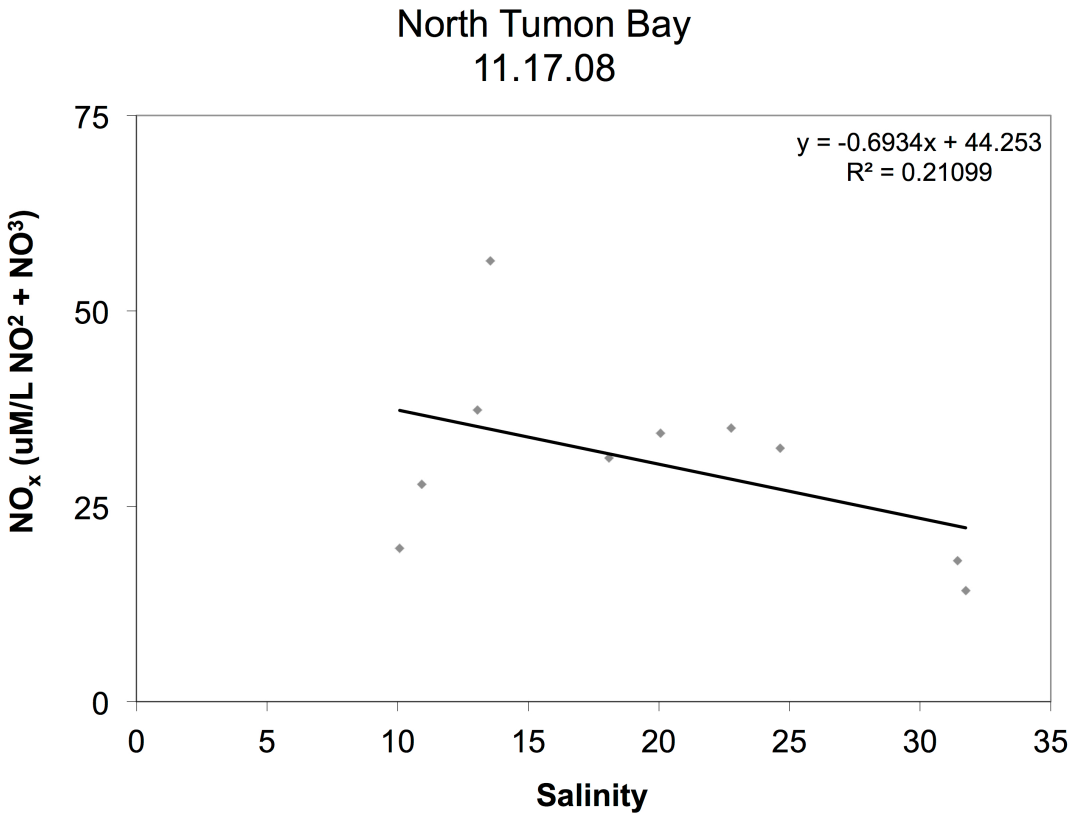

Figure 4.29. Salinity vs. NO_x (solid gray diamonds) at North Tumon Bay on November 17, 2008 fitted with a linear trendline (black line).

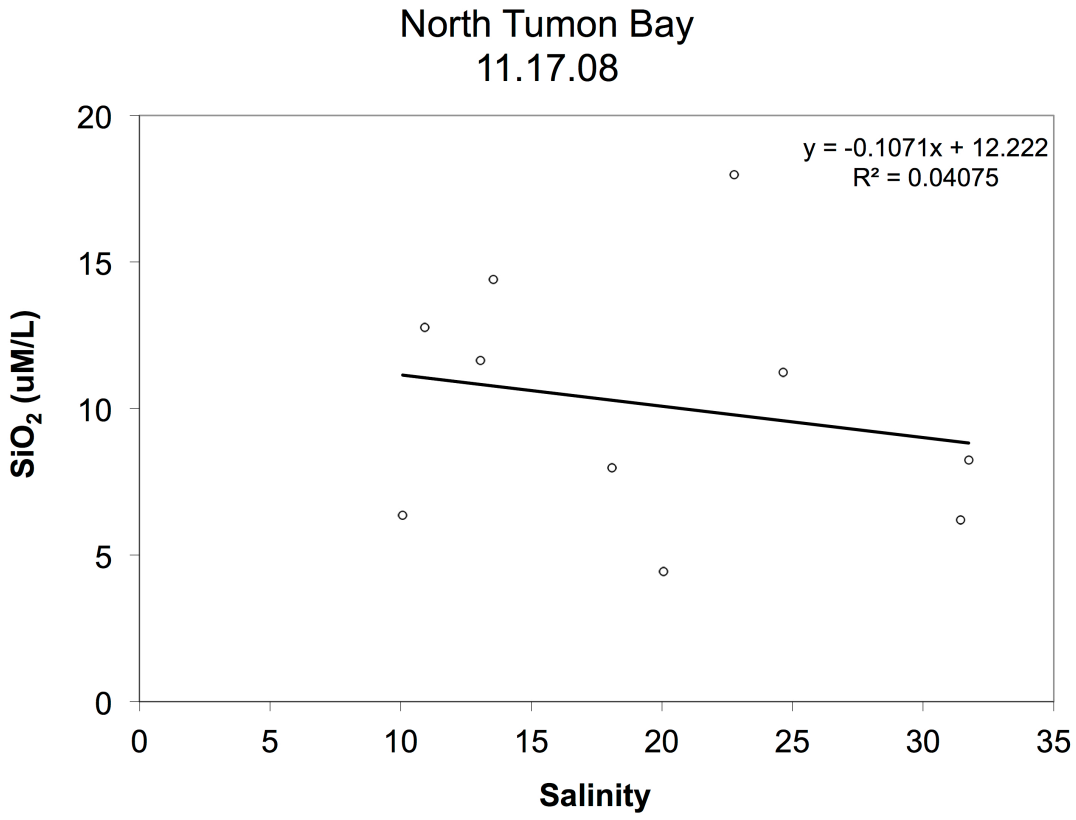

Figure 4.30. Salinity vs. SiO_2 (open circles) at North Tumon Bay on November 17, 2008 fitted with a linear trendline (black line).

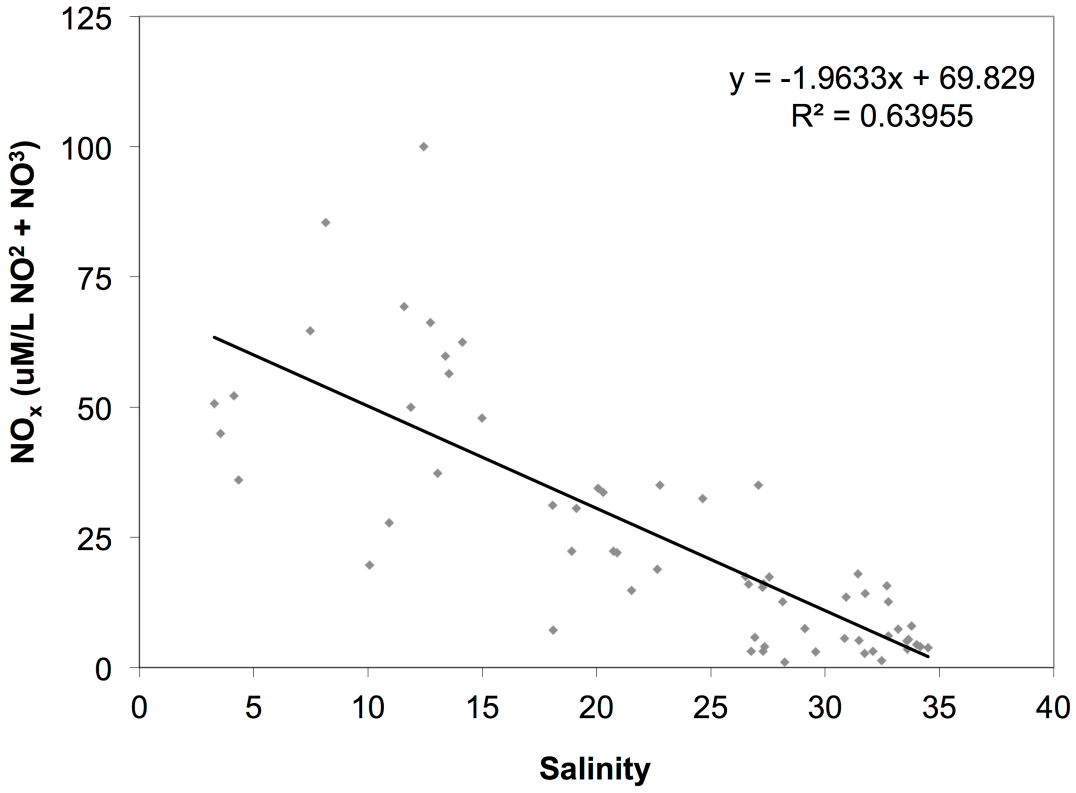

Figure 4.31. Salinity vs. NO_x (solid gray diamonds) of all Tumon Bay samples fitted with a linear trendline (black line).

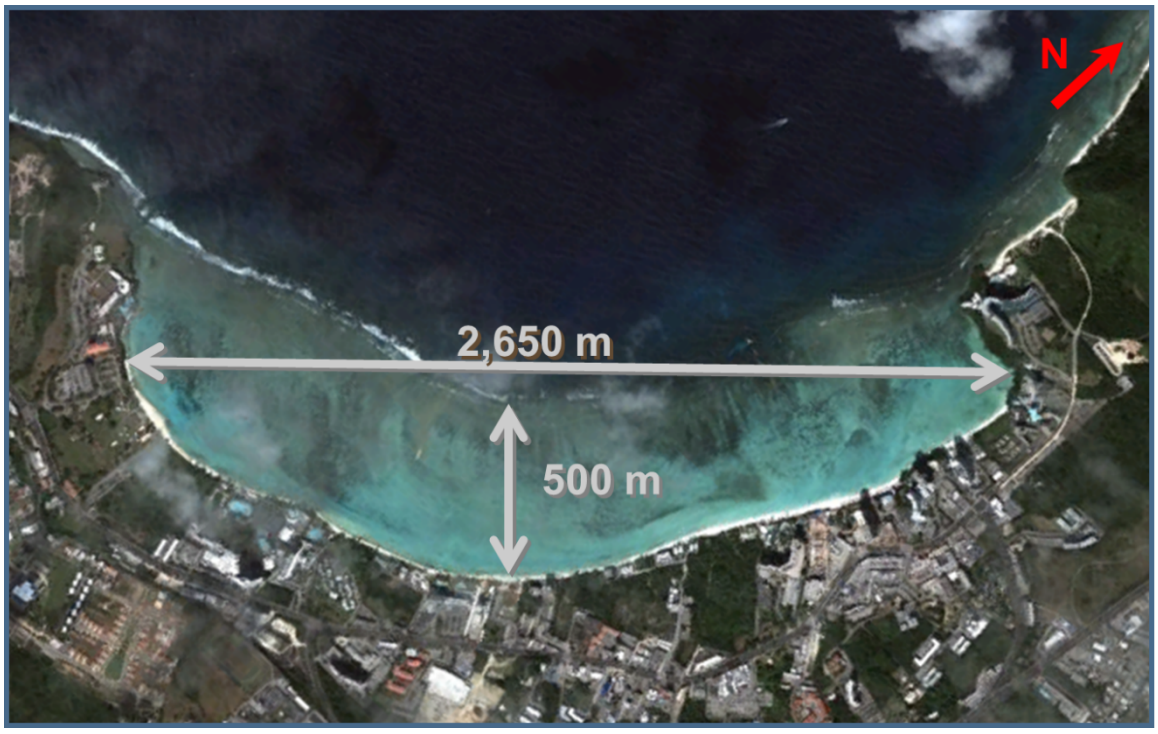

Figure 4.32. Map of Tumon Bay. White arrows indicate length and width of the bay. Red arrow indicates north direction. Map from Google Earth.

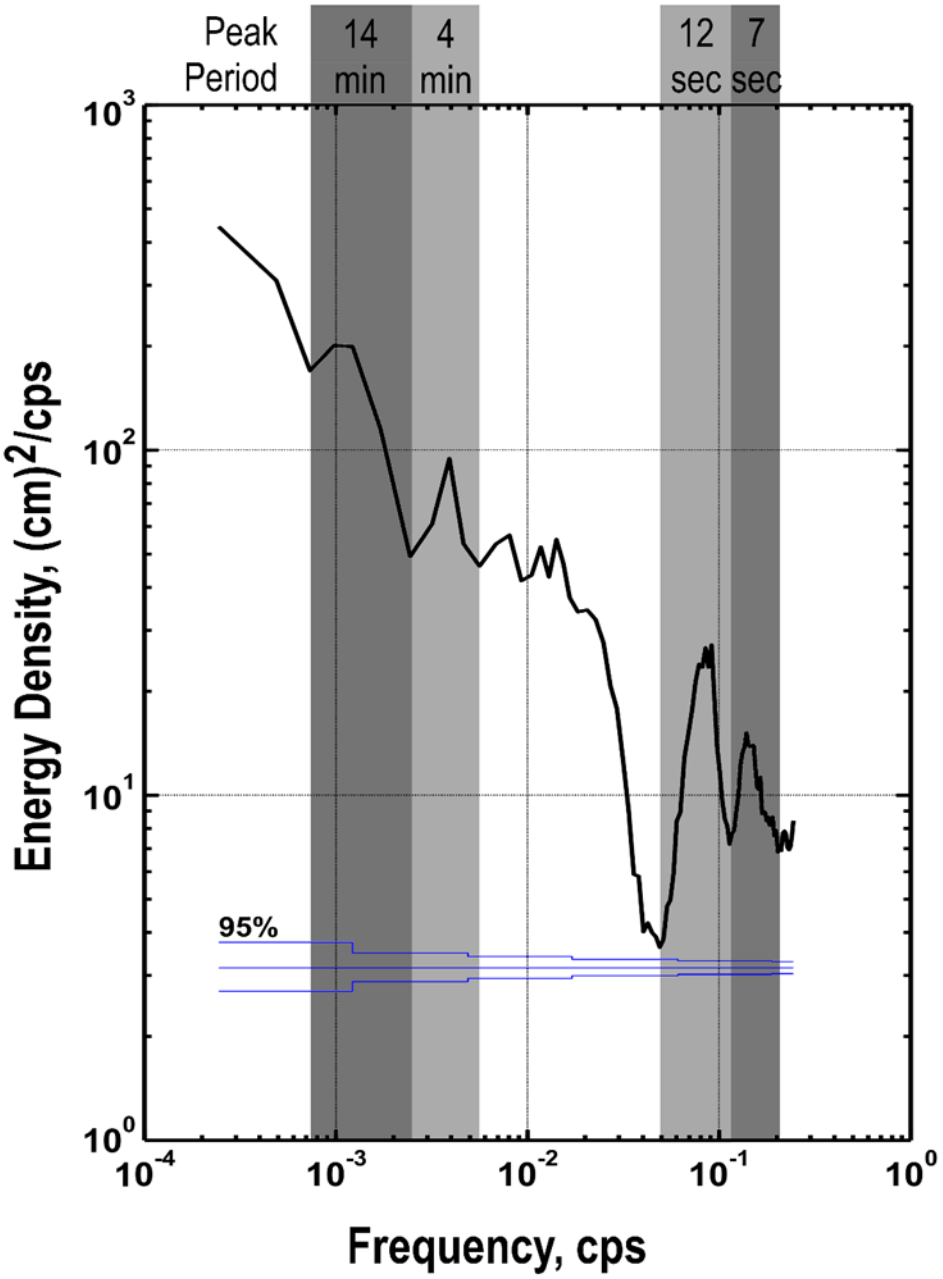

Figure 4.33. Spectral analysis of water levels in Tumon Bay. Frequency vs. energy density graph indicates four primary peaks (highlighted with gray bars) with periods corresponding to 14 min, 4 min, 12 sec, and 7 sec. Blue bar indicates range of 95% confidence.

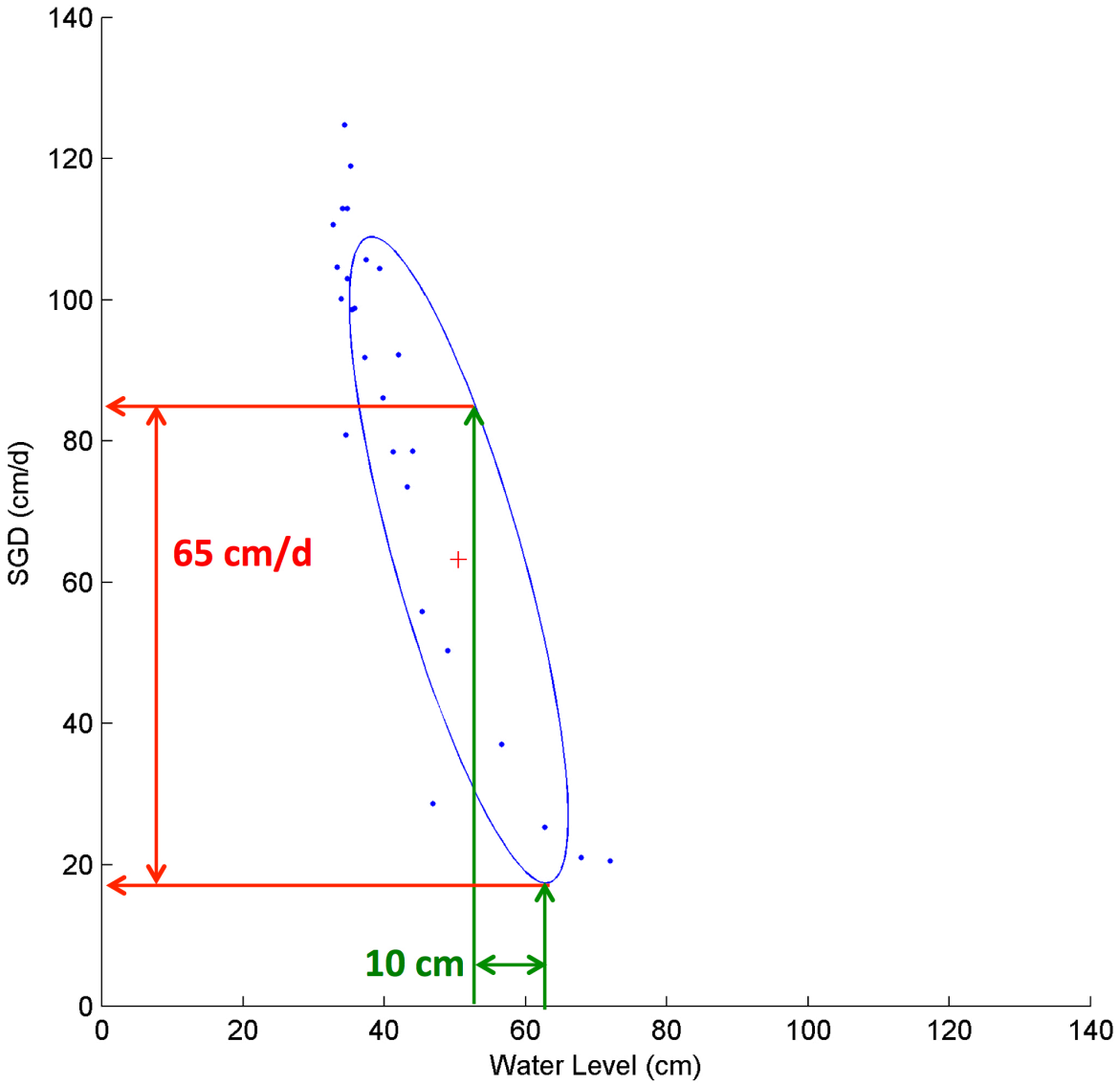

Figure 4.34. Ellipse of South Tumon Bay from November 11, 2008 device A. A 10 cm change in water level (green arrows) can yield a 65 cm/d change in SGD (red arrows).

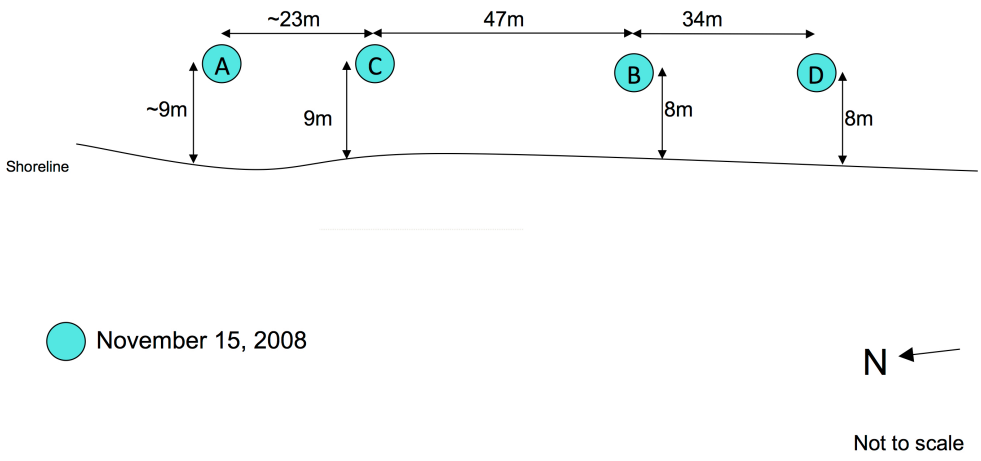

Figure 4.35. Sketch of SE Pacific site. Lettered circles represent device locations, solid black line indicates shoreline position and large arrow indicates north. Figure is not to scale.

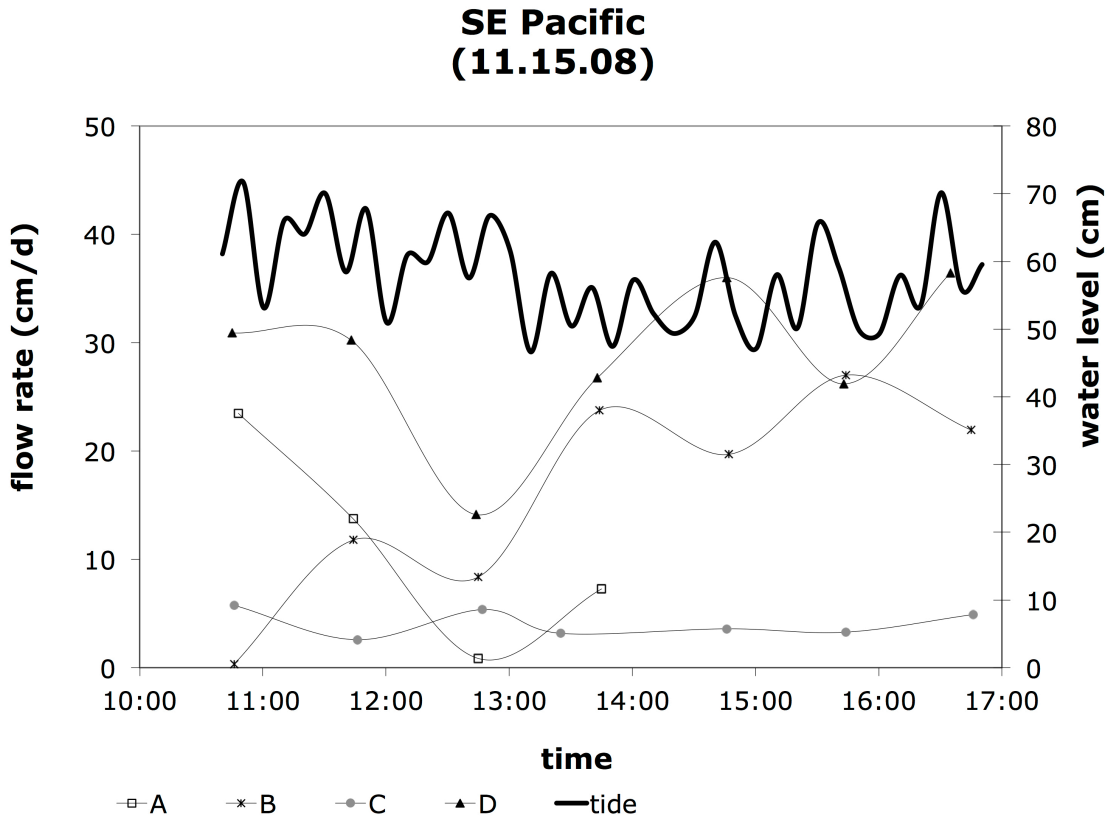

Figure 4.36. SGD results for SE Pacific on November 15, 2008: tide (black line) and four SGD time series, devices A (open squares), B (star), C (gray solid circle), and D (black solid triangle).

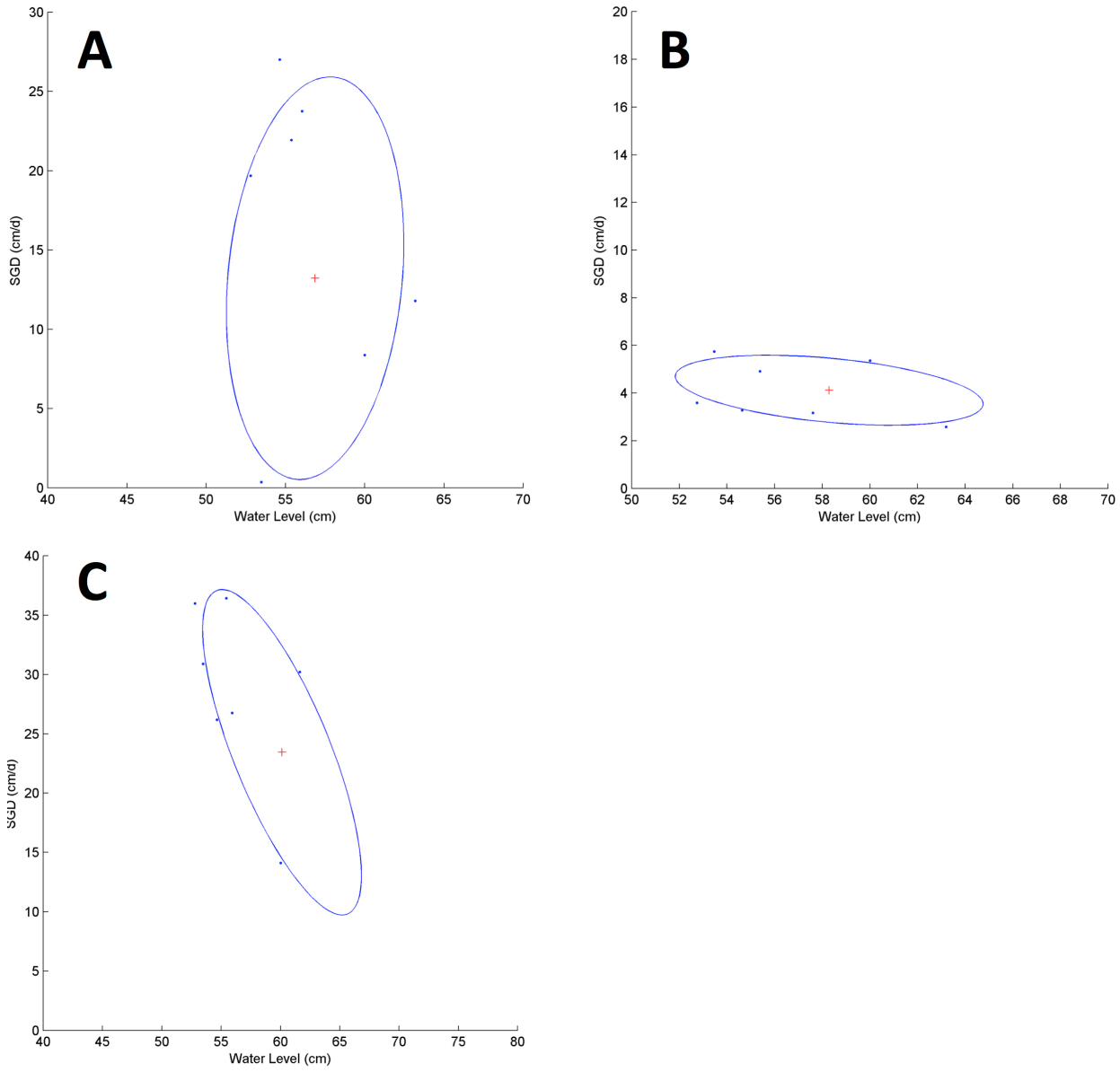

Figure 4.37A-C. SE Pacific ellipse fit for November 15, 2008. Upper left (A) is device B, upper right (B) is device C, and lower left (C) is device D. Blue points are data, blue ellipse is the fit ellipse, and the red cross is the center of the ellipse. Note different axes on subplots

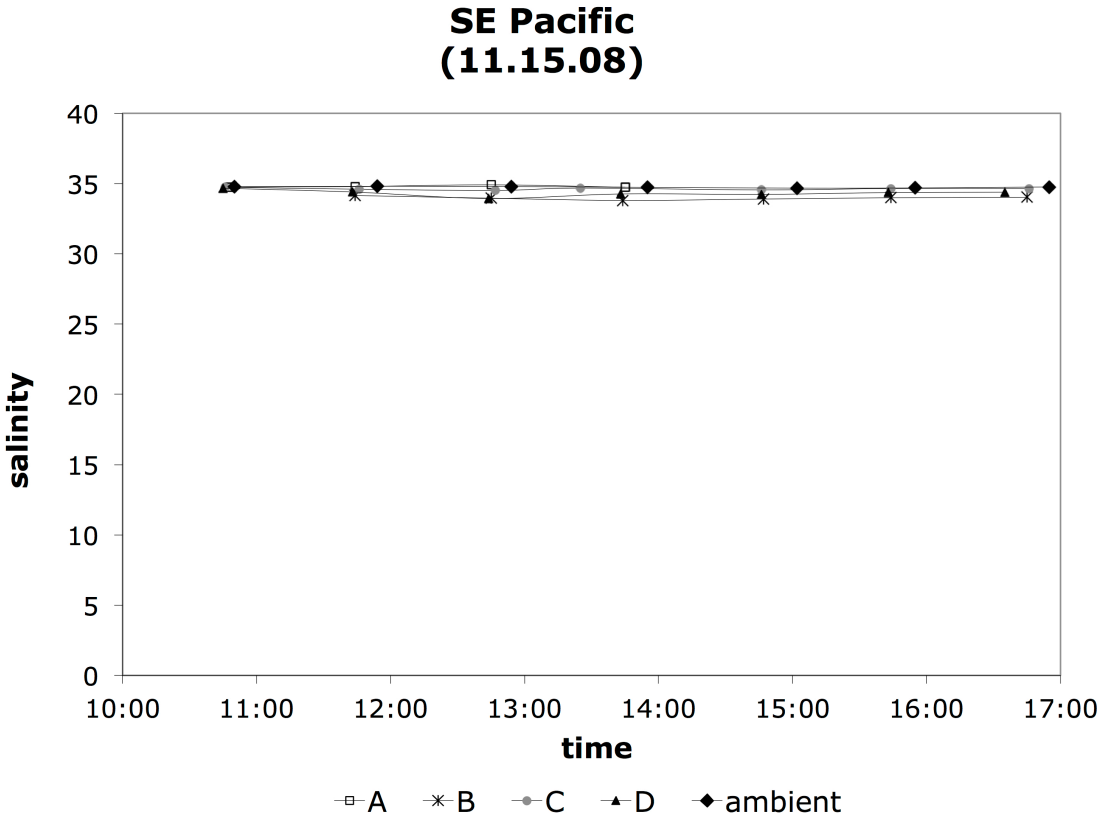

Figure 4.38. Salinity trends at SE Pacific for November 15, 2008. Time vs. salinity for devices A (open squares), B (black star), C (solid gray circle), and D (solid black triangle), ambient salinity (solid black diamond) and a spring exposed on the beach face that was directly sampled (open diamond).

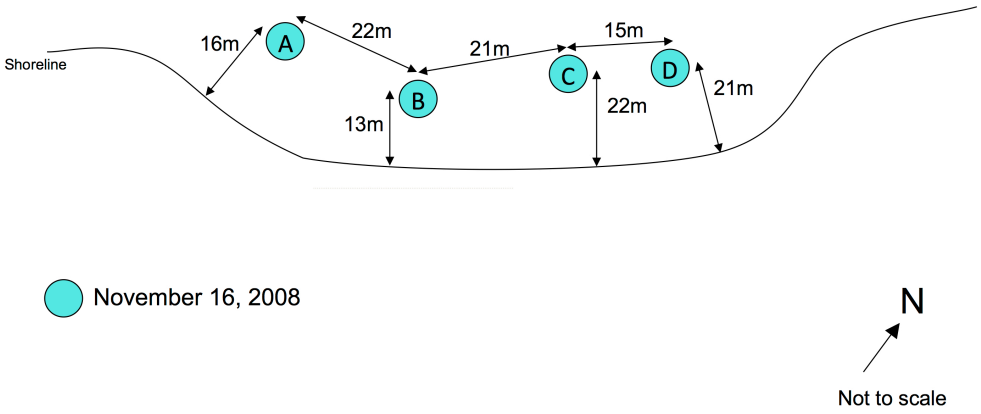

Figure 4.39. Sketch of Nimitz site. Lettered circles represent device locations, solid black line indicates shoreline position and large arrow indicates north. Figure is not to scale.

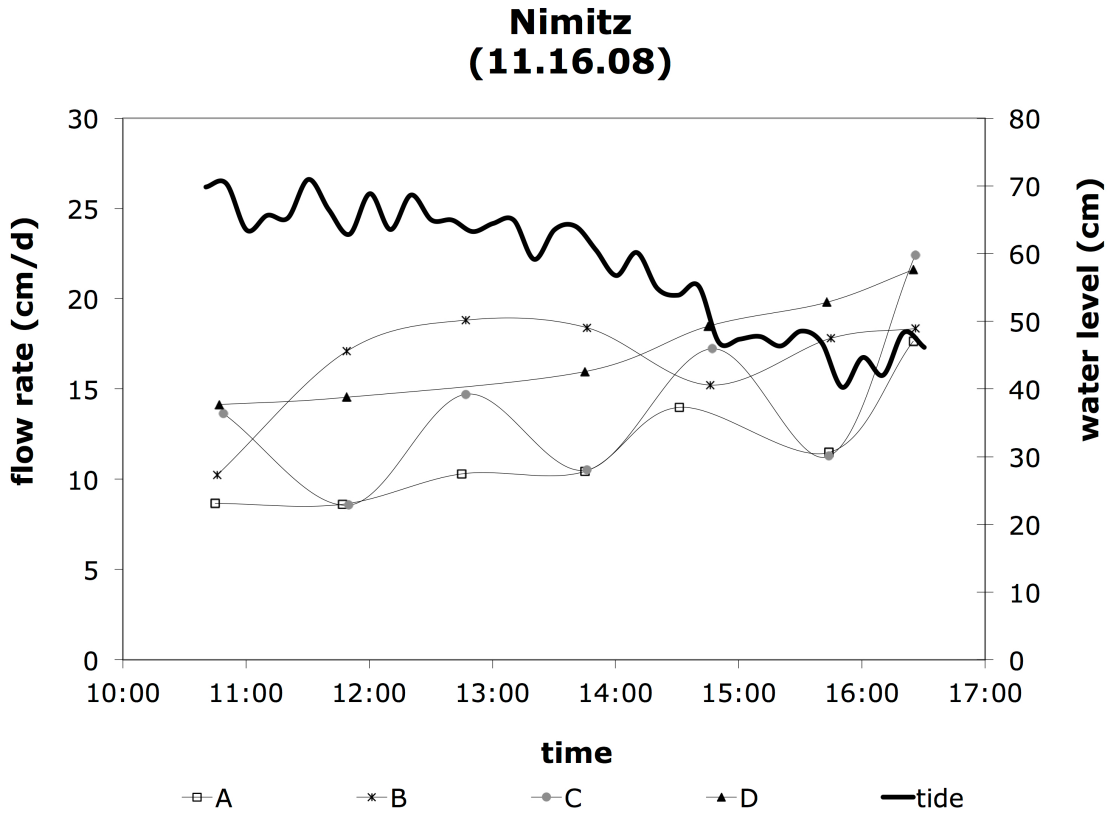

Figure 4.40. SGD results for Nomitz on November 16, 2008: tide (black line) and four SGD time series, devices A (open squares), B (star), C (gray solid circle), and D (black solid triangle).

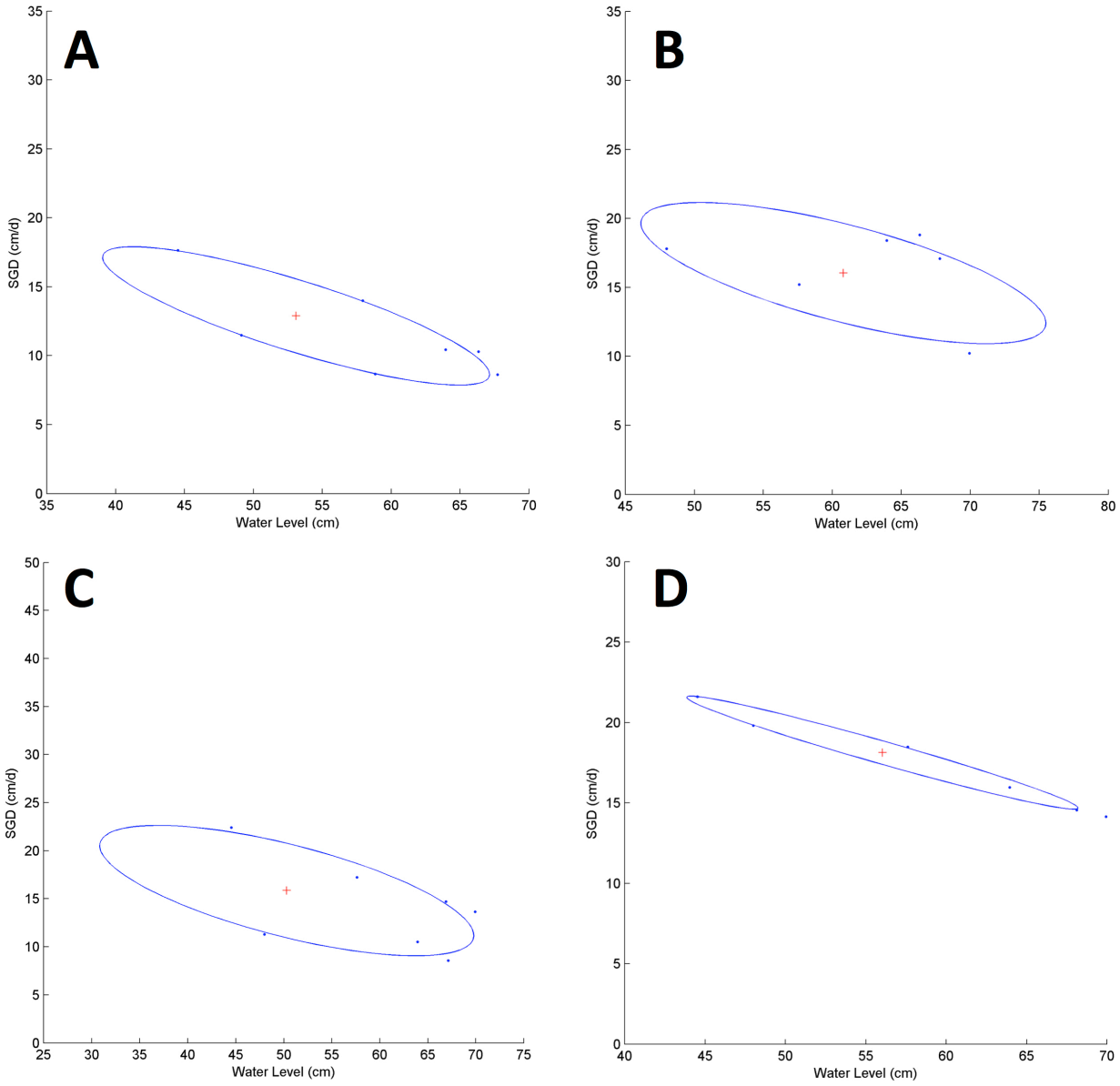

Figure 4.41A-D. Nimitz ellipse fit for November 16, 2008. Upper left (A) is device A, upper right (B) is device B, lower left (C) is device C and lower right (D) is device D. Blue points are data, blue ellipse is the fit ellipse, and the red cross is the center of the ellipse. Note different axes on subplots

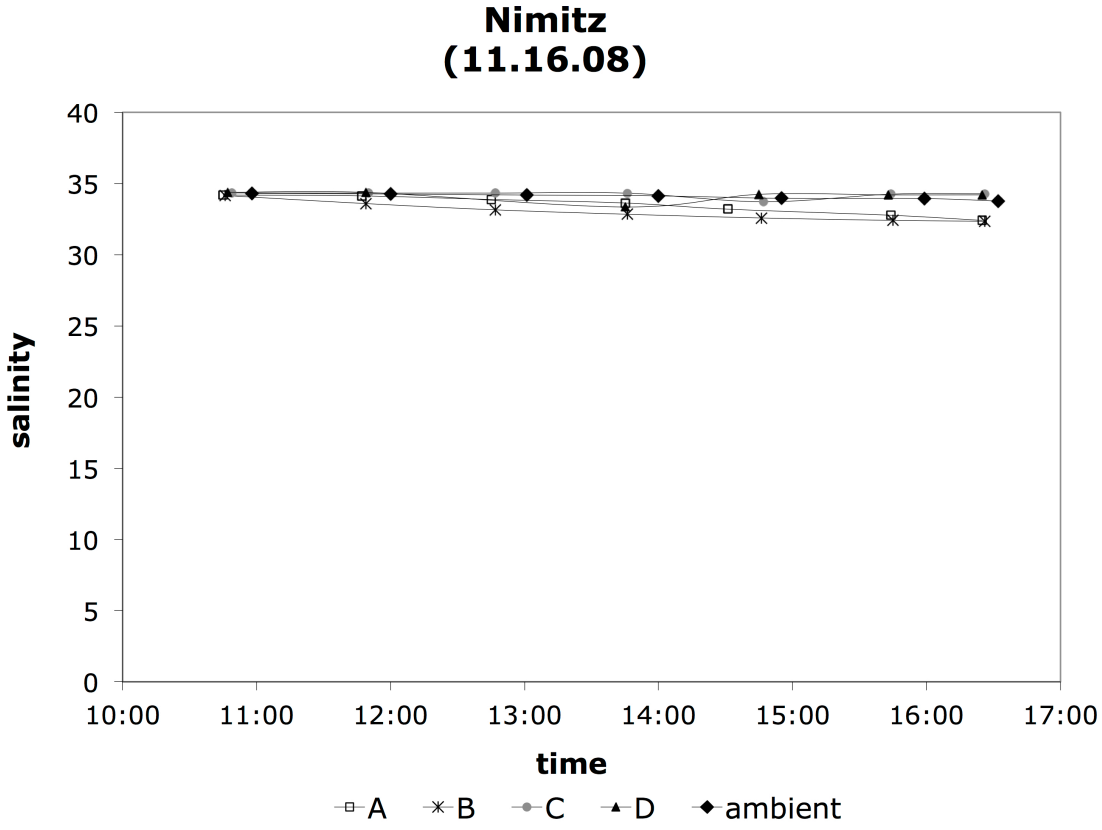

Figure 4.42. Salinity trends at Nimitz for November 16, 2008. Time vs. salinity for devices A (open squares), B (black star), C (solid gray circle), and D (solid black triangle), ambient salinity (solid black diamond) and a spring exposed on the beach face that was directly sampled (open diamond).

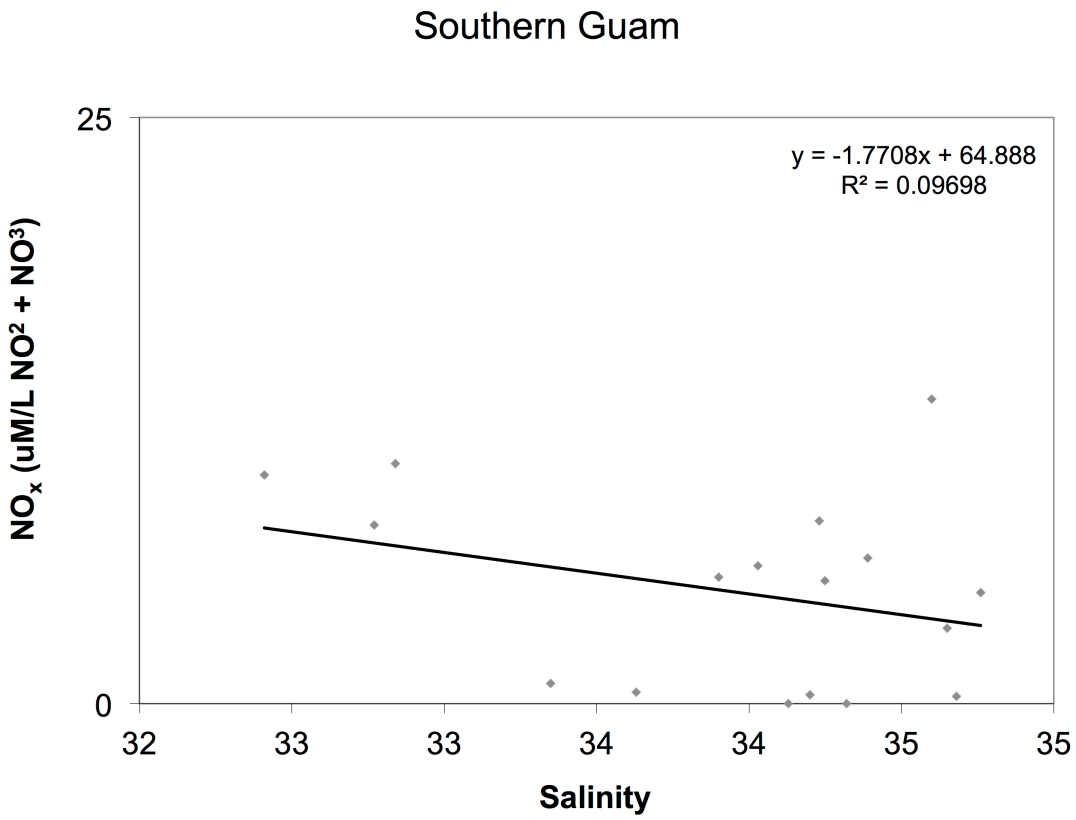

Figure 4.43. Salinity vs. NO_x (solid gray diamonds) both Southern Guam sites fitted with a linear trendline (black line).

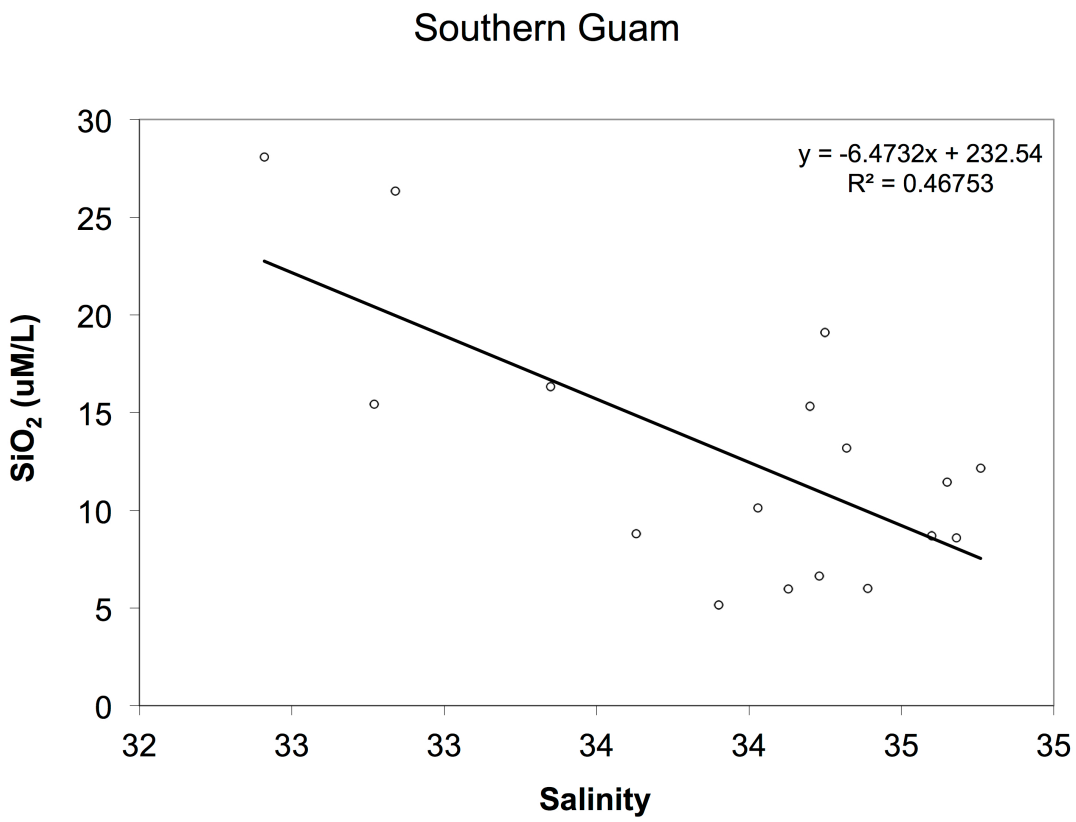

Figure 4.44. Salinity vs. SiO_2 (open circles) at both Southern Guam sites fitted with a linear trendline (black line).

Tables

*Table 4-1. Tumon Bay Results. Device locations, dates, ID, average SGD, SGD range, high discharge anomalies (starred devices had at least one measurement in excess of 100 cm/d), salinity, average ambient salinity and freshwater component (** indicates lowest freshwater component; *** indicates highest freshwater component).*

Location	Date	Seepage Meter ID	Average SGD (cm/d)	SGD Range (cm/d)	High Discharge Anomalies (>100 cm/d)	Salinity	Average Ambient Salinity	Freshwater Component (%)
South Tumon Bay	11 November 2008	A	63	21 – 125	*	11.28	32.86	66
		B	25	14 – 44		26.52	32.86	19
		C	35	28 – 43		26.51	32.86	19
		D	31	18 – 41		27.26	32.86	17
Central Tumon Bay	13 November 2008	A1	37	0 – 78		19.12	33.67	43
		B1	45	1 – 80		18.10	33.67	46
		C1	16	8 – 26		32.10	33.67	5**
		D1	76	24 – 143	*	13.39	33.67	60
	18 November 2008	A2	76	48 – 111	*	20.68	34.16	39
		B2	66	43 – 106	*	26.84	34.16	21
		C2	35	21 – 55		29.03	34.16	15
		D2	35	19 – 49		31.39	34.16	8
North-Central Tumon Bay	12 November 2008	A	147	65 – 246	*	3.28	33.90	90**
		B	75	24 – 100	*	7.47	33.90	78
		C	73	23 – 153	*	30.85	33.90	9
		D	13	8 – 17		28.24	33.90	17
North Tumon Bay	17 November 2008	A	35	12 – 63		22.08	31.85	31
		B	80	6 – 160	*	8.13	31.85	74
		C	71	9 – 139	*	11.86	31.85	63
		D	74	16 – 134	*	11.59	31.85	64

Table 4-2. Freshwater component correlations. Correlation coefficient and significance for freshwater component and flow rate.

Categories		***Correlation Coefficient (R)***	***Significance (p)***
Freshwater Component	Average High Flow Rate	0.83	7.1×10^{-6}
	Peak High Flow Rate	0.75	1.3×10^{-4}
	Average Flow Rate	0.76	8.8×10^{-5}
	Flow Rate Range	0.78	4.9×10^{-5}

Table 4-3. Southern Guam Results. Device locations, dates, ID, average SGD, SGD range, salinity, average ambient salinity and freshwater component. Average SGD reported is from ellipse fit method except where indicated by a star (*) when traditional arithmetic average is used due to ellipse fit issues.

Location	Date	Seepage Meter ID	Average SGD (cm/d)	SGD Range (cm/d)	Salinity	Average Ambient Salinity	Freshwater Component (%)
South-East Pacific	15 November 2008	A	11*	1 – 23	34.74	34.75	0
		B	13	0 – 27	34.03	34.75	2
		C	4	3 – 6	34.65	34.75	0
		D	23	14 – 36	34.39	34.75	1
Nimitz Bay	16 November 2008	A	13	9 – 18	32.41	34.08	5
		B	16	10 – 19	32.35	34.08	5
		C	16	9 – 22	34.28	34.08	-1
		D	18	14 – 22	34.20	34.08	0

Chapter 5 Bimini, Bahamas

Introduction

Bimini is a grouping of small, carbonate islands located in the North Atlantic Ocean about 80 km east of Miami, FL. They are the westernmost district in The Commonwealth of the Bahamas. Bimini's two principal islands, North and South Bimini, cover a combined area of about 10 km^2. This estimated area does not include areas covered by mangroves submerged at high tide. North and South Bimini are separated by a strait. The channel between these islands (170 m wide) is regularly dredged, leading to saltwater intrusion across the sea floor at depth (Duncan, 1972). Increased intrusion would lead to more saltwater infiltration and, possibly, a reduction of potable groundwater (Duncan, 1972). Neglecting the mangrove perimeter, the shoreline is about 33 km in length. The oceanic tides have a range of about 1 m. Both islands lie on the northwestern portion of the Great Bahama Bank. The average, summer air temperature is 28°C and average, summer, marine-water temperature is 28°C (Carew and Mylroie, 1997). The islands are mostly covered by pine and, occasionally, by broadleaf coppice and palmetto palm (Carew and Mylroie, 1997).

Bimini receives an average of 1250 mm of rainfall annually, 25% of which is estimated to contribute to groundwater recharge (Whitaker and Smart, 1997a). Recharge therefore provides about 3.125 million m^3/y. With an average elevation less than 10 m and a maximum of 22 m, there is no orographic precipitation. Although almost 90% of the Bahamas' population relies on groundwater supplies for potable water, on Bimini, desalination plants provide all freshwater. The daily *per capita* demand is about 284 liters (Rolle, 2010, personal communication), amounting to a total of 200,000 m^3/y. Bimini is home to approximately 1,900 permanent residents, but the islands may be visited by between 1,900 and 5,000 tourists on a monthly basis, arriving by air and sea respectively (Bahamas Department of Statistics, 2012) increasing the water demand.

Carbonate islands typically have high permeability due to their karstic nature and increased secondary permeability as a result of dissolution. Across the Bahamian Archipelago, groundwater reserves are contained in two carbonate units: the Lucayan Limestone and the Holocene Aquifer. The Lucayan Limestone is a Pleistocene unit consisting of calcitic packstones

or wackestones (Whitaker and Smart, 1997a). The irregularly cemented unit has a high hydraulic conductivity formed through dissolution and, as a result, is the primary freshwater aquifer on most islands (Whitaker and Smart, 1997a). The Holocene Aquifer is made up of unconsolidated to partially consolidated calcareous sands. The Lucayan Limestone is commonly found throughout the archipelago but the distribution of a Holocene Aquifer is irregular among the various islands. In some locations, the Holocene Aquifer forms a fringe around the circumference of the island. Due to low transmissivity, the fringe has been shown to retard freshwater discharge and tidal mixing (Whitaker and Smith, 1997a). The islands in the north of the Bahamian Archipelago tend to receive more precipitation and have a larger freshwater lens than the more southern islands. For Bimini, the freshwater lens has been estimated to contain 1.25 million m^3. This volume is only 40% of the average annual groundwater recharge. The freshwater reservoir is considered to be at risk due to the infiltration of liquid wastes and sewer systems, and while the freshwater needs of Bimini are supplied by desalination, preserving a freshwater reservoir could be an important water supply safety net.

Like the rest of the Bahamas, Bimini is a karst terrain characterized by areas of high, localized flow through channels formed by dissolution. In the mangrove swamp there is a submerged spring locally known as the “Healing Hole”, which is a popular, though remote, tourist attraction believed to have restorative and curative properties. The Bimini Healing Hole was visited briefly on June 16, 2010 at times of both low and high tide. The odor of sulfur was especially strong at low tide. Salinity was measured at 36 near the sediment, and there was a perceptible coldness at the bottom of the water column. Due to soft and loose sediment, frequent mangrove roots and limited time, no seepage meters were installed at the Healing Hole.

There are few water-table wells on Bimini. One notable well is the “Fountain of Youth”, built to commemorate Ponce de Leon’s search for the Fountain of Youth (The Bahamian, 2010). As I will discuss, this appears to access a perched water table.

High permeability systems, like those in the Bahamas, may enhance the recirculation of seawater into the groundwater system. In nearby South Andros Island, tidally driven ocean waters had substantial effects on the carbonate aquifer under the island (Whitaker and Smart, 1997b). Circulated seawater increases the dissolution potential of carbonate sediments. The saline groundwater is depleted in calcium compared to open seawater, leading to a possible formation of marine calcite cements in these parts of the aquifer below meteoric water mixing and in areas where the bank’s groundwater contains a large seawater fraction (Whitaker and Smart, 1997b). An increase in circulation of seawater, perhaps as a result of sea level rise, would likely augment calcite cementation and/or dolomitization forming a digenetic barrier to seaward groundwater seepage (Moore, 1989).

Methods

SGD measurements were collected at six locations (Figure 5.1). A Schlumberger "CTD-Diver" pressure sensor (model DI261: 10m/80 mS/cm) was attached to record water elevations. Measurements were made using Lee-type seepage meters using the method previously described in Chapter 1. Average SGD reported are those derived by the ellipse fit method described in Chapter 1, except where noted. Salinity measurements were taken from each device and measured with a refractometer.

Results

South Bimini Island

Groundwater discharge was measured at three different locations on the island of South Bimini: two along the western end of the island (Bimini Sands Resort and Blue House Beach) and one on the southern end along the shore at the Bimini Biological Field Station (Figure 5.1).

SGD along the beach at the Bimini Sands Resort (Figure 5.1; 25.707N, 79.301 W) was sampled on three dates: June 14, 17 and 24, 2010. The devices among the three sample dates were not all in the same location on the beach, but in the same general vicinity in order to determine a random sample of groundwater discharge patterns.

On June 14, devices were arranged in a transect perpendicular to shore (Figure 5.2). Device B showed a weak inverse relationship with the tide height and ranged from 8 to 16 cm/d, device D had a stronger inverse relationship ranging from 9 to 18 cm/d and device F had a direct relationship with the tide ranging from 6 to 11 cm/d (Figure 5.3). They showed a slight decrease in discharge as distance from shore increased (Figure 5.4). Using the exponential expedient, as described in Chapter 1, yields an integrated SGD value of 14 m^3 per meter of shoreline per day. Average SGD was 13 cm/d at device B closest to shore, 12 cm/d at the intermediate device D, and 9 cm/d furthest from shore at device F (Figure 5.5A-C). No dilution could be detected; SGD samples were of ambient salinity (32); the freshwater component of SGD was not large enough to dilute and flush the chambers.

On June 17, devices were positioned between two groins parallel to the shore (Figure 5.2) in an attempt to substantiate reports of cold spots as indication of submerged springs of fresh groundwater. The centrally located device showed higher discharge than the adjacent devices. Devices B and D showed a direct relationship with the tide ranging from 6 to 12 cm/d at device B and 6 to 16 at device D. Device F showed an inverse relationship with the tide ranging from 5 to 10 cm/d (Figure 5.6). The average discharge was 9 cm/d at device B, 11 cm/d at device D, and 7 at device F (Figure 5.7A-C). No difference between SGD samples and ambient salinity (39) could be detected.

On June 24, devices were also arranged parallel to shore (Figure 5.2) and All devices showed an inverse relationship with the tide; device B ranged from 9 to 20 cm/d, device D ranged from 13 to 23 cm/d and device F ranged from 13 to 22 cm/d (Figure 5.8). Average discharges were 15 cm/d for device B, 17 cm/d for device D and 17 cm/d for device F (Figure 5.9A-C). Salinity was not measured at this site.

SGD at Blue House Beach was sampled on June 20, 2010 (Figure 5.1; 25.70156 N, 79.30244 W) with the devices arranged parallel to shore (Figure 5.10). All three devices showed an inverse relationship with the tide; device B ranged from 6.6 to 12.6 cm/d, device D ranged from 4 to 11 cm/d and device F ranged from 6 to 9 cm/d (Figure 5.11). Average discharges were 14 cm/d for device B, 8 cm/d for device D and 8 cm/d for device F; devices D and F averages are the arithmetic mean, not ellipse average due to an inaccurate fit of the ellipses to the data (Figure 5.12A-C). There was no difference between SGD samples and ambient salinity, which was 39.

The southern side of South Bimini was sampled on June 15, 2010 at a site near the Bimini Biological Field Station (a.k.a. the Shark Lab; Figure 5.1; 25.69916 N, 79.29664 W) with three devices installed perpendicular to the shoreline (Figure 5.13). Discharges were low with no discernible trend with distance from shore, and none of the devices showed a strong relationship with the tide; SGD at device B ranged from 4 to 7 cm/d; device D ranged from 3 to 6 cm/d; device F ranged from 4 to 8 cm/d. SGD of 6 cm/d was recorded from device B closest to shore, 4 cm/d from device D and 6 cm/d from device F furthest from shore (Figure 5.14, Figure 5.15A-C). Discharge and ambient salinities were all 32 at the end of the sampling period.

The South Bimini Island had a grand average groundwater discharge of 11 cm/d.

Water Table and Tidal Response

Two pressure sensors were deployed on June 15, 2010 to investigate the responsiveness of the water table to changes in tidal level. One pressure sensor was deployed with the SGD collection devices at the Bimini Biological Field Station and another was temporarily installed inside a water well, known locally as the Fountain of Youth (25.70828 N, 79.28913 W). Tidal signature is clearly evident in the pressure sensor at the Bimini Biological Field Station while the pressure sensor at the Fountain of Youth shows no change in water level over the same time period (Figure 5.16). Any observed changes in the pressure record at the Fountain of Youth greater than one cm are attributed to visitors using a provided bucket to collect the fresh water from the well (Figure 5.17). The well water was fresh but apparently intersected a perched water table without hydrological connection to the sea.

North Bimini Island

On the island of North Bimini, groundwater discharge was measured at three locations: two on the western side of the island at Alice Town and the Bimini Bay Resort and one on the eastern side of the island at East Well (Figure 5.1).

Alice Town, the center of development on Bimini (Frommers, 2013), was sampled for groundwater discharge on June 18, 2010 with three devices installed perpendicular to shore (Figure 5.18; 25.72440 N, 79.29954 W). At this time, the beach was bounded on the landward edge by a 3 m scarp, the base of which acted as the high water line. The pressure sensor failed so no water level data was recorded, precluding the use of the ellipse fit method of determining average. The arithmetic means for the three devices show a slight decrease in SGD as distance from shore increases; 7 cm/d was recorded at device B closest to shore, 7 cm/d at device D and 6 cm/d at device F furthest from shore. SGD appeared to be inversely correlated with published tidal predictions (Figure 5.19). Salinities of groundwater and ambient samples remained constant at 37 over the sampling period.

Groundwater discharge was sampled just south of the Bimini Bay Resort on June 21, 2010 with three devices installed parallel to shore (Figure 5.20; 25.74557 N, 79.28589 W). Device B recorded an average discharge of 8 cm/d, ranging from 4 to 13 cm/d, device D had an average of 11 cm/d and a range of 5 to 13 cm/d and device F recorded the lowest discharges with an average of 7 cm/d and a range from 5 to 10 cm/d (Figure 5.21, Figure 5.22A-C). All three devices show a slight inverse relationship with the tide and all water samples, groundwater and ambient, salinity remained at 39 over the sampling period.

SGD was measured on the eastern side of North Bimini Island at a site called East Well on June 23, 2010 (Figure 5.23; 25.75368 N, 79.24368 W). Devices were installed parallel to shore just offshore of an extensive sea grass bed. Groundwater at device B recorded an average SGD of 5 cm/d and ranged from 4 to 8 cm/d, device D showed the largest average discharge measured on either Bimini island with an average SGD of 21 cm/d, ranging from 16 to 25 cm/d, and discharge at device F ranged from 7 to 15 cm/d with an average of 9 cm/d (Figure 5.24, Figure 5.25A-C). Devices B and F showed slight inverse relationships with the tide while device D shows a slight direct relationship with the tide. Both the groundwater and ambient seawater had a salinity of 40, which was unchanged through the course of the sampling period.

The North Bimini Island had a grand average discharge of 9 cm/d.

Discussion

The nearly uniformly consistent salinity measured in the discharged groundwater that did not vary from ambient water salinities, the low average discharges and the apparent disconnect

between the water levels in the fresh groundwater and the sea level indicate that discharge at the shoreline is the result of tidal pumping rather than the expected discharge driven by the hydraulic head of the freshwater lens.

A preliminary water budget for Bimini might be constructed to take advantage of SGD measurements. Direct precipitation amounts to about 30 million m^3/y. Of that, 7.5 million m^3/y is recharged. Desalination provides another 0.2 million m^3/y, which can be expected to also be recharged through septic systems. Assuming a discharge zone one hundred meters wide at the shoreline, SGD would amount to an average of about 110 million m^3/y. This is supported by the integrated SGD of 14 m^3 per meter of shoreline per day approximated using the exponential expedient at the Bimini Sands Resort location on June 14, 2010, which, when multiplied by the 33 km of shoreline and converted to yearly values, translates to 169 million m^3/y, on the same order of magnitude as the expected value. However, considering that there was no observed freshening of groundwater samples on either Bimini island, the majority of this discharge must be circulated seawater. This is not an uncommon situation. Seawater has often been found to be the dominant component of SGD, contributing up to 97% of SGD (Taniguchi *et al*., 2002). In Great South Bay, NY, for example, SGD was assessed to be composed of 90% re-circulated seawater (Beck *et al*., 2008).

The Holocene aquifer contains perched water tables isolated from the beach aquifer that the Fountain of Youth has accessed, and where there is no tidal variation and no measurable salinity. The deeper aquifer may also be supplying water through fissures or dissolution channels in spots up through the sand blanket to support higher discharge areas like the Healing Hole. From the salinity measurement of the bottom water, it seems unlikely that a submerged, *freshwater* spring feeds water to the Healing Hole, though the looseness of the sea floor and the perceptible coldness of the water indicates that there may be a submerged saline spring in that location. In the mangrove swamp, groundwater may seep directly through the sediment as interstitial pore-water (Susilo *et al*., 2006). Seawater may also be flushed through animal burrows during the tidal cycle (Stieglitz *et al*., 2000). It would seem that seawater, carried into the mangrove swamp by the tide, migrates through the sediment. The discharge is then focused into the deep Healing Hole after its residence in the substrate.

Conclusion

As might be expected, the karstic, surficial, freshwater aquifer of Bimini is neither homogeneous nor isotropic. Nevertheless, SGD can approach 25 cm/d. Seawater recirculated through the beach or the mangrove root zone is the only observed component of SGD around the island. Seawater seeping through mangrove sediments to eventual discharge into local deeps, like the Healing Hole. Along the open-ocean shoreline, about 100 million m^3/y seems to be recirculated through the carbonate platform. Despite the undetectable contribution from

terrestrial fresh groundwater, chemical transformations in the subterranean estuary may still be a substantial factor controlling the water quality in the coastal zone if anthropogenic elevation of septic contaminants is high.

References

Bahamas Department of Statistics, 2012. Key Statistics > Population & Census > Pop. By Sex & Age Bimini. Key Statistics > Tourism Statistics. http://statistics.bahamas.gov.bs/ Last accessed: 30 April 2013.

Beck, A.J., J.P. Rapaglia, J.K. Cochran, H.J. Bokuniewicz, and S. Yang. 2008. Submarine groundwater discharge to Great South Bay, NY, estimated using Ra isotopes: Marine Chemistry, v. 109, p. 279-291

Carew, J.L. and J.E. Mylroie. 1997. Geology of the Bahamas. In H.L. Vacher and T. Quinn (Ed.), Geology and Hydrogeology of Carbonate Islands. Developments in Sedimentology 54 pp. 91-133. Amsterdam: Elsevier B.V.

Duncan, D.A., 1972. High Resolution Seismic Survey, Port Royal Sound Environmental Study. S. C. Water Resources Commun., Columbia SC, pp. 85-106.

Frommers Travel Section for Bimini http://www.frommers.com/destinations/bimini/0263010001.html Last accessed: 19 April 2013.

Moore, C.H., 1989. Carbonate Diagenesis and Porosity. Developments in Sedimentology 46, Elsevier, Amsterdam, 38 pp.

Moore, W.S. and R. Arnold. 1996. Measurement of 223Ra and 224Ra in coastal waters using a delayed coincidence counter. Journal of Geophysical Research. 101: 1321–1329.

Rolle, O. 2010. Personal communication. June 2010. Bimini water supplier.

Stieglitz T., P.V. Ridd and P. Muller. 2000. Passive irrigation and functional morphology of crustacean burrows in atropical mangrove swamp. Hydrobiologia 421: 69–76.

Susilo, A., P.V. Ridd and S. Thomas. 2006. Comparison between tidally driven groundwater flow and flushing of animal burrows in tropical mangrove swamps. Wetlands Ecology and Management 13: 377–388

Taniguchi, M., W.C. Burnett, J.E. Cable and J.V. Turner. 2002. Investigation of submarine groundwater discharge: Hydrological Processes, v. 16, p. 2115- 2129.

The Bahamian. 2010. http://islands.thebahamian.com/bimini.html Last accessed: July 2010.

Whitaker, F.F. and P.L. Smart. 1997a. Hydrogeology of the Bahamian Archipelago. pp. 183-212 in H.L. Vacher and T. Quinn (Ed.), Geology and Hydrogeology of Carbonate Islands. Developments in Sedimentology Vol. 54

Whitaker, F.F. and P. Smart. 1997b. Groundwater circulation and geochemistry of a karstified bank-marginal fracture system, South Andros Island, Bahamas. Journal of Hyrdology 197: 293-315.

Figures

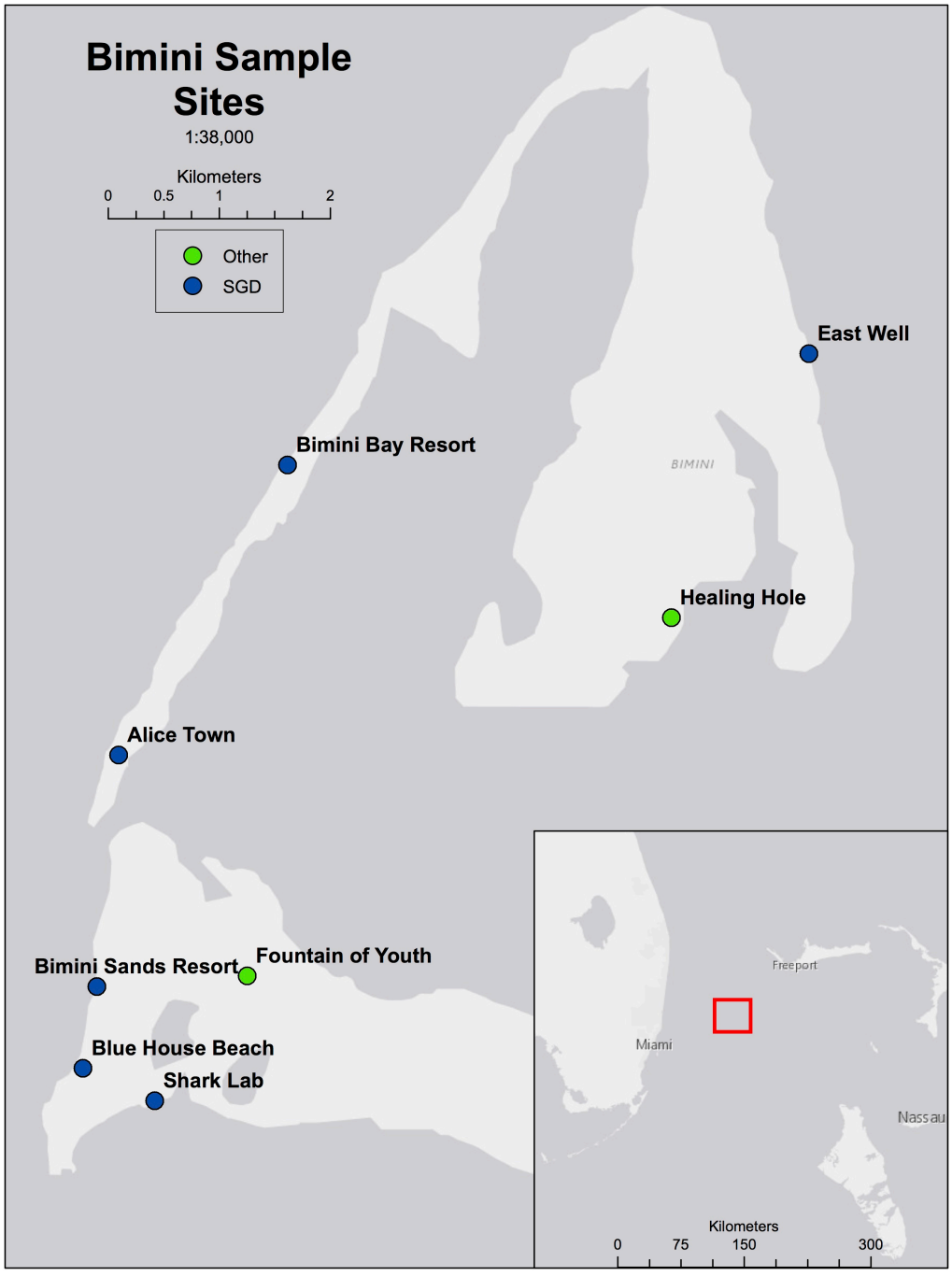

Figure 5.1. Bimini Map. Blue markers indicate SGD field sites, green markers indicate water samples taken without SGD devices. Map produced by Michael White, SoMAS.

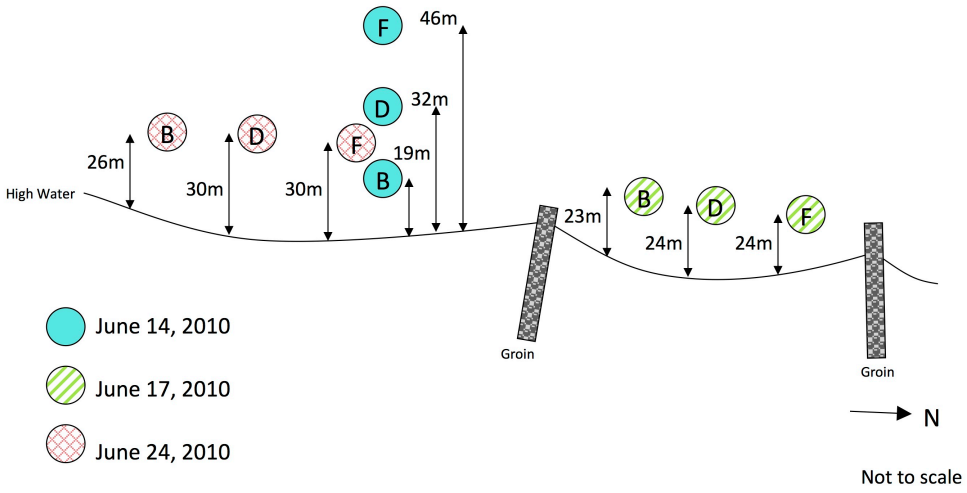

Figure 5.2. Sketch of Bimini Sands Resort site. Lettered circles represent device locations (fill patterns indicate different sampling dates), solid black line indicates shoreline position and large arrow indicates north. Figure is not to scale.

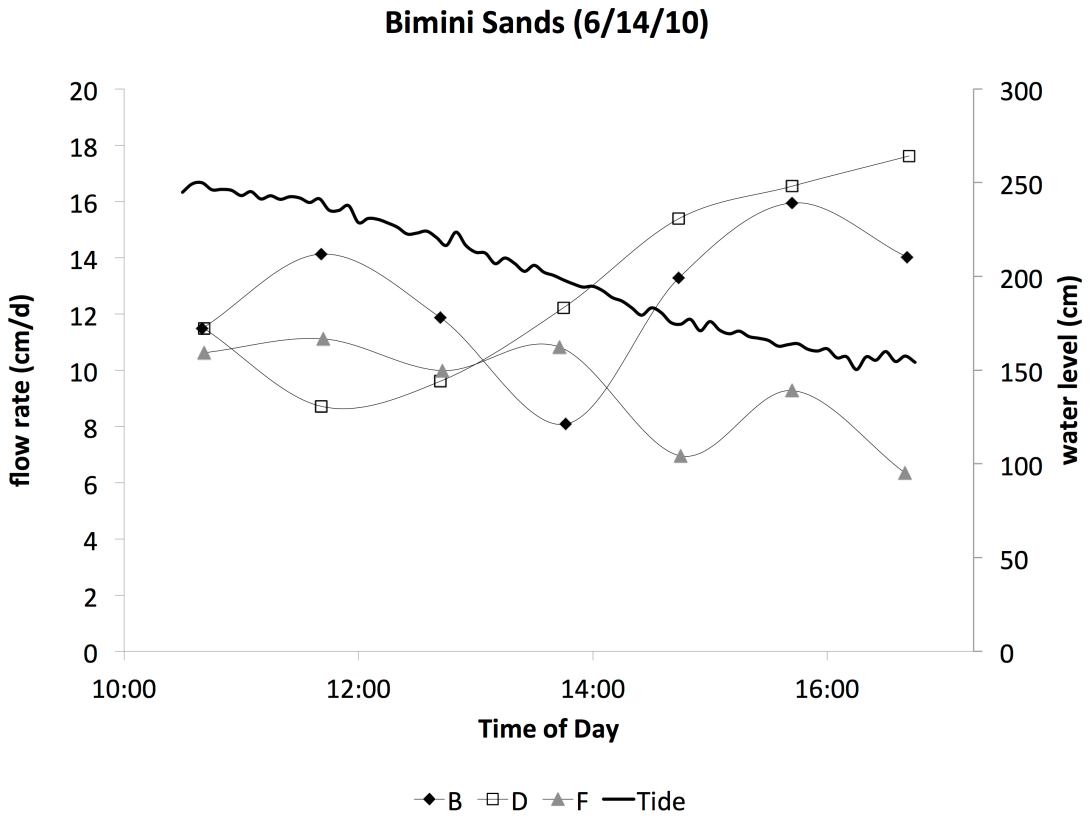

Figure 5.3. Bimini Sands flow rates for June 14, 2010. Devices B (black closed diamonds), D (black open squares), and F (grey closed triangles) with relation to the tide (thick black line).

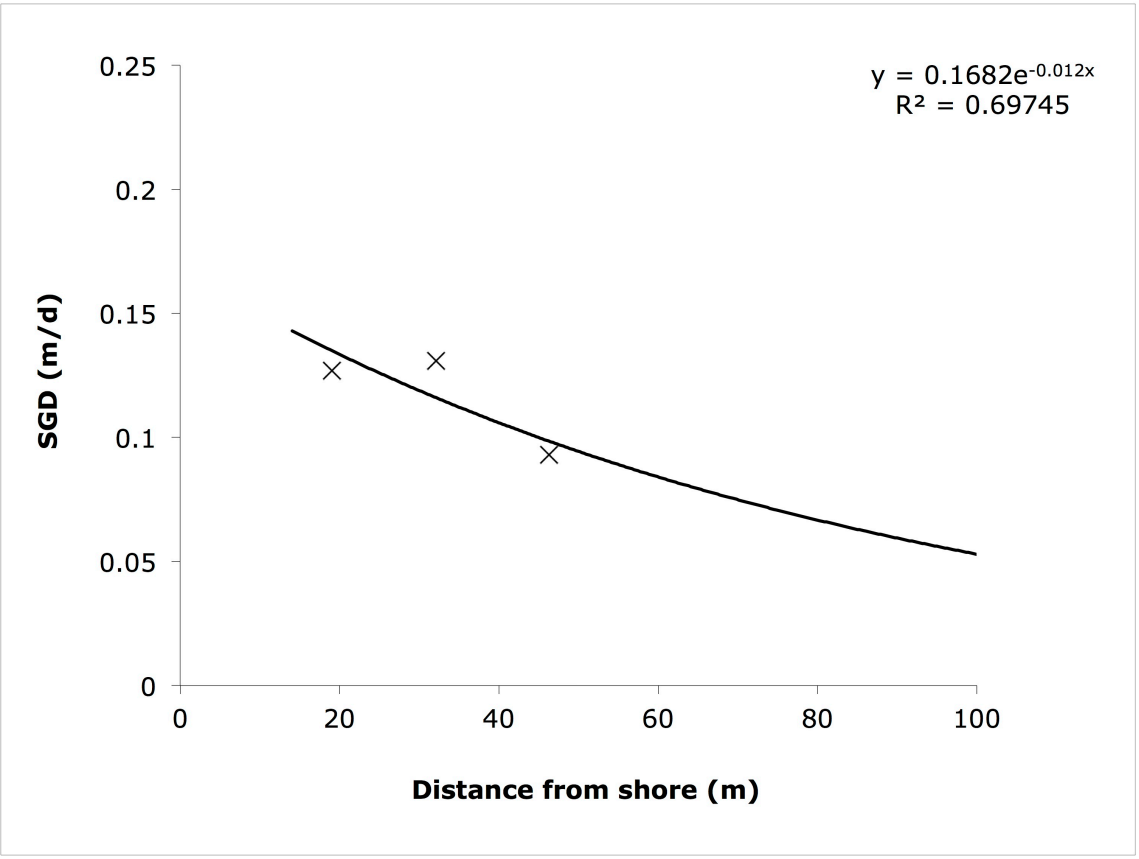

Figure 5.4. SGD decrease with increasing distance from shore at the Bimini Sands Resort on June 14, 2010.

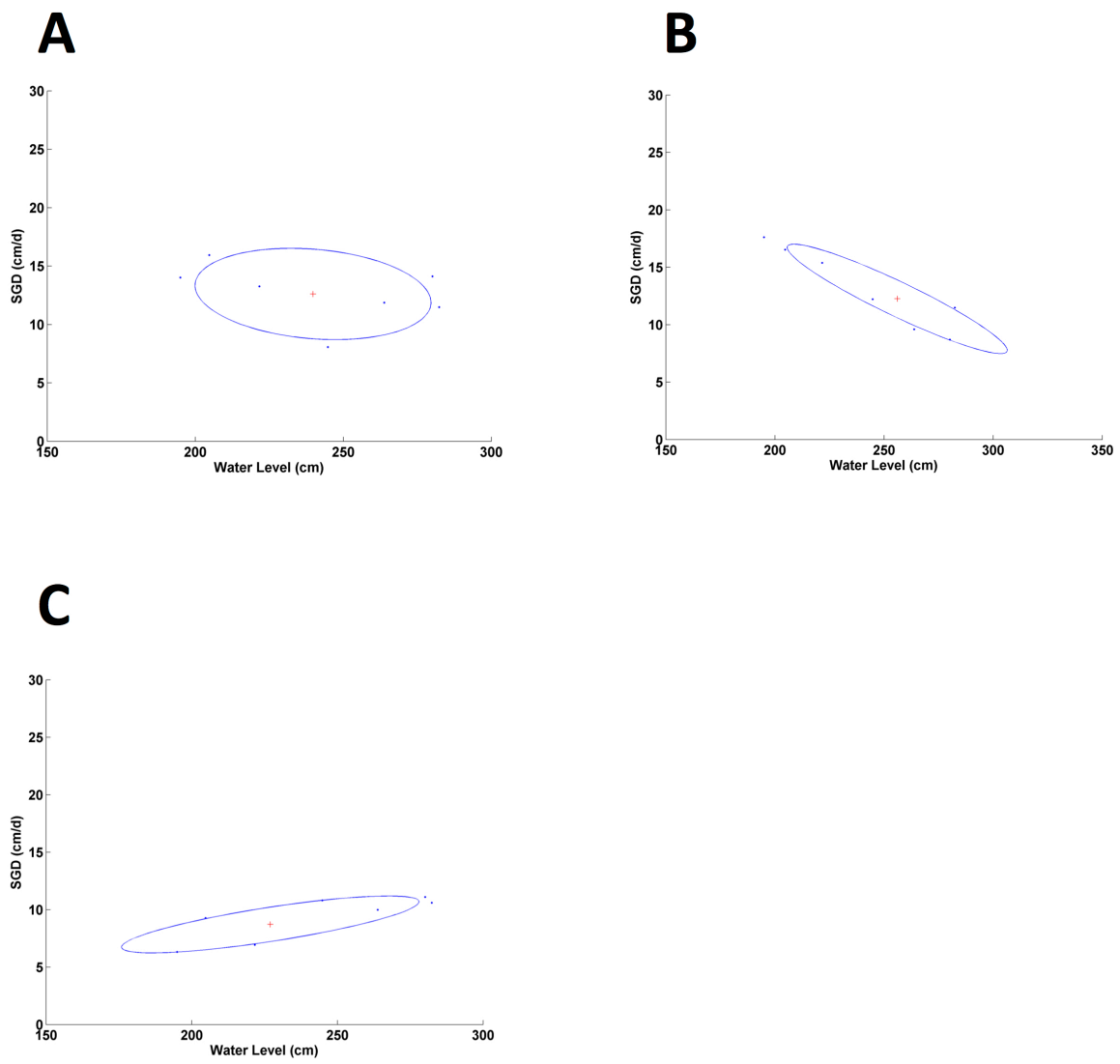

Figure 5.5A-C. Bimini Sands Resort ellipse fit for June 14, 2010. Upper left (A) is device B, upper right (B) is device D, and lower left (C) is device F. Blue points are data, blue ellipse is the fit ellipse, and the red cross is the center of the ellipse. Note different axes on subplots.

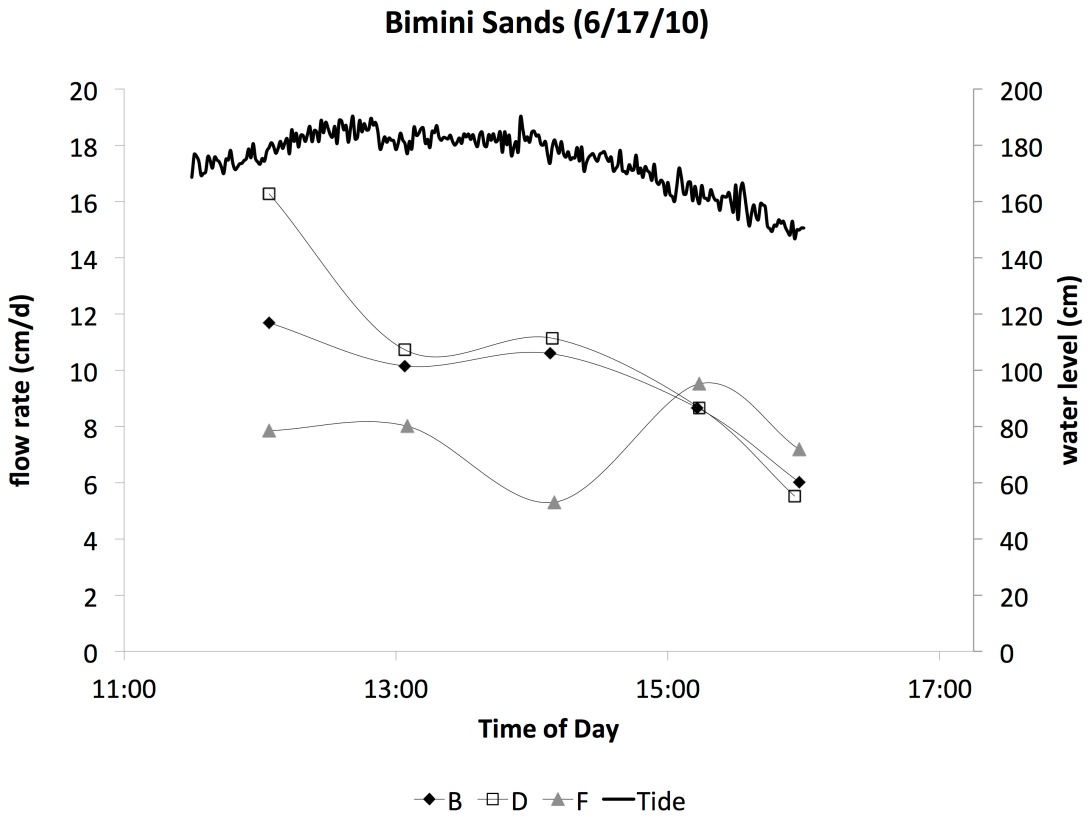

Figure 5.6. Bimini Sands flow rates for June 17, 2010. Devices B (black closed diamonds), D (black open squares), and F (grey closed triangles) with relation to the tide (thick black line).

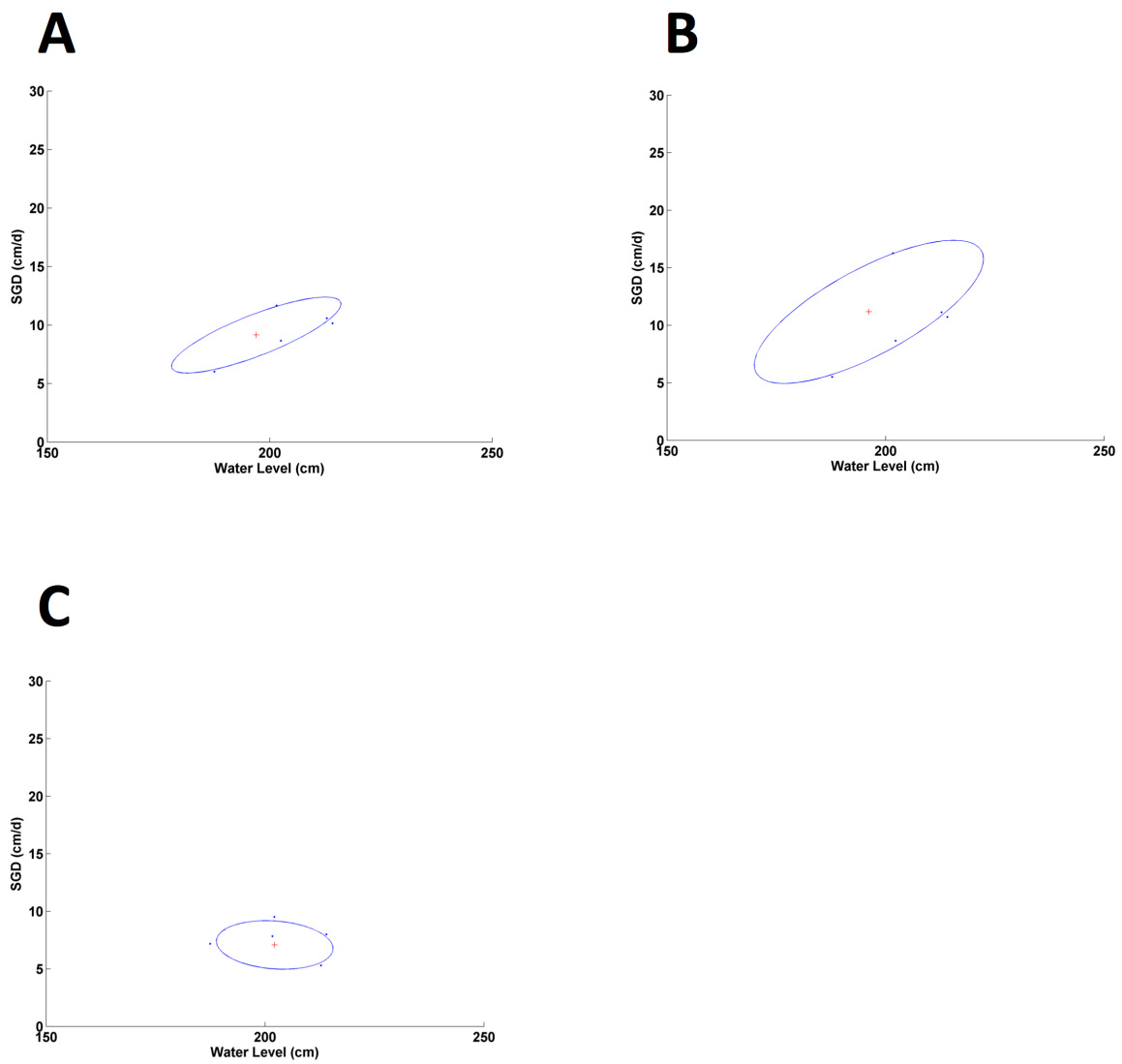

Figure 5.7 A-C. Bimini Sands Resort ellipse fit for June 17, 2010. Upper left (A) is device B, upper right (B) is device D, and lower left (C) is device F. Blue points are data, blue ellipse is the fit ellipse, and the red cross is the center of the ellipse. Note different axes on subplots.

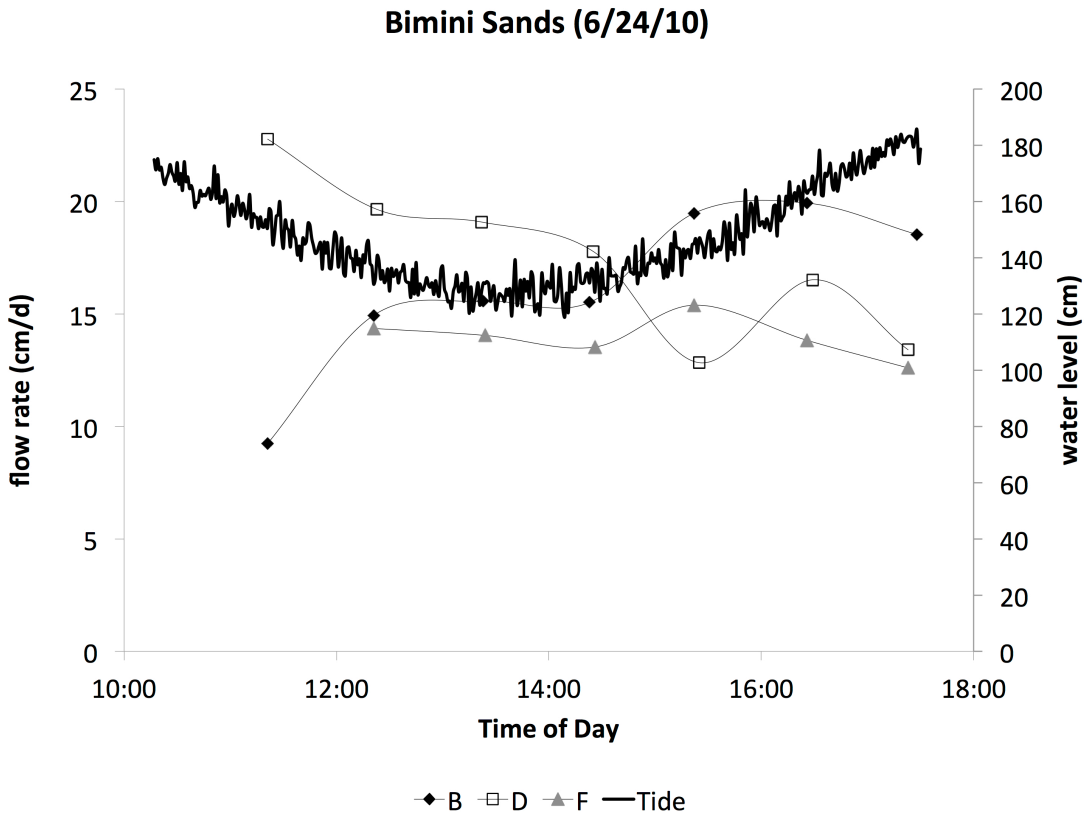

Figure 5.8. Bimini Sands flow rates for June 24, 2010. Devices B (black closed diamonds), D (black open squares), and F (grey closed triangles) with relation to the tide (thick black line).

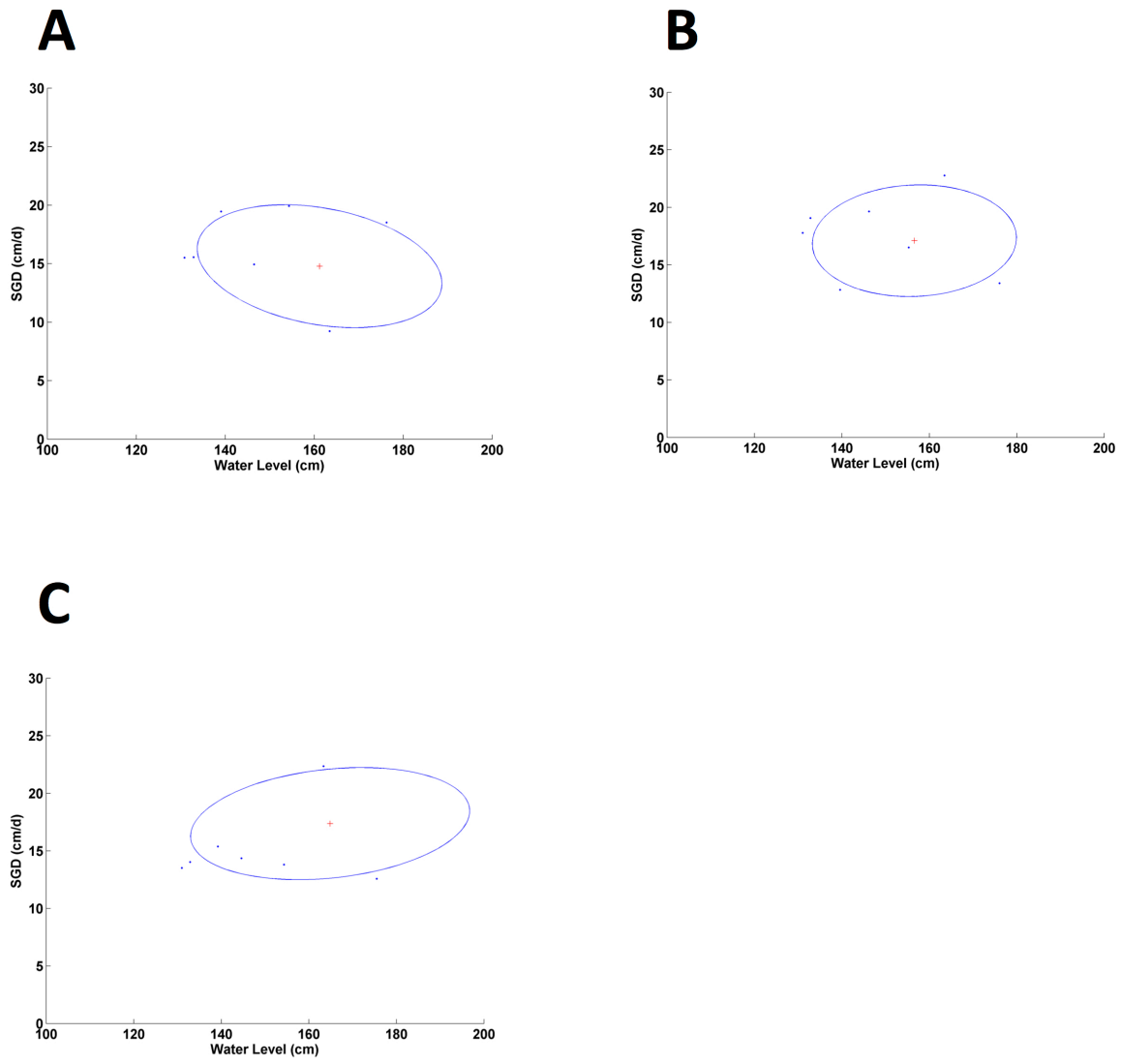

Figure 5.9 A-C. Bimini Sands Resort ellipse fit for June 24, 2010. Upper left (A) is device B, upper right (B) is device D, and lower left (C) is device F. Blue points are data, blue ellipse is the fit ellipse, and the red cross is the center of the ellipse. Note different axes on subplots.

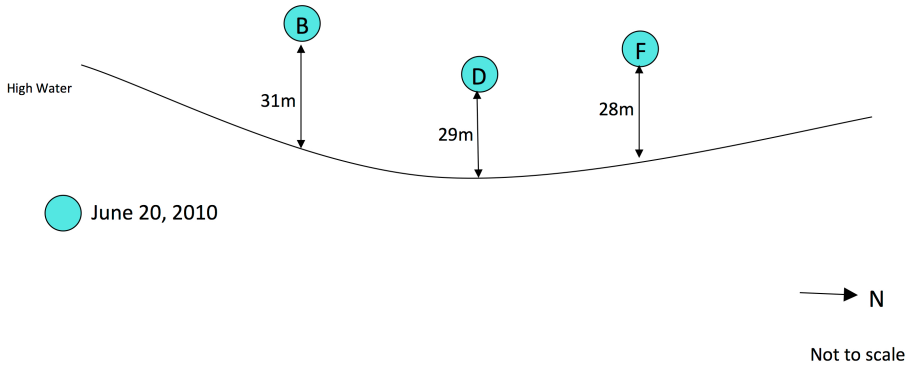

Figure 5.10. Sketch of Blue House Beach site. Lettered circles represent device locations, solid black line indicates shoreline position and large arrow indicates north. Figure is not to scale.

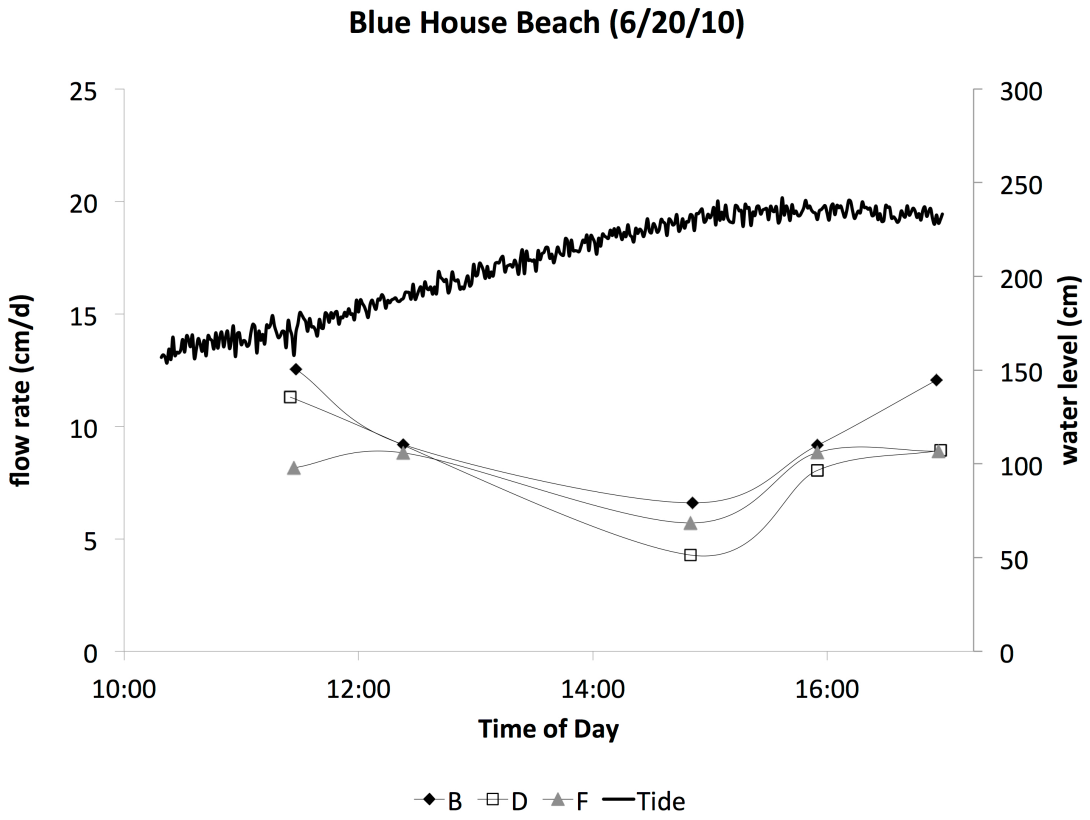

Figure 5.11. Blue House Beach flow rates for June 20, 2010. Devices B (black closed diamonds), D (black open squares), and F (grey closed triangles) with relation to the tide (thick black line).

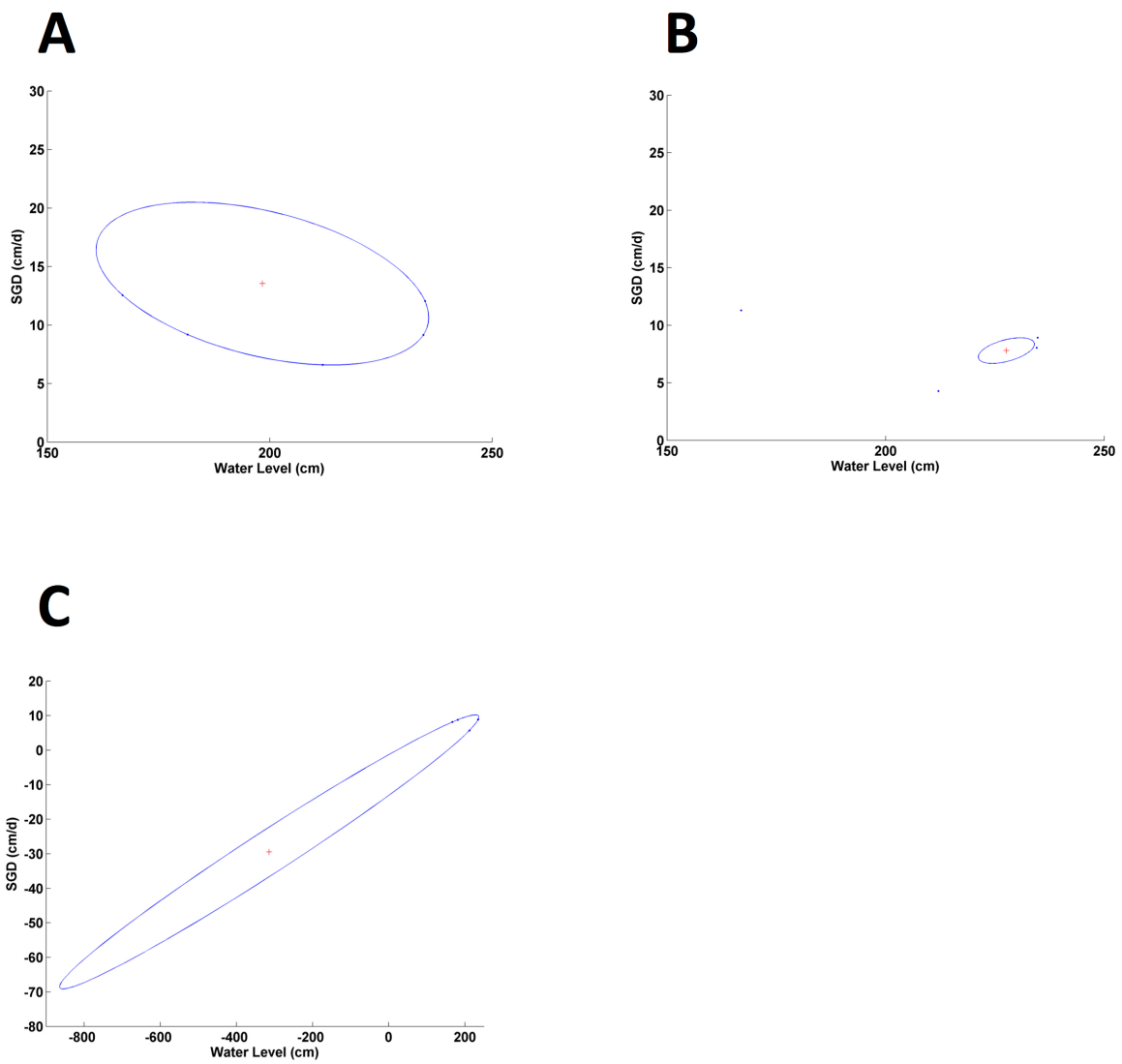

Figure 5.12 A-C. Blue House Beach ellipse fit for June 20, 2010. Upper left (A) is device B, upper right (B) is device D, and lower left (C) is device F. Blue points are data, blue ellipse is the fit ellipse, and the red cross is the center of the ellipse. Note different axes on subplots. Also note poor ellipse fit for devices D and F (subplots B and C respectively).

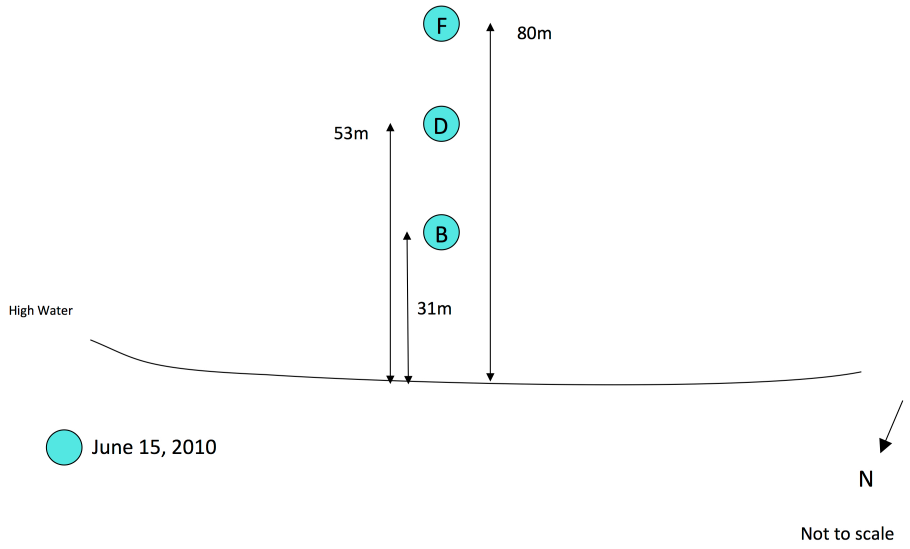

Figure 5.13. Sketch of Bimini Biological Field Station (a.k.a. Shark Lab) site. Lettered circles represent device locations, solid black line indicates shoreline position and large arrow indicates north. Figure is not to scale.

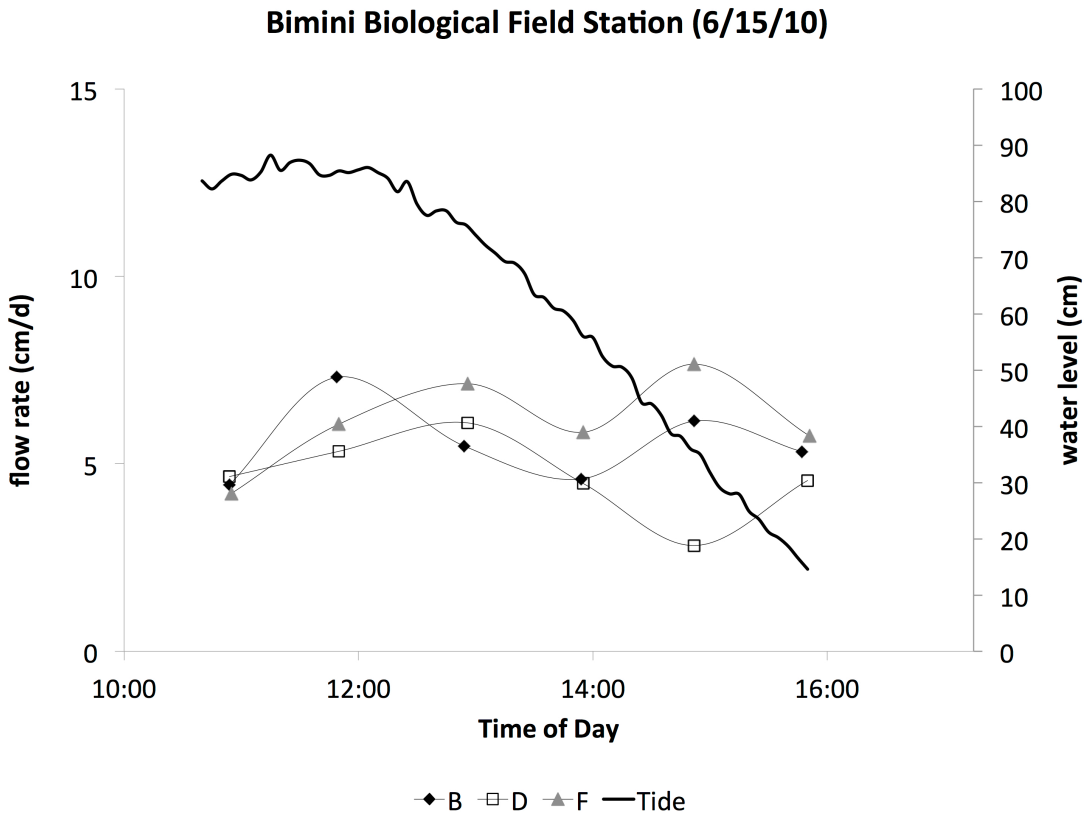

Figure 5.14. Bimini Biological Field Station (a.k.a. Shark Lab) flow rates for June 15, 2010. Devices B (black closed diamonds), D (black open squares), and F (grey closed triangles) show an inverse relationship to the tide (thick black line).

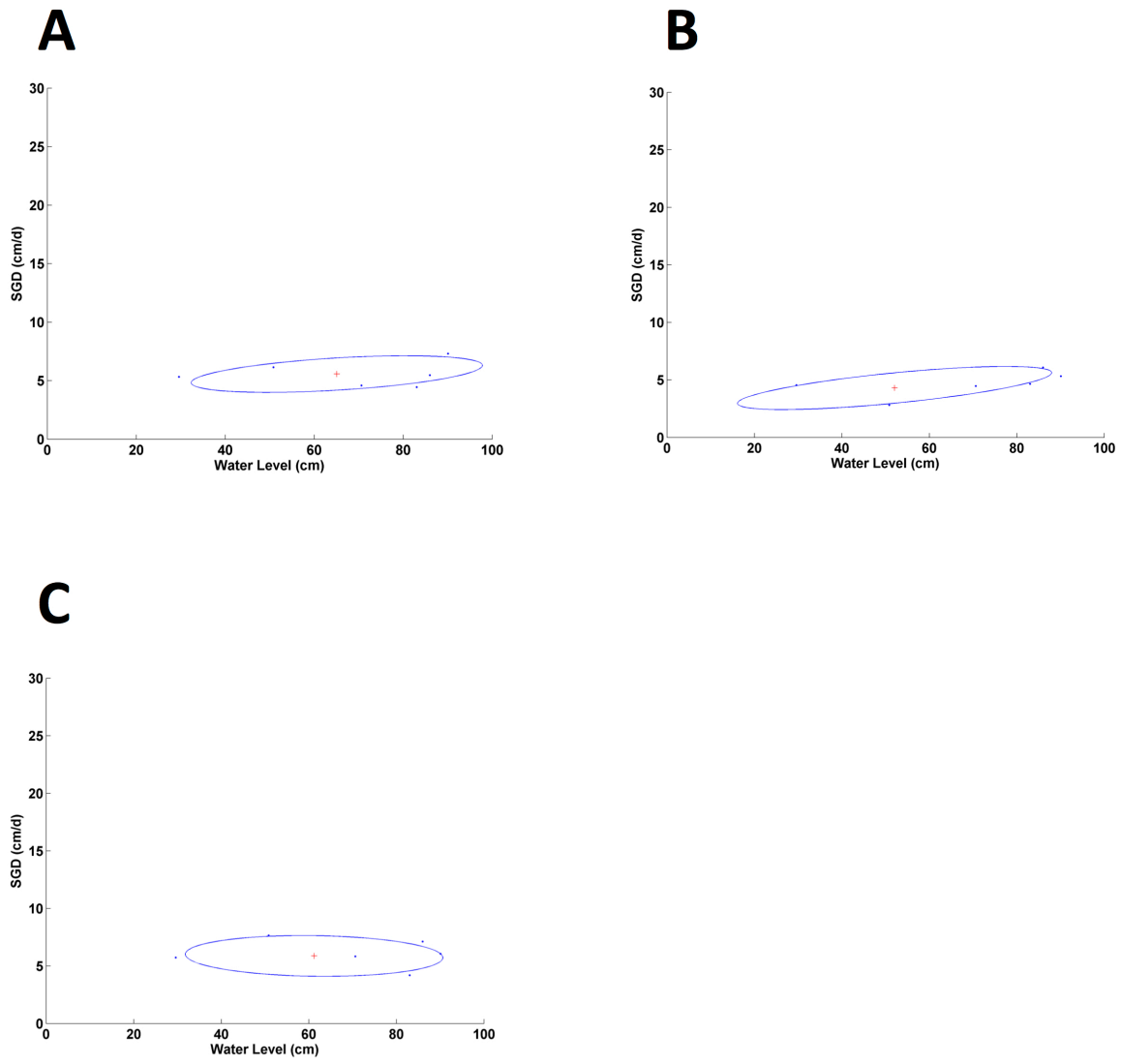

Figure 5.15 A-C. Bimini Biological Field Station (a.k.a. Shark Lab) ellipse fit for June 15, 2010. Upper left (A) is device B, upper right (B) is device D, and lower left (C) is device F. Blue points are data, blue ellipse is the fit ellipse, and the red cross is the center of the ellipse. Note different axes on subplots.

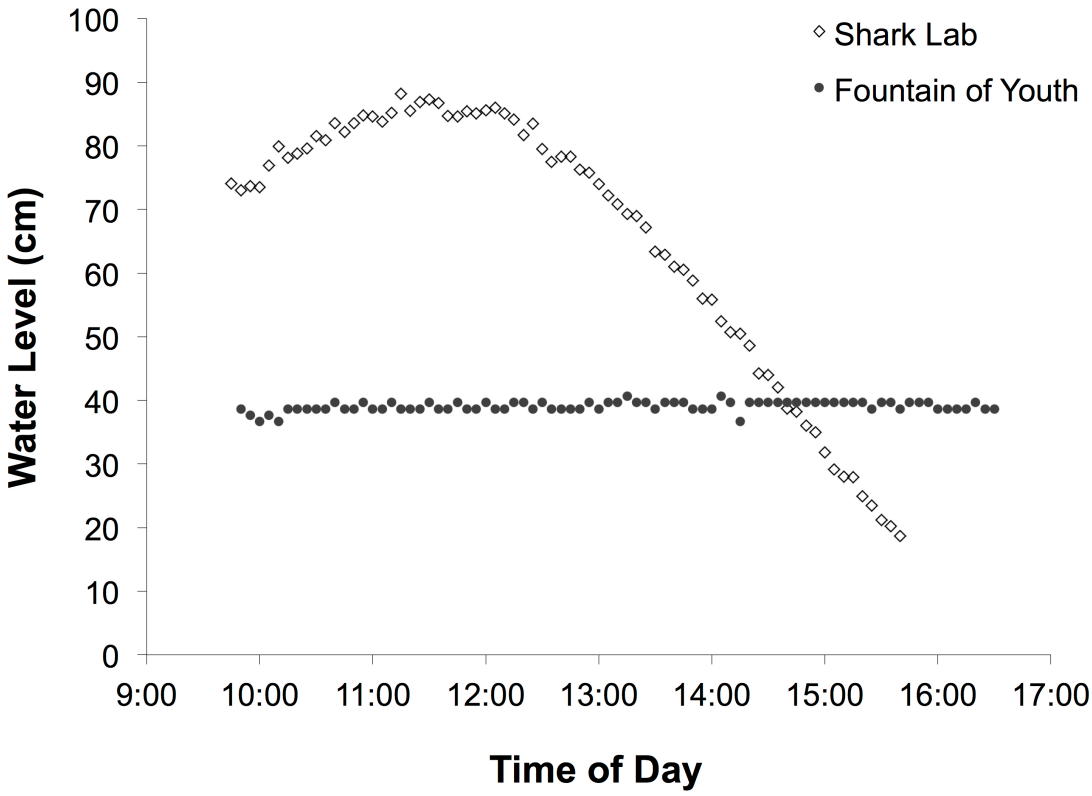

Figure 5.16. Pressure sensor comparison. A time series of water level elevations from the Shark Lab (open water; open diamonds) and the Fountain of Youth (aquifer well; closed circles).

Figure 5.17. Photos of the Fountain of Youth. Credit Ruth Coffey.

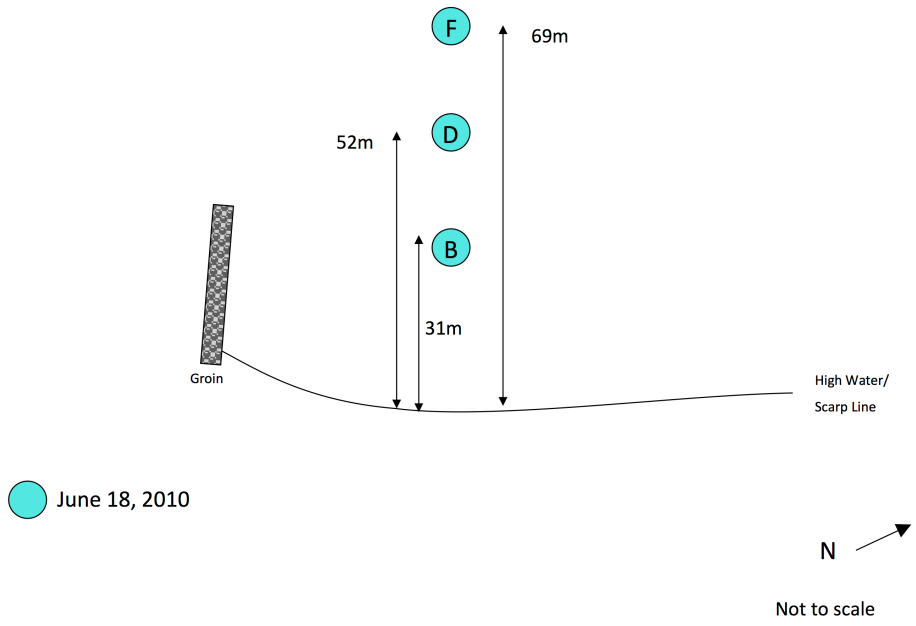

Figure 5.18. Sketch of Alice Town site. Lettered circles represent device locations, solid black line indicates shoreline position and large arrow indicates north. Figure is not to scale.

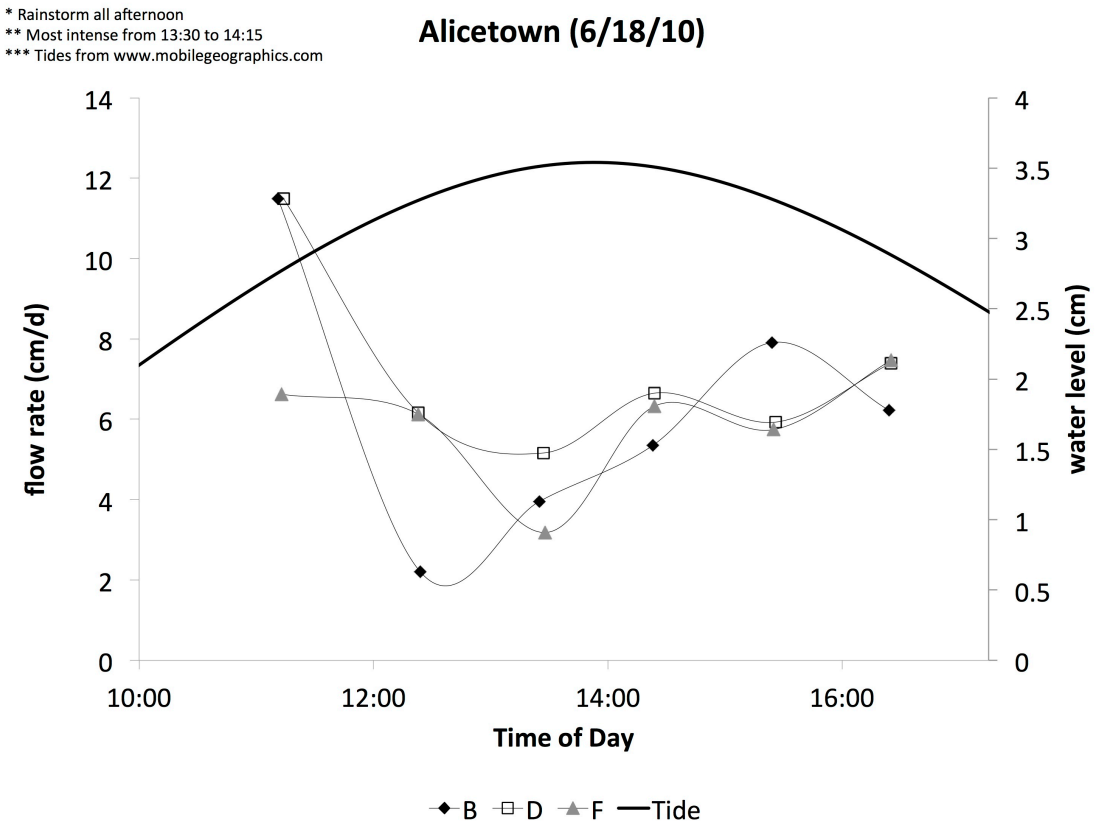

Figure 5.19. Alice Town flow rates. Devices B (black closed diamonds), D (black open squares), and F (grey closed triangles) show an inverse relationship to tidal prediction (thick black line).

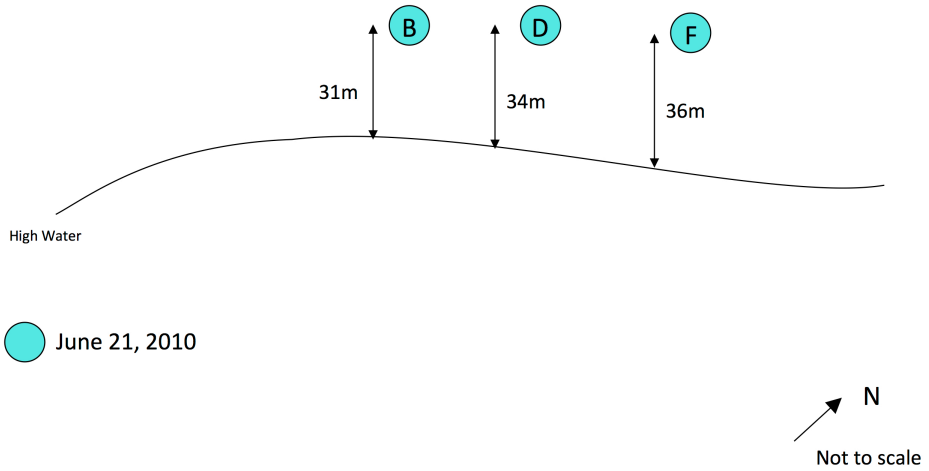

Figure 5.20. Sketch of Bimini Bay Resort site. Lettered circles represent device locations, solid black line indicates shoreline position and large arrow indicates north. Figure is not to scale.

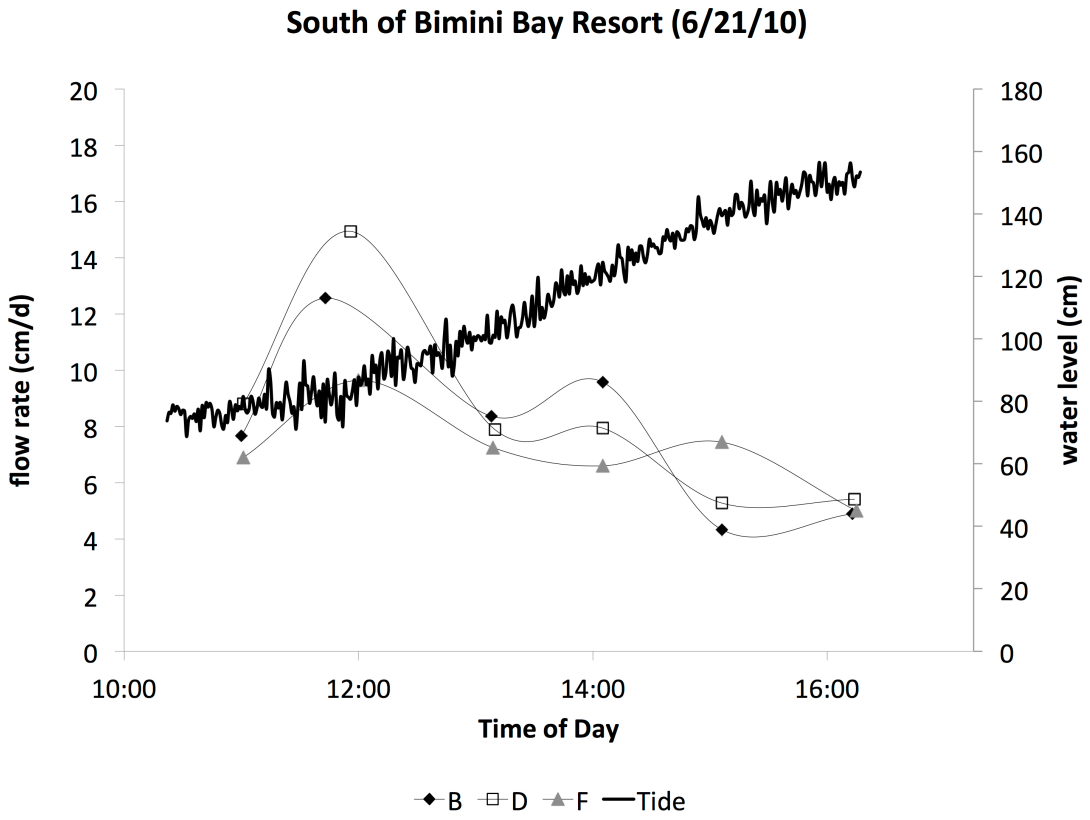

Figure 5.21. Bimini Bay Resort flow rates for June 21, 2010. Devices B (black closed diamonds), D (black open squares), and F (grey closed triangles) show an inverse relationship to the tide (thick black line).

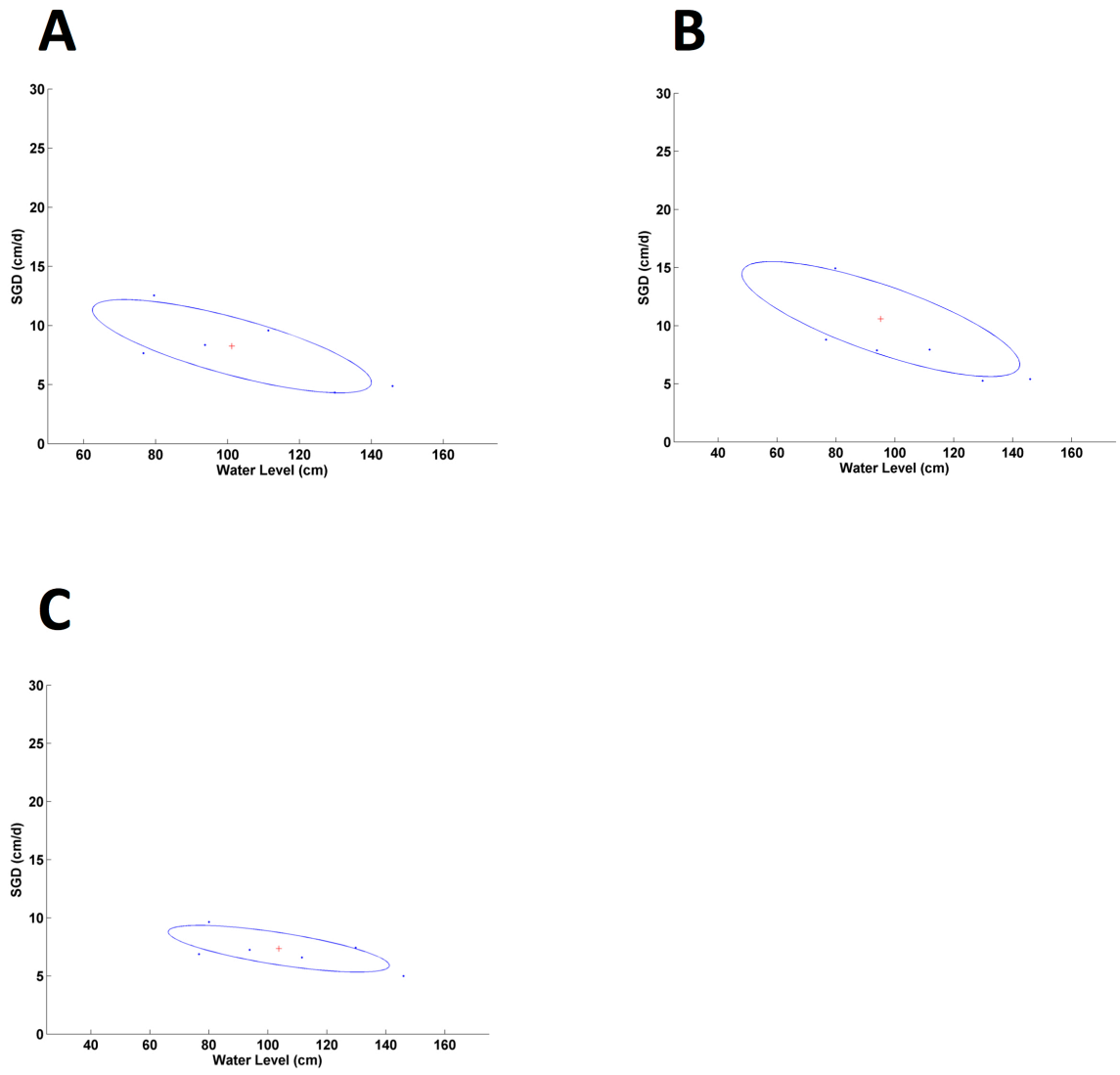

Figure 5.22 A-C. Bimini Bay Resort ellipse fit for June 21, 2010. Upper left (A) is device B, upper right (B) is device D, and lower left (C) is device F. Blue points are data, blue ellipse is the fit ellipse, and the red cross is the center of the ellipse. Note different axes on subplots.

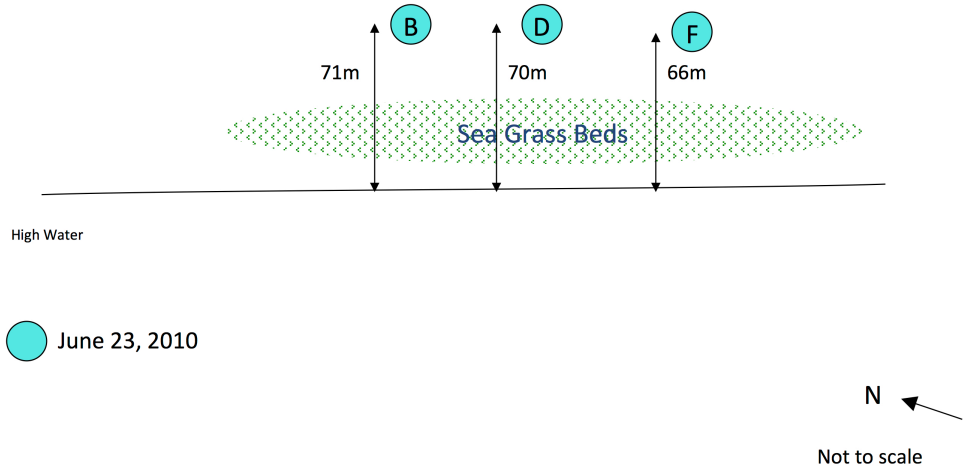

Figure 5.23. Sketch of East Well site. Lettered circles represent device locations, shaded area indicates presence of sea grass beds, solid black line indicates shoreline position and large arrow indicates north. Figure is not to scale.

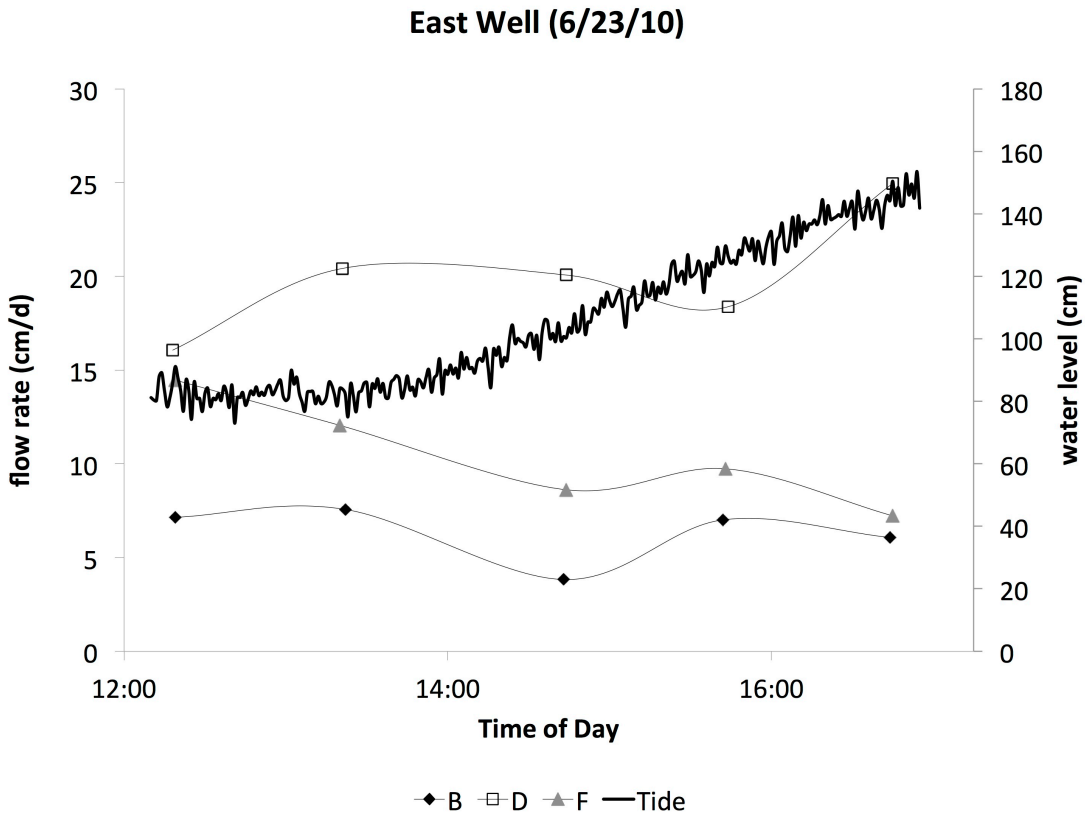

Figure 5.24. East Well flow rates for June 23, 2010. Devices B (black closed diamonds), D (black open squares), and F (grey closed triangles) with relation to the tide (thick black line).

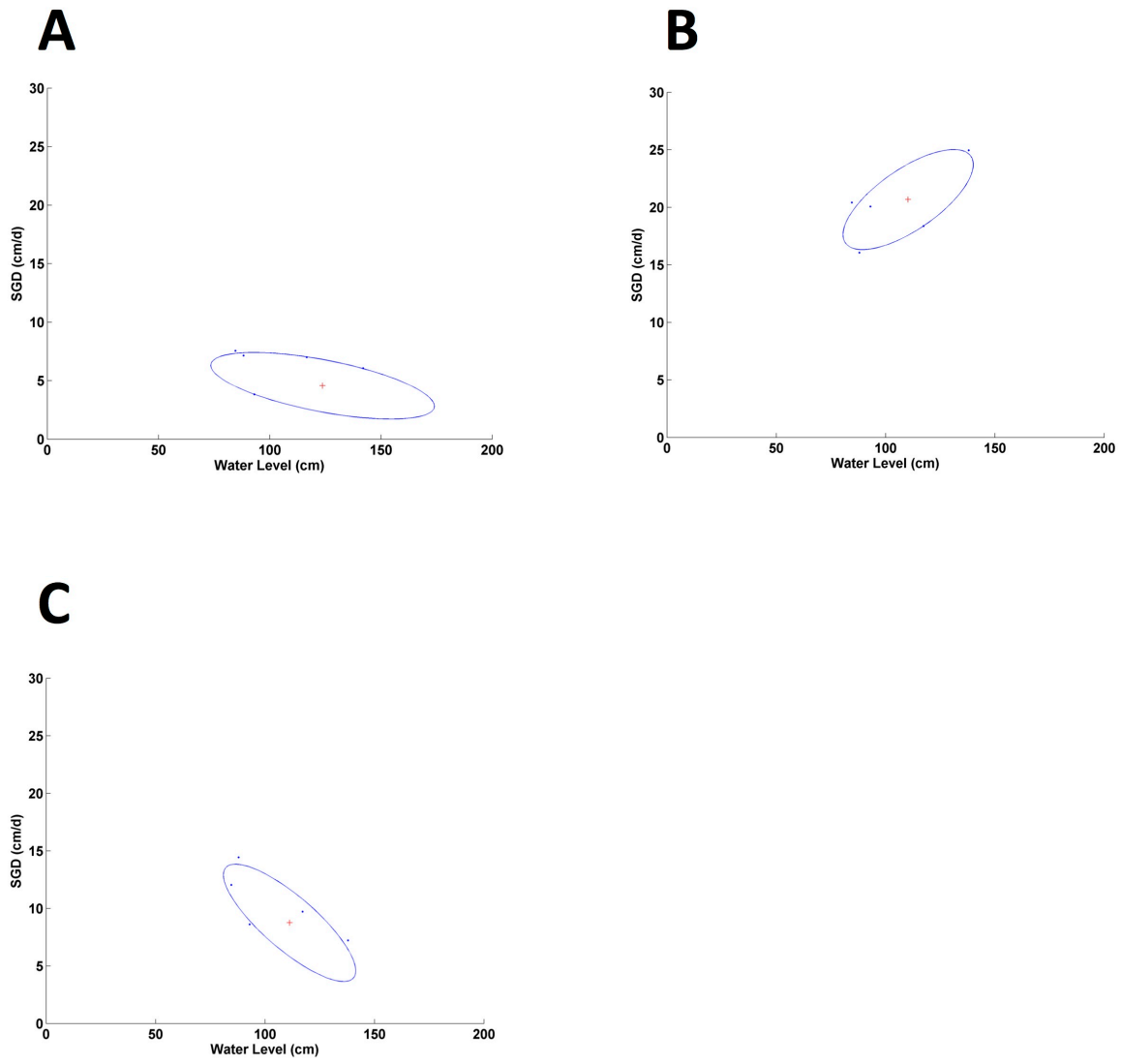

Figure 5.25 A-C. East Well ellipse fit for June 23, 2010. Upper left (A) is device B, upper right (B) is device D, and lower left (C) is device F. Blue points are data, blue ellipse is the fit ellipse, and the red cross is the center of the ellipse. Note different axes on subplots.

Chapter 6 Synthesis

Introduction

Environmental science cannot simply be the description of natural processes. The goal of environmental science and the policies developed from that science should be the sustainable development that balances a healthy environment, a healthy population and economic growth (Lutz, 1994). Unfortunately, though, the interaction between humans and the environment cannot be boiled down to a simple cause and effect relationship; rather, it is a complex system of feedbacks between demographic, economic, developmental and environmental variables. For example, tourism on a small oceanic island will impact water resources through freshwater demand and wastewater disposal contributing to the local economy at a cost. The indigenous population, agriculture and industry must cope with diminished freshwater reserves and degraded water quality. Tourist preference for a destination is dependent on the quality and availability of environmental and cultural resources to attract them, so if the environment is degraded by poor wastewater disposal techniques, the island becomes a less attractive option for tourists, feeding back into the economy and also the demographic constitution of the resident population (e.g. sector employment, emigration and immigration). Different sectors of a population, be they resident or transient, have different requirements of and impacts on the ecosystem. A population model, development model or environment model alone will, by definition, fail to incorporate the complexity of interactions between the population, development and the environment (PDE); an interdisciplinary PDE model must be used to explicitly investigate these interactions, develop effective policies, evaluate the long-term effect of these policies and make a definitive step towards sustainable development (Lutz, 1994).

A successful model supports the goals outlined. A PDE model that supports a shift towards sustainable development through tourism must not only meet the requirements for sustainable development, but also for sustainable tourism. Sustainable development is defined as "a process of change in which the exploitation of resources, the direction of investments, the orientation of technological development; and institutional change are all in harmony and enhance both current and future potential to meet human needs and aspirations" (Brundtland Report, 1987). Sustainable tourism, then, needs to develop in such a way as to balance economic growth, preservation of the natural and heritage environment that appeals to and attracts tourists

and the well being of the residents. The World Tourism Organization defined sustainable tourism as "tourism that takes full account of its current and future economic, social and environmental impacts, addressing the needs of visitors, the industry, the environment and host communities" (UNEP WTO, 2005). A PDE model, then, needs to incorporate all of these factors into a system that can make recommendations for policy makers.

The operational framework of a PDE model was well-developed by Lutz (1994). One formulation applied concepts of PDE modeling to Mauritius. It was pointed out that small island nations might be particularly appropriate for the PDE approach because resources, water especially, have "tangible finiteness" so that even a small loss might be 'painful' (Lutz, 1994). In addition, because of the small area of islands and high population densities, even small environmental degradation can have widespread impacts and, further, fragile island ecosystems may not be able to recover from environmental insults leading to irreversible losses (Lutz, 1994).

Lutz (1994) also points out that a lack of data and uncertainties "inhibit the building of detailed models". Focusing attention on one resource, water, helps, but at the expense of consideration of other resources such as agricultural products, biological resources, like fisheries, or mineral resources although development of all of these other resources depend to some extent on the quality and quantity of water. This approach may not be appropriate for all places. In some areas, air pollution or deforestation, for example, may take precedence. Certainly for the case study of Mauritius, water issues were predominant and the same is likely true on Barbados.

There are also multiple pathways that might be chosen by individual island nations to secure sustainable development, such as the exploitation of non-renewable resources, minerals or oil and gas; or the exploitation of renewable resources such as timber or fish; or the growth of agriculture. Some island nations may be able to shift sugar cane production to the generation of ethanol for export, much like Brazil was able to do after the fuel crisis in the 1970s (Hira and de Oliveira, 2009). Many island economies seemed to have forged a path of expanding tourism to fuel their island economies. In what follows, I too will assume a path to sustainable development through the expansion of tourism, even though many other options are available.

With these simplifying assumptions, the dilemma becomes one of ensuring an adequate supply of potable water both for the resident population and the tourists, while maintaining water quality at the beaches required to continue to attract tourists, many of whom visit island nations for the beach and water recreation activities.

The PDE framework (Lutz, 1994; Lutz *et al*., 2000) was proposed along these lines. In the module on water budget, "seepage" was identified but not explicitly included in the analysis because the state-of-the-knowledge had not yet been sufficiently advanced. Even now, SGD remains an under-explored topic beyond the community of researchers studying the phenomenon itself. My intent here is to demonstrate how SGD measurements can fit into the PDE framework.

The PDE model of Mauritius showed that early remediation of pollution is less costly and more effective than treatment being postponed until the environment surpassed a predetermined "critical" point (Lutz *et al*., 2002) and I will support a similar result.

SGD is a ubiquitous link between land-based activities and the coastal ocean, and as such, it can be leveraged as a valuable parameter to evaluate impacts of land-use, agricultural practices and climate change on the economic and environmental aspects within the coastal zone. To incorporate SGD as a factor in a PDE model, it is necessary to explicitly create the linkages between SGD conditions and the various environmental and population parameters involved. A PDE model, with its connections between population, economics and environmental qualities, can then be used to answer questions that lead to effective management strategies. The kinds of questions that could be answered by a PDE model include: What conditions, environmental and population related, will lead to a steady state or to an unstable situation? What effect does choosing an "optimal" economy have on the environment, and what feedbacks can complicate this? What effects do management strategies, such as investment in wastewater treatment or "best management practices" for agriculture have on population structure, economic viability and environmental quality? What effects will climate change have on the dynamics between population, development and the environment? Relevant characteristics of SGD, however, are complex. One component is the underflow or the seepage of fresh groundwater under the shoreline. This component carries with it contaminants introduced from the varied uses upland. A second, and often much larger component of SGD is seawater circulated through the coastal aquifer. The components are mixed and chemically altered as they transit the subterranean estuary (STE). The impact of SGD on the freshwater reserves depends on the underflow and associated saltwater intrusion, while the coastal water quality depends on the total SGD and its chemical composition after alterations in the STE. In the previous chapters, I have demonstrated how total SGD and the freshwater component might be determined and how SGD water quality can be considered.

As I have said, separate and distinct studies of both SGD characterization and PDE modeling have been done in Mauritius. Mauritius is a nearly 2,000-km^2 island in the western Indian Ocean. It has one of the highest population densities in the world, and more than half of the population's water demands are supplied by the island's volcanic aquifers (Burnett *et al.*, 2006). A thorough evaluation of the SGD field studies in Mauritius may be found in Chapter 1 of this thesis. Earlier, in 1994, the International Institute for Applied Systems Analysis (IIASA) had used the island of Mauritius as a case study for a PDE model. This model showed that early remediation is less costly and more effective than postponing treatment until a predetermined environmental "critical" point was surpassed (Lutz *et al.*, 2002). This PDE model, while it used a simple representation of the environment and did not incorporate SGD as a specific factor in water quality, provides the foundation for my research in incorporating this field-science explicitly into a module that could be used in a PDE framework.

In previous chapters, I have developed the field methods for assessing SGD on oceanic islands. For the module development, I will use Barbados as a case study, primarily because I had the opportunity there to collect seasonal data, which, as I will discuss, is useful for exploring the impacts of seasonal dynamics. Barbados is a 431 km^2 karstic island in the Caribbean Sea. SGD evaluations (Chapter 3 of this thesis) have demonstrated two different SGD regimes along the western coast of the island; the first, typified by the Alleynes Bay site, is a freshwater-dominated SGD driven by terrestrial hydraulic gradients that is the primary transport mechanism for dissolved inorganic nitrogen in the form of nitrate and nitrite (NO_x) into the coastal ocean, the second regime, typified by the Queens Fort Beach site, is SGD dominated by recirculated seawater driven by oceanographic processes with little contribution of NO_x to the coastal waters. Using data collected by Lewis (1987), 60% of the western shoreline of Barbados is similar to the Alleynes Bay site with a freshwater influence, and it is this portion of the shoreline that will be focused on in this chapter as a pathway for terrestrial NO_x input to the coastal ocean.

In this chapter, I will employ these characteristics of SGD as an environmental "currency" or a natural asset, and explore how it might be incorporated as a factor among the other various economic drivers for tourism. Field measurements, as documented in previous chapters of this thesis, can be designed to characterize SGD for a shoreline and can then be incorporated in a model that evaluates tourist preference for coastal water quality, as represented by nutrient contribution *via* SGD. This model can then support the idea that wastewater treatment is important for sustainable tourism on small islands. I must emphasize that this is not a full PDE model, but a suggestion on how new information on SGD might be incorporated into the quantification of "seepage" in the environmental module of a PDE model.

Economic choices: for simplicity, I will assume that the connection between anthropogenic nutrient input and water quality hinges on sewage treatment. As pointed out by Lutz (1994), it is not possible to build in a large number of defendable feedback relationships that might allow feedback to tourism. Options like governmental controls on hotel capacity, investment in desalination, limits on energy consumption, subsidies to fisheries or other interests, all open economic pathways that I cannot consider here. My goal is merely to show how new information on SGD might be incorporated into a water module of a PDE model.

Methods

I will incorporate the following specific characteristics of SGD: SGD flux for the wet and dry seasons and the freshwater component for the wet and dry seasons. While other aspects of an island's water resources are usually available, SGD characteristics are unlikely to be known for any particular island. In the previous chapters, I have demonstrated methods of estimating these parameters in an efficient manner. The flow of information in this element of a PDE model, then, was designed to link tourism to fluxes of both nutrients and water (Figure 6.1). The aquifer is

segmented into two reservoirs, a "pristine" potable water reservoir and a reservoir of wastewater. Water enters the potable reservoir as recharge (Figure 6.1 flow line A). Water is withdrawn from the potable reservoir (flow line B) and returned to the wastewater reservoir (flow line C) primarily through sewage systems and leaching from agricultural fertilizers. Recharge is balanced by SGD (flow line H), which is made up of a combination of freshwater (flow lines D and E) and circulated seawater (flow line F). The major parameters within the model (Figure 6.1) are the nitrogen contribution to the aquifer by the total population, both resident and transient tourist (flow line C), the aquifer's natural ability to remove nitrogen from the water, the demographic composition of the total population, tourism contribution to GDP, the sensitivity of the tourists to coastal water quality conditions (flow line G) and the changes in precipitation and recharge between the seasons.

Nitrogen is the nutrient of concern, primarily dissolved inorganic nitrogen in the forms of nitrate and nitrite (expressed as NO_x). Nitrate can be a major concern in the potable groundwater reserve and nitrogen is often a nutrient limiting production in the open, coastal waters. Tourists of course, are not themselves sensitive to nitrogen levels in the coastal ocean, but rather to the condition of eutrophication, which may manifest in algal blooms or fish kills. Such conditions generally appear when nitrogen concentrations exceed the assimilative capacity of the particular coastal ocean (Howarth and Marino, 2006; Teichberg *et al*., 2010; Rodellas *et al.*, 2014). Concentrations of nitrogen above which eutrophication conditions begin to materialize vary depending on the environment and recommending agency; the US EPA criteria for the streams and rivers (considered in the current context to be analogous to SGD) of 14 "ecoregions" of the United States range from 0.1 to 2.2 mg/L TN (total nitrogen, which is organic nitrogen as well as dissolved inorganic nitrogen; EPA, 2014), other sources cite 1 mg/L of dissolved inorganic nitrogen as the concentration to characterize impairment of coastal waters (Quinn *et al.*, 1989; Camargo and Alonso, 2006). As mentioned previously, field data for Barbados revealed two SGD regimes, only one of which transported terrestrially derived anthropogenic nitrogen into the coastal ocean (Alleynes Bay site; Chapter 2 of this thesis). To delve into the linkages between tourism and environmental quality as a function of SGD-driven nitrogen transport, I focused an island-wide model on the field measurements from Alleynes Bay.

Population

The residents of Barbados include both the permanent resident population as well as the transient tourist population. Resident population growth characteristics are determined by data from a UN population growth projection model for Barbados (World Population Prospects, 2012) and can be represented as:

$$R = -0.0395t^3 - 2.7686t^2 + 1067.4t + 272093 \qquad [7.1]$$

where t is the time in years and R is the population of residents.

Monthly arrivals of stay-over tourists for the years 1997-2010 were obtained from the Barbados Ministry of Tourism (2006; 2011). Stay-over tourists for this period grew from 513,242 to 532,889 tourists (Barbados Ministry of Tourism, 2006; Barbados Ministry of Tourism 2011). Tourism has continued to change with similar magnitudes of fluctuations from 2011 to 2013, (567,724 in 2011, 536,303 in 2012 and 508,520 in 2013; respectively, Barbados Statistical Service, 2012; Barbados Statistical Service, 2013; and Barbados Statistical Service, 2014). The transient tourist population is determined by creating a "resident equivalent" as:

$$T_{re} = \frac{T_a t_{stay}}{d} \quad [7.2]$$

where T_{re} is the resident equivalent tourist, T_a is the seasonal tourist arrivals for the year 2000, t_{stay} is the average length of stay for the tourists, length of stay is the total number of nights spent by a tourist on the island, and d is the length of the season in days. Tourists have initial values of 10,848 resident equivalents for the dry season and 10,089 for the wet season for the year 2000 (t_0 in the model). Using historical tourism data, average values can be calculated for growth and declines in tourism for both the wet and dry seasons. Year-to-year changes in seasonal tourist arrivals was categorized into years of seasonal tourist growth (increase in tourist arrivals) and seasonal tourist declines (decrease in tourist arrivals), the average of each of these categories provides an approximation for the scale at which tourism changes historically (Table 6-1). Tourism arrivals, then, can be determined as:

$$T_{season} = H\Delta t + T_{season-1} \quad [7.3]$$

where H is the historical value of change in tourist arrivals for the season and direction of change, Δt is the time interval, and $T_{season-1}$ is the value for tourists during that season of the previous year.

The resources available also constrain the population of tourists. Tourism is a function of many complex factors, from preference for destination-specific environmental characteristics such as the width of beaches (Morgan, 1999; Klein *et al*., 2004; Valdemoro and Jiménez, 2006), quality of sand (Morgan, 1999), to destination-specific institutional constraints like governmental policies governing tourism (Jenkins and Henry, 1982; Bramwell, 2011; Ruhanen, 2013), as well as more general limitations like the global economic and social stability (Causevic and Lynch, 2013) and the personal budgets of the tourists (Alegre *et al*., 2010), or availability of attractive alternative destinations (Butler, 1991). There are several methods, both theoretical and empirical, for incorporating some of these factors into modeling tourism dynamics (Casagrandi and Renaldi, 2002; Schubert *et* al., 2011; Sen *et al*., 2014) but that complexity of tourism dynamics is not intended to be within the scope of this study.

Acknowledging that there are multitude factors governing tourism limits, for this model example, I will use bed availability and potable water availability as simple limits to tourism

growth. Bed availability grows with time based on statistics from the Barbados Central Bank (2006) through the equation:

$$T_{bed\ availability} = 0.7495T_{t-1} + 4656.9 \quad [7.4]$$

where T_{t-1} is the number of tourists during that season of the previous year. This growth is capped at 19,000 beds, a theoretical maximum number of beds that could be supported on Barbados, as space and resources for hotels are not infinite. The initial condition for bed limitation is 12,240 visitors (Barbados Central Bank, 2006). Within this model, $T_{bed\ availability}$ does not include tourist contribution to gross domestic product (GDP); while there is positive correlation between overall tourist contribution to GDP and beds available two years later (assuming time for construction), it is weak (Figure 6.3; $R^2 = 0.47$).

Island Water Characteristics

For SGD in Barbados, I have assumed qualities similar to the field location Alleynes Bay. I have estimated in Chapter 3 that Alleynes Bay is representative of 60% of the Barbados shoreline based upon previous work by Lewis (1987). It is important to note that this study, as well as that of Lewis (1987), was completed only on the western shoreline of Barbados, due to high surf and insufficient beach width on the eastern shore. While it is likely that the differences in hydraulic gradient affect the magnitude of SGD, without field data to support that idea, I am making the assumption that SGD on the eastern shore is similar to that on the western shore. To take this estimate of similarity into account, I have modified all land area related parameters within equations by 60%.

The land area for Barbados is 431 km^2 and its shoreline length is 92 km. Based on data about the distribution of the geologic unit containing the aquifer from Jones (2002) the effective surface area of the aquifer is 85% of the total land area. Average saturated aquifer thickness is 15 m, as derived from approximate aquifer base elevations subtracted from water table elevations (Jones Figure 5-3 and Table 5-2, respectively, 2002). Aquifer average porosity is 45% and the specific yield[2] is 15% (Jones, 2002). These factors are incorporated to calculate the volume of water in the aquifer as:

$$V = ATnS_y \quad [7.5]$$

where V is the saturated volume, A is the area, T is the average saturated thickness of the aquifer, n is the porosity and S_y is the specific yield.

[2] Specific yield is the ratio of the volume of water from a rock or soil sample *via* gravity drainage to the total volume of the rock or soil sample (Fetter, 2001).

Both wet and dry season SGD fluxes measured in field studies (Chapter 3 of this thesis) were included in the calculation as well as ties these seasonal fluxes to climatic variables. Climatic variables include wet and dry season precipitation (1.01 and 0.22 m/season respectively) as well as the duration of the dry season in months (wet and dry seasons both 6 months in duration). Duration of the seasons is important in evaluating effects on the system as a result of climate change. Current projections for precipitation on Barbados indicate that, in the short-term, annual precipitation will likely stay the same, however, the duration of the seasons will be altered; the wet season will contract, so rainfall will be more intense[3] (Nurse, 2014 personal communication). Climate model scenarios suggest that in the Caribbean in the short-term, annual precipitation may remain constant from current conditions but the length of the seasons may change, resulting in longer dry seasons and shorter, more intense wet seasons. This will likely also be reflected in changes in SGD magnitude and nutrient concentrations in the discharged water. Assuming the relationship between rainfall and SGD is linear (Figure 6.2), we can determine a governing equation to determine SGD changes as a result of incremental extensions of the dry season. This equation is:

$$SGD_{field} = 63.13p + 5.74 \quad [7.6]$$

where p is the seasonal monthly average rainfall and SGD_{field} is the average monthly SGD measured in the field. These can then be translated into a shoreline flux as:

$$SGD_m = SGD_{field} 0.6LW \quad [7.7]$$

where SGD_m is the modeled SGD, SGD_{field} is the SGD determined from field values, 0.6 is the adjustment for 60% of the shoreline being similar to the Alleynes Bay field site, L is the length of the shoreline, and W is the width of the discharge zone in meters offshore. If data are available, this can be estimated from the exponential decrease of SGD with distance from shore. It has often been shown, and assumed, to be on the order of 100 m (Burnett *et al.*, 2006).

Tourist-Water Interactions

In addition to the bed limitations discussed earlier, the quantity of potable water available also serves as a limit to tourist expansion. Here the water limit ($T_{water\ limit}$) is defined as the number of tourists that can be supplied by 10% of the seasonal recharge to the aquifer, using this as an arbitrary theoretical maximum of water use.

[3] Changes in precipitation patterns will likely also affect tourist arrivals directly, though this is not considered within this study.

Also included in the model is a minimum value of tourists (T_{min}) to prevent the total collapse of the tourism sector and to allow for recovery of tourism if conditions improve, this value is set at an arbitrary value of 1,000 tourists seasonally.

Tourists are ultimately determined by a series of nested logical statements that incorporate all of these components (Figure 6.4).

$$\text{IF } T_{season_{t-1}} < T_{min}, \quad [7.8]$$

$$\text{THEN } T_{season_{t-1}} + (T_{min} - T_{season_{t-1}} + 1), \text{ OR ELSE} \quad [7.9]$$

$$\text{IF } T_{season_{t-1}} > T_{water\ limit} \quad [7.10]$$

$$\text{OR } T_{season_{t-1}} > T_{bed\ availability} \quad [7.11]$$

$$\text{THEN } T_{season} = T_{season_{t-1}}, \text{ OR ELSE} \quad [7.12]$$

$$\text{IF } [N]_{t-0.5} > [N]_{threshold} \quad [7.13]$$

$$\text{OR } [N]_{t-1} > [N]_{threshold} \quad [7.14]$$

THEN T_{Season} = Seasonal Decline (Equation 7.3; *H* decline value)

OR ELSE T_{Season} = Seasonal Growth (Equation 7.3; *H* growth value)

where $[N]_{t-0.5}$ is the concentration of NO_x in the measured SGD from the previous season, $[N]_{t-1}$ is the concentration of NO_x in the measured SGD during the same season of the previous year and $[N]_{threshold}$ is the concentration of NO_x to which tourists respond. If the tourist arrivals during the same season of the previous year ($T_{season\ t-1}$) are less than the minimum value, the tourist equation brings the current tourist arrivals (T_{season}) above the minimum by an arbitrary value of one tourist. If previous tourist arrivals are above the minimum, then the tourist equation tests how the previous arrivals compare to the water and bed availability limitations. If either limit is exceeded, there is no change in tourist arrivals. If the previous arrivals are below both water and bed limits, the tourist equation then compares the concentration of nitrogen in SGD from the two preceding seasons ($[N]_{t-0.5}$ and $[N]_{t-1}$) to the NO_x threshold and adjusts the current tourist arrival value according to the season and direction of change (*e.g.* NO_x in SGD exceeding the NO_x threshold results in a decline in tourist arrivals, the value of which is specific to the current season).

Freshwater consumption has been reported to vary by a factor of three between residents and tourists; tourists, individually as well as through the tourist industry services supporting them, consume more water *per capita* than residential use. Greenidge and Greenidge (2011) cite Barbados Water Authority values for water use of 6.7 m^3/month *per capita* for local residential

use and 20.3 m^3/month *per capita* for resort and hotel use (proxy for tourist use). Pumping of freshwater is calculated as:

$$P = D[(U_{resident}R) + (U_{tourist}T_{seasonal})] \quad [7.15]$$

where P is the pumping of freshwater in m^3/season, D is the duration of the season in months, $U_{resident}$ and $U_{tourist}$ are, respectively, the residential and tourism monthly water use rates in m^3/month *per capita*.

The aquifer is divided into two distinct volumes: potable and wastewater. Initial conditions assume the whole aquifer is potable and there is zero wastewater. Potable water volume (V_P) is:

$$V_P = V_{P_{t-1}} - P - SGD_P + Re \quad [7.16]$$

where V_{Pt-1} is the potable water volume from same season of the previous year, P is the pumping, SGD_P is the potable volume contribution to SGD and Re is the recharge to the aquifer. The volume of potable water is reduced by removal by use (pumping) as well as loss to the coastal ocean (SGD), and recharged by precipitation. Freshwater recharge is:

$$Re = 0.6APr_{season}Re_{fraction} \quad [7.17]$$

where 0.6 is the adjustment for 60% of the shoreline being similar to the Alleynes Bay field site, Pr_{season} is the seasonal precipitation, and $Re_{fraction}$ is the fraction of precipitation that recharges the aquifer (25%; Jones, 2002). The wastewater volume (V_W) is:

$$V_W = V_{W_{t-1}} + P - SGD_W \quad [7.18]$$

where V_{Wt-1} is the potable water volume from the same season of the previous year, P is the pumping, SGD_W is the wastewater volume contribution to SGD. The volume of wastewater is increased by the conversion of freshwater through use (pumping) and is reduced by loss to the coastal ocean (SGD).

The freshwater component of SGD is assumed to balance recharge to the aquifer, which keeps the aquifer volume and the location of the freshwater-saltwater interface constant. Both of the aquifer volumes, potable and wastewater, contribute proportionally to the freshwater SGD flux.

$$SGD_P = \frac{Re}{1+\left({}^{V_W}/_{V_P}\right)} \quad [7.19]$$

$$SGD_W = Re - SGD_P \quad [7.20]$$

Initial conditions for the first season of the year 0 are set so that all freshwater SGD is from the potable volume, and there is no wastewater component.

Nitrogen input to the aquifer is from both sewage and fertilizer application. The nitrogen contribution from agricultural fertilizer application is assumed to be evenly distributed between the wet and dry seasons. Total nitrogen is calculated as:

$$N_T = \left(\frac{D}{12} N_{sewage}(R + T_{seasonal})\right) + \left(\frac{D}{12} A A_C F_a F_l\right) \quad [7.21]$$

where N_{sewage} is the NO_x contributed from the total population (residents and tourists) (8.65 kg/y *per* capita; Goolsby *et al.*, 1997), A is the total land area, A_c is the percentage of cultivated land area (60%; Jones, 2002), F_a is the application of fertilizer (0.013 kg N/m^2/y; Jones, 2002), and F_l is the percentage of fertilizer that leaches to the groundwater (23%; Jones, 2002).

The amount of nitrogen provided to the coastal ocean by SGD is also impacted by chemical and biological alterations along the groundwater flowpaths, represented by the "cleaning" of the aquifer. Denitrification within the vadose zone in Barbados is unlikely to be an important factor due to the high porosity and rapid infiltration (Jones, 2002), however alterations within the subterranean estuary may still be important (Ullman *et al*., 2003). The cleaning (K) was estimated using field data results from freshwater well samples and direct seepage samples collected during the January 2007 season:

$$K = \frac{Well - Seep}{Well} \quad [7.22]$$

where *Well* is the NO_x concentration in the freshwater well, *Seep* is the NO_x concentration at the beach-face at Alleynes Bay where groundwater was directly seeping (Chapter 3 of this thesis) and K is the fraction of NO_x lost during transport from the well to the shoreline, which would include any alterations within the STE. For the *Well* value, the highest NO_x concentration from among the freshwater well samples was chosen as a best-case scenario for maximal removal of NO_x within the aquifer.

For scenarios investigating the effects of sewage treatment, removal of dissolved nutrients requires a tertiary level treatment with a denitrification filter to remove NO_x. Depending on the system used, 30-99% of the nitrogen may be removed (Ahn, 2006). Ahn (2006) compared the performance of different systems for nitrogen removal, and the average N removal was 75%. Costs for construction a 2 MGD (million gallons per day) tertiary sewage treatment plant is approximated to be 50 million Barbados dollars (BDS), based on sewering projects and costs from the Suffolk County Department of Public Works (Wright, 2006, personal communication). Nitrogen removed through sewage treatment is:

$$S_T = \frac{C * D}{P} S_R N_{sewage} \quad [7.23]$$

where S_T is the removal from sewage treatment, C is the capacity of the sewage treatment plant (m^3/month), D is the duration of the season, P is the volume of wastewater from pumping,

S_R is the percent nitrogen removed through treatment, N_{sewage} is the nitrogen from sewage. Construction of the sewage treatment plant is initiated when a threshold of GDP loss is surpassed, two scenarios for this GDP loss threshold were considered – an early intervention scenario with a GDP loss of 5%, and a late intervention scenario with a GDP loss of 35%. GDP loss is assessed on a yearly basis (in the wet season, or the second season of the model year) and it is assumed that the full cost of construction is imposed immediately, and subsequent years invoke an annual maintenance cost. The model assumes that it takes two years to begin treating wastewater after initiating construction.

The NO_x that is dissolved in the groundwater and makes it to the coastline as SGD, or the effective nitrogen, is a combination of the sources of NO_x, the removal along the flowpath as well as possible removal from treatment of sewage, expressed as:

$$N_e = N_T(1 - K - S_T) \quad [7.24]$$

where N_e is the effective NO_x, K is the loss during transport to the shoreline, and S_T is the removal from sewage treatment, all in kg/season.

The effective nitrogen that makes it to the shoreline to be incorporated in SGD can also be expressed as:

$$[N]_{SGD_m} = \frac{N_e}{SGD_m} \quad [7.25]$$

where effective nitrogen (N_e) is divided by the modeled SGD (SGD_m).

Results

A sensitivity analysis shows the relationship of tourism and its resulting economic contribution to GDP and the nitrogen concentration, or $[N]_{threshold}$, to which tourism (i.e. water quality) is sensitive (Figure 6.5). This may translate into an economic development choice between a focus on attracting high-end, upscale tourists who, presumably, would demand higher water quality, and high-volume, less expensive package tours which might attract tourists who accept a somewhat lower water-quality standard. In either case, the higher the $[N]_{threshold}$ is, the more tourists can be sustained and environmental quality no longer limits tourist growth. Tourism becomes limited by resource availability (available beds and water) at the upper bound of the $[N]_{threshold}$ sensitivity analysis (Figure 6.5; blue highlighted data series). Lower $[N]_{threshold}$ values increase the responsiveness of tourists to environmental quality until the tourism is in a steady decline and remains suppressed, which occurs at the lower bound of the $[N]_{threshold}$ sensitivity analysis (Figure 6.5; red highlighted data series).

Under the conditions of a high $[N]_{threshold}$ value that allows growth of the tourism industry ([N]=1.99), no sewage treatment and current climate conditions, there is a steady increase in

tourist arrivals until model year (MY) 16 when tourists become limited by the growth of the beds available, slowing the growth until 23MY when tourist arrivals begin to approach the maximum bed availability value (Figure 6.6). GDP profit follows the same pattern as the tourist arrivals (Figure 6.7). The volume of potable water declines sharply in the first four years of the model, and then the decline slows as the volume stabilizes with the stabilizing total population (Figure 6.7). Variations in seasonal precipitation and changes in tourist arrivals are responsible for the seasonal oscillations shown in all parameters (tourist population, GDP profit and volume of potable water).

Under a scenario with a lower $[N]_{threshold}$ vaue that causes the maximum decline of the tourism industry ([N]=1.79), no sewage treatment and current climate conditions, there is a continual decrease in tourism until 16MY when tourism in the wet season is below the tourist minimum and 20MY when tourism in the dry season is below the tourist minimum (Figure 6.8). The remainder of the model run to MY30.5 shows oscillation around the minimum tourist value (Figure 6.8). GDP profit also follows the same pattern as the tourist arrivals (Figure 6.9). The volume of potable water declines sharply in the first three years of the model and then the decline slows as the volume stabilizes along with the total population. The volume of potable water at the end of the model run for the declining tourism industry is 8.1% higher than the volume of potable water at the end of the model run for a growing tourism industry. In a tourist-free scenario, the volume of potable water shows the same trend, decreasing rapidly in the first three years and then stabilizing (Figure 6.10). The volume of potable water at the end of a tourist-free scenario is 8.4% higher than the growing tourism industry scenario, and 0.3% higher than the declining tourism industry scenario. This indicates that the tourists have a slight persistent effect on the volume of potable water, even 10MY after the crash of the tourism industry.

Under the lower $[N]_{threshold}$ scenario ([N]=1.79), sewage treatment construction initiated when GDP loss surpasses a 5% yearly loss (an early intervention), construction begins at 1MY, and treatment of water begins at 3MY. Assuming a reduction of 75% nitrogen by the treatment plant, recovery of the tourist arrivals begins at 4MY (Figure 6.11). A late intervention (GDP loss that surpasses a 35% yearly loss) occurs when tourist arrivals have already dropped to the minimum, and results in construction initiation at 19MY, treatment of wastewater at 21MY and tourist recovery at 22MY (Figure 6.12). Intervention *via* construction of a sewage treatment plant changes the sensitivity analysis' lower bounds of the $[N]_{threshold}$ slightly; the upper bound remains the same (Figure 6.13). The lower bound with early intervention is 3.5% lower than the limit during a late intervention.

Global climate change, for Barbados, is projected to change the duration of the seasons while total seasonal rainfall remains constant, intensifying rainfall during the wet season and drought during the dry season. Incremental changes in the duration of the dry season manifest in a sensitivity analysis of the model as changing the upper and lower bounds of the $[N]_{threshold}$ to tourism stability. Increases in the length of the dry season results in increasing values of the

upper and lower $[N]_{threshold}$ (Figure 6.14). The relationships between dry season duration and tourism sensitivity to NO_x in the measured SGD is non-linear, approximated by the following polynomial equations (R-squared 0.99982 and 0.99981 respectively):

Upper Bound $$y = -0.0084x^2 + 0.20 + 1.1$$ [7.17]

Lower Bound $$y = -0.0076x^2 + 0.18 + 1.00$$ [7.18]

With increasing duration of the dry season, there is a decrease in the GDP benefit of early intervention, delaying intervention decreases the GDP profit, while there is no difference between a late intervention and no intervention (Figure 6.15).

Discussion

The variety of $[N]_{threshold}$ values that have been highlighted by the sensitivity analyses (1.4 mg/L to 2.2 mg/L) are on the same order of magnitude as those found in the field at Alleynes Bay (0.10 mg/L at salinity 34, 2.53 mg/L at salinity 3.2; Chapter 3 of this thesis), as well as those recognized as potentially indicative of eutrophic conditions (0.1 to 2.2 mg/L; Quinn *et al.*, 1989; Camargo and Alonso, 2006; EPA, 2014) . However, the $[N]_{threshold}$ is not intended to be interpreted as a goal concentration for environmental quality. It is, rather, a measure of the sensitivity of tourists to the environmental conditions. Tourists that are highly responsive to environmental conditions have an $[N]_{threshold}$ that is low; tourists that do not readily respond to environmental conditions have an $[N]_{threshold}$ that is high. The upper and lower bounds of the $[N]_{threshold}$, then, define the region of environmental quality within which tourist response to environmental conditions is plastic and sensitive to policies that change the amount of nitrogen in the coastal waters. This is also the region where intervention *via* installation of a sewage treatment plant will have the most impact (Figure 6.13). The lower $[N]_{threshold}$ lower boundary during the early intervention scenario indicates that a proactive sewage treatment plan allows for a tourist industry that can persist, even with a slightly more sensitive tourist population. The constant upper bound of the $[N]_{threshold}$ indicates that initiation of sewage treatment at any point does not have an effect on upper limits of the [N]-tourism relationship; insensitive tourists are not affected by the treatment of sewage.

Global climate change intensifying the seasons in Barbados results in a decrease in the sensitivity of the tourists. What this translates to is that environmental quality will be degraded more by the tourism industry with more intense seasons (a higher $[N]_{threshold}$ is necessary to sustain a tourism industry), and more selective tourists will not be attracted to Barbados, the more intense the seasonality becomes. Another way to think about this is that the nitrogen contribution by the population has a larger effect during the dry season, and a prolonged dry season leads to a more quickly degrading environment. Sewage treatment helps ameliorate this effect somewhat, but only with the earliest intervention scenarios. There is a diminishing return

on sewage treatment intervention the later it is implemented and the more intense the disparity between seasons.

The applicability of this model for inclusion in a broader PDE framework for a location depends on whether the location meets three criteria: tourism ought to contribute a sizeable portion to the economy, there should be limited avenues for surface drainage of water and the SGD needs to have a high freshwater component. The first criterion is self-explanatory, modeling the dynamics of tourism is unnecessary where tourism is not a large enough component of the economy to be a concern. The second and third relate to the degree of the effect of SGD on the coastal water quality. Limited surface drainage indicates that groundwater discharge is the primary pathway for water to move from land into the coastal ocean, and the freshwater component is the portion of groundwater discharge that acts as a pathway for anthropogenic nutrients. All three study sites in this thesis, Barbados, Guam and Bimini, pass the first criterion; tourism is a major component of their economies. For Barbados, Northern Guam and Bimini, surface drainage is minimal, but Southern Guam has a well-developed drainage basin. As discussed earlier in this thesis, Barbados (the 60% of the western shoreline similar to Alleynes Bay) and Northern Guam both have relatively high freshwater components; 26-34% and 39% respectively, Bimini and Southern Guam, however do not have detectible influences of freshwater. This assessment would indicate that this methodology could be applied, and further developed, for Barbados and Northern Guam, but would not be appropriate for Southern Guam or Bimini.

Future Work

An interesting avenue for future development would be to use SGD water quality as a method to assign a monetary value on coastal water quality in areas where SGD is the predominant source of anthropogenic influence on the coastal ocean. This can also included an expanded scope to investigate phosphorus contribution to water quality dynamics, as studies have suggested that certain coastal environments may be phosphorus-limited rather than nitrogen-limited (Smith, 1984). The field methods used in this thesis were incompatible with investigating phosphorus, as the steel of the manual seepage meters used would likely scavenge phosphate from discharged water (Charette, 2008, personal communication). Use of less reactive field equipment would be required to expand this aspect of the research.

For future developments, another avenue to explore for the tourism water limit is the maximum tourist population that can be supplied by the infrastructure currently as well as the inclusion of the ability to upgrade infrastructure in favorable economic climates.

While this study has only focused specifically on the linkages between the environment and tourism using SGD, this work can also be expanded to incorporate how coastal water quality intersects with all sectors of the economy and evaluate how environmental quality drives

transitions between different sectors. And specifically look at competing interests between tourism, fisheries and agriculture.

References

Ahn, Y.-H. 2006. Sustainable nitrogen elimination biotechnologies: A review. Process Biochemistry (2006) 1709-1721.

Alegre, J., S. Mateo and L. Pou. 2010. An analysis of households' appraisal of their budget constraints for potential participation in tourism. Tourism Management. 31: 45-56.

Barbados Central Bank. 2006. Website: http://www.centralbank.org.bb/documents/ASD07H.pdf. Last accessed: 7/17/14.

Barbados Ministry of Tourism. 2006. 2006 Statistical Digest. Website: http://www.tourism.gov.bb/reports/2006_STATISTICAL_DIGEST.pdf. Last accessed: 7/17/14.

Barbados Ministry of Tourism. 2011. Tourism Statistics for 2007-2011. Website: http://www.tourism.gov.bb/images/stories/Reports/tourism%20statistics%20for%202007%20-2011.pdf. Last accessed: 7/17/14.

Barbados Statistical Service. 2012. Comparison of tourist arrivals by country of residence: December 2010 to December 2011. Website: http://www.barstats.gov.bb/files/documents/Dec_2010_and_2011_compared.pdf. Last accessed: 10/31/14.

Barbados Statistical Service. 2013. Comparison of tourist arrivals by country of residence: December 2011 to December 2012. Website: http://www.barstats.gov.bb/files/documents/Dec_2011_and_2012_compared.pdf. Last accessed: 10/31/14.

Barbados Statistical Service. 2014. Comparison of tourist arrivals by country of residence: December 2012 to December 2013. Website: http://www.barstats.gov.bb/files/documents/Dec_2012_and_2013_compared.pdf. Last accessed: 10/31/14.

Bramwell, B. 2011. Governance, the state and sustainable tourism: a political economy approach. Journal of Sustainable Tourism. 19(4-5): 459-477.

Brundtland Report, UN World Commission on Environment and Development. 1987. Our Common Future. Oxford Unversity Press. 383 pp. Website: http://www.un-documents.net/our-common-future.pdf. Last accessed: 10/23/14.

Burnett, W.C., P.K. Aggarwal, A. Aureli, H. Bokuniewicz, J.E. Cable, M.A. Charette, E. Kontar, S. Krupa, K.M. Kulkarni, A. Loveless, W.S. Moore, J.A. Oberdorfer, J. Oliveira, N. Ozyurt, P. Povinec, A.M.G. Privitera, R. Rajar, R.T. Ramessur, J. Scholten, T. Stieglitz, M. Taniguchi, J.V. Turner. 2006. Quantifying submarine groundwater discharge in the coastal zone *via* multiple methods. Science of the Total Environment. 367(2-3): 498-543.

Butler, R.W. 1991. Tourism, Environment and Sustainable Development. Environmental Conservation. 18(3): 201-209.

Camargo, J.A. and A. Alonso. 2006. Ecological and toxicological effects of inorganic nitrogen pollution in aquatic ecosystems: A global assessment. Environment International. 32(2006): 831-849.

Casagrandi, R. and S. Rinaldi. 2002. A Theoretical Approach to Tourism Sustainability. Conservation Ecology. 6(1): 13 [online]. Website: http://www.consecol.org/vol6/iss1/art13/.

Causevic, S. and P. Lynch. 2013. Political (in)stability and its influence on tourism development. Tourism Management. 34: 145-157.

Charette, M. 2008. Personal communication. Woods Hole Oceanographic Institution.
EPA. 2014. Summary Table for the Nutrient Criteria Documents. Website: http://www2.epa.gov/sites/production/files/2014-08/documents/criteria-nutrient-ecoregions-sumtable.pdf. Last accessed: 10/23/14.
Fetter, C.W. 2001. Applied Hydrogeology, 4th edition. Prentice-Hall, Inc. Upper Saddle River, NJ. 598 pp.
Goolsby, D.A., W.A. Battaglin and R.P. Hooper. 1997. Sources and Transport of Nitrogen in the Mississippi River Basin. Presentation. American Farm Bureau Federation Workshop "From the Corn Belt to the Gulf...Agriculture and Hypoxia in the Mississippi River Watershed", July 14-15, 1997, St. Louis, Missouri.
Greenidge K. and N. Greenidge. 2011. Sustainable Tourism Development: The Case of Barbados. The Central Bank of Barbados Economic Review. Volume XXXVII, Issues 1&2: 83-125.
Hira, A. and L.G. de Oliveira. 2009. No substitute for oil? How Brazil developed its ethanol industry. Energy Policy. 37(6): 2450-2456.
Howarth, R.W, and R. Marino. 2006. Nitrogen as the limiting nutrient for eutrophication in coastal marine ecosystems: Evolving views over three decades. Limnology and Oceanography. 51(1, part 2): 364-376.
Jenkins, C.L. and B.M. Henry. 1982. Government involvement in tourism in developing countries. Annals of Tourism Research. 9(4): 499-521.
Jones, I.C. 2002. Geochemical evolution of groundwater in the Pleistocene limestone aquifer of Barbados. Doctoral Thesis. University of Texas, Austin, TX. 273 pp.
Klein, Y.L., J.P. Osleeb and M.R. Viola. 2004. Tourism-Generated Earnings in the Coastal Zone: a Regional Analysis. Journal of Coastal Research. 20(4): 1080-1088.
Lewis, J.B. 1987. Measurements of groundwater seepage flux onto a coral-reef – spatial and temporal variations. Limnology and Oceanography. 32(5): 1165-1169.
Lutz, W. (Ed.) 1994. Population-Development-Environment: Understanding their Interactions in Mauritius. Springer-Verlag, Berlin, Germany. 400 pp.
Lutz, W., L. Prieto and W.C. Sanderson. 2000. Population, Development and Environment on the Yucatan Peninsula: from Ancient Maya to 2030. International Institute for Applied Systems Analysis, Laxenburg, Austria. 257 pp.
Lutz, W., W.C. Sanderson and A. Wils. 2002. Toward Comprehensive P-E studies. Population and Development Review, 28(Supplement: Population and Environment: Methods of Analysis): 225-250.
Morgan, R. 1999. Preferences and Priorities of Recreational Beach Users in Wales, UK. Journal of Coastal Research. 15(3): 653-667
Nurse, L. 2014. Personal Communication. University of West Indies, Cave Hill Campus, Barbados. August 2014.
Quinn, H., J. Tolson, J. Klein, S. P. Orlando, and C. Alexander. 1989. Strategic assessment of near coastal waters: Susceptibility of east coast estuaries to nutrient discharges: Albemarle/Pamlico Sound to Biscayne Bay. NOAA/EPA summary report. U.S. Department of Commerce, National Oceanic and Atmospheric Administration, Silver Spring, MD.
Rodellas, V., J. Garcia-Orellana, A. Tovar-Sánchez, G. Basterretxea, J. M. López-Garcia, D. Sánchez-Quiles, E. Garcia-Solsona, P. Masqué. 2014. Submarine groundwater discharge as a source of nutrients and trace metals in a Mediterranean bay (Palma Beach, Balaeric

Islands). Marine Chemistry. 160(2014): 56-66.
Ruhanen, L. 2013. Local government: facilitator or inhibitor of sustainable tourism development? Journal of Sustainable Tourism. 21(1): 80-98.
Schubert, S.F., J.G. Brida and W.A. Risso. 2011. The impacts of international tourism demand on economic growth of small economies dependent on tourism. Tourism Management. 32: 377-385.
Sen, A., A.R. Harwood, I.J. Bateman, P. Munay, A. Crowe, L. Brander, J. Raychaudhuri, A.A. Lovett, J. Foden and A. Provins. 2014. Economic Assessment of the Recreational Value of Ecosystems: Methodological Development and National and Local Application. Environmental and Resource Economics. 57: 233-249.
Smith, S.V. 1984. Phosphorus versus Nitrogen Limitation in the Marine Environment. Limnology and Oceanography. 29(6): 1149-1160.
Teichberg, M., S.E. Fox, Y.S. Olsen, I. Valiela, P. Martinetto, O. Irabarne, E.Y. Muto, M.A.V. Petti, T.N. Corbisier, M. Soto-Jiménez, F. Páez-Osuna, P. Castro, H. Freitas, A. Zitelli, M. Cardinaletti and D. Tagliapietra. 2010. Eutrophication and macroalgal blooms in temperate and tropical waters: nutrient enrichment experiments with *Ulva* spp. Global Change Biology. 16(9): 2624-2637.
Ullman, W.J., B. Chang, D.C. Miller, and J.A. Madsen. 2003. Groundwater mixing, nutrient diagenesis, and discharges across a sandy beachface, Cape Henlopen, Delaware (USA). Estuarine, Coastal and Shelf Science 57(2003): 539-552.
UNEP WTO (United Nations Environment Programme and World Tourism Organization). 2005. Making Tourism More Sustainable: A Guide for Policy Makers. Website: http://www.unep.fr/shared/publications/pdf/DTIx0592xPA-TourismPolicyEN.pdf. Last accessed 10/23/14.
Valdemoro, H. and J. Jiménez. 2006. The Influence of Shoreline Dynamics on the Use and Exploitation of Mediterranean Tourist Beaches. Coastal Management. 34: 405-423.
World Population Prospects. 2012. Population Division of the Department of Economic and Social Affairs of the United Nations Secretariat, World Population Prospects: The 2012 Revision, http://esa.un.org/unpd/wpp/index.htm. Last accessed 4/24/14.
Wright, Benjamin. 2006. Suffolk County Department of Public Works. Personal communication April 20, 2006.

Figures

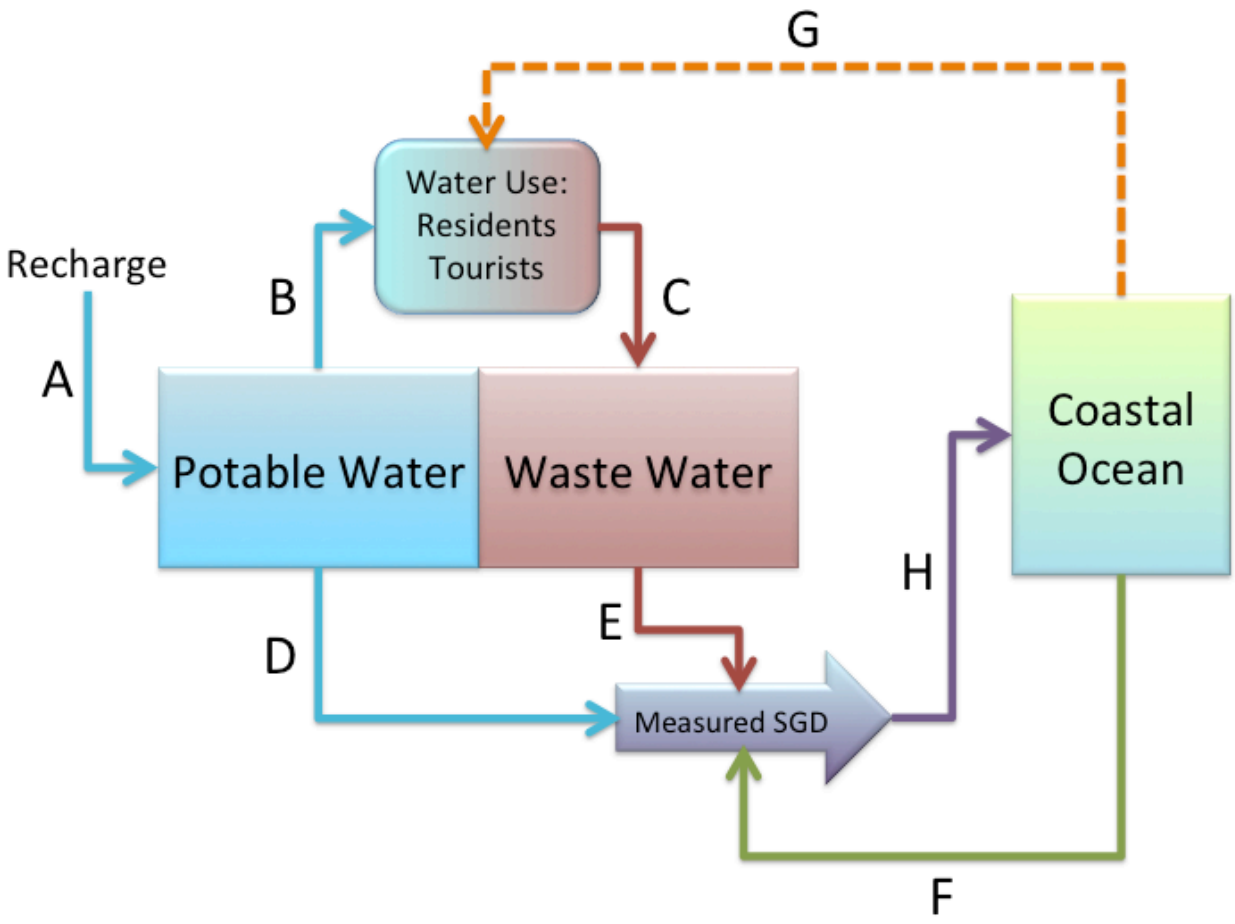

Figure 6.1: Box model schematic.

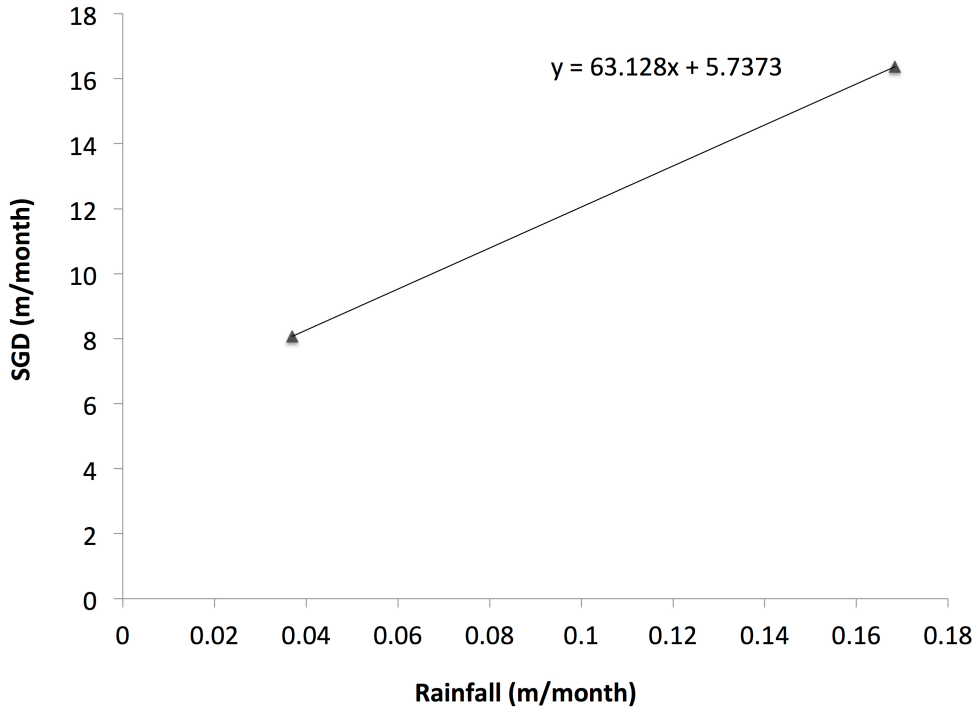

Figure 6.2. Seasonal rainfall and SGD.

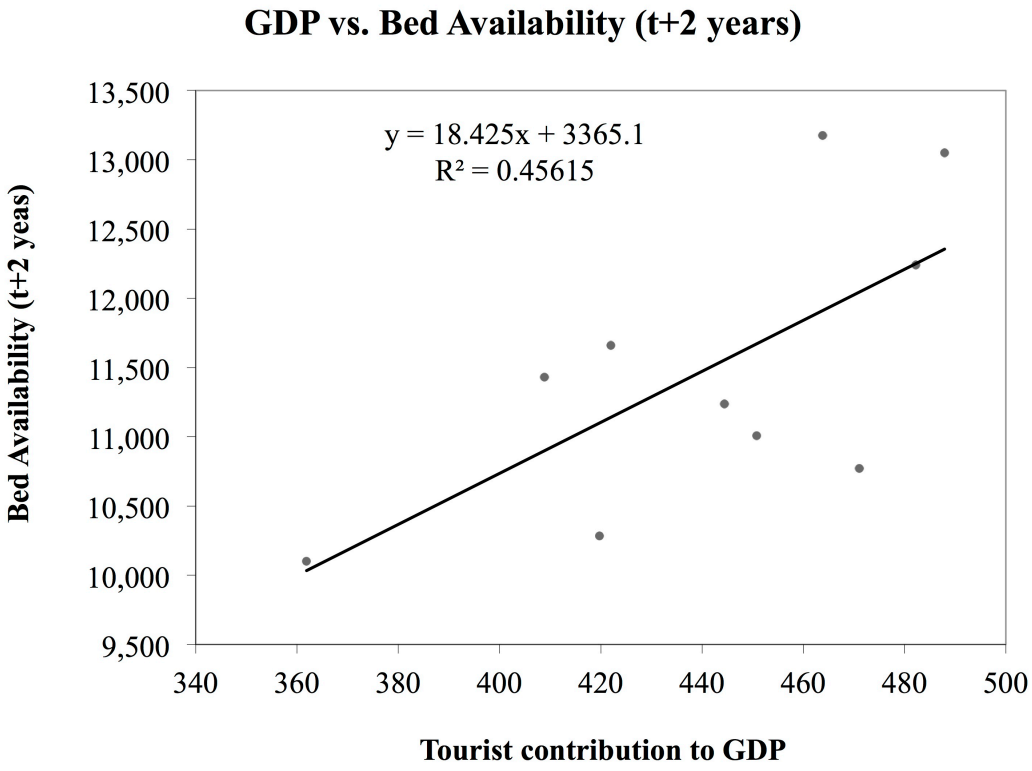

Figure 6.3. GDP versus Bed Availability. Bed availability values are selected with a two-year lag behind the GDP values.

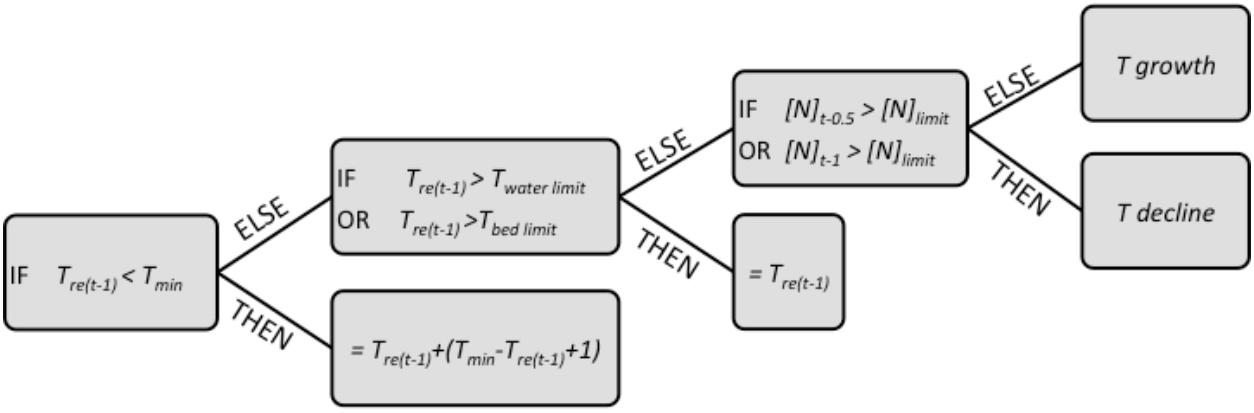

Figure 6.4: Schematic of logical tourist equation.

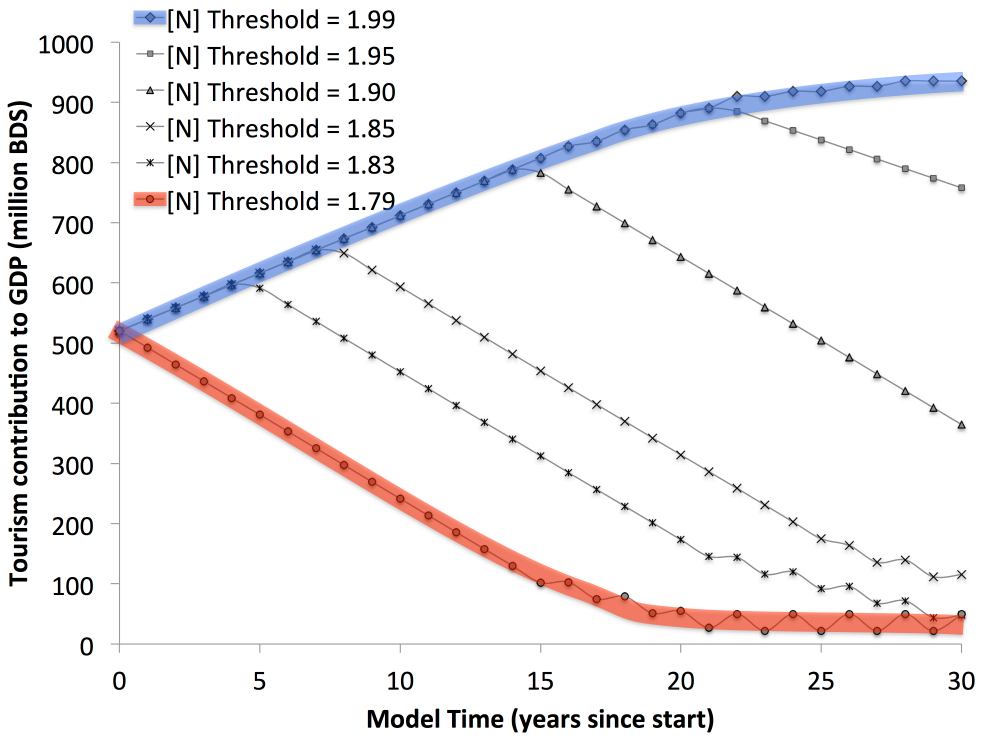

Figure 6.5. Sensitivity of tourist revenue to environmental conditions. Different [N] threshold values show changes in the tourism contribution to GDP (million BDS). Blue line indicates the [N] threshold that has maximum sustained tourist growth. Red line indicates the [N] threshold that has continued tourist decline.

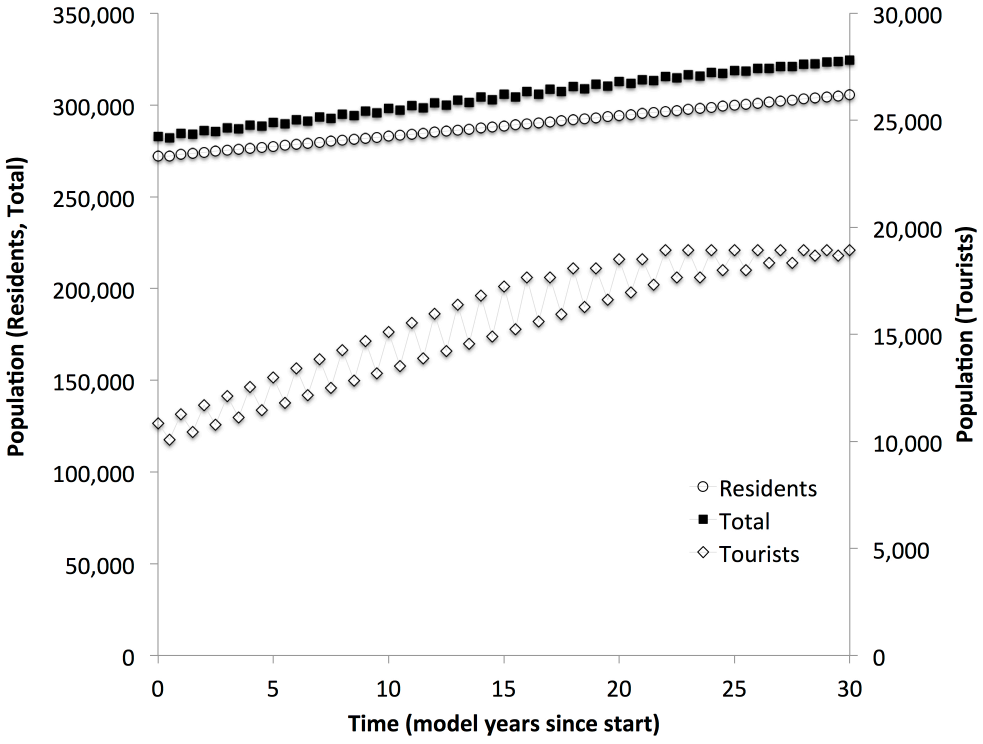

Figure 6.6. Time series of population growth with an [N] threshold that allows growth. Tourist population (triangles) is on the right axis, resident population (square) and total population (diamond) are on the left axis. The x-axis is in time, years since the beginning of the model.

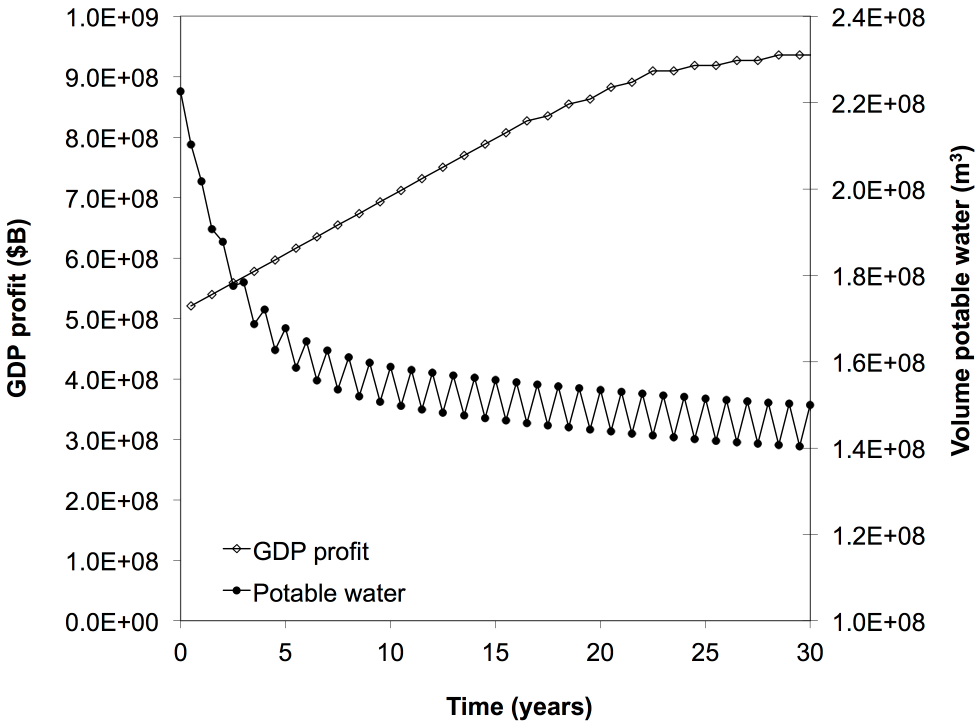

Figure 6.7. Time series of annual GDP profit (diamonds; left axis) and seasonal Potable Water volume (stars; right axis) during tourist growth conditions.

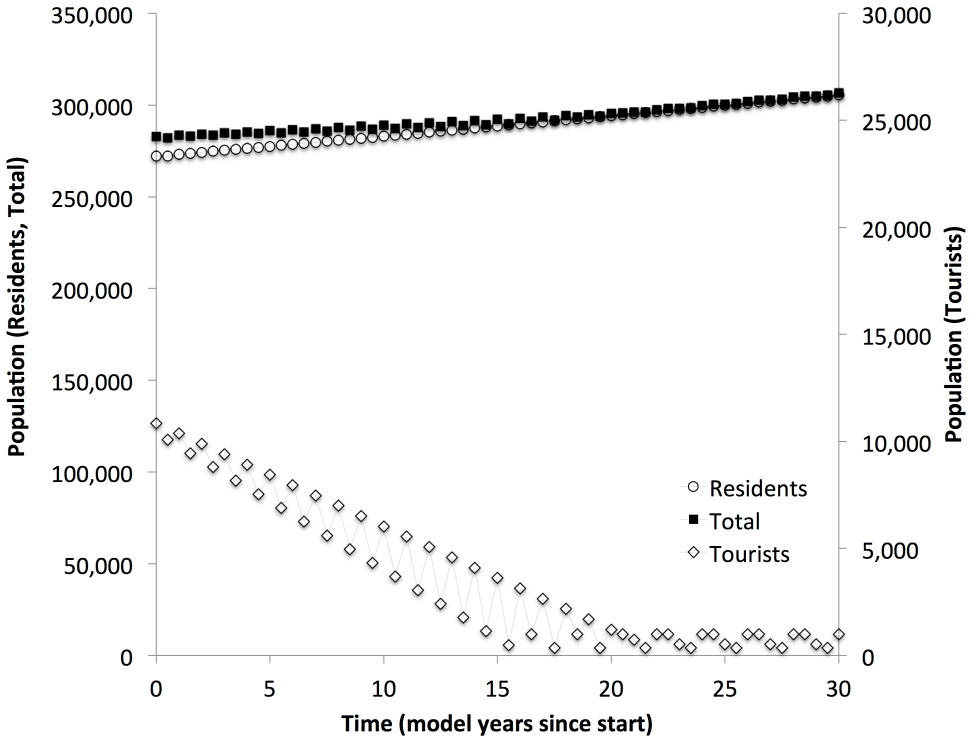

Figure 6.8. Time series of population growth with an [N] threshold that does not allow growth. Tourist population (triangles) is on the right axis, resident population (square) and total population (diamond) are on the left axis. The x-axis is in time, years since the beginning of the model.

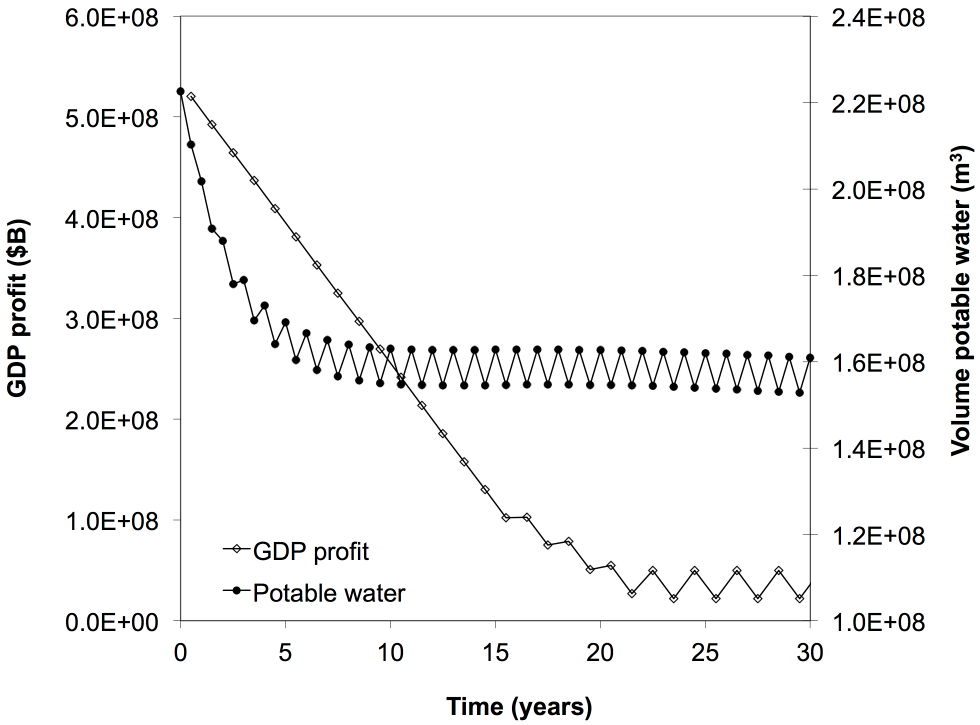

Figure 6.9. Time series of annual GDP profit (diamonds; left axis) and seasonal Potable Water volume (stars; right axis) during tourist decline conditions.

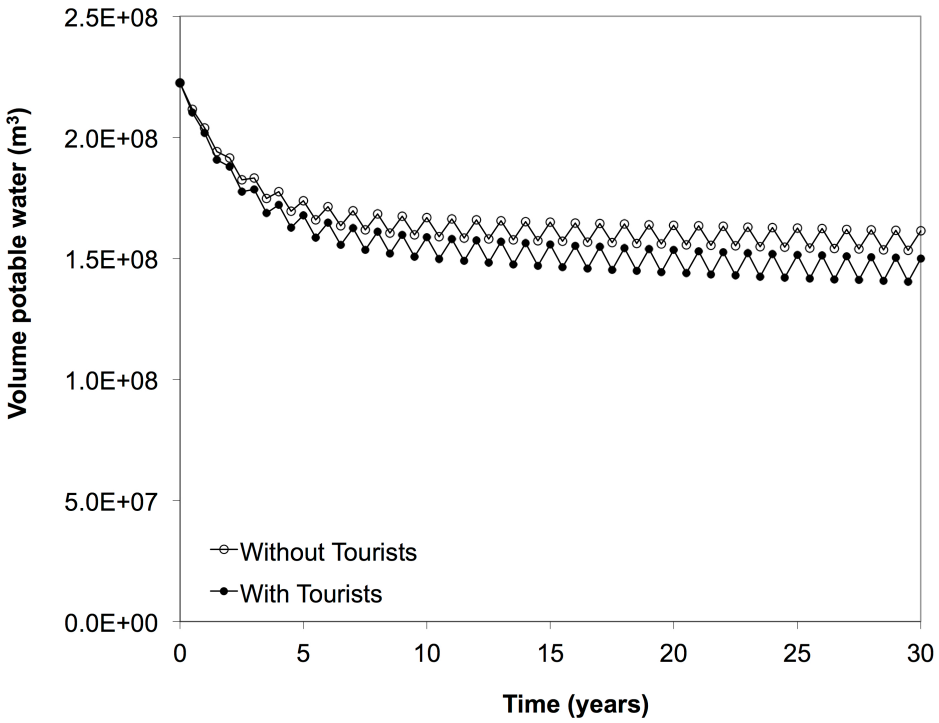

Figure 6.10. Time series of the volume of potable water in a tourist-free model.

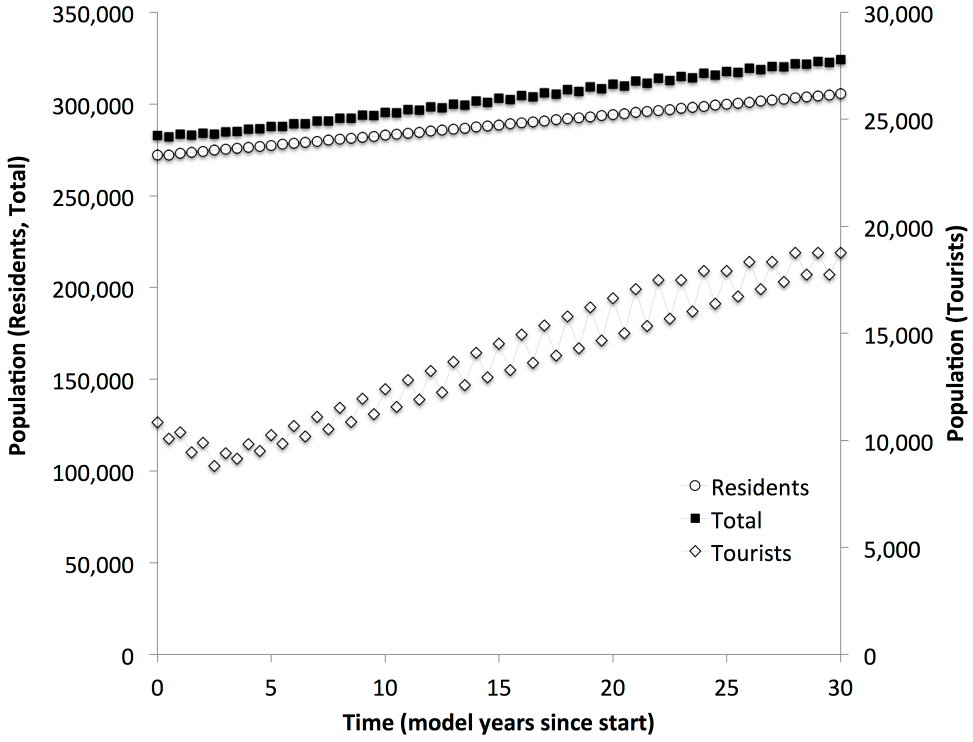

Figure 6.11. Strict [N] threshold with early intervention with sewage treatment.

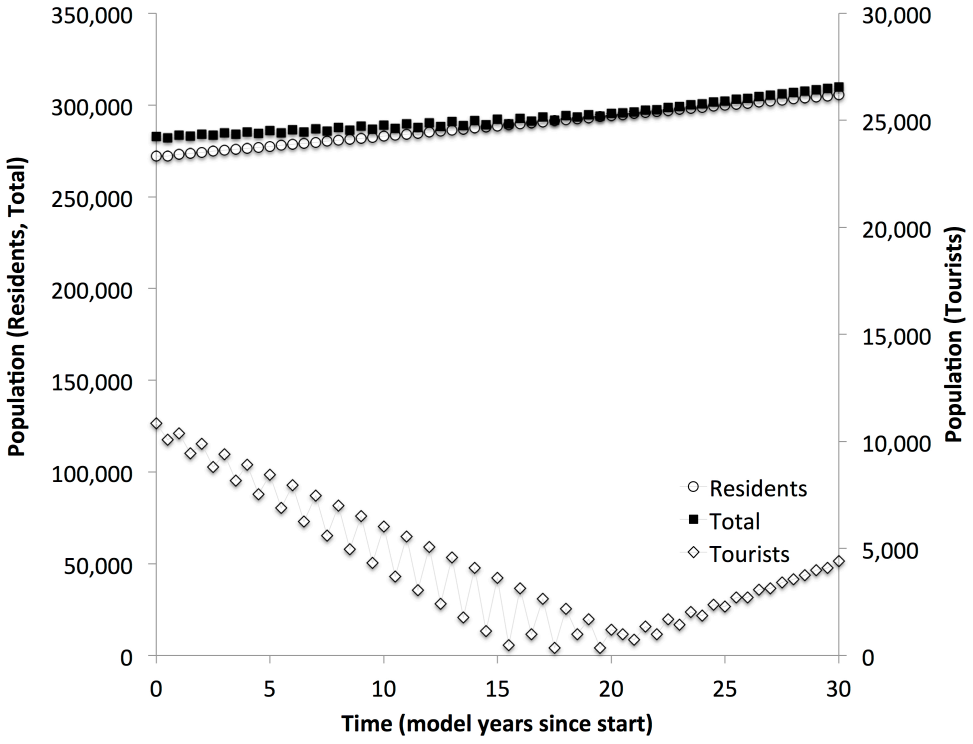

Figure 6.12. Strict [N] threshold with late intervention with sewage treatment.

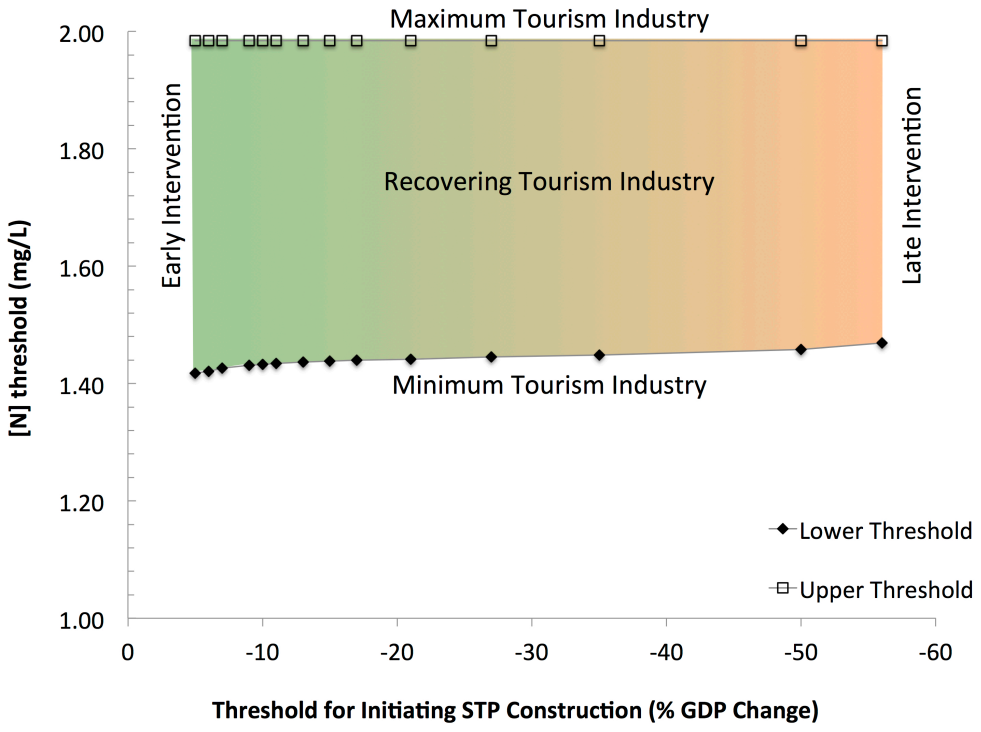

Figure 6.13. STP Intervention timing and [N] threshold as a proxy for tourist sensitivity.

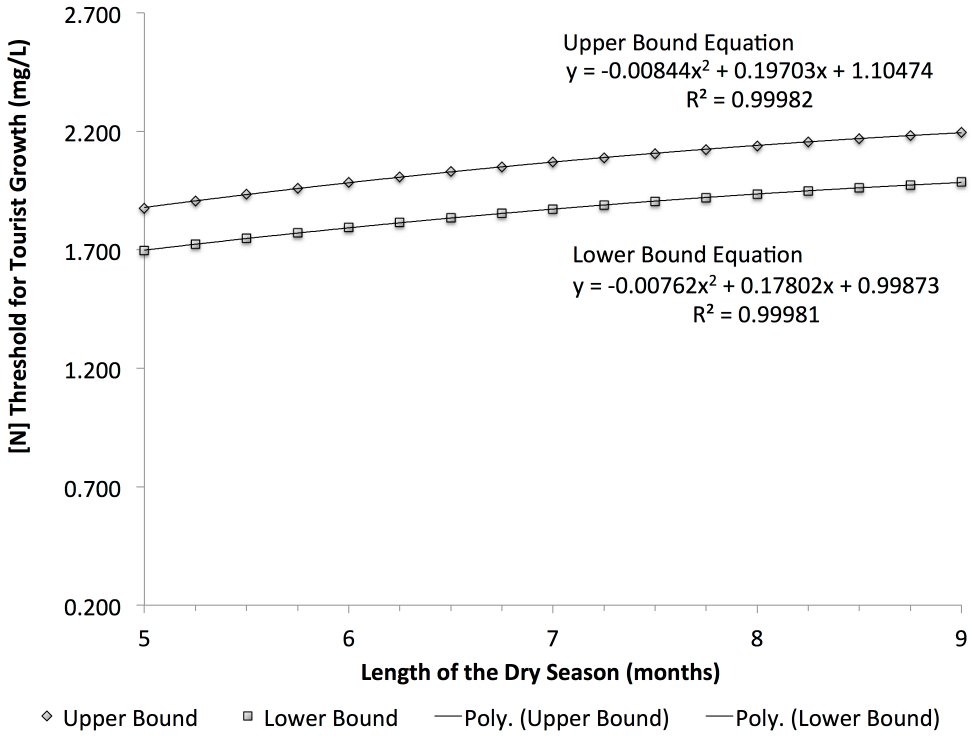

Figure 6.14. Tourism sensitivity to climate change. The effects of climate change on the upper (diamonds) and lower (squares) bounds to [N] threshold sensitivity.

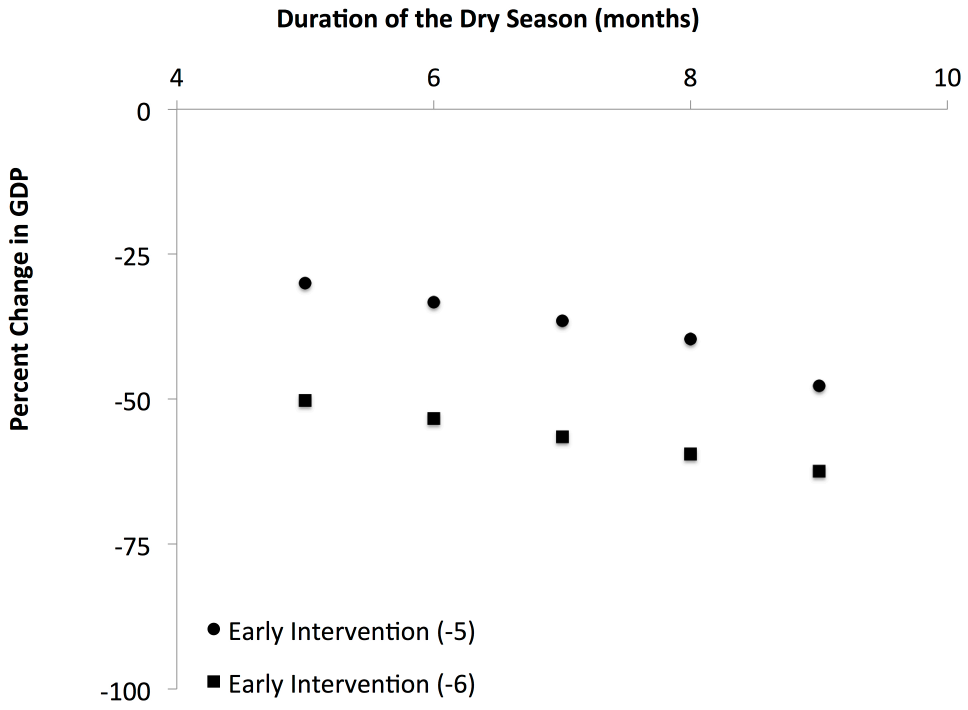

Figure 6.15. Intervention with Climate Change. [N] threshold chosen as the median value between climate change scenario-specific upper and lower bounds. Percent change in GDP for final model year relative to initial conditions. Two scenarios are presented: early intervention at GDP loss of 5% (circles), early intervention at GDP loss of 6% (squares).

Tables

Table 6-1. Tourism changes by season.

Seasonal Variation in Tourist Arrivals	Historical Average Value (*H*)
Dry Season Growth	426
Dry Season Decline	-482
Wet Season Growth	344
Wet Season Decline	-640

Bibliography

Ahn, Y.-H. 2006. Sustainable nitrogen elimination biotechnologies: A review. Process Biochemistry (2006) 1709-1721.

Alegre, J., S. Mateo and L. Pou. 2010. An analysis of households' appraisal of their budget constraints for potential participation in tourism. Tourism Management. 31: 45-56.

AQUASTAT. 2000. Food and Agriculture Organization of the United Nations. Information System on Water and Agriculture: Barbados. http://www.fao.org/nr/water/aquastat/countries/barbados/index.stm Last accessed: 12 August 2008.

Bahamas Department of Statistics, 2012. Key Statistics > Population & Census > Pop. By Sex & Age Bimini. Key Statistics > Tourism Statistics. http://statistics.bahamas.gov.bs/ Last accessed: 30 April 2013.

Barbados Central Bank. 2006. Website: http://www.centralbank.org.bb/documents/ASD07H.pdf. Last accessed: 7/17/14.

Barbados Ministry of Tourism. 2006. 2006 Statistical Digest. Website: http://www.tourism.gov.bb/reports/2006_STATISTICAL_DIGEST.pdf. Last accessed: 7/17/14.

Barbados Ministry of Tourism. 2011. Tourism Statistics for 2007-2011. Website: http://www.tourism.gov.bb/images/stories/Reports/tourism%20statistics%20for%202007%20-2011.pdf. Last accessed: 7/17/14.

Barbados Statistical Service. 2012. Comparison of tourist arrivals by country of residence: December 2010 to December 2011. Website: http://www.barstats.gov.bb/files/documents/Dec_2010_and_2011_compared.pdf. Last accessed: 10/31/14.

Barbados Statistical Service. 2013. Comparison of tourist arrivals by country of residence: December 2011 to December 2012. Website: http://www.barstats.gov.bb/files/documents/Dec_2011_and_2012_compared.pdf. Last accessed: 10/31/14.

Barbados Statistical Service. 2014. Comparison of tourist arrivals by country of residence: December 2012 to December 2013. Website: http://www.barstats.gov.bb/files/documents/Dec_2012_and_2013_compared.pdf. Last accessed: 10/31/14.

Basterretxea, G., A. Jordi, E. Garces, S. Angles, A. Rene. 2011. Seiches stimulate transient biogeochemical changes in a microtidal coastal ecosystem. Marine Ecology Progress Series: V423: 15-28.

Basterretxea, G., A. Tovar-Sanchez, A.J. Beck, P. Masqué, H.J. Bokuniewicz, R. Coffey, C.M. Duarte, J. Garcia-Orellana, E. Garcia-Solsona, L. Martinez-Ribes, R. Vaquer-Sunyer. 2010. Submarine Groundwater Discharge to the Coastal Environment of a Mediterranean Island (Majorca, Spain): Ecosystem and Biogeochemical Significance. Ecosystems. 13(5) pp. 629-643.

Beck, A.J., J.P. Rapaglia, J.K. Cochran, H.J. Bokuniewicz, and S. Yang. 2008. Submarine groundwater discharge to Great South Bay, NY, estimated using Ra isotopes: Marine Chemistry, v. 109, p. 279-291

Bokuniewicz, H.J. 1980. Groundwater Seepage into Great South Bay, New York. Estuarine and Coastal Marine Science 10 pp. 437-444.

Bokuniewicz, H.J. 1992. Analytical Descriptions of Subaqueous Groundwater Seepage. Estuaries15:458-462
Bokuniewicz, H.J. 2001. Towards a coastal groundwater typology. Journal of Sea Research: 46: 99-108.
Bokuniewicz, H.J. 2004. Personal Communication. Stony Brook University.
Bokuniewicz, H.J. and M.J. Zeitlin. 1980. Characteristics of Ground-Water Seepage into Great South Bay. Marine Sciences Research Center. Special Report 35. pg. 30.
Bokuniewicz, H, E Kontar, M Rodrigues, DA Klein. 2004. Submarine Groundwater Discharge (SGD) Patterns through a fractured rock: A case study in the Ubatuba, coastal area, Brazil. Asociacion Argentina de Sedimentologia Revista, 11: 9-16.
Bokuniewicz, H., J. Rapaglia and A. Beck. 2007. Submarine groundwater discharge (SGD) from a volcanic island: A case study in Mauritius Island. International Journal of Oceans and Oceanography, submitted.
Bramwell, B. 2011. Governance, the state and sustainable tourism: a political economy approach. Journal of Sustainable Tourism. 19(4-5): 459-477.
Brock, T.D., D.R. Lee, D. Janes and D. Winek. 1982. Groundwater seepage as a nutrient source to a drainage lake; Lake Mendota, Wisconsin. Water Research. 16: 1255-1263.
Brodie, R.S., S. Baskaran, T. Ransley and J. Spring. 2009. Seepage meter: progressing a simple method of directly measuring water flow between surface water and groundwater systems. Australian Journal of Earth Sciences. 56(1): 3-11.
Brundtland Report, UN World Commission on Environment and Development. 1987. Our Common Future. Oxford Unversity Press. 383 pp. Website: http://www.un-documents.net/our-common-future.pdf. Last accessed: 10/23/14.
Burdick, D. 2006. Guam Coastal Atlas. University of Guam Marine Laboratory. Technical Report 114. http://www.guammarinelab.com/coastal.atlas/ (last accessed 5/24/11)
Burnett, W.C., M. Taniguchi, J. Oberdorfer. 2001. Measurement and significance of the direct discharge of groundwater into the coastal zone. Journal of Sea Research 46(2): 109-116.
Burnett, W.C., P.K. Aggarwal, A. Aureli, H. Bokuniewicz, J.E. Cable, M.A. Charette, E. Kontar, S. Krupa, K.M. Kulkarni, A. Loveless, W.S. Moore, J.A. Oberdorfer, J. Oliveira, N. Ozyurt, P. Povinec, A.M.G. Privitera, R. Rajar, R.T. Ramessur, J. Scholten, T. Stieglitz, M. Taniguchi, J.V. Turner. 2006. Quantifying submarine groundwater discharge in the coastal zone *via* multiple methods. Science of the Total Environment. 367(2-3): 498-543.
Butler, R.W. 1991. Tourism, Environment and Sustainable Development. Environmental Conservation. 18(3): 201-209.
Cable, J.E., J.B. Martin, C. Pounder, L. Inniss, A. Moseley and E. Smith. 2010. Submarine Groundwater Discharge from a Carbonate Aquifer, Worthing Beach, Barbados. American Society for Limnology and Oceanography Summer Meeting. June 6-11, 2010. Santa Fe, New Mexico, USA.
Camargo, J.A. and A. Alonso. 2006. Ecological and toxicological effects of inorganic nitrogen pollution in aquatic ecosystems: A global assessment. Environment International. 32(2006): 831-849.
Capone, D.G. and M.F. Bautista. 1985. A groundwater source of nitrate in nearshore marine sediments. Nature. 313: 214-216.
Carew, J.L. and J.E. Mylroie. 1997. Geology of the Bahamas. In H.L. Vacher and T. Quinn (Ed.), Geology and Hydrogeology of Carbonate Islands. Developments in Sedimentology 54 pp. 91-133. Amsterdam: Elsevier B.V.

Casagrandi, R. and S. Rinaldi. 2002. A Theoretical Approach to Tourism Sustainability. Conservation Ecology. 6(1): 13 [online]. Website: http://www.consecol.org/vol6/iss1/art13/.
Causevic, S. and P. Lynch. 2013. Political (in)stability and its influence on tourism development. Tourism Management. 34: 145-157.
Charette, M. 2008. Personal communication. Woods Hole Oceanographic Institution.
Corbett, D.R. and J.E. Cable. 2003. Seepage Meters and Advective Transport in Coastal Environments: Comments on "Seepage Meters and Bernoulli's Revenge" by EA Shinn, CD Reich and TD Hickey. 2002. Estuaries. 25: 126-132.
Crotwell, A.M., and W.S. Moore. 2003. Nutrient and radium fluxes from submarine groundwater discharge to Port Royal Sound, South Carolina. Aquatic Geochemistry 9(3): 191-208.
Denton, G.R.W., L.P. Concepcion, H.R. Wood and C.M. Sian Denton. 2005. Nutrient Status of Tumon Bay in Relation to Intertidal Blooms of the Filamentous Green Alga, *Enteromorpha clathrata*. Water and Environmental Research Institute of the Western Pacific, University of Guam. Technical Report No. 110.
Destouni, G. and C. Prieto. 2003. On the possibility for generic modelling of submarine groundwater discharge. Biogeochemistry. 66: 171-186.
Dore, J.E., T. Houlihan, D.V. Hevel, G. Tien, L. Tupas and D.M. Karl. 1996. Freezing as a method of sample preservation for the analysis of dissolved inorganic nutrients in seawater. Marine Chemistry 53: 173-185.
Duncan, D.A., 1972. High Resolution Seismic Survey, Port Royal Sound Environmental Study. S. C. Water Resources Commun., Columbia SC, pp. 85-106.
Emery, K.O. and J.P. Foster. 1948. Water Tables in Marine Beaches: Journal of Marine Research. 7(3): 644-654.
EPA. 2014. Summary Table for the Nutrient Criteria Documents. Website: http://www2.epa.gov/sites/production/files/2014-08/documents/criteria-nutrient-ecoregions-sumtable.pdf. Last accessed: 10/23/14.
Falkland, A. 1991. Hydrology and water resources of small islands: a practical guide. United Nations Educational, Scientific and Cultural Organization, Paris. 435 pp.
Fetter, C.W. 2001. Applied Hydrogeology, 4th edition. Prentice-Hall, Inc. Upper Saddle River, NJ. 598 pp.
FitzGerald, W.J. 1978. Environmental Parameters Influencing the Growth of *Enteromorpha clathrata* (Roth) J. Ag. In the Intertidal Zone on Guam. Botanica Marina: V21 pp. 207-220.
Fitzgibbon, A.W., M. Pilu and R.B. Fisher. 1999. Direct Least Squares Fitting of Ellipses. IEEE Transactions on Pattern Analysis and Machine Intelligence. 21(5): 476-480.
Folk, R.L. 1966. A Review of Grain-Size Parameters. Sedimentology 6(1966): 73.93.
Frommers Travel Section for Bimini http://www.frommers.com/destinations/bimini/0263010001.html Last accessed: 19 April 2013.
Garrison, G.H., C.R. Glenn and G.M. McMurtry. 2003. Measurement of Submarine Groundwater Discharge in Kahana Bay, O'ahu, Hawai'i. Limnology and Oceanography. 48(2): 920-928.
Goolsby, D.A., W.A. Battaglin and R.P. Hooper. 1997. Sources and Transport of Nitrogen in the Mississippi River Basin. Presentation. American Farm Bureau Federation Workshop "From the Corn Belt to the Gulf...Agriculture and Hypoxia in the Mississippi River

Watershed", July 14-15, 1997, St. Louis, Missouri.
Greenidge K. and N. Greenidge. 2011. Sustainable Tourism Development: The Case of Barbados. The Central Bank of Barbados Economic Review. Volume XXXVII, Issues 1&2: 83-125.
Hahn, J., Y. Lee, N. Kim, C. Hahn and S. Lee. 1997. The groundwater resources and sustainable yield of Cheju volcanic island, Korea. Environmental Geology. 33(1): 43-53.
Harris, W.H. 1971. Groundwater-carbonate rock chemical interactions, Barbados, West Indies. Ph.D. thesis, Brown Univ. 384 pp.
Hira, A. and L.G. de Oliveira. 2009. No substitute for oil? How Brazil developed its ethanol industry. Energy Policy. 37(6): 2450-2456.
Howarth, R.W, and R. Marino. 2006. Nitrogen as the limiting nutrient for eutrophication in coastal marine ecosystems: Evolving views over three decades. Limnology and Oceanography. 51(1, part 2): 364-376.
Huettel, M., G. Gust. 1992. Impact of bioroughness on interfacial solute exchange in permeable sediments. Mar. Ecol. Prog. Series. 89: 253-267.
Huettel, M., W. Ziebis and S. Forster. 1996. Flow-induced uptake of particulate matter in permeable sediments. Limnology and Oceanography. 41(2): 309-322.
Huettel, M., W. Ziebis, S. Forster and G.W. Luther III. 1998. Advective transport affecting metal and nutrient distributions and interfacial fluxes in permeable sediments. Geochim. Cosmochim. Acta. 62(4): 613-631.
Hwang, D.-W., Y.-W. Lee and G. Kim. 2005. Large submarine groundwater discharge and benthic eutrophication in Bangdu Bay on volcanic Jeju Island, Korea. Limnology and Oceanography. 50(5): 1393-1403.
Jenkins, C.L. and B.M. Henry. 1982. Government involvement in tourism in developing countries. Annals of Tourism Research. 9(4): 499-521.
Jocson, J.M.U., J.W. Jenson and D.N. Contractor. 2002. Recharge and aquifer response: Northern Guam Lens Aquifer, Guam, Mariana Islands. Journal of Hydrology 260: 231-254.
Jones, I.C. 2002. Geochemical evolution of groundwater in the Pleistocene limestone aquifer of Barbados. Doctoral Thesis. University of Texas, Austin, TX. 273 pp.
Kim, G., K.-K. Lee, K.S. Park, D.-W. Hwang and H.-S. Yang. 2003. Large submarine groundwater discharge (SGD) from a volcanic island. Geophysical Research Letters. 30(21): 2098.
Kim, G., J.-S. Kim and D.-W. Hwang. 2011. Submarine groundwater discharge from oceanic islands standing in oligotrophic oceans: implications for global biological production and organic carbon fluxes. Limnology and Oceanography. 56(2): 673-682.
Klein, Y.L., J.P. Osleeb and M.R. Viola. 2004. Tourism-Generated Earnings in the Coastal Zone: a Regional Analysis. Journal of Coastal Research. 20(4): 1080-1088.
Knee, K.L., B.A. Layton, J.H. Street, A.B. Boehm, A. Paytan. 2008. Sources of Nutrients and Fecal Indicator Bacteria to Nearshore Waters on the North Shore of Kaua'i (Hawai'i, USA). Estuaries and Coasts 31: 607-622.
Lander, M.A. and C.P. Guard 1. 2003 Creation of a 50-Year Rainfall Database, Annual Rainfall Climatology, and Annual Rainfall Distribution Map for Guam. Water & Environmental Research Institute of the Western Pacific, University of Guam. Technical Report No. 102.
Lee, D.R. 1977. Device for measuring seepage flux in lakes and estuaries. Limnology and Oceanography. 22(1): 140-147.

Lee, J.-M. and G. Kim. 2007. Estimating submarine discharge of fresh groundwater from a volcanic island using a freshwater budget of the coastal water column. Geophysical Research Letters. 34: L11611.
Lewis, J.B. 1987. Measurements of groundwater seepage flux onto a coral-reef – spatial and temporal variations. Limnology and Oceanography. 32(5): 1165-1169.
Li L., D. Barry, F. Stagnitti, J.P. Parlange. 1999. Submarine groundwater discharge and associated chemical input to a coastal sea. Water Resource Research. 35: 3253–3259.
Lutz, W. (Ed.) 1994. Population-Development-Environment: Understanding their Interactions in Mauritius. Springer-Verlag, Berlin, Germany. 400 pp.
Lutz, W., L. Prieto and W.C. Sanderson. 2000. Population, Development and Environment on the Yucatan Peninsula: from Ancient Maya to 2030. International Institute for Applied Systems Analysis, Laxenburg, Austria. 257 pp.
Lutz, W., W.C. Sanderson and A. Wils. 2002. Toward Comprehensive P-E studies. Population and Development Review, 28(Supplement: Population and Environment: Methods of Analysis): 225-250.
Matson, E.A. 1993. Nutrient flux through soils and aquifers to the coastal zone of Guam (Mariana Islands). Limnology and Oceanography 38(2), 361-371.
Mayers, B. 2007. Personal Communication. January 2007, University of the West Indies, Cave Hill Campus, Barbados.
McBride, M.S., and H.O. Pfannkuch. 1975. The distribution of seepage within lake beds. Journal of Research of the United States Geological Survey. 3: 505-512.
Mesolella, K.J., R.K. Matthews, W.S. Broeker and D.L. Thurber. 1969. The astronomical theory of climatic change: Barbados Data. Journal of Geology. 77: 250-274.
Metcalf, W., H. Bokuniewicz and A. Terchunain. 1995. Water-table variations on a reflective ocean beach: Quoque Beach, New York. Northeastern Geology. 17(1): 61-67.
Michael, H.A., J.S. Lubetsky and C.F. Harvey. 2003. Characterizing submarine groundwater discharge: A seepage meter study in Waquoit Bay, Massachusetts. Geophysical Research Letters. 30: 1297.
Michael, H.A., A.E. Mulligan and C.F. Harvey. 2005. Seasonal oscillations in water exchange between aquifers and the coastal ocean. Nature. 436(25): 1145-1148.
Moore, C.H., 1989. Carbonate Diagenesis and Porosity. Developments in Sedimentology 46, Elsevier, Amsterdam, 38 pp.
Moore, W.S. 1999. The subterranean estuary: a reaction zone of ground water and sea water. Marine Chemistry 65(1-2): 111-125.
Moore, W.S. 2006. The role of submarine groundwater discharge in coastal biogeochemistry. Journal of Geochemical Exploration 88(1-3): 389-393.
Moore, W.S. and R. Arnold. 1996. Measurement of 223Ra and 224Ra in coastal waters using a delayed coincidence counter. Journal of Geophysical Research. 101: 1321–1329.
Morgan, R. 1999. Preferences and Priorities of Recreational Beach Users in Wales, UK. Journal of Coastal Research. 15(3): 653-667
Murdoch, L.C. and S.E. Kelly. 2003. Factors affecting the performance of conventional seepage meters. Water Resour. R. 39(6): 1163, doi:10.1029/2002WR001347.
Nielsen, P. 1990. Tidal Dynamics of the Water Table in Beaches. Water Resources Research. 26: 2127-2134.
NOAA. 2007. Tidal Station Locations and Ranges. http://tidesandcurrents.noaa.gov/tides07/tab2ec4.html#117. Accessed 12 August 2008.

Nurse, L. 2014. Personal Communication. University of West Indies, Cave Hill Campus, Barbados. August 2014.
Nymphea Middle East. 2013. Company Profile. http://www.oceanologyinternational.com/__novadocuments/43497?v=635242597726870000 Last accessed: 28 January 2014.
Paulsen, R.J., D. O'Rourke, C.F. Smith and T.F. Wong. 2004. Tidal load and salt water influences on submarine groundwater discharge. Ground Water. 42(7): 990-999.
Paytan, A., G.G. Shellenbarger, J.H. Street, M.E. Gonneea, K. Davis, M.B. Young, W.S. Moore. 2006. Submarine groundwater discharge: an important source of new inorganic nitrogen to coral reef ecosystems. Limnology and Oceanography. 51(1): 343-348.
Peterson, R.N., W.C. Burnett, C.R. Glenn and A.G. Johnson. 2009. Quantification of point-source groundwater discharges to the ocean from the shoreline of the Big Island, Hawaii. Limnology and Oceanography 54(3) p 890-904.
Povinec P.P, W.C. Burnett, A. Beck, H. Bokuniewicz, M. Charette, M.E. Gonneea, M. Groening, T. Ishitobi, E. Kontar, L. Lion Wee Kwong, D.E.P. Marie, W.S. Moore, J.A. Oberdorfer, R. Peterson, R. Ramessur, J. Rapaglia, T. Stieglitz, Z. Top. 2012. Isotopic, geophysical and biogeochemical investigation of submarine groundwater discharge: IAEA-UNESCO intercomparison exercise at Mauritius Island. Journal of Environmental Radioactivity. 104(2012): 24-45.
Prieto, C. and G. Destouni. 2005. Quantifying hydrological and tidal influences on groundwater discharges into coastal waters. Water Resources Research. 41: W12427.
Proctor and Redfern International Ltd. 1983. Coastal conservation project, V.2; sect. 8: Drainage and groundwater models. 50 p.
Quinn, H., J. Tolson, J. Klein, S. P. Orlando, and C. Alexander. 1989. Strategic assessment of near coastal waters: Susceptibility of east coast estuaries to nutrient discharges: Albemarle/Pamlico Sound to Biscayne Bay. NOAA/EPA summary report. U.S. Department of Commerce, National Oceanic and Atmospheric Administration, Silver Spring, MD.
Rocha, C. 2000. Density-driven convection during flooding of warm, permeable intertidal sediments: the ecological importance of the convective turnover pump. Journal of Sea Research. 43: 1-14.
Rodellas, V., J. Garcia-Orellana, A. Tovar-Sánchez, G. Basterretxea, J. M. López-Garcia, D. Sánchez-Quiles, E. Garcia-Solsona, P. Masqué. 2014. Submarine groundwater discharge as a source of nutrients and trace metals in a Mediterranean bay (Palma Beach, Balaeric Islands). Marine Chemistry. 160(2014): 56-66.
Rolle, O. 2010. Personal communication. June 2010. Bimini water supplier.
Rosenberry, D.O., R.W. Sheibley, S.E. Cox, F.W. Simonds and D.L. Naftz. 2013. Temporal variability of exchange between groundwater and surface water based on high-frequency direct measurements of seepage at the sediment-water interface. Water Resources Research. 49: 2975-2986.
Ruhanen, L. 2013. Local government: facilitator or inhibitor of sustainable tourism development? Journal of Sustainable Tourism. 21(1): 80-98.
Salarashayeri A.F. and M. Siosemarde 2012. Prediction of Soil Hydraulic Conductivity from Particle-Size Distribution. World Academy of Science, Engineering and Technology 6: 395-399.
Schubert, S.F., J.G. Brida and W.A. Risso. 2011. The impacts of international tourism demand

on economic growth of small economies dependent on tourism. Tourism Management. 32: 377-385.
Sen, A., A.R. Harwood, I.J. Bateman, P. Munay, A. Crowe, L. Brander, J. Raychaudhuri, A.A. Lovett, J. Foden and A. Provins. 2014. Economic Assessment of the Recreational Value of Ecosystems: Methodological Development and National and Local Application. Environmental and Resource Economics. 57: 233-249.
Senal, M.I.S., G.S. Jacinto, M.L. SanDiego-McGlone, F. Siringan, P. Zamora, L. Soria, M. B. Cardenas, C. Villanoy and O. Cabrera. 2011. Nutrient inputs from submarine groundwater discharge on the Santiago reef flat, Bolinao, Northwestern Philippines. Marine Pollution Bulletin. 63(2011):195-200.
Shaw, R.D. and E.E. Prepas. 1989. Anomalous, short-term influx of water into seepage meters. Limnology and Oceanography. 34(7): 1343-1351.
Shinn, E.A., C.D. Reich and T.D. Hickey. 2002. Seepage Meters and Bernoulli's Revenge. Estuaries. 25: 126-132.
Smith, A.J., D.E. Herne and J.V. Turner. 2009. Wave effects on submarine groundwater seepage measurement. Advances in Water Resources. 32: 820-833.
Smith, S.V. 1984. Phosphorus versus Nitrogen Limitation in the Marine Environment. Limnology and Oceanography. 29(6): 1149-1160.
Stieglitz T., P.V. Ridd and P. Muller. 2000. Passive irrigation and functional morphology of crustacean burrows in atropical mangrove swamp. Hydrobiologia 421: 69–76.
Sunamura, T. 1984. Quantitative predictions of beach-face slope. Geological Society of America Bulletin 95: 242-245.
Susilo, A., P.V. Ridd and S. Thomas. 2006. Comparison between tidally driven groundwater flow and flushing of animal burrows in tropical mangrove swamps. Wetlands Ecology and Management 13: 377–388
Taniguchi, M. 2002. Tidal effects on submarine groundwater discharge into the ocean. Geophysical Research Letters. 29(12): 1561.
Taniguchi, M. and Y. Fukuo. 1996. An effect of seiche on groundwater seepage rate into Lake Biwa, Japan. Water Resources Research 32(2), 333-338.
Taniguchi, M., W.C. Burnett, J.E. Cable and J.V. Turner. 2002. Investigation of submarine groundwater discharge: Hydrological Processes, v. 16, p. 2115- 2129.
Taniguchi, M., W.C. Burnett, H. Hulaiova, F. Siringan, J. Foronda, G. Wattayakorn, S. Rungsupa, E.A. Kontar and T. Ishitobi. 2008. Groundwater Discharge as an Important Land-Sea Pathway into Manila Bay, Philippines. Journal of Coastal Research. 24(sp1):15-24.
Teichberg, M., S.E. Fox, Y.S. Olsen, I. Valiela, P. Martinetto, O. Irabarne, E.Y. Muto, M.A.V. Petti, T.N. Corbisier, M. Soto-Jiménez, F. Páez-Osuna, P. Castro, H. Freitas, A. Zitelli, M. Cardinaletti and D. Tagliapietra. 2010. Eutrophication and macroalgal blooms in temperate and tropical waters: nutrient enrichment experiments with *Ulva* spp. Global Change Biology. 16(9): 2624-2637.
The Bahamian. 2010. http://islands.thebahamian.com/bimini.html Last accessed: July 2010.
Ullman, W.J., B. Chang, D.C. Miller, and J.A. Madsen. 2003. Groundwater mixing, nutrient diagenesis, and discharges across a sandy beachface, Cape Henlopen, Delaware (USA). Estuarine, Coastal and Shelf Science 57(2003): 539-552.
UNEP WTO (United Nations Environment Programme and World Tourism Organization). 2005. Making Tourism More Sustainable: A Guide for Policy Makers. Website:

http://www.unep.fr/shared/publications/pdf/DTIx0592xPA-TourismPolicyEN.pdf. Last accessed 10/23/14.
United Nations Department of Economic and Social Affairs, Division for Sustainable Development. 2014. SIDS Members. URL: http://sustainabledevelopment.un.org/index.php?menu=1520 Last accessed: 10 September 2014.
Valdemoro, H. and J. Jiménez. 2006. The Influence of Shoreline Dynamics on the Use and Exploitation of Mediterranean Tourist Beaches. Coastal Management. 34: 405-423.
Ward, P.E., S.H. Hoffard and D.A. Davis. 1965. Hydrology of Guam. Geological Survey Professional Paper 403-H, Washington, H1-H28.
Weisstein, Eric W. 2014a "Eccentricity." From MathWorld--A Wolfram Web Resource. http://mathworld.wolfram.com/Eccentricity.html Last accessed: 3 February 2014.
Weisstein, Eric W. 2014b "Conic Section." From MathWorld--A Wolfram Web Resource. http://mathworld.wolfram.com/ConicSection.html Last accessed: 3 February 2014.
Wellington, C. and R. Moore. 2004. Barbados' first national communications to the United Nations Framework Convention on Climate Change. http://unfccc.int/essential_background/library/items/3599.php?rec=j&priref=3229 Last accessed: 12 August 2008.
Wentworth, C.K. 1922. A Scale of Grade and Class Terms for Clastic Sediments. Journal of Geology 30(5): 377-392.
Whitaker, F.F. and P.L. Smart. 1997a. Hydrogeology of the Bahamian Archipelago. pp. 183-212 in H.L. Vacher and T. Quinn (Ed.), Geology and Hydrogeology of Carbonate Islands. Developments in Sedimentology Vol. 54
Whitaker, F.F. and P. Smart. 1997b. Groundwater circulation and geochemistry of a karstified bank-marginal fracture system, South Andros Island, Bahamas. Journal of Hyrdology 197: 293-315.
World Population Prospects. 2012. Population Division of the Department of Economic and Social Affairs of the United Nations Secretariat, World Population Prospects: The 2012 Revision, http://esa.un.org/unpd/wpp/index.htm. Last accessed 4/24/14.
Wright, Benjamin. 2006. Suffolk County Department of Public Works. Personal communication April 20, 2006.
Xin, P., C. Robinson, L. Li, D.A. Barry and R. Bakhtyar. 2010. Effects of wave forcing on a subterranean estuary. Water Resources Research. 46.
Zektser, I.S. 2000. Groundwater and the Environment: Applications for the Global Community. Lewis Publishers, Boca Raton: 175 pp.